

Investigations into Optically Controlled Phase Contrast, Polarisation Switchable Narrow Band RF Detection Techniques.

By
Terry Quinlan



A Thesis submitted for the degree of Doctor of Philosophy
School of Computer Science and Electronic Engineering
University of Essex

September 2015

Table of Contents

Acknowledgments	6
Abstract	7
Chapter 1 Introduction	
1.1 Radio Frequency Detection.....	8
1.2 Signal Quality.....	10
1.3 Reflection and Dielectric Effects.....	12
1.4 Antenna Configurations.....	14
1.5 Polarisation Technique.....	16
1.6 Wide Bandwidth Signals.....	17
1.7 Phase Techniques.....	18
1.8 Outline of Thesis.....	19
List of References.....	21
Chapter 2 Short Range Systems	
2.1 General Techniques.....	23
2.2 Medical Imaging.....	24
2.3 Ground penetrating Radar.....	39
2.4 Microwave Non-Destructive Evaluation.....	44
2.5 Phase unwrapping.....	46
2.6 Suitable Antenna Designs.....	47
2.7 Phase preservation.....	58
2.8 Optical Remoting.....	60

2.9	Polarisation.....	61
2.10	Conclusions.....	62
	List of References.....	65
Chapter 3	Initial Experimental Work	
3.1	Aims and Objectives.....	70
3.2	Radio Frequency System (Proof of Concept).....	72
3.3	Tri – Antenna Array.....	77
3.4	Initial Investigations.....	82
3.5	E Plane Measurements.....	88
3.6	Conclusions.....	89
	List of References.....	92
Chapter 4	Radio over Fibre - Phase Preservation	
4.1	Introduction.....	93
4.2	Quadrature Amplitude Modulation and phase preservation.....	94
4.3	Error Vector Magnitude.....	96
4.4	Reflected Modulation Method.....	98
4.5	Coarse Wavelength Division Multiplexing Method.....	102
4.6	Directly Modulated VCSELs.....	103
4.7	Outline of Some Devices used.....	111
4.8	Conclusions.....	118
	List of References.....	120

Chapter 5	Optical Transmission System	
5.1	Introduction.....	122
5.2	Reflective Transducer Approach.....	123
5.3	CWDM Approach.....	136
5.4	Final CWDM system.....	151
5.5	Conclusions.....	161
	List of References.....	165
Chapter 6	Modelling of Polarisation Switchable Antenna	
6.1	Design Considerations.....	166
6.2	Patch Antenna background.....	168
6.3	Design Methodology.....	173
6.4	Linearly Polarised Square Patch.....	177
6.5	Polarisation Switchable Square Patch.....	182
6.6	Linearly Polarised Rectangular Patch.....	188
6.7	Polarisation Switchable Crossed Rectangular Patch.....	191
6.8	Conclusions.....	196
	List of References.....	198
Chapter 7	Implementation of Antenna Design	
7.1	Introduction.....	200
7.2	Input / Feed Measurements.....	201
7.3	Polarisation Isolation Measurements.....	204
7.4	Gain Measurements.....	205
7.5	Conclusions	206

Chapter 8	Polarisation Switchable Measurement System	
8.1	Final System overview.....	208
8.2	Antenna to antenna measurements.....	210
8.3	Radio over fibre comparison.....	212
8.4	Conclusions.....	214
	Reference.....	215
Chapter 9	Summary of Chapters and Further Work.....	216
Authors Relevant Publications.....		226
Appendix 1	Definitions.....	231
Appendix 2	Alphabetical List of Acronyms.....	232

Acknowledgments

Well I guess it is true to say that I have never had a conventional view of life and consequently rarely do things in a “normal” way in the “usual” order. Labelled at Curwen primary school, London, circa 1956 as “a plodder who gets there in the end” it is no surprise then that I found myself doing this toward the end of my research career rather than at the beginning. As it took so long to get here I think it is more appropriate to thank and acknowledge those who were broadly instrumental in putting a set of circumstances together that allowed this work to come about rather than the more orthodox mentioning of individuals.

Firstly I must thank people I have worked with in the department of ESE / EES here at the University for all the Inspiration, encouragement, discouragement and sometimes “character building experiences” over my time in the department. Then the people from whom I have learnt during that time, the many students and colleagues that I have been involved with on a large number of projects covering a wide range of sometimes seemingly unrelated subjects.

Also I must acknowledge the many wise and interesting people I have encountered whilst travelling in various parts of the world. The wisdom, experience of reality and the lessons in patience and appreciation of what is important in life that they so often imparted has proved invaluable and totally unreplaceable.

Having said that certain people must be thanked for their close involvement and support as well. Stuart Walker, head of the Access Networks Group for facilitating this work and providing a research friendly environment. But above all I must thank my wife, Lesley Quinlan for all of the help, support, encouragement, companionship and wise counsel given that enabled me to cope with and survive the many challenging and sometimes impossible situations that arose during the course of this work.

Finally, as I think I have now forgotten most of what I had learned at school I must now also
acknowledge the wisdom of the guy below.

“Education is what remains after one has forgotten what one has learned in school.”

Albert Einstein

Abstract

This thesis describes an investigation into S-band microwave frequency phase-contrast imaging. Resolution is a critical issue so system enhancements such as optical remote connection and polarisation-dependant sensing have been implemented within an end-to-end sensing system. Initially, the feasibility of phase-contrast measurements was considered and the limits of phase and amplitude measurements established. A switching matrix was then designed and incorporated into a tri-antenna array to demonstrate triangulation-based location. Commercial, linearly-polarised antennas were then used to demonstrate basic object location. A comprehensive experimental investigation into optical transmission of phase sensitive data using Radio over Fibre (RoF) techniques is then described. Reflective technology and directly modulated Vertical Cavity Surface Emitting Lasers (VCSELs) are assessed for suitability as are Coarse Wavelength Division Multiplexed (CWDM) architectures. These are believed to be a novel contribution in the imaging context as are the techniques employed to enhance and extend the matching and performance of the optical devices. A directly modulated VCSEL based CWDM method was then used over the extended range of 1 km of standard single mode optical fibre. Subsequently, dual polarisation plane techniques were used to generate sequential, orthogonally-separated measurements, which required the development of a suitable antenna. The design, modelling, construction and deployment of a high cross-polar isolation, patch antenna is then described. An antenna with single symmetrical forward lobes (on both polarisation planes) and low back radiation pattern was devised so enabling sensing from a single coincident point. With the device integrated into the final measurement system the resulting “Polarisation Switched, Narrowband, RF Probe System Using a VCSEL Optical Feed” was used to demonstrate improved resolution of a phase contrast RF measurement system at an optically-remoted distance of 1km.

Chapter 1 Introduction

1.1 Radio Frequency Detection

Radio frequency detection emerged in its most well-known form at the beginning of the 1940's with the implementation of Radio Detection and Ranging (RADAR). Pioneered by Watson Watt et al, at Bawdsey, Suffolk and based on ideas for the use of radio for the detection of thunderstorms using effects generated by lightning [1.01]. Radar in its most basic form uses a signal sent from a directional transmitting antenna; this signal will then scatter off any obstacles in its path. Some of the energy will inevitably be reflected back to a receiving antenna in the form of an "echo". By processing this signal information about the distance and direction of the source of the reflection can be obtained. This principle forms the basis of a plethora of radio frequency location techniques in applications as diverse as air traffic control to medical imaging. In its rudimentary form a radar detection system consists of a number of building blocks common to the majority of all RF imaging techniques. An antenna system, an RF switching matrix, transmitting and receiving amplifiers, a frequency synthesizer and pulse modulator and radio frequency mixers. Digital signal processing equipment is added after the "core" detection arrangement to reconstruct images, remove unwanted signals (clutter and noise), enhance the information gathered and interpret and analyse the received signals. At the "front end" of the system is a single antenna, this alternates between transmit and receive modes using an RF switching arrangement. In order to select the frequency of operation a synthesiser is incorporated, and is commonly fed to the antenna via a pulse modulator, so as to provide a signal burst which can be "gated" on in transmit mode and off in receive mode as well as create a pulse. With the creation of this modulated pulse it is then necessary to provide amplification before application to the antenna and transmission can

be implemented. Following this, receive mode can be selected as the system waits for the “echo” or return pulse to arrive. After detection by the antenna the “return pulse” is amplified and can be down converted and demodulated, using RF mixers that are also locked to the synthesised frequency. In this way it is possible to reconstruct a signal that has a finite delay with reference to the original transmitted pulse. As the speed of propagation of an electromagnetic (radio) signal in a given medium (Air) is known (approx. 299,792,458 m / s) the distance of an object can be calculated, taking into account delays inherent to the radar system itself by equation (1).

$$R = c\tau_d / 2 \quad (1)$$

Where R is the distance of the target (range), c is the speed of light and τ_d is the propagation delay (round trip time) attributed to the returning signal. This “return path” time is then divided by two to give the distance travelled by the pulse. [1.02] An indication of the direction of the target (azimuth) can be obtained if a highly directional antenna is utilised. If such an antenna is rotated it can be synchronised with a display in such a way as to reveal the direction of the object of interest (hence the familiar rotating dish antenna). A notable exception to the method outlined above is Doppler Shift Radar. Doppler Shift radar is only used to detect the speed of an approaching object. Using frequency measurements from the reflected signal, the speed of an object can be calculated from

$$f_d = 2v_r / \lambda \quad [\text{Hz}] \quad (2)$$

where f_d is the change in frequency, v_r is the speed of the object and λ is the wavelength of the radar carrier signal. This change in frequency (wavelength) can then be translated to speed [1.03]. Radio frequency detection systems are dependant not only on the physical properties of the building blocks already described, but also that of the medium in which the system is to operate. Factors including attenuation, background noise and scattering will influence the received signal, reducing signal integrity and so undermining the accuracy of the resulting measurements [1.03].

1.2 Signal Quality

Scattering of the reflected signal is caused by the presence of irrelevant objects. Examples of these may include fixed obstacles that give rise to shrouding reflections (cliffs, trees and buildings), the “chaff” emitted from military aircraft that provides many small noise like reflections and material inhomogeneity in Non Destructive Evaluation (NDE) and medical applications. Generally known as “clutter” this phenomenon is mainly related to long range radar systems, the effect, increasing with target distance due to signal attenuation. Although having a similar effect, clutter differs from noise, in that it can be from a stationary object (point clutter) or distributed source (volume clutter). In both cases this is either dealt with using Doppler information or by a process known as “clutter fixing”, using pre-determined “clutter maps” to cancel the anomaly. Such techniques though, clearly require the use of a priori knowledge of the operating environment. As with most electronic systems, ultimate performance is largely dependent on Signal to Noise Ratio (SNR). This is dependant not only on the levels of residual noise present, but also on how the signal is affected by the transmission medium. At high frequencies materials can often exhibit properties that render them lossy to specific frequencies. An example being the high atmospheric absorption at 60GHz due to Oxygen absorption.

Returned signals are inherently small due to the amount being reflected from the target ie. the Radar Cross Section (RCS). In addition it has to travel twice the distance from transmitter to the target so limiting the operating range of any system. Selecting a suitable frequency of operation will drastically affect system performance in terms of SNR; this ability can lead to significant benefits. An example is shown in Fig. 1.1, this shows plots

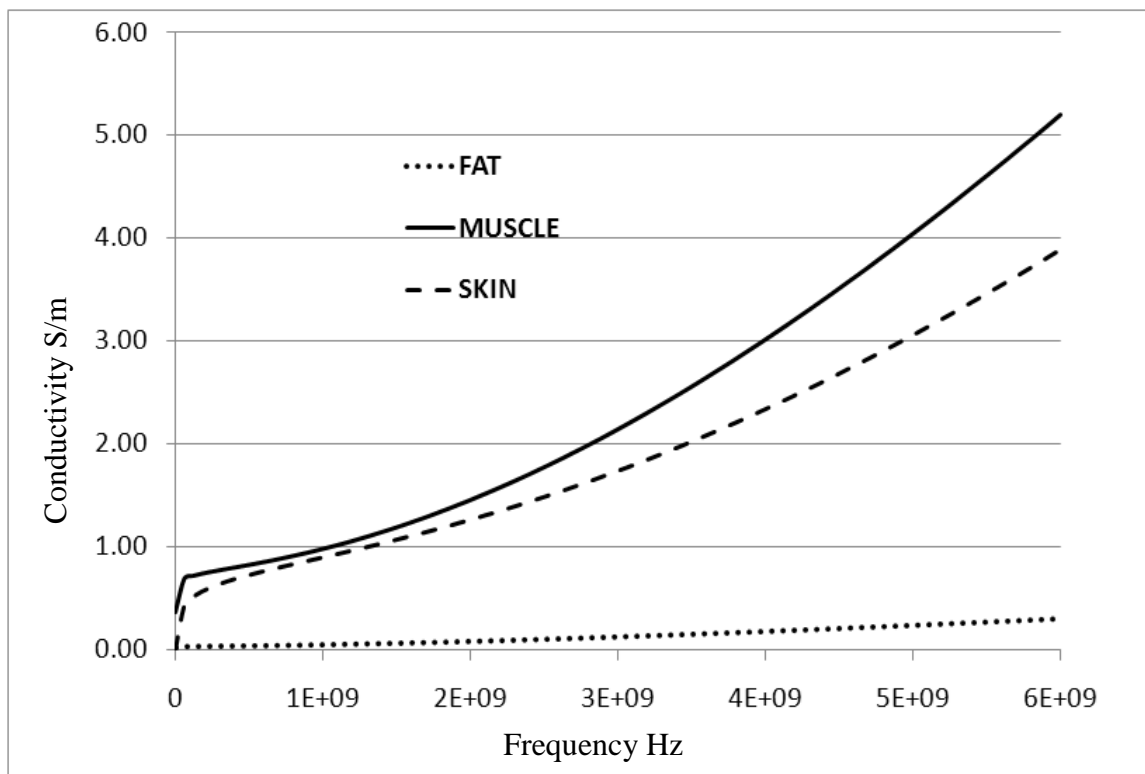


Fig.1.1. Conductivity variation with frequency [1.04].

of the variation of electrical conductivity with frequency for three types of human tissue [1.04]. As conductivity increases the more rapidly electromagnetic energy is dissipated, and so the more opaque the material appears at that frequency [1.05]. It can be seen that the conductivity of skin and muscle increases with frequency, while fat remains relatively constant. At frequencies below 10GHz, conductivity, and so, attenuation is low in all cases, making these frequencies a good choice in terms of SNR for this (medical)

application. Higher frequencies, while having the potential for higher resolution are rapidly dissipated leading to poor SNRs and consequently indistinct return signals. If used to try to penetrate these materials any resolution advantages will be quickly lost in a noisy signal. However this relative opacity can be used to advantage if a signal reflected by these materials is detected through a low loss medium such as air. An example of this is the airport style full body and baggage scanners that operate at mm wavelengths and Terahertz systems. Notoriously, airport full body scanners can provide very detailed images because they will only penetrate relatively light clothing, body tissues being highly reflective. Similarly the use of Terahertz scanners such as those commercially available from companies such as Teraview <http://www.teraview.com/> are confined to either surface observations (ie basal cell carcinomas) or spectroscopic analysis uses. Most “airport style” high resolution image scanning uses modified Computer Tomography (CT) technology similar to that used for medical imaging (<http://www.analogic.com/products-security.htm>) and employs the use of X-rays to produce high penetration, high quality results.

1.3 Reflection and Dielectric Effects

All radio frequency detection systems are dependent on a reflection from the object of interest. As discussed earlier the amount of the signal power returned by an object to a detector of a given size (aperture), is influenced by the size and shape of any such target.

$$P_r = \frac{P_t G_t}{4\pi r^2} \sigma \frac{1}{4\pi r^2} A_{eff} \quad [1.06] \quad (3)$$

Where: P_t = power transmitted, G_t = transmitting antenna gain, r = range, σ = RCS,

A_{eff} = effective aperture of receiving antenna and P_r = returned power. Known as the radar Cross Section this can be described as the amount of power that is scattered isotropically when a target intercepts the radar signal and is dependent on several factors, especially shape and size. A spherical object for example will scatter the signal in many directions, returning only a small proportion being returned to the detector as an echo and so would present a small RCS. Just as with an antenna, a large object will intercept and reflect more signal, this signal scattering is also dependant on target size relative to the detecting signal wavelength and so is also frequency dependant. Conversely it is also possible to increase the power of the received signal by increasing the effective aperture (area) of the antenna so as to capture more of the reflected signal. Apart from simply building large structures (which may not always be practical) a technique known as Synthetic Aperture Radar (SAR) sets out to accomplish this in one of two ways. The first method uses a series of pulses transmitted from a single mobile antenna. These are then collected at known intervals and then combined during a post processing procedure. Effectively this sums each “snapshot”, combining coherent material so effectively amplifying the pulse while the incoherent background noise is averaged to a very low level. This is only of use where the object of interest is stationary i.e. geographic mapping. A second method may be implemented by deploying multiple antennas over a large area, the return signals from each location can once again be coherently recombined [1.07], [1.08] effectively producing an antenna with a very large area. In this way widely scattered, low power reflections from a moving object can be time gated, added and resolved. In the first case the antenna is moved but the object of interest must be stationary and in the second case, multiple antennas are stationary but at known intervals, so the object can be moving. Multi antenna configurations can also be found in sensing processes that rely on signals that are transmitted between antennas. In applications

involving purely reflective objects it may only be necessary to measure the “time of flight” of a pulse bounced off the target. Other applications however may require the signal to be passed through a non-reflective object as may be the case for medical imaging systems. In this case the object of interest may be relatively large compared to the overall range of the system. Also, if radio frequency wavelengths are deployed in these applications, these may be long in comparison to both the object under investigation and the distances involved. In these cases the dielectric properties of the object may also be of interest as variations in the dielectric constant (ϵ_r) of the material will lead to wavelength shortening within the material. As a consequence real and relative phase changes to a sensing signal may occur. This will lead to scattering in wideband signals as well as the possibility of bending of the beam (refraction). Whereas this may be insignificant for long range and long wavelength radar, at smaller scales it will become a significant effect. Microwave short distance ranging and sensing applications can often capitalise on these effects.

1.4 Antenna Configurations

Antenna arrangements for radio frequency based detection systems mostly fall into one of three categories:

1. **Monostatic;** where the transmit and receive antennas are located close to one another. Often a single dual function antenna only is used, this being time gated between transmit and receive modes.
2. **Bistatic;** where the transmit and receive antennas are separated by a distance comparable to, or greater than that of the object of interest. In this case detection is that of forward scatter from the transmitting antenna to the target and then on to

the receiving device, not reflection and is particularly useful where the RCS of the object is small as the target silhouette is often illuminated. Antennas in this configuration can be at an angle up to 180 degrees with respect to the target.

3. **Multistatic**; where multiple transmit and receive stations interact with each other. These systems can be widely spaced, switched or combined, forming a grid that will further enhance the effective performance of individual elements within the array. This will frequently lead to an improvement in the data gathering ability and accuracy of an overall system.

Frequently antenna performance and function can be manipulated by grouping antennas into arrays. Techniques deployed in these cases can often include Phased Array and Multi Input Multi Output (MIMO) configurations. Phased Arrays are of particular interest as they support the possibility to manipulate the radiation pattern of the array so as to implement Beam Steering. Individual elements are arranged such that when switched “in” or “out” the radiated signal from each will either constructively or destructively add to produce a different radiation pattern. In this way the beam pattern and gain can be altered. The angle of the radiated signal can also be manipulated enabling the array to effectively be pointed in many directions without the need for physical rotation. Although not commonly used in radar applications MIMO encompasses the techniques outlined above. A combination of the multistatic radar technique that deploys multiple transmitters and receivers and Phased Array technique that uses interaction between array elements, MIMO offers the opportunity for much improved signal control and processing. Spatial diversity also offers immunity to multi-path fading that could lead to inaccuracies in any centimetre wavelength imaging application [1.09].

1.5 Polarisation Technique

Electric “E plane” plane radiation from a linearly polarised antenna can be isolated into horizontal and vertical planes of radiation. Dependant on the antenna design these polarisation planes can be manipulated to be strongly independent from each other, allowing the possibility of using each plane independently. In the case of Polarimetric Radar linearly polarised antennas are used to illuminate the target in a number (usually two) of differing planes [1.10]. These polarisation planes are usually arranged orthogonally to each other so providing radar cross sections that are set at 90 degrees. This can be particularly useful in imaging systems, but care must be taken that the antennas polarisation characteristics are known and stable. Individual antennas of this type are, because of their construction, either horizontally or vertically polarised; this being dependant on antenna orientation. For short range, imaging applications because of the system scale the use of individual antennas is undesirable as it is very difficult to arrange for a common radiation point. Switching between antennas is undesirable as it infers a significant change in position. In long range, large scale detection methods these changes in antenna position are, however, insignificant. At the microwave frequencies to be considered patch antennas seem a viable choice of device, they can be small in size, directional and can be excited by a number of different feed methods. These devices can be made square in shape and radiate from the edge of the patch. Careful selection of the feed point can result in radiation from either the vertical or horizontal edges [1.11], making orthogonal polarisation switching from a single device a possibility. With careful design it should be possible to attain a single symmetrical area of radiation in both polarisation planes. Patch antennas normally radiate at around half wavelength dimensions, so lend themselves for operation at centimetre wavelengths of propagation in small short range system applications.

1.6 Wide Bandwidth Signals

Although conventional patch type antennas offer a convenient radiation solution, they are generally limited to only a few percent fractional bandwidth. A number of methods can be employed to overcome this limitation. These include the use of aperture feeding arrangements, stacked designs and the use of thick, low dielectric constant substrates to produce devices with a low “Q” factor. This gives the possibility to use signals within the Ultra Wide Band (UWB) frequency spectrum allocation of 3.1GHz to 10.2GHz. The European allocation is restricted to 3.1GHz to 4.7GHz, with free space wavelengths between approximately 6cms to 10cms. With the correct choice of dielectric substrate and careful design, patch antennas can be made small enough at these frequencies to be a practical reality. UWB radar has found applications in medical imaging and the field of non-destructive evaluation, the wide bandwidth availability enables significant resolution to be obtained, for example, it has been shown to be possible to detect the breathing motion of a person in a room [1.12]. Non-invasive imaging systems have shown that UWB frequencies have a high degree of penetration (Fig. 1.) and may have uses in specialised imaging applications [1.13]. Synthetic aperture techniques, as outlined earlier, have also been put forward [1.14] to further improve data gathering when used for non-invasive scanning. All the above use narrow pulses to generate the desired UWB signal of the required bandwidth, the imaging information being obtained by measuring reflection time of the pulse. Multi Band UWB, using discrete frequencies being largely unexplored. An exception to this can be found in [1.15] where a swept frequency is generated using a network analyser. This is then “gated” to a transmit antenna amongst a switchable bistatic antenna array. On transmission the signal is reflected from an external shield to the selected receiving antenna in the array and this “time of flight” recorded. This Time Domain Reflectometry (TDR) technique has been shown to offer surprisingly high

resolution possibilities of around 1mm. [1.16]. Whilst this represents a valuable technique, currently image resolution is still an issue using standard pulse “time of flight” and reflective measurements, the detection of anomaly features and size variations below 4 – 5 mm may be difficult to achieve [1.17].

1.7 Phase Techniques

Phase contrast microscopy is an optical technique whereby light passing through an object with varying refractive index regions is changed in phase by wavelength shortening in these areas. On recombination this leads to constructive and destructive interference effects, which in turn give rise to enhanced light and dark regions in a sample. This principle can also be applied to radio frequency imaging and is used to good effect in conjunction with SAR in Interferometric Synthetic Aperture Radar (IfSAR) geographic survey applications to improve resolution [1.18]. Often used by satellites this method requires multiple scans to build up an image. Two satellites each gather information via a reflected monostatic signal. Phase differences in this case being caused by the differing return path times due to each satellite. Information is gathered from these sources is mapped and then overlaid, so obtaining an interferometric image. Since the number of cycles of phase shift is usually unknown the accuracy of such systems is dependent on the use of phase unwrapping algorithms to deliver absolute topographic information.

“Three measurements are required to reconstruct the three-dimensional (3-D) coordinate of a point in an IfSAR image: the range, azimuth, and elevation. The first is obtained by timing the return of the radar pulse, the second by measuring the Doppler shift, and the last by measuring the phase difference between the signals received at two displaced antennae” [1.19].

1.8 Outline of Thesis

With these basic principles of ranging and detection now explored the next task was to explore how these techniques were adapted for use in short range applications. A number of techniques and applications were examined and discussed along with associated devices and scenarios. It was shown that under these short range conditions the issues of signal characteristics, clutter and resolution become increasingly challenging. Unlike the long range systems discussed in this chapter these short range sensing applications invariably need to operate in environments that are inconsistent in nature. To compound this these systems often use sensing signals that have pulse rise times and wavelengths that are comparable to or larger than the object of interest. The majority of these methods employ time of flight based measurement methods that rely heavily on the use of high frequencies and fast rise times to resolve relatively small objects. Even so this gives rise to resolution limitations that are primarily due to signal rise times exceeding the propagation time due to the size of the object of interest and so “masking” the object and blurring detail. These issues frequently compound to limit the resolution of microwave frequency detection systems. As a consequence currently reported systems are limited in resolution to no better than 3mm. The focus of the remainder of this thesis will concentrate on physical techniques that alleviate some of these issues with an aim of improving the resolution of these microwave sensing methods. A phase contrast based measurement technique was employed that had the advantage of using a single frequency, narrow band sensing signal to enable sub millimetre resolution. A significant problem then existed in that cable based transmission methods were unreliable in the delivery of phase sensitive information. The development and implementation of a number of techniques were then described that when combined form a complete end to end sensing system that can deliver sub millimetre resolution. Initially, using a centimetre wavelength

signal a proof of concept examination established the validity of a single frequency phase contrast method in providing measurements at these sub millimetre levels of accuracy. Using commercial linearly polarised antennas the concept of taking measurements on separate planes was established. Using information from concurrently conducted experiments into Radio over Fibre transmission the phase preserving nature of optical transmission techniques at microwave frequencies was established. These techniques were then used to complement the phase sensitive measurement system as conventional cables were not sufficiently phase stable. Two optical transmission systems were investigated, a reflective transducer based scheme and a standard configuration based around optical splitters. Both systems used dual wavelengths to separate the upstream and downstream signal paths and both required the use of directly modulated laser devices. Some novel techniques were required in the deployment of these devices and components and are described in detail later. Following this, the design, modelling and practical implementation of a dual polarisation patch antenna was discussed. The criteria for this device was that it should have moderate gain, should possess a single radiating lobe and be capable of operation on two orthogonally separated polarisation planes that possessed a high degree of separation. With this established it was then shown to be possible to incorporate all these items into the then complete measurement system and conduct simultaneous measurements about two orthogonal planes. The thesis was then drawn to a conclusion with a summary of the work described and an outline of the possible future directions the work might take.

References

- [1.01] Robert Watson-Watt and J. F. Herd. “An instantaneous direct-reading radiogoniometer.” Journal of the Institution of Electrical Engineers, Volume 64, Pages 611-622. Published in 1926.
- [1.02] Simon Kingsley and Shaun Quegan, “Understanding Radar Systems”, pages 3-5. McGraw-Hill. 1992.
- [1.03] Simon Kingsley and Shaun Quegan, “Understanding Radar Systems”, pages 19-20. McGraw-Hill. 1992.
- [1.04] Source data, <http://niremf.ifac.cnr.it/tissprop/> , Istituto di Fisica Applicata, Italy.
- [1.05] http://en.wikipedia.org/wiki/Electrical_conductivity#Complex_conductivity
- [1.06] http://en.wikipedia.org/wiki/Radar_cross_section
- [1.07] http://en.wikipedia.org/wiki/Synthetic_aperture_radar
- [1.08] P.R.P. Hoole, “Smart Antennas and Signal Processing, pages 191 – 193. WIT Press, 2001.
- [1.09] Paulraj, Nabar and Gore, “Introduction to Space-time Wireless Communications, pages 7&8. Cambridge University Press 2003.
- [1.10] Harold Mott, “Remote Sensing with Polarimetric Radar” Page 108. Wiley, 2007
- [1.11] Zhi Ning Chen and Michael Chia, “Broadband Planar Antennas”, page 39. Wiley, 2005
- [1.12] A.G. Yarovoy & L.P. Ligthart. “UWB Radar for Human Being Detection”. Aerospace and Electronic Systems Magazine, IEEE. Vol 23, issue 5, May 2008.
- [1.13] E.M.Staderini. “UWB radars in medicine” Aerospace and Electronic Systems Magazine, IEEE. Vol 17, issue 1, Jan 2002.
- [1.14] Zhuge, X. Savelyev, T.G. Yarovoy, A.G. Ligthart, L.P. Matuzas, J. Levitas. “Human body imaging by microwave UWB radar”. European Radar Conference (EuRAD) Oct 2008. Pages 148-151.
- [1.15] I.J. Craddock, M. Klemm, J. Leendertz, A.W. Preece, and R. Benjamin. “Development and application of a UWB radar system for breast imaging”. Loughborough Antennas and Propagation Conference, March 2008. Pages 24- 27.
- [1.16] T. J. Quinlan, S.E.M.Dudley and S.D.Walker “Time-Resolved Bragg Effects in an Ultra Wideband Leaky Feeder Antenna Array Based on Semi-Rigid Coaxial Cable”. Loughborough Antenna and Propagation Conference March 2008

- [1.17] Xu Li, Essex J. Bond, Barry D. Van Veen and Susan Hagness, “An overview of ultra-wideband microwave imaging via space-time beamforming for early stage breast cancer detection”. IEEE Antennas and Propagation Magazine, Vol 47, No 1, Feb 2005.
- [1.18] http://en.wikipedia.org/wiki/Interferometric_synthetic_aperture_radar
- [1.19] David A. Imel, “Accuracy of the Residual-Delay Absolute-Phase Algorithm”. IEEE Transactions on Geoscience and Remote Sensing. Vol.36, No 1, Jan 1998.

Chapter 2 Short Range Systems

2.1 General Techniques

The previous chapter concentrated on general techniques associated with Radio Frequency detection in long range applications and geological mapping. Time domain measurement techniques are foremost, often supplemented with Doppler shift measurement and phase overlay mapping, to detect motion or increase accuracy. Short distance ranging and imaging applications use similar techniques but often need to operate in more complex environments, this, along with the comparatively long wavelengths used, leads to considerable challenges to system accuracy. The focus now will be to explore short distance ranging and RF imaging techniques such as those used in medical imaging, ground penetrating radar and non-destructive evaluation, in particular those found in difficult, confined or hazardous areas. With the emphasis on exploring existing work in the above areas, various methods are evaluated with the aim of identifying potential advantages suggested by the work to date. Short range microwave radar measurements conveniently lend themselves to the use of the Vector Network Analyser (VNA). This instrument is most commonly used in its swept frequency mode, to record measurements of forward transmission and reflected signal magnitudes. Other relevant measurements that can be made with this instrument include phase and impedance evaluations as well as the use of time domain reflectometry. Typically in the sensing applications that follow these responses are measured at various object rotations or positions, and may be then correlated to the scattering target across a range of frequencies if desired. Refinements of these techniques can include multi-port adaptations to accommodate multistatic antenna arrangements, with the aim of increasing resolution and sensitivity [2.01]. In a development of the swept frequency method, UWB radars

employ extremely wide bandwidth instantaneous signals, generated by means of a short pulse. Such imaging radars are now being proposed [2.03] for use in applications involving subsurface sensing and medical scanning. The very high bandwidths generated support a relatively high resolution capability and the pulse format is ideal for time domain orientated imaging systems. As might be expected, signal attenuation is not uniform across the entire UWB frequency band. It may be necessary to make a compromise between the high frequency, high resolution signal component that has poor penetration, and the lower frequency, high penetration fragment of the frequency spectrum. An ability to select the frequency range is a great advantage and is relatively easily achieved by alterations to the signal pulse width and the use of pre-emphasis. Whereas both swept frequency and pulse generated UWB signals can be produced with relative ease, they place extreme demands on the propagating antenna which in itself often leads to signal degradation or the need for complicated, difficult to fabricate designs [2.02].

2.2 Medical Imaging

The electrical properties of various body tissues exhibit considerable variation, this being largely dependent on factors such as water content and levels of non-conducting fatty tissues as well as levels of mineral elements present. Tissues such as skin, fat and bone have a low water content and so exhibit low conductivity, muscle, blood and most internal organs with a higher water content are more conductive. Tumours, by virtue of their cellular structure, fall into the more conductive category, and so, if situated in an area of contrasting low conductivity, can be illuminated by microwave radiation [2.03][2.05]. As shown previously in Fig 1.1, microwaves at centimetre wavelengths also penetrate body tissues easily, this in conjunction with the variation in dielectric constants

of material with the body, has led to the emergence of UWB radar for medical imaging and detection applications. As previously mentioned these systems use nanosecond pulse width generation to create signals with a very high instantaneous bandwidth. With dielectric constant variation producing impedances from 112Ω to 49Ω in soft tissue, any such pulse would experience measurable propagation delay variation. If used to monitor organ movements as with the heart beating, these delays can be predicted and accounted for (Fig 2.1.) [2.04]. A significant advantage of microwave imaging methods of this type over the very effective ultrasound techniques currently in use, is that it may not be necessary for any sort of patient contact, and that the effect of clothing etc. can be considered to be largely negligible. Such techniques would have considerable patient benefits in that it could allow for continual un-intrusive remote patient monitoring to be implemented.

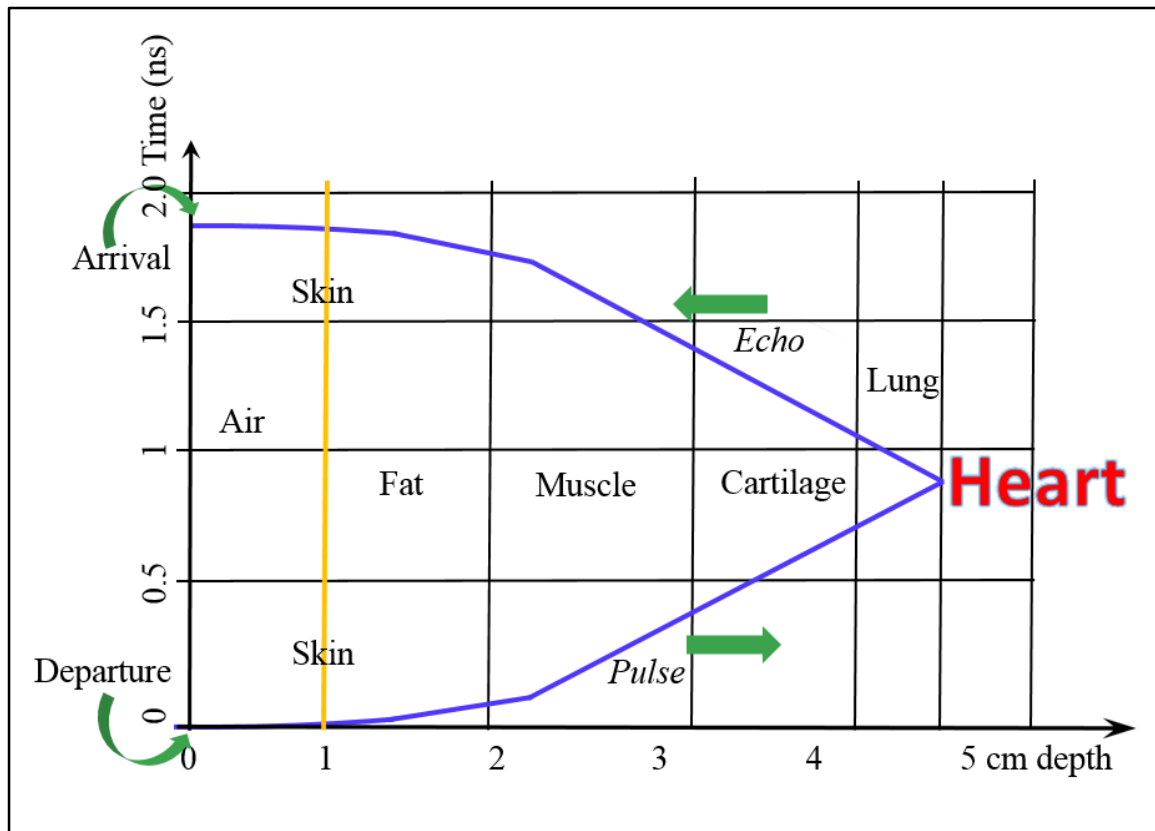


Fig. 2.1. Predicted pulse delay in human thorax tissue [2.04]

Due to the largely homogenous nature of the tissues involved, there has been much interest in microwave imaging for the detection of breast cancer. Taking advantage of the known dielectric differences between malignant and normal breast tissue this technique promises a cost effective and less distressing option to conventional imaging methods, although it is unlikely to ever achieve the same resolution as Xray or Magnetic Resonance Imaging. Another significant advantage is that microwave techniques may offer a safer alternative to methods employing ionising radiation. Maximum Permissible Exposure levels as set out by IEEE standard C95.1 – 1999 are given as 1.6W/kg over frequencies ranging from 100kHz to 6GHz, it would not be unreasonable to expect that any centimetre wavelength system could operate at levels far below this. Early imaging systems used continuous wave (CW) signals to measure transmission loss [2.05] or looked at the transmission / reflection ratio. The presence of a dielectric anomaly would produce unexpected reflections (scattering) or attenuation, resulting in VSWR (Voltage Standing Wave Ratio) and / or transmitted power variations. These measurement procedures were carried out between multiple antennas in various transmit and receive configurations, sometimes across a range of frequencies. In this way differing amplitudes can be mapped and a “picture” built up of the dielectric / loss properties at a particular point. By moving the array it is possible to see any changes and draw conclusions as to the position of any anomaly, in this case, by comparison of the data with results obtained from a predictive model. These methods form the basis for Microwave Tomography. Such systems (Fig. 2.2.) are claimed to be capable of resolutions down to one twelfth of the wavelength used.

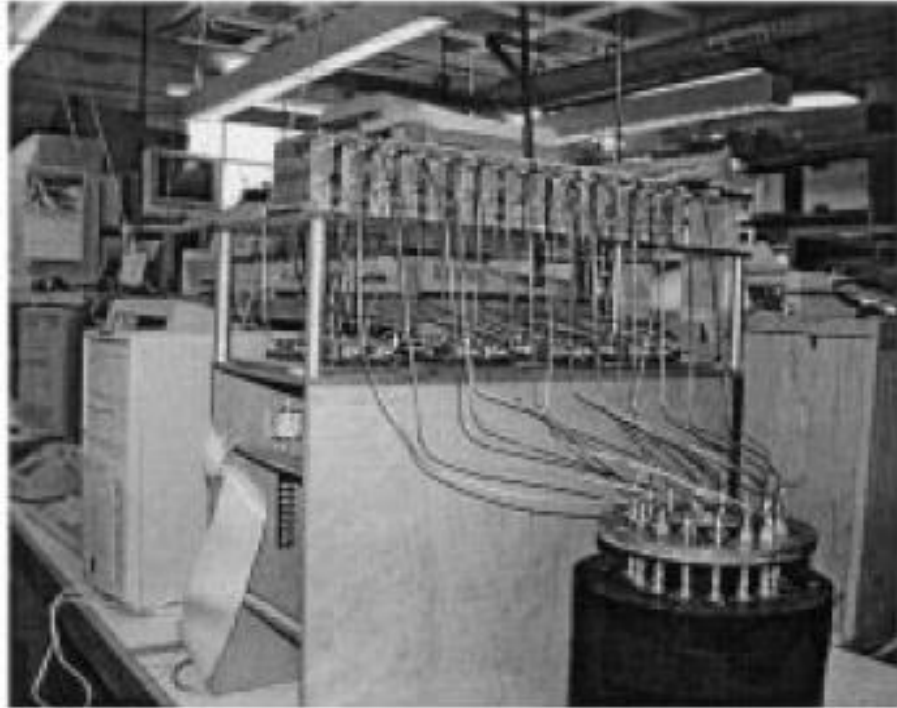


Fig. 2.2. Prototype imaging system proposed by Dartmouth University [6].

Fig. 2.2. shows the prototype system described above [2.06], operating at frequencies up to 900MHz, a maximum resolution of just over 3mm is claimed to be possible. With a claimed operating dynamic range of 130dB the system used matching fluids and monopole antennas to map dielectric variations. Such a system was bulky and difficult to implement practically and the use of matching fluids largely negates any advantage over ultrasound methods.

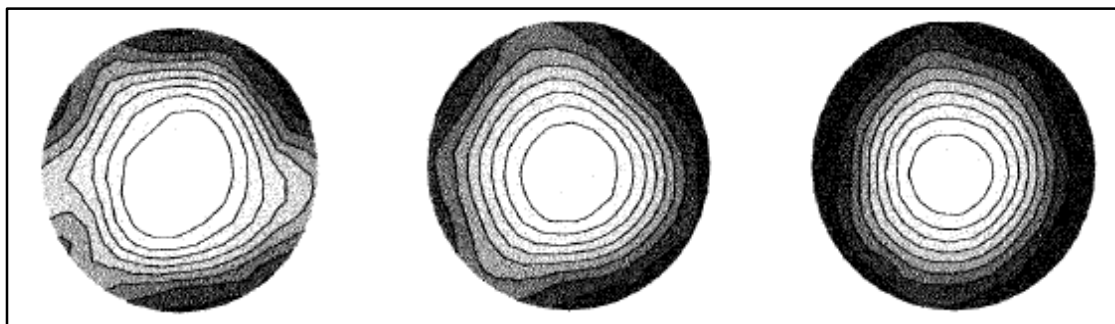


Fig. 2.3. Some of the resulting plots from the Dartmouth system [2.06].

Shown in Fig. 2.3. are the resulting images of dielectric variation zones taken at three different vertical positions; this was achieved by raising and lowering of the antenna array. As will be discussed in more detail later later, the monopole antennas used here are not ideal for the purpose. Lack of gain and multidirectional, radiation patterns lead to spurious reflections and ill defined measurement zones due to the resulting difficult to control scattering. Comparison of measured results with that of a model may offer a practical way forward in the interpretation of the recieved data. As mentioned earlier pulsed UWB radar systems have recieved much attention with respect to medical imaging, and in particular, its application to the detection of tumours associated with breast tissue. Most of these radars use signal generation and recovery methods similar to those previously outlined, the short UWB pulse width giving rise to the possibility of higher resolution. Hemispherical antenna array configurations are a popular and effective choice for breast tumour detection systems. In the case illustrated in Fig. 2.4. a simulated system is studied [2.07] An assumed 8mm diameter is positioned deeply in the otherwise largely homogenous tissue, dielectric constant and conductivity values are taken as shown in the plots below (Fig. 2.5.). As can be seen this shows the tumour as having significantly different electrical properties from the surrounding fatty tissue. Also that the dielectric values show little variation with frequency across expected UWB frequency range. The conductivity values shown in this study differ from those derived earlier and so cannot be verified but this work gives a good indication of the potential for such methods. A UWB pulse is launched from an antenna at position "A9", after propagation through the tissue, the reflection from the "high contrast" target is recieved, in turn by antennas "A1" to "A8". Subtraction of the propagation time of the pulse from the previously obtained "tumour free" calibration values indicates the position of the object. Calibration is achieved in the simulation by randomly positioning the "tumour" and

averaging the resulting reflections, it is then suggested that the same result could be obtained by randomly moving the antennas.

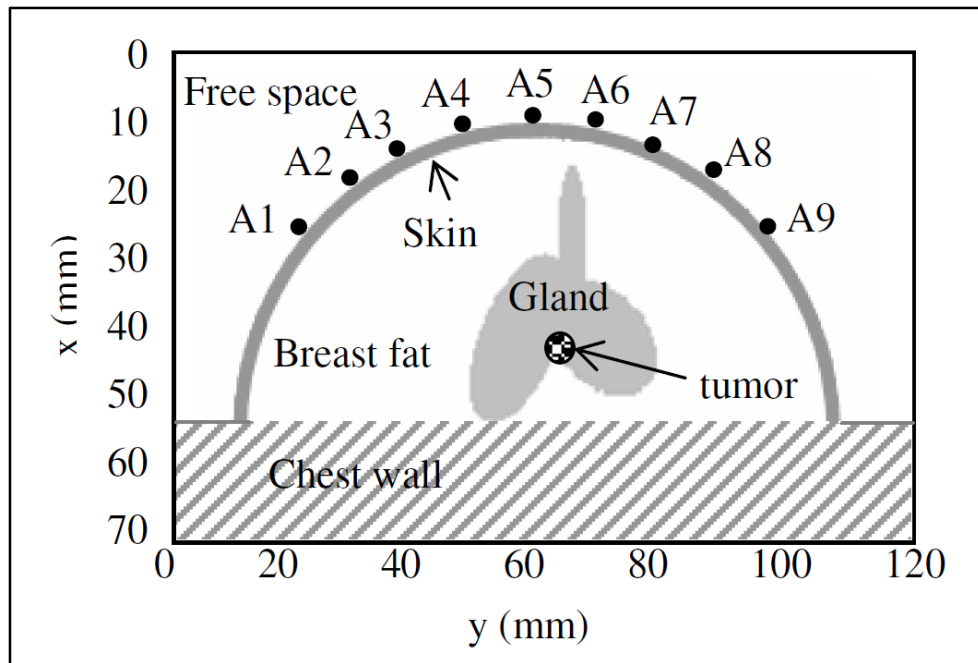


Fig. 2.4. Antenna arrangement, Hiroshima University study [7]

This method does not take into account the characteristics of the antenna, or how the propagated signal may diffuse within the material around the tumour. Unless the antenna radiation pattern produces a beamwidth much smaller than the target, at the point of intersection, reflections will occur that are related to the tumour.

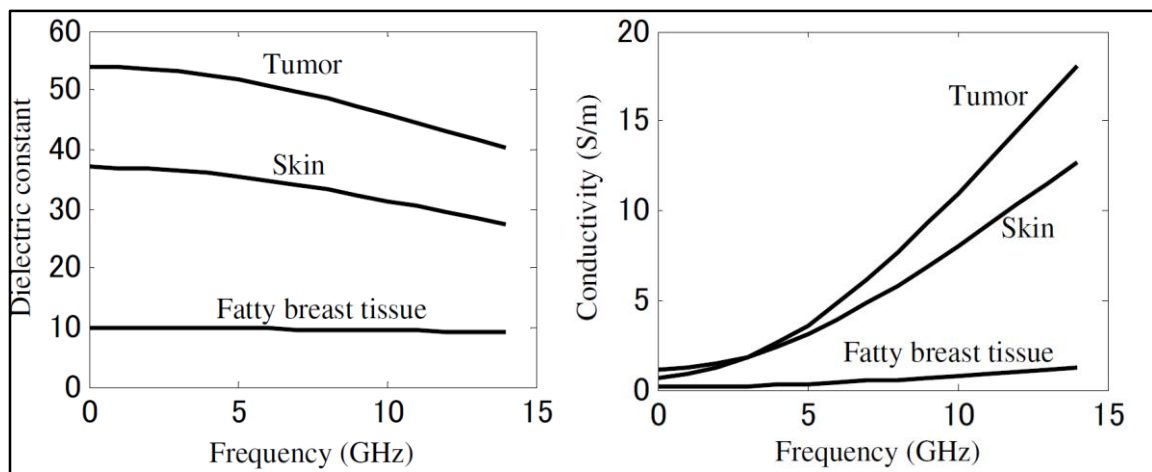


Fig. 2.5. Dielectric constant and conductivity values used [2.07]

In practice this would require the use of very high gain antennas that may not be achievable at these frequencies and bandwidths within the dimensions allowed. Calibration and reference establishment is always a challenge with imaging systems and an adaption of the averaging method described may produce results, especially within a homogenous propagation medium. In reality the homogenous nature of tissues cannot be certain, and in any case as shown earlier, electrical properties will vary according to tissue type, layer thickness, water content etc. As might be expected these variations will have an overall impact on system resolution as they lead to an increase in the possibilities in scattering of a reflected signal [2.08]. Here Resolution is defined as the ability to separate objects and contrast as the definition possible amongst clutter. The system modelled consists of a 5 x 5 antenna array with the central antenna being used to transmit to the remaining 24 receivers. The model (Fig. 2.6.) consists of layers of material with dielectric properties that approximate breast tissue and the tumour is allocated a dielectric constant of 50, contrasting strongly with the surrounding material. As with the majority of proposed systems a coupling material at the antenna tissue interface is assumed, so as reduce reflection caused by the air / skin disparity. In this reflective model it is further assumed that the cross sectional resolution is dependant on the synthetic aperture of the antenna array and the bandwidth of the imaging signal. Variations in the dielectric make up of the model lead to diffraction at the material interfaces, effectively concentrating the imaged volume. It is claimed that this gives the possibility of increased resolution. Results from the model show that it is possible to detect and resolve reflected energy peaks from two 2mm tumours at a separation of 16mm and a depth of 50mm. However, when random variation of up to 10% in the dielectric properties of the "breast tissue layer" is introduced, random scattering leads to reduced contrast. The antenna array described in

this system is of a planar design and as such this will tend to define individual antenna element performance.

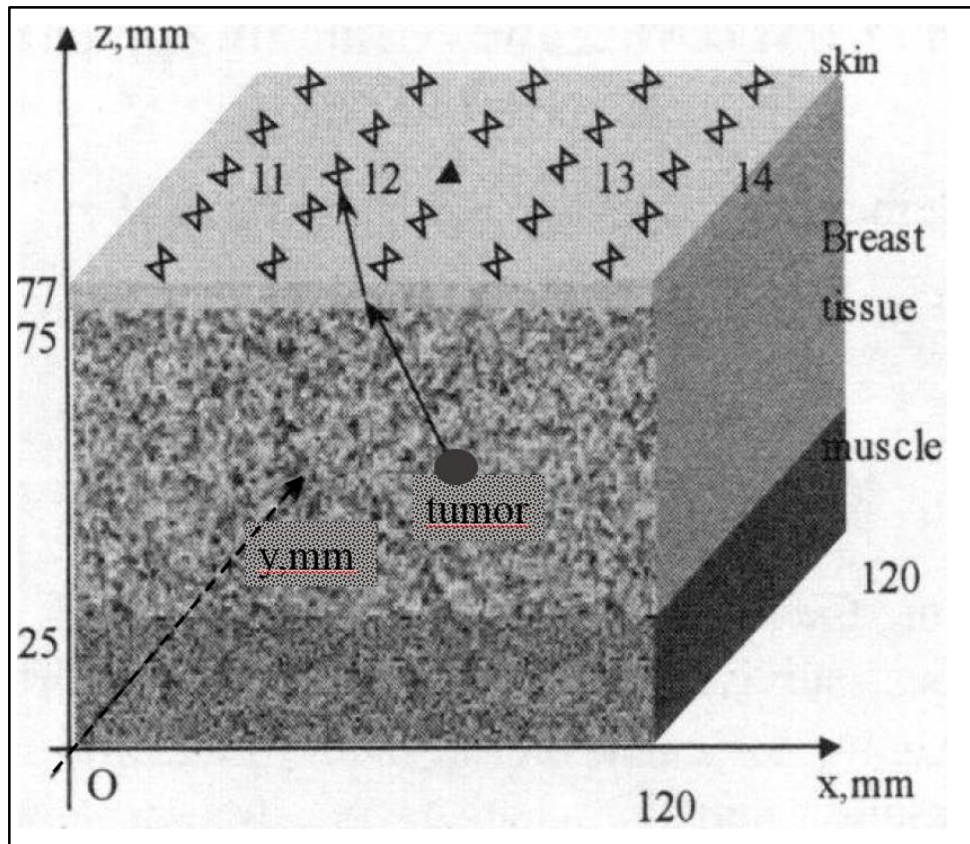


Fig. 2.6. Structure of tissue model [2.08]

As suggested previously calibration or a zeroing function may be possible by either moving antennas or using angular variation to provide multiple signal paths and using averaging to remove the effect of material inhomogeneity. A development of this method may be to use a multistatic approach, each antenna transmitting in turn, all other antennas receiving. Used in conjunction with a data adaptive algorithm known as Multi-static Adaptive Microwave Imaging (MAMI) [2.09] [2.11] this claims increased noise immunity and resolution. Apart from the proposed conformal nature of the antenna array the principle strength of this approach lies in the diversity of transmitting and receiving antennas used. In this case each antenna is used as a transmitter in turn, with the rest receiving the reflected signals and so producing multiple paths, without the need to move

the array. The model described here is based around hemispherical antenna array and a 3D simulation of breast tissue, also in common with most studies, a Finite Difference Time Domain (FDTD) method is used to construct the model. MAMI uses beamforming techniques to post process the received information from the reflected signals. Based on this, a beamforming technique is used to estimate scalar information, which can then be used to derive information on the target from the backscattered energy. The reported results indicated that this processing technique yielded an increased resistance to the effects of noise and clutter and offered clearly defined images of a 4mm diameter object in a realistically constructed model. Comparisons are made with the bistatic Amplitude and Phase ESTimation (APES) and the monostatic Microwave Imaging through Space Time (MIST) [2.10] algorithms, both of which proved to be inferior. As the author acknowledges, a significant issue existed with the large number of antennas deployed in this study. This array of 72 antennas yielded excellent results but the study did not take into account the physical size of the necessary to accommodate this number of devices. Antenna size is dependant on wavelength, and so a small size can only be achieved using high dielectric materials or high frequencies. The use of high dielectric materials will lead to a high Q factor antenna, which in turn imply a narrow bandwidth device which is unsuitable for use with UWB signals. With a reduction in the number of antennas reduced to a more manageable 18, the quality of the recovered image was greatly diminished as shown in Fig. 2.7. due to the reduced number of signal paths from which to derive the necessary information, but was still comparable to other systems deploying many more antennas. MAMI represents a very powerful method of image recovery when used with UWB pulsed signals and multistatic aquisition arrangements. Although dismissed here, direct aquisition of phase and amplitude information such as the used in APES may lead to a simplified approach and is discussed later.

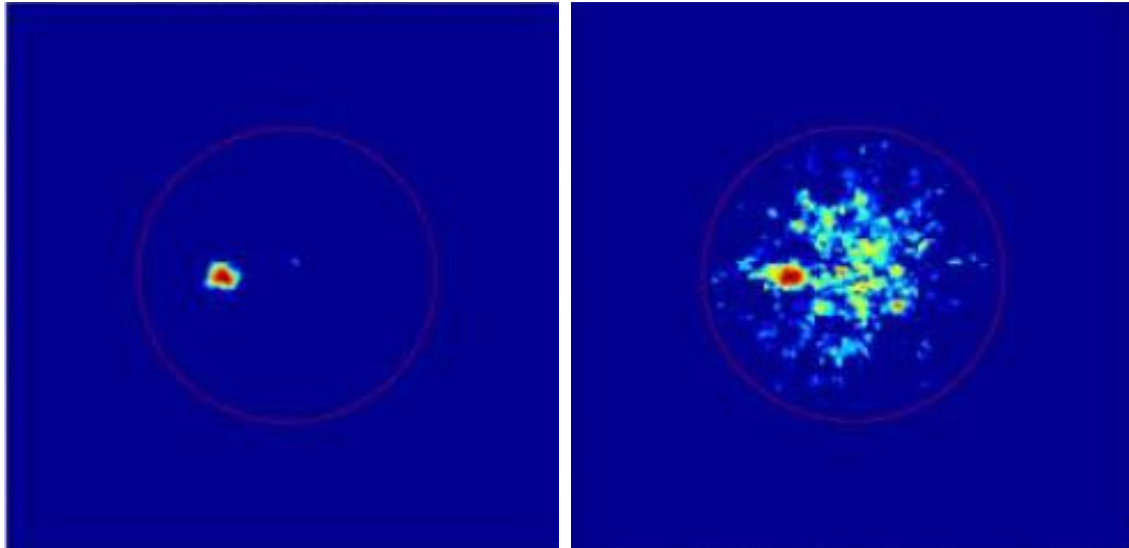


Fig. 2.7. Difference in recovered image 72 antennas (left) 18 antennas (right)

[2.09][2.11]

Of great interest though is the method of calibration prior to the imaging process. In common with most of the applications discussed, before imaging can proceed it is necessary to remove undesired reflections resulting from normal tissue (or any background material) and parasitic interaction between antennas. Signals that contain the normally stronger responses from these, as well as the tumour or other target responses, are acquired. A calibration signal may then be obtained by the averaging of the signals made up of the undesired information (clutter). The resulting signal may then be subtracted from information obtained in the imaging process, leaving mostly the backscattered information resulting from the tumour (or target). This technique was adapted from [2.12], here the use of wide bandwidth signals is justified at the outset, with the claim that it permitted the use of simplified reconstruction algorithms. The antenna system is now specified, being of 17 monopoles in a conformal array spanning 8cm. Each of these antennas is used in monostatic mode in turn to launch and receive a 110ps bipolar pulse. Also allowance is made for the propagation of the signal through the medium in that a radial diffusion from the point of launch is assumed, representing a

good approximation to a realisable system. Backscattered signals are gathered and given a fixed delay time, effectively moving them in distance, these are then added, creating a virtual “point of focus”. This process was then repeated across the breast by adjusting these time delays producing new “points of focus” and the reflected waveforms stored. These waveforms are then summed. In areas of high dielectric contrast, the clearly defined reflections tended to add coherently, areas of low contrast produced noise like clutter reflections which added incoherently, and so tended to average out. From this the position of the anomaly can be determined by the time delay, and the dielectric variation from the norm, by the amplitude of the reflection. A picture can then be assembled by assigning grey scale values to the amplitude information and appropriate mapping of the return signal delays. Delay and sum techniques (DAS), such as this are widely used for image recovery in many proposed microwave imaging applications. Antenna radiation patterns will be critical for such applications as the radiated beams not only need to overlap but must also be well defined. These simulation studies give a good indication as to the potential for the use of microwaves in medical imaging applications, but often do not explore the practical difficulties that may exist. Probably the most demanding of these is the characteristics and design of the antennas to be deployed. If very wide bandwidths are to be used antenna design can become particularly challenging. Factors including gain, directionality and radiation pattern, mutual coupling within the array, as well as the antenna bandwidth have a direct impact on system performance and need careful consideration. For example the monopole antennas frequently suggested in the studies examined so far, have, as explained earlier, multidirectional radiation patterns which produces an inherently low gain, so they are not ideal as factors such as dynamic range and system noise may be compromised. Devices such as patch antennas, being planar and small and typically having a gain of up to 9dBi would seem a more suitable choice. With

sufficient ground plane, low back radiation characteristics can also be expected and although sometimes complicated a variety of feed arrangements are available that can facilitate wide bandwidths. In the study described in [2.13], initially a 16 element planar patch antenna array that is capable of operating over a range of 4GHz to 10GHz is described. In an attempt to negate the normally narrow bandwidth limitations associated with patch antennas whilst preserving their gain advantages, this design uses a microstrip feed on the reverse face of the substrate to excite the radiating patch. This is a well known method of producing a wide bandwidth feed. Although initial results proved encouraging, the aim was to implement a hemispherical array, due to the necessary ground plane and patch dimensions required this proved impractical. Further modifications were then made to the antenna structure, reducing the radiator dimensions and enclosing each element in a screening container to reduce back radiation [2.14]. The addition of this screening enclosure was now necessary to ensure signal confinement and integrity due to the now greatly reduced ground plane dimensions for each individual structure. Reduction of the antenna size necessitated a complete re-design of the structure layers and feed arrangements in order to preserve the antenna gain and bandwidth characteristics. Details of the adopted design are shown in Fig. 2.8. In this microstrip fed, slot coupled, stacked patch design the dimensions of the feeding strip and dielectric constant (ϵ_r) of the associated substrate are chosen so as to provide the desired 50Ω input impedance match. As the antenna feeding procedure is often the cause of bandwidth limitation, a resonant slot technique is employed at this point to couple power from the feeding strip to the intermediate patch (patch 2). This slot coupling method is well known to provide a good impedance match over a wide frequency range. Immediately above the feeding slot is a layer of material of ϵ_r 10.2, this relatively high value is chosen in order to provide a reduced wavelength dimension both in the radiating slot and the intermediate resonating

patch (patch 2). A second resonating patch is now added, separated by a layer of ϵ_r 2.2 material. While this will lead to an increase in wavelength, dielectric loss will be minimised and coupling into the final resonant patch, (patch 1) achieved efficiently. Unusually this final element is designed to operate directly into a material of ϵ_r 10.2 and so is located beneath a further layer of ϵ_r 10.2 material. As this value is similar to that of skin, this gives the structure the ability to radiate directly into the body with minimal mismatching and undesired reflections, removing the need for the matching fluids used previously. This type of structure provides a very effective method of propagating wide bandwidth signals with little back radiation. Providing high fractional bandwidths and consistent radiation patterns over its frequency range this structure will be discussed in more detail later [2.15].

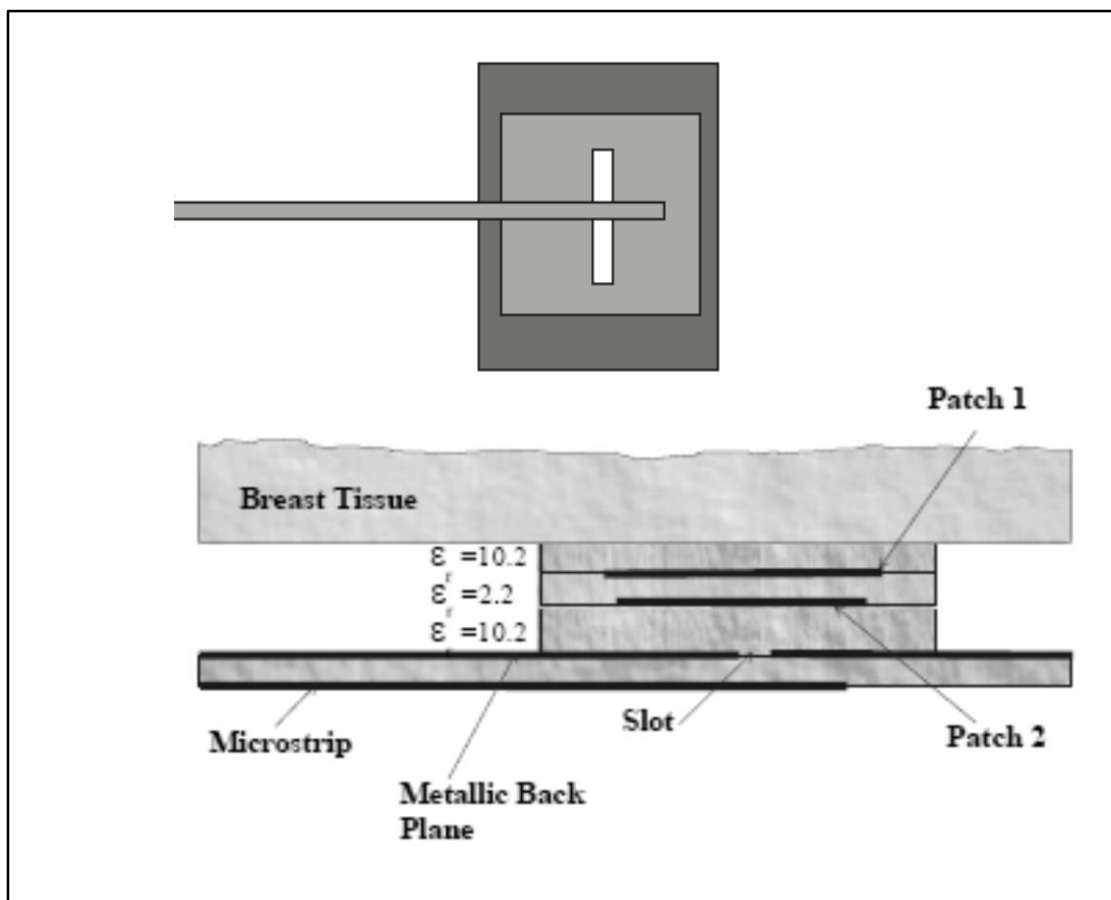


Fig. 2.8. Structure of microstrip fed slot coupled stacked patch antenna. [2.14]

With the antenna design established, a 16 element hemispherical array was constructed [2.16][2.18] as shown in Fig. 2.9. This represents the culmination of a number of published results and is one of very few implemented studies. The smaller size of the re-designed antennas allows a symmetrical distribution with the array operating in multistatic mode, each antenna having a radiation angle of 80 degrees and cross polar isolation of 40dB [2.15]. In [2.16][2.17][2.18] this multistatic approach provides 120 different signal paths and also avoids the use of the directional couplers that would be required in monostatic operation. Experimental results were analysed using DAS and MAMI type algorithms, and the performance of each then compared. These were chosen as they have been shown to outperform MIST [2.09][2.11] when used in combination with a multistatic antenna array in simulation studies. These studies, however, were based around “idealised point source antennas”. Successful detection of spherical tumour phantoms of 4mm is claimed.

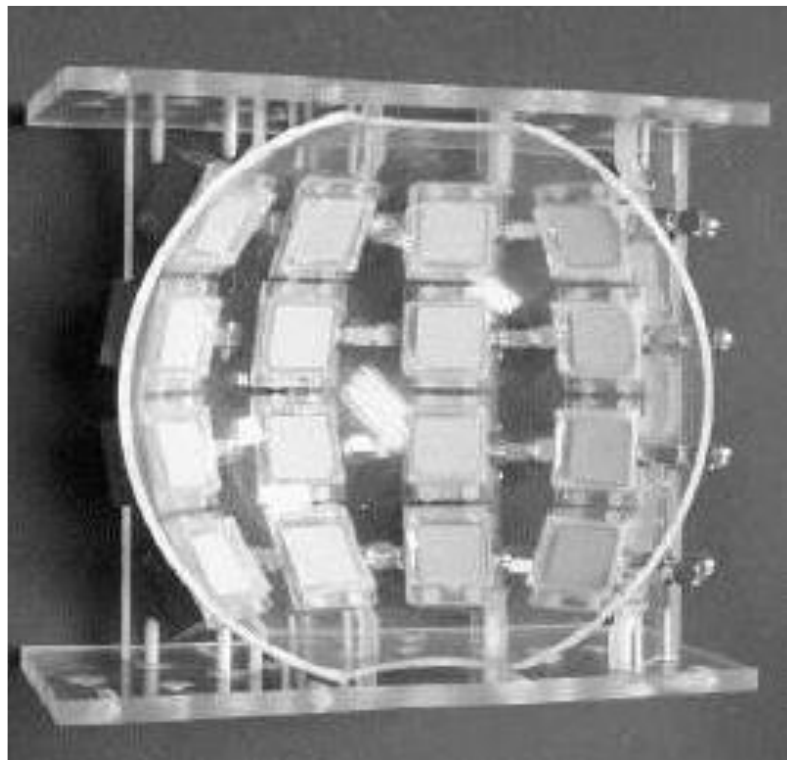


Fig. 2.9. Finalised hemispherical array [2.16][2.18]

In order to achieve this, the array needed to be rotated by 10 degrees in a pre-processing operation in order to remove the unwanted reflections due to imperfect antenna coupling into the skin etc. and produce a zero calibration condition. These appear as identical time responses and are removed, the tumour reflection, unless it is on the axis of rotation, appears at differing times between the two measurements. A high degree of tissue homogeneity is assumed and necessary, as with all these systems. Fig. 2.10a. and 2.10b. shows the worst case 4mm tumour size reconstructed images, here because of the resolution demands, clutter becomes much more prevalent. Grey scale values are equated to contour maps of normalised linear values of energy returns. The high dielectric contrast tumour is clearly visible on both plots but there is greatly reduced clutter present on the plot using the MAMI reconstruction algorithm. In the methods described above all use a UWB pulse that relies on dielectric contrast to induce a reflection and time of flight variations. In a simulation study, [19] proposes the use of APES type techniques and claims increased resolution and clutter resilience.

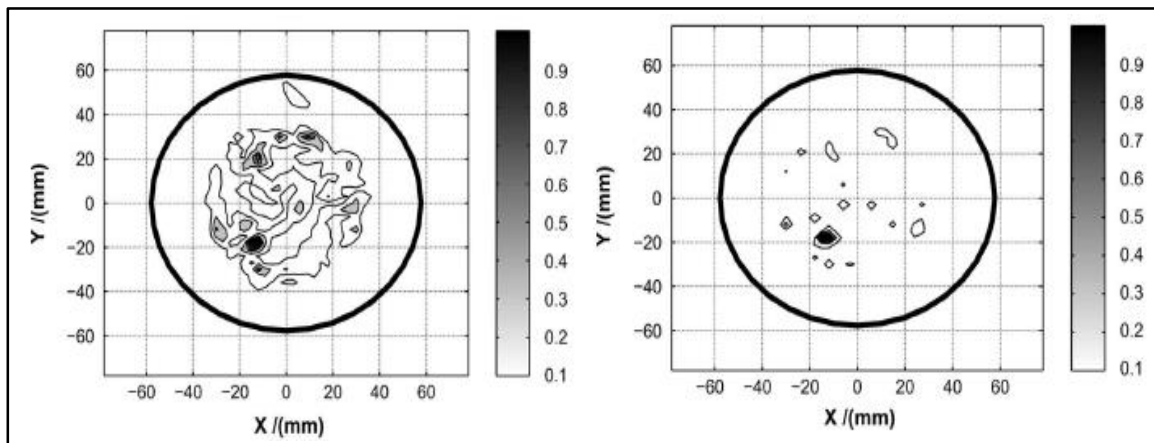


Fig. 2.10a.

Fig. 2.10b.

Comparison of reconstructed images using DAS (2.10a) and MAMI (2.10b) [2.18]

Whilst still employing a UWB pulse and using similar time realignment methods to those outlined earlier in order to remove unwanted responses the simulated method assumes knowledge of the transmitted pulse to make a phase comparison. Using a pair of antennas

in a bistatic configuration that are moved around multiple locations, the position of the target is then estimated by measuring a combination of the pulse attenuation compared to that of the straight line path and the degree of time alignment needed to duplicate the original signal. The phase shifting due to the delay potentially being cyclic. Whilst this simulation offers an insight to the capability of phase measurements there are a number of assumptions that may not easily translate into practice. Sufficiently accurate and repeatable antenna positioning will be difficult to achieve, small variations will lead to large phase differences. Also possibly unrealistic prior knowledge of the transmission medium would seem to be assumed. For any sort of estimation of delay or attenuation necessary for weighting to be realistic, the transmission medium (tissue) would need to be very uniform. Also no allowance is made for the inevitable pulse spreading that would be introduced by the antennas.

2.3 Ground Penetrating Radar

Ground penetrating radar (GPR) poses similar problems as those found in medical imaging in that the propagation medium may have varying and unknown dielectric properties. In addition to this, there are unavoidable problems with the antenna interface due to unpredictable and uneven ground contours. This situation is further compounded by difficulties with signal propagation at microwave frequencies, due to soil moisture content and conduction properties [2.20] that can lead to severe signal attenuation and so give rise to a poor SNR performance. Uneven ground profile and varying sub-surface conditions present considerable challenges for any time domain based detection and ranging process. Such anomalies lead to highly variable return times for the reflected pulse and so can lead to high levels of clutter [2.21] and return signal anomalies. Despite this, GPR has found many uses in areas as diverse as space exploration [2.22] and sewer

inspection [2.23]. Discussed in [2.22] is the unique set of circumstances encountered by the recent Mars survey probes to date that serves to outline some of the issues. The detection of sub-surface water is a well-known priority for planetary exploration and is well suited to detection by GPR. Concern was raised however, that whereas the Martian sub surface contains amongst other things, frozen CO₂ mixed with dust, which would prove very suitable for survey by GPR, the prolific distribution of magnetic minerals and the Martian permafrost would prove highly lossy and so disruptive. A frequency dependant simulation study was conducted to determine the attenuation that may be expected to be attributed to the expected materials that would be encountered. Four frequencies were selected at 225, 450, 900 and 1200 MHz as shown in Fig. 2.11, unsurprisingly attenuation rose nearly linearly with frequency and generally increased in the presence of ice. When the simulation was run for a mixture of CO₂ powder and varying sizes of basalt rock it was found that attenuation also varied with particle size as well as frequency. Probably due to Rayleigh scattering.

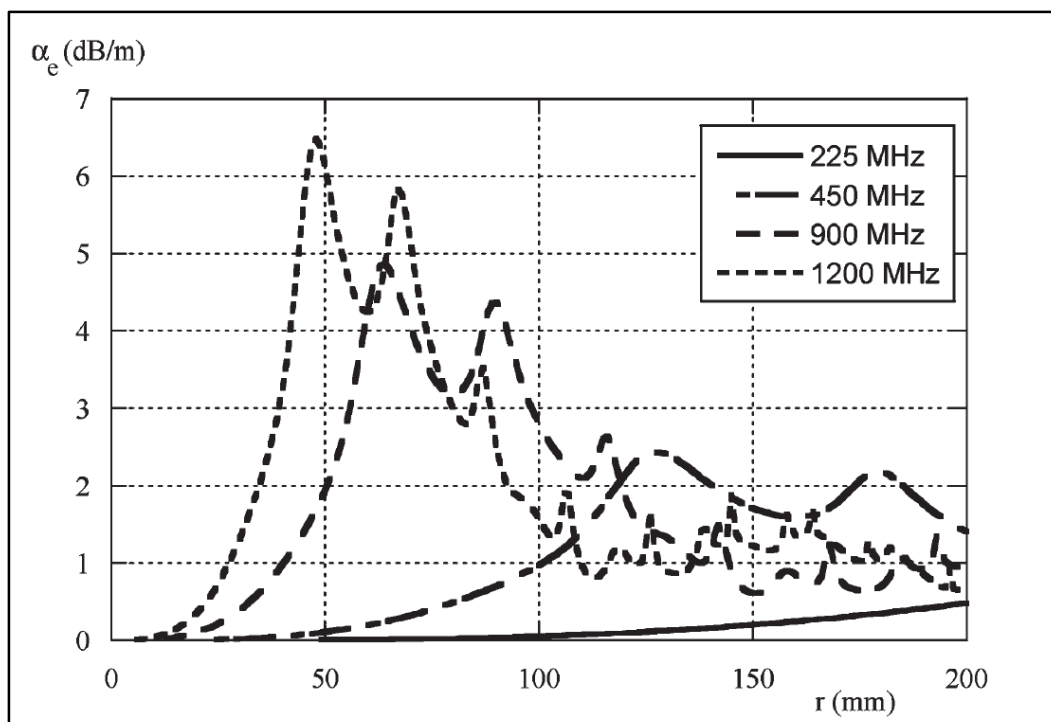


Fig. 2.11. Signal attenuation - variation with particle size [2.22]

Also with suggested operating frequencies between 200MHz and 1 GHz, [2.23] explores possibilities of using multiple frequency RF imaging for underground inspection of sewer pipes. Taking advantage of dielectric variations, due largely to the water content of surrounding soil, a multi- frequency antenna system launches modulated pulses at 200MHz, 500MHz and 1GHz. The reflected signals are then time analysed and conclusions drawn as to the dielectric properties (propagation speed), of the signal in the surrounding medium. A trade-off has to be made between resolution and depth of penetration. The longer wavelength 200 MHz signal provides highest penetration but is compromised in terms of resolution. At this frequency penetration into the soil is sufficient to provide information on moisture content, and so, leakage, as this only requires a low degree of accuracy. At closer range the 500MHz system is deployed and finally the 1GHz is used to examine the structure at close range and in more detail. Detection of faults (cracks) in any pipes at these frequencies can be a problem however for this approach, as it seems relatively insensitive, having difficulty distinguishing the dielectric properties of materials such as concrete and plastic from that of air.

Table 2.1 Dielectric properties of relevant materials [2.23]

		Frequency	100MHz	1GHz	10GHz
Material	Relative Permittivity	Propagation Velocity cm/ns	Wavelength cm		
Air	1	30	300	30	3
Concrete	9	10	100	10	1
Water	80	3.35	33.5	3.35	0.335

Advantages of this approach over conventional camera based inspection systems are that it can detect issues that are out of the direct field of vision and that may not also be visible to infra-red detection. Further, such systems are not as vulnerable as camera based

solutions to obstructions covering lenses, dirt etc. The lack of resolution however is a serious handicap, a hybrid camera / RF system may represent an ideal combination. More conventional GPR methods have much in common with the medical imaging systems already outlined. As discussed in the comprehensive study described in [2.24] much of this work is focussed on the detection of large buried objects such as landmines and the removal of clutter caused by surface rocks and uneven surface profiles. Multistatic, “multi look” methods and DAS techniques are used to reduce effects due to these anomalies. In order to accomplish this, system operation in a number of different environments was studied. In this study a linear antenna array is raised some distance above the ground thereby creating a predictable and even layer. Similar reflections arrive at differing times over the possible eight bistatic paths created (Fig. 2.12.). These can then be time aligned, identified as clutter and removed in the post processing procedure to produce a calibration state. It may be possible to remove these “early arrival” responses with the use of time-gating techniques similar to that used in TDR enabled Vector Network Analysers . By necessity GPR antenna arrays need to be mobile, calibration often being carried out at multiple locations. With surface effects minimised, subterranean anomalies can be identified by the return times of a pulses transmitted between each of the multistatic antenna pairs. These times being dependant on the reflected path lengths and speed of signal propagation through the transmission medium under investigation (see Table 2.1.). Assumptions are made that the pulse will have constant, but different, velocities in the three materials considered here, air, sand and rock and that there are no intermediate variations in the dielectric properties of the materials studied. Return times of the pulses between each of the bistatic antenna pairs were coherently summed, so approximating a multistatic antenna array system having the potential to facilitate increased resolution.

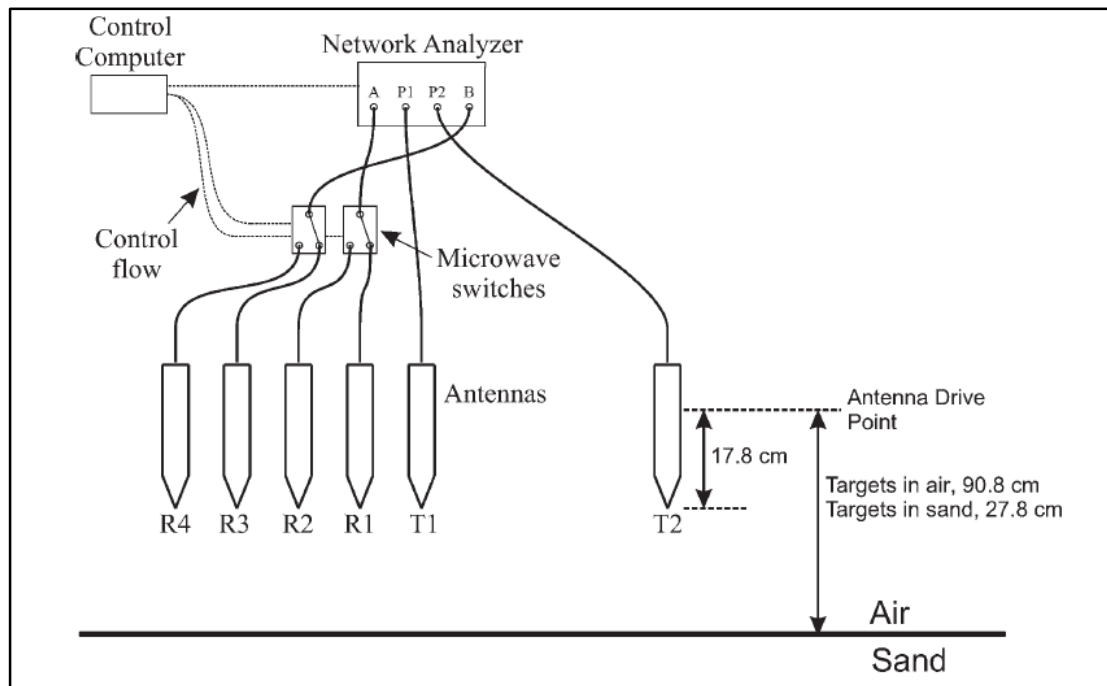


Fig. 2.12. Multistatic GPR experimental arrangement [2.24]

A linear array of resistive vee antennas is deployed in this work. This unusual design is effectively a resistively loaded dipole with a low radar cross section. Importantly this purely resistive design has the ability to cope with short pulses because, unlike a conventional dipole, it has minimal reflections along each arm. Designs such as this do however require an impedance matching balun that may well limit their usable bandwidth and will be discussed in more detail later. Shown in Fig 2.13. is a system developed specifically for humanitarian land mine clearance [2.25] describes a UWB vehicle mounted GPR survey system. As indicated in [2.23] frequencies at the higher end of the UWB range will be rapidly attenuated in soil conditions. Whilst higher frequency content is essential for good resolution, penetration can be minimal so this system operates at frequencies toward the lower end of the microwave spectrum of between 1GHz and 3GHz. This being frequency range being restricted by the transmitted pulse shape as with the medical systems discussed earlier. This frequency range conveniently also allows for the use of loop antennas in the receiver, which, because of the necessary quarter wavelength dimensions, can be difficult to fabricate at higher frequencies.

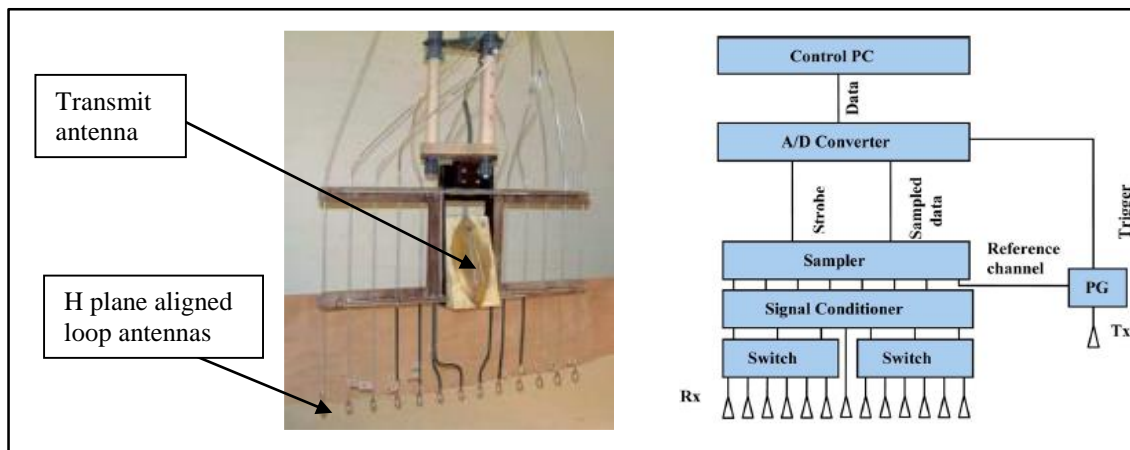


Fig. 2. 13. Linear, switched array [2.25]

The transmit antenna is of a dielectric wedge design designed to illuminate an area covered by the entire receive array. Each of the elements in the receive array has a torroidal E plane radiation pattern that is aligned with that of the transmitting antenna. Mutual coupling between the receive array elements was analysed and found to be dependent on loop diameter as well as spacing. A combination of coupling effects and practical limitations led to a final element spacing of 7cms. Each antenna was then connected via an RF switch and Low Noise Amplifier and Sampler, to an Analogue to Digital converter. Control of the scanning beam is achieved by selective switching and combining of the loop elements. This effectively enables a complete left to right scan to be made, without the degradation of SNR that would result from single element switching. This type of beam steering has been used to great effect in phased array radar and wireless systems [2.26], to provide fast scan rates and shape beam profiles.

2.4 Microwave Non-Destructive Evaluation

Microwave based Non-Destructive Evaluation (NDE) and anomaly detection is now being used increasingly in industrial inspection and verification applications with

companies such as MVG (<http://www.microwavevision.com/>) marketing continuous scanning devices that measure the dielectric properties within materials using multi antenna non-contact RF scanning techniques. Although unclear from the available literature, these methods appear to operate by making loss measurements through the material being examined so detecting density variations. Claimed resolution is still quite poor though at an object detection size lower limit of 10mm. Post construction inspection and maintenance of buildings has led to applications of the techniques previously outlined being adopted for civil engineering uses. Typically, this could involve confirming the presence and location of metal reinforcing rods within a concrete structure. A convincing demonstration of microwave imaging capability in this application is shown in [2.27]. Using a 45ps rise time, 10GHz bandwidth unipolar pulse and suitable horn antennas, a 2.5cm metal rod is detected and imaged beneath 15cms of concrete. Intuitively this choice of frequency might be thought to be rather high for use in this type of material at this depth. Experimental investigations presented in [2.28] found that frequencies in the 6GHz to 10GHz frequency range were useable up to a depth of 10cms. This system uses eleven discrete frequencies spaced over the operating range. Detection here is based on phase change induced by dielectric variation, results being shown for both conductive and non-conductive materials buried in a concrete slab. Phase shift is measured between antenna pairs that are in contact with the surface of the concrete using a vector network analyser. Apart from the previously discussed issues of material homogeneity and contact there are issues raised with antenna spacing, mutual coupling and phase shifting due to cables. This, as well as the necessity to compensate for multiple (cyclic) phase shifting, are dealt with by the use of measurement subtraction of the air based condition and a phase unwrapping algorithms. These steps may be rendered unnecessary if a through calibration between antenna pairs is performed as this will effectively remove all system

anomalies. As distances here are in the centimetre range, single wavelength frequencies could be used to effect without loss of resolution as these type of phase measurements have been shown to be very sensitive [2.29].

2.5 Phase Unwrapping

As mentioned earlier, phase measurements are sometimes used in conjunction with time domain returns in geographic IfSAR radar to produce higher resolution images than standard time domain techniques allow. When measuring the phase difference between signals arriving at two antennas, it is difficult to know how many cycles of shifting have occurred [2.30]. Most of these methods require *a priori* knowledge to provide an estimated distance on which to base an assumed amount of initial phase shift. For this reason these methods are used in conjunction with standard time domain techniques or previously mapped regions. In short range imaging a similar problem will exist if target distances exceed one wavelength as suggested in most studies, this being necessary to maximise resolution. A significant solution to this “phase unwrapping” problem is described in [2.31]. Presented there is a method of combining log amplitude and phase measurement to measure distance. Unlike the mapped interferometric method of IfSAR, here signal amplitude is measured solely as a function of time and so claims to not require any *a priori* information. Operating at spot frequencies between 500MHz and 900MHz and with antennas spaced around a circle of a diameter of 15cm, wavelengths are very long (60cms to 33cms) in comparison to the array dimensions. If the imaging process can be contained within a distance of no more the one wavelength, then phase unwrapping is superfluous. It was shown to be possible to map dielectric variation using phase changes due to wavelength shortening, this method giving surprising resolution even at these long

wavelengths. These results, whilst simulated, still present a realistic solution to this issue so lending optimism for the development of practical systems.

2.6 Suitable Antenna Designs

Many of the systems described above use the well known antenna designs of monopole, dipole and loop. These exhibit near spherical or toroidal radiation patterns and consequently are low gain devices, and in these cases, are only required to operate over narrow bandwidths. Printed monopole antennas can be designed to operate at the high bandwidths required to satisfy the demands made by UWB microwave detection processes. In addition, these designs can be made small in size by taking advantage of the dielectric properties of the substrate employed. An example of one such design is discussed in [2.32]. This design benefits from using a substrate with a dielectric constant (ϵ_r) of 10.2

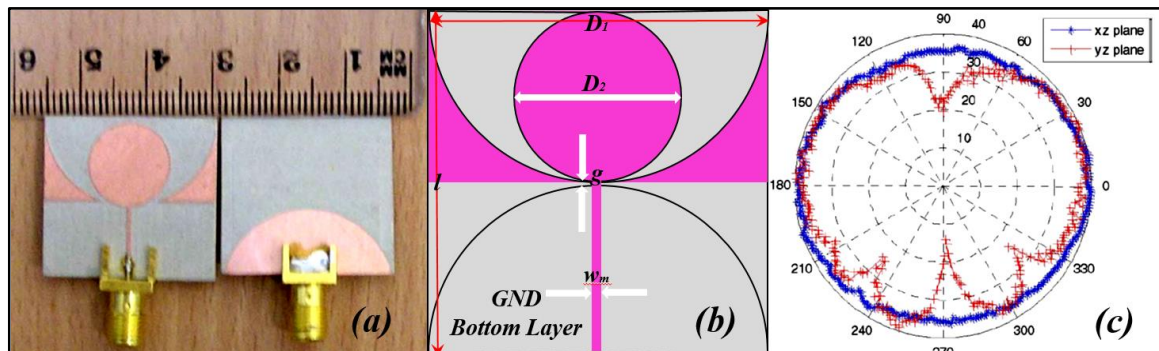


Fig. 2.14. Construction and radiation pattern (6GHz) of UWB monopole antenna [2.32]

(Rogers RT6010LM) to produce a planar structure that is 28mm x 28mm (Fig. 2.14 a&b) and has a toroidal, omni directional radiation pattern (Fig. 2.14c). A -10dB bandwidth of 3.1GHz to 14.5GHz allows this design across the entire UWB bandwidth allocation of 3.1GHz to 10.2GHz. This monopole design also allows the use of a very thin substrate (0.64mm) without compromising bandwidth, making fast pulse response times possible,

as can be seen in Fig. 2.15. This shows a comparison between the transmitted and received pulses between two antennas spaced at a distance of 45cm apart. As is often the case, the design was finalised by empirically using suitable microwave simulation software, but detailed dimensions are given, mostly being derived from standard equations some of which will be discussed in Chapter 6. Here the 50Ω stripline antenna feed is situated above a semicircular ground plane with a diameter of half the effective wavelength of the lowest required frequency (Fig. 14b, D_1). Dimension “ l ” comprises the radius associated with D_1 , a gap “ g ” which is half the feed stripline width, and a circular quarter wavelength patch of diameter D_2 . Around this, a slot resulting from the removal of a copper area of diameter D_1 from around the circular patch. Radiation occurs at the boundary of the quarter wavelength circular patch and the slot. Whilst the wide radiation patterns of these designs is useful to provide coverage, this will also introduce the problem of receiving returns from unwanted or irrelevant sources in the surrounding vicinity. Screening the array, or the introduction of a surrounding grounded backplane, will effectively provide a solution but may also adversely affect the bandwidth performance of the antenna elements as capacitive effects come into play. As can be seen in Fig. 2.15. below considerable spreading of the generated pulse results from passage through the devices being assessed. In medical applications and in particular, mamography, the area of interest is relatively small and so elements that can facilitate a dense spacing, without the multidirectional radiation pattern of the printed monopole, would be desirable. Stacked patch antenna designs can provide such a solution as discussed earlier in [2.14]. Details of the frequency and impulse responses of this design, as well as the predicted frequency dependent radiation patterns in the propagation medium are given in [2.15].

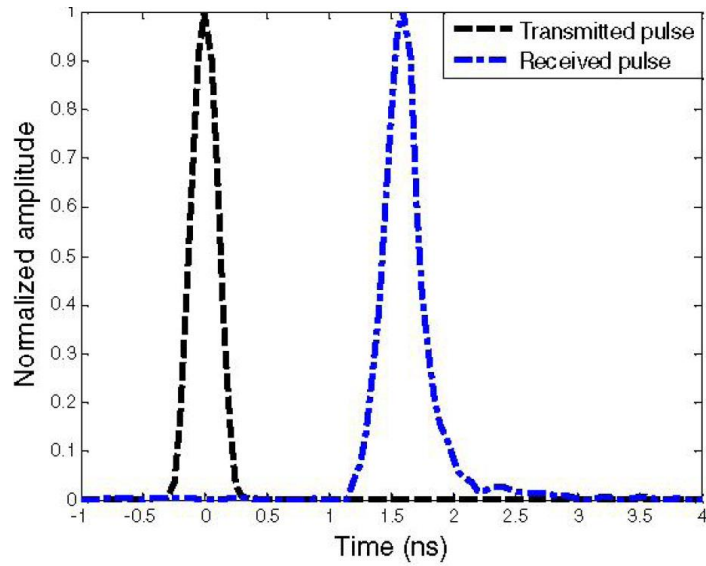


Fig. 2.15. Pulse degradation between two antennas [2.32]

Fig. 2.16 (a). shows the orientation of the patch, indicating the two measurement planes studied. Predicted co-polar radiation patterns of this antenna on each of the two orthogonal planes are shown in Fig. 2.16(b) & 2.16(c). This indicates a tendency towards a hemispherical radiation pattern that is fairly typical for a patch antenna.

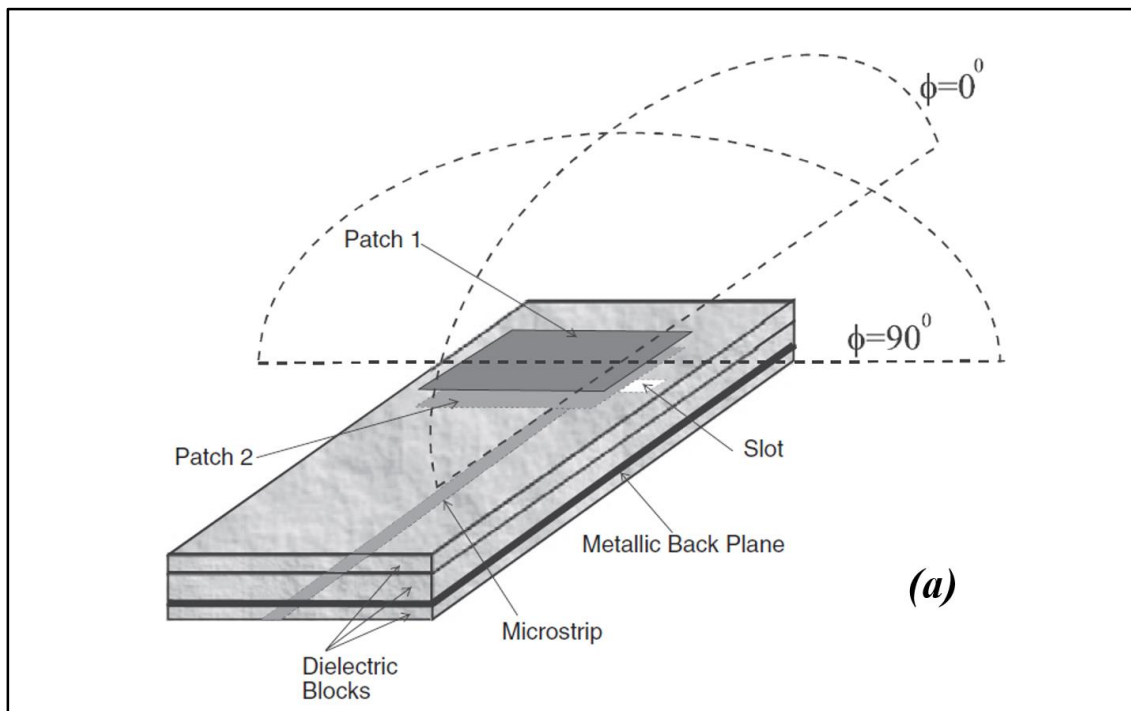


Fig. 2.16(a). Radiation patterns for stacked patch antenna [2.15]

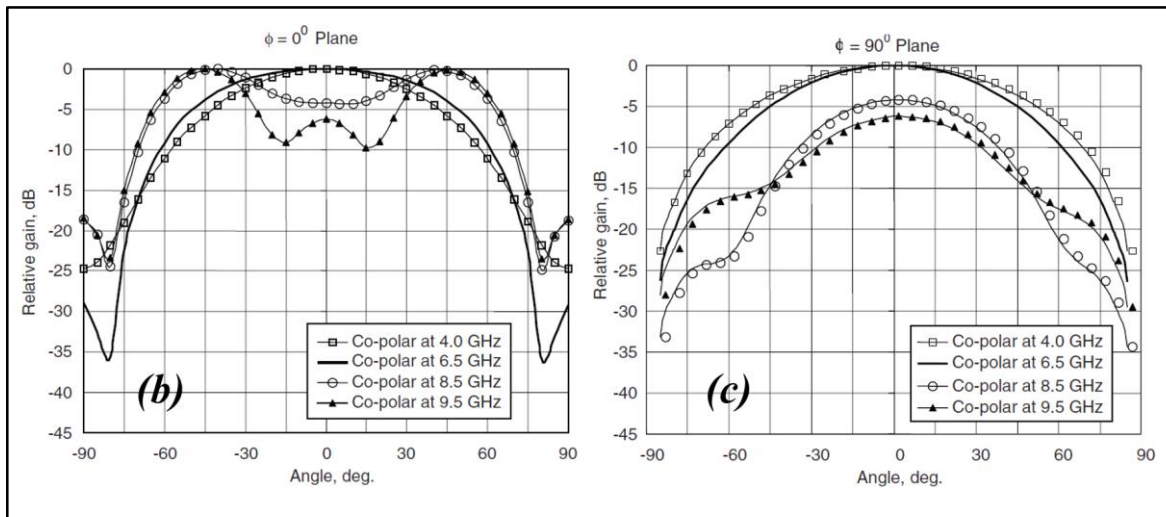


Fig. 2.16(b) & 2.16(c).. Radiation patterns for stacked patch antenna [2.15]

In the case of very broadband devices it is not uncommon for the radiation pattern to vary considerably with frequency, as is the case here. It would appear from the above plots that apart from at the higher end of the frequency spectrum, the radiation angle is around +/- 40 degrees, which is again to be expected from a patch. Cross polar plots are 40dB lower in amplitude than those for co-polar, indicating that the antenna is strongly linearly polarised. As can be seen in Fig. 2.17. the pulse response of this design is inferior to that of the monopole. Fig. 2.17a. shows the input pulse and Fig. 2.17b. the pulse after reception, as can be seen, the received pulse is subject to a significant level of “ringing”. Patch antennas by nature of their “plate type” construction, are prone to capacitive effects that may well in turn lead to the device being compromised when dealing with fast rise and fall times. Despite being slightly compromised when dealing with fast edges, the useable bandwidth of this device is very wide, as can be seen in the S_{21} (forward transmission) plot shown in Fig. 2.18. Also shown in this plot is the signal attributed to radiation at the rear of the patch.

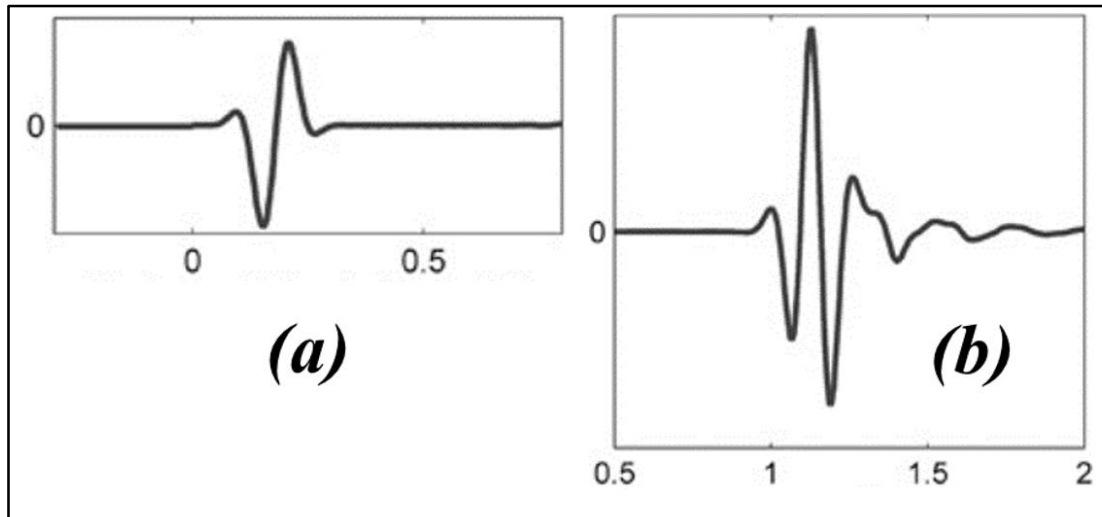


Fig. 2.17. Pulse response of antenna [2.15]

Unlike the printed monopole there is a significant difference of at least 10dB in the measured signal levels at the front and rear of the antenna, although no information is given as to how this is spacially distributed.

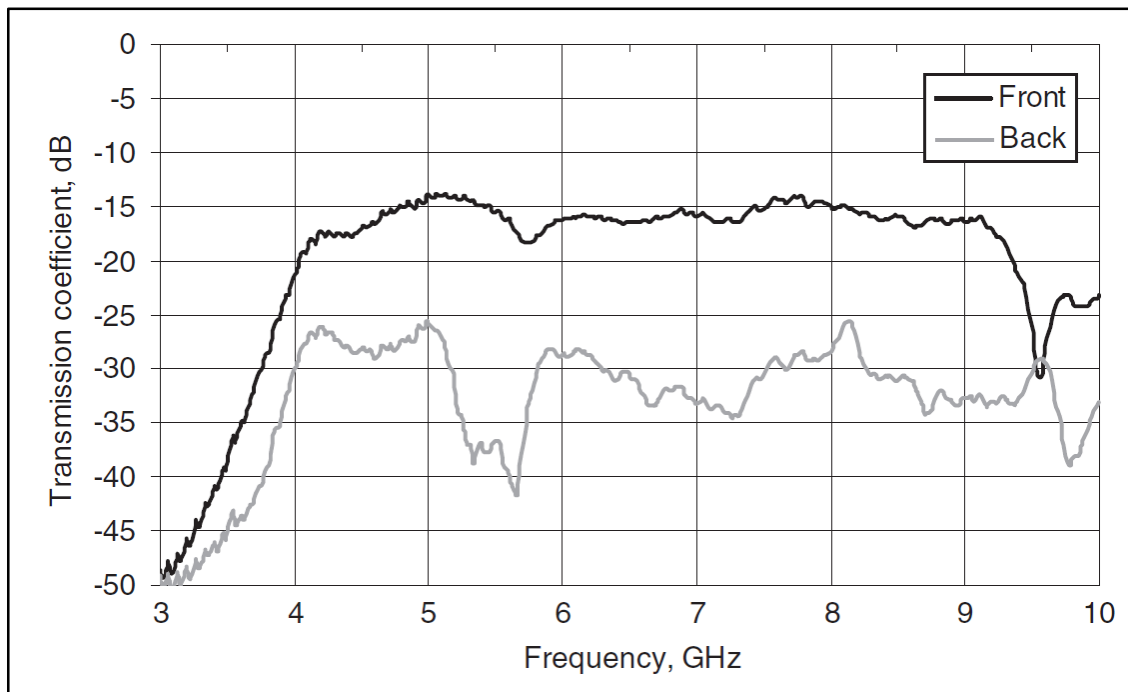


Fig. 2.18. S_{21} showing front and back radiation [2.15]

Stacked patches are effective and small in size but are difficult to fabricate as contact between layers is difficult to control as is their alignment and positioning. Using the wideband slot feeding technique leads to linear polarisation, which may be used to advantage in a polarimetric system, but this configuration may present difficulties when a switched or a circular polarisation antenna is required as the feed geometry becomes difficult. A possible solution is to use a cross slot feed to produce circular polarisation as put forward in [2.33], but this design operates over a narrow bandwidth, however it does indicate a possibility of controlling the polarisation plane. Taking advantage of “dielectric scaling” to reduce the antenna dimensions, the horn antenna described in [2.34] is designed to operate whilst immersed in a high permittivity liquid (Acetone E_r 20.7) so as to approximate operation in body tissue. In this design two “ridges” form part of the horn interior (Fig. 2.19a.), these are adjustable and are used to fine tune the antenna feed input impedance match when immersed.

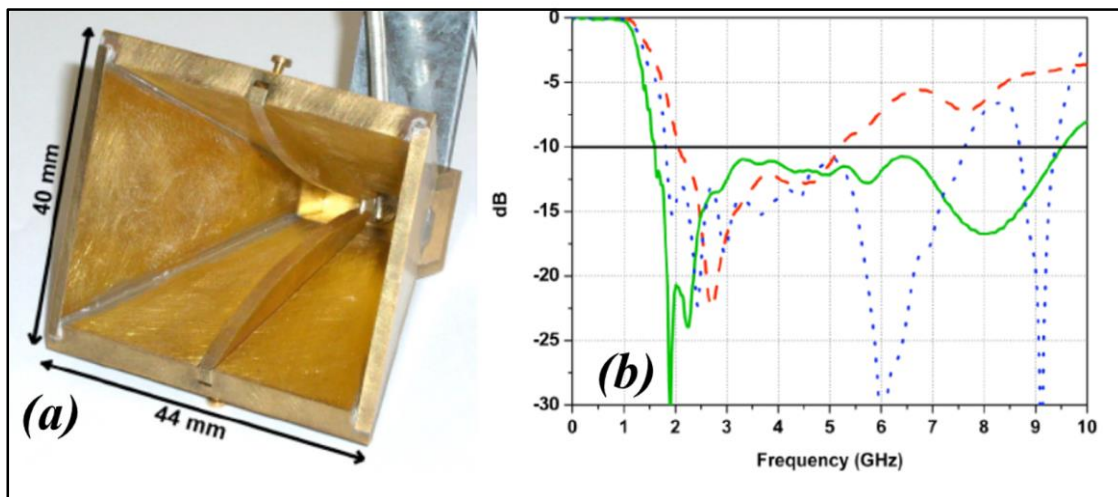


Fig. 2.19. Adjustable ridged horn [2.34]

Impedance matching at this point is critical to ensure wide bandwidth source coupling. Fig. 2.19b. shows the final dimensions of the horn (a) and the (b) S₁₁ impedance match

both before (red dotted line) and after immersion (green line), the blue line is a simulation plot. This measurement may not be truly indicative of the antenna's radiation bandwidth, since as can be seen in figure 20. The radiation patterns broaden with decreasing frequency, (blue 1.5GHz, red 3GHz, green 5GHz), implying a reduction in antenna gain at the lower frequencies.

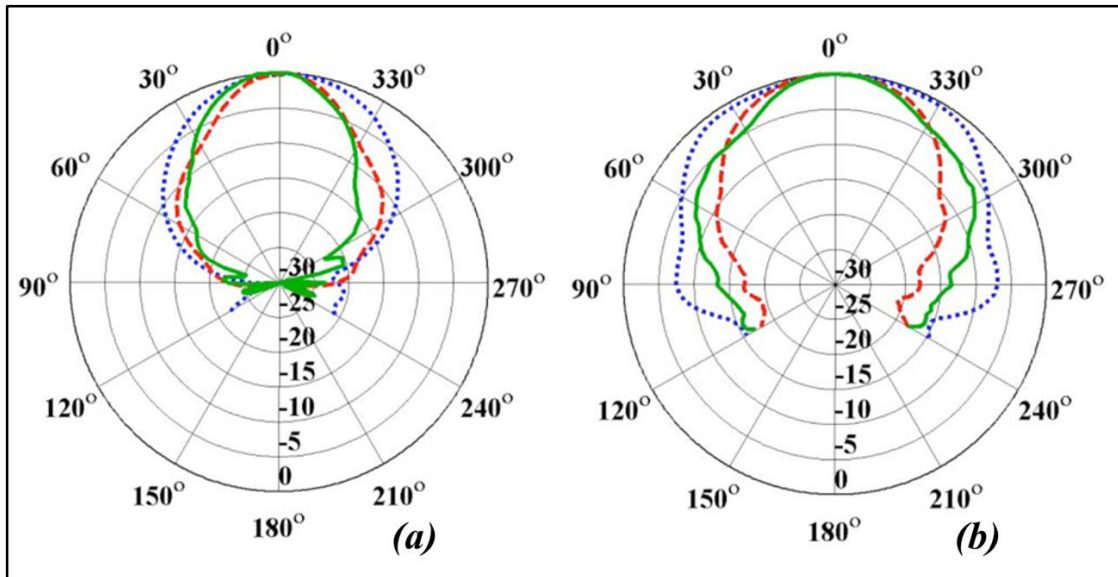


Fig. 2.20. Frequency dependant radiation patterns in acetone (a) and air (b) [2.34]

Narrowing of the radiation pattern in acetone (Fig. 2.20a) as compared to air (Fig. 2.20b) is not surprising as in these conditions ($E_r 20.7$), the electric field will be concentrated in comparison to that of air ($E_r 1$). Although horn antennas are a well proven design with desirable radiation characteristics the final structure is relatively large in comparison with the alternative printed designs. Such a design is the Vivaldi antenna, a planar printed structure that uses an exponential flare in much the same way as a horn design. Such an antenna is described in [2.35], this device exhibits many of the desirable features already outlined, a wide bandwidth, fast pulse response and up to 11dBi gain. Having dimensions of 5cm x 5cm (Fig. 2.21a.) it would seem large in comparison to the

other devices described, but being an end fire device, it represents the smallest area presented to a target of any of the designs examined.

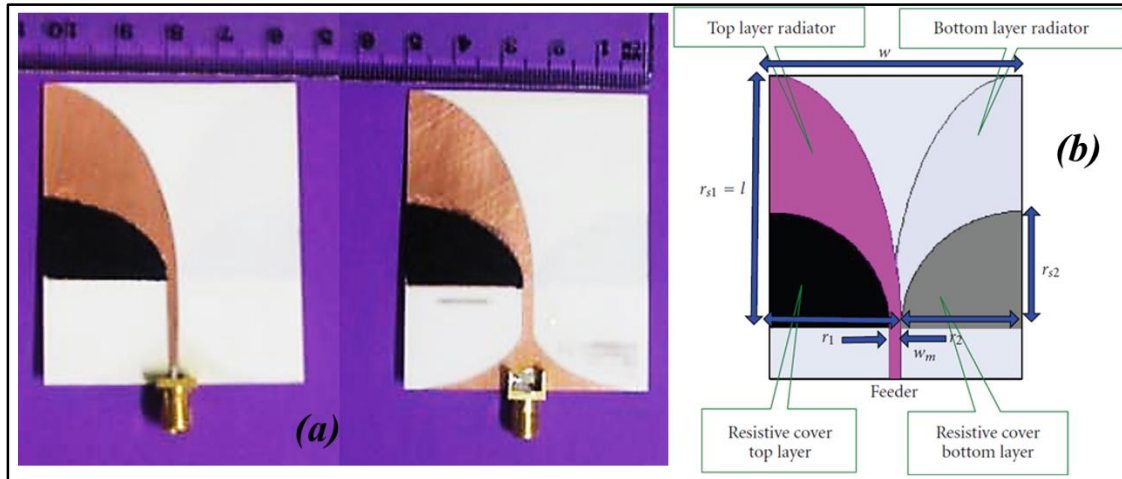


Fig. 2 .21. Vivaldi horn antenna construction [2.35]

As with all printed designs the antenna dimensions are largely determined by the dielectric constant of the substrate, in this case $E_r = 3.38$, and its thickness 0.508mm. Shown in Fig. 2.21b are the construtlional details where w is set to be half the wavelength of the lowest operating frequency, the legnth of the flare l is also this half wavelength value, the length of the 50Ω stripline feed making up the final dimension.

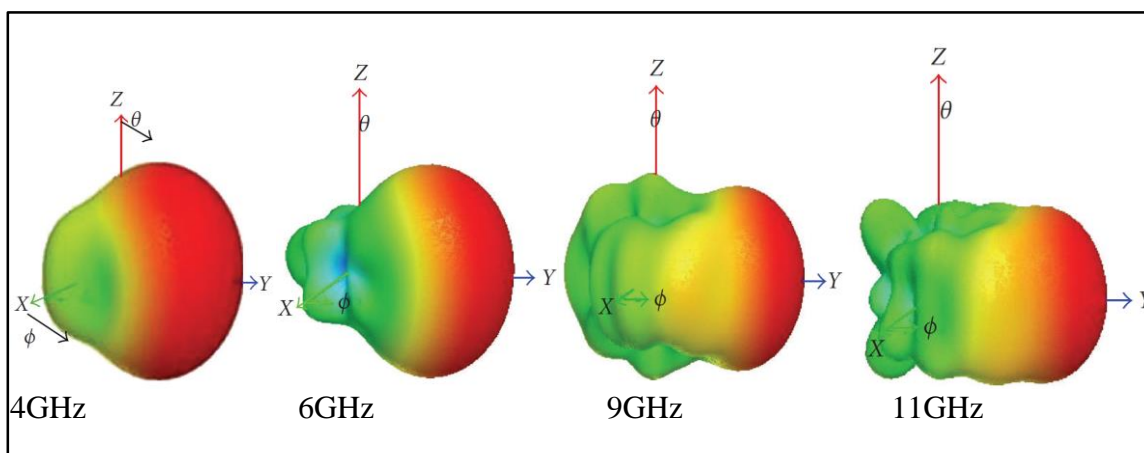


Fig .22.Vivaldi horn radiation pattern variation with frequency [2.35]

A quarter elliptical geometry forms the “inner” part of the metallised flare, whilst the “outer” part of the shape is formed from a quarter ellipse radii r_2 and r_{s2} . In order to minimise back radiation a resistive chemical layer is added to the void created by the formation of the ellipse r_2 / r_{s2} . As can be seen from the modelled radiation patterns in Fig. 2.22. there is still considerable predicted back radiation at 4GHz which diminishes with increasing frequency.

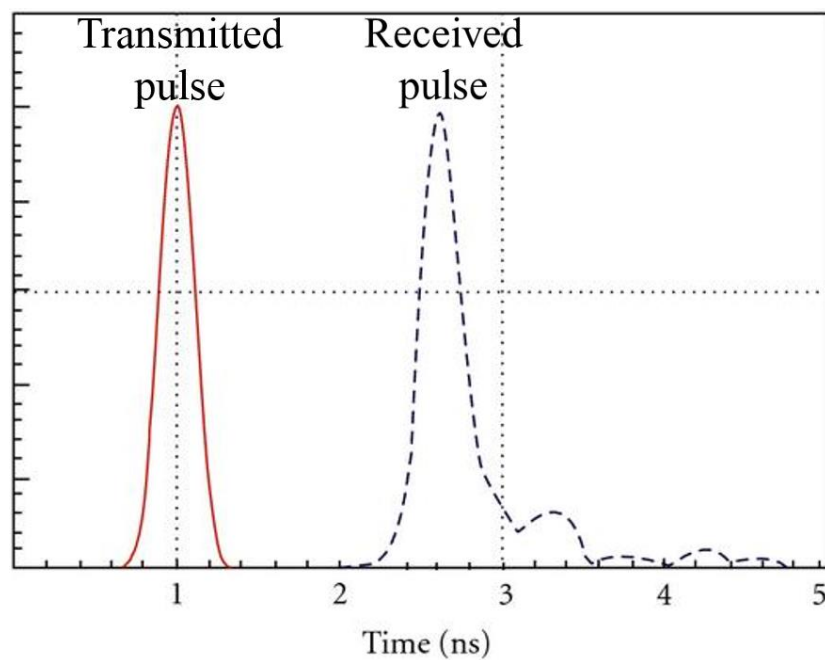


Fig. 23. Pulse response comparable to monopole [2.35]

This combined with a predicted narrowing of the radiation pattern is confirmed by the antenna gain measurements, stated as 4.3dBi at 3GHz rising to 10.8dBi at 10.6GHz. Fig. 2.23. Shows the predicted pulse response of the Vivaldi design, this would appear to be comparable to that of the low capacitance monopole design shown earlier. Such a result would indicate that this design possesses not only wide bandwidth properties but also sufficient gain to ensure sufficient dynamic range if used in an imaging environment. Vivaldi antennas of this type are linearly polarised, the E field existing between the

metalised regions of the structure. The use of orthogonally opposed devices may however lead to circular polarisation, or use in a switched polarisation scheme. Being a planar, end fire device, this configuration lends itself for use in densely packed antenna arrays.

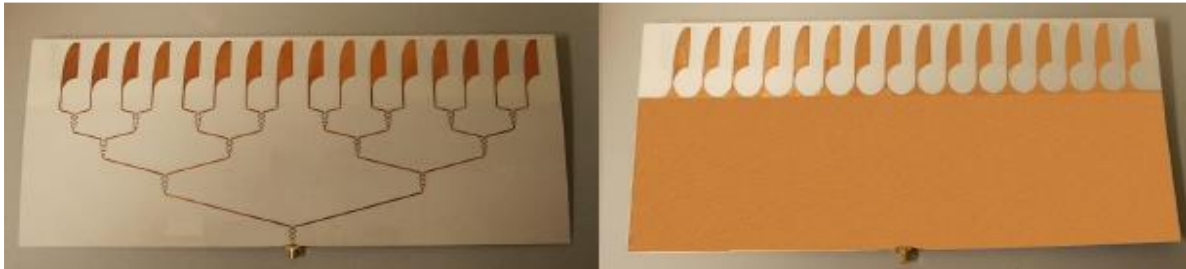


Fig. 2.24 Vivaldi antenna array [2.36]

Using similar antenna elements to that outlined above, [2.36] develops a 16 element linear Vivaldi array. Fig. 2.24. shows the printed layout, illustrating the potential density of such an array. Element design in this array was not optimal, having an individual gain of less than 7 dBi; this along with large insertion losses associated with the Wilkinson splitter network, is a likely to be the cause of the disappointing final array gain of 12 dBi. The final two antenna designs to be discussed are specific to GPR and NDE applications. The first of these is used in a frequency tuneable ground penetrating radar [2.37], In this example varying pulse widths are used to generate operating bandwidths between 0.5GHz and 6GHz so as to take advantage of the differing penetration / resolution capabilities of these signals. Described in this paper, this unusual antenna design is divided into two separate but identical transmit and receive sections. Each section consists of a tapered transmission line radiator and a ground plane separated by a polystyrene foam insert to form a “quasi- horn” structure (Fig. 2.25). Such a transmit / receive configuration simplifies system electronics but may introduce the need for delay compensation to account for spacial separation of the two, effectively independent

antenna sections. Also due to length of this, and any horn based device, the path length of the reflected signal will vary with frequency, leading to the need for further compensation. A credible gain of 15dBi at a frequency of 4 GHz is claimed for this device.

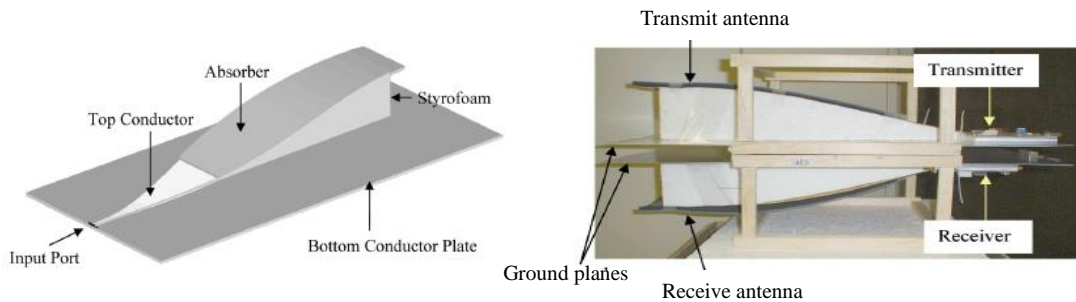


Fig. 2.25. Quasi horn antenna for GPR [2.37]

As mentioned earlier in [2.24], the final design to be discussed is that of a resistive vee antenna (Fig. 2.26). Based on a dipole, each arm uses progressive linear resistive loading along its length, from feed to air interface, so as to eliminate reflection from the normally mis-matched (377Ω) open end of the element. This method was first put forward by Wu and King [2.38] as a way of reducing conflict between outward and inward travelling waves in a cylindrical antenna. Whilst this produces a structure that is capable of generating undistorted pulses, the price paid is a reduction of up to 50% in the antenna efficiency. This is largely due to the suppression of the radiation generated by the continued reflection of the returned signal.

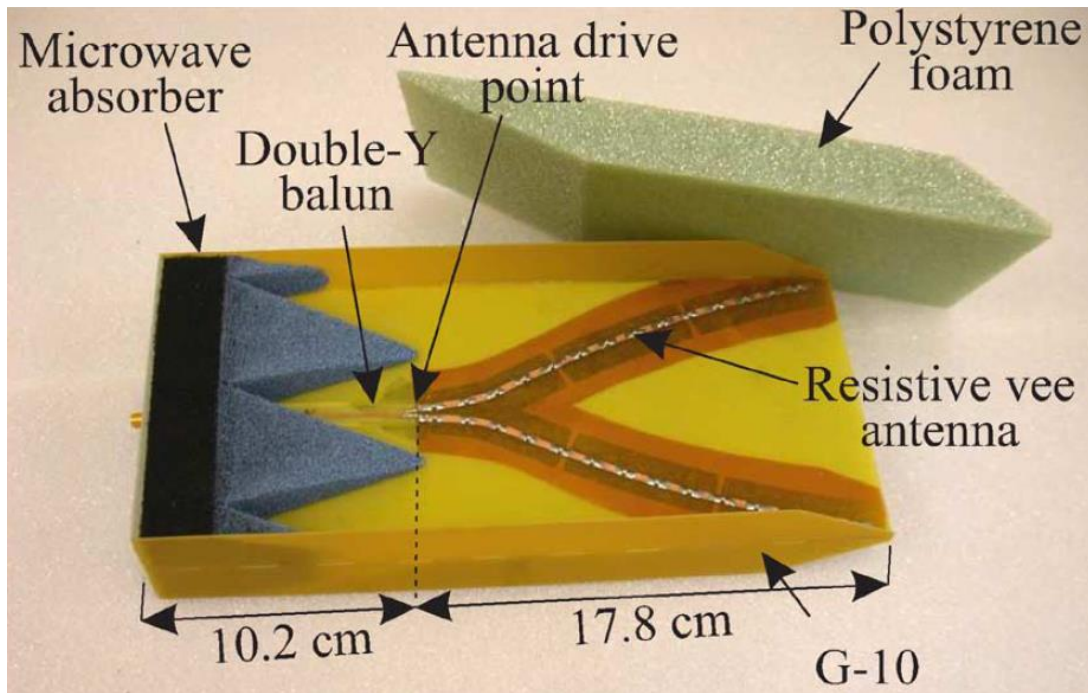


Fig. 2.26. Resistive vee antenna [2.24]

2.7 Phase Preservation

Imaging methods that rely on the recovery of phase related information at GHz frequencies will experience anomalies related to movements associated with interconnecting co-axial cables. A significant cause of this is because when cable movement occurs it inevitably causes localised changes in the density of dielectric separator in the cable. This then leads to changes in the dielectric constant of the material in these areas and so variations in signal wavelength occur. Such variation then goes on to influence phase stability in the cable. In order to assess this [2.39] uses the experimental setup shown in Fig. 2.27. to measure the phase modulation, due to a 12 foot cable undergoing a vibration test. This was part of an experiment to assess the effect of vibration on microwave components; it was found that in these tests that the effect of these mechanical deformations in the cable “sets the noise floor” in the experimental set up and so was significant. As can be seen below this test bed consisted of a reference

oscillator with its output split two ways. One half is sent to the test cable mounted on a vibration table, the other to a delay line and a phase shifter. This was necessary to ensure a zero phase difference when the signal was applied to an RF mixer used as a phase comparator. If a difference in the phase on one arm of the mixer occurs, there is an output at the IF port which is then amplified and sent to a spectrum analyser. This is then displayed as peaks either side of the centre frequency set by the reference oscillator.

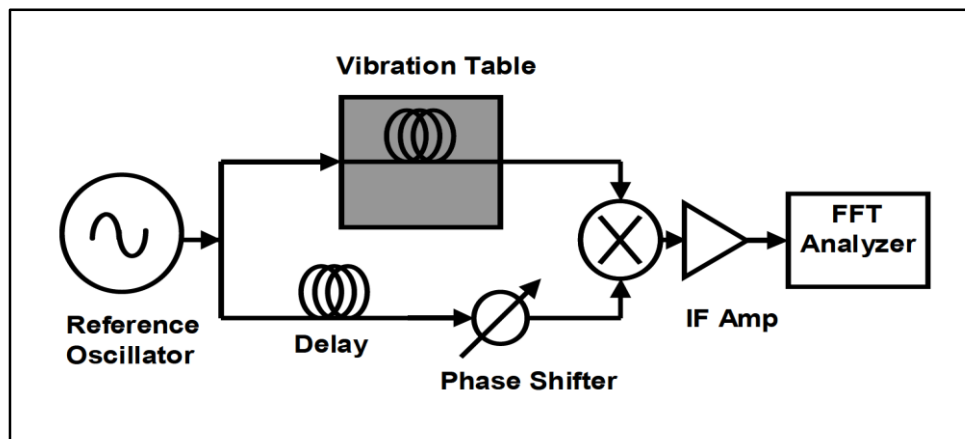


Fig. 2.27. Phase sensitivity test rig [2.39]

Shown in Fig. 2.28. is the resulting plot from a system being vibrated at 100Hz showing peaks at +/- the vibration frequency on either side of the central frequency of the oscillator caused by phase variation induced outputs from the RF mixer. These tests were carried out on flexible, semi rigid and rigid cables; similar levels of movement sensitivity were recorded. Phase instabilities of this type due to movement in interconnecting cables, would pose significant accuracy problems for GHz frequency phase related measurement systems. The use of optical interconnections would lessen this problem and will be investigated as a possible solution in this application.

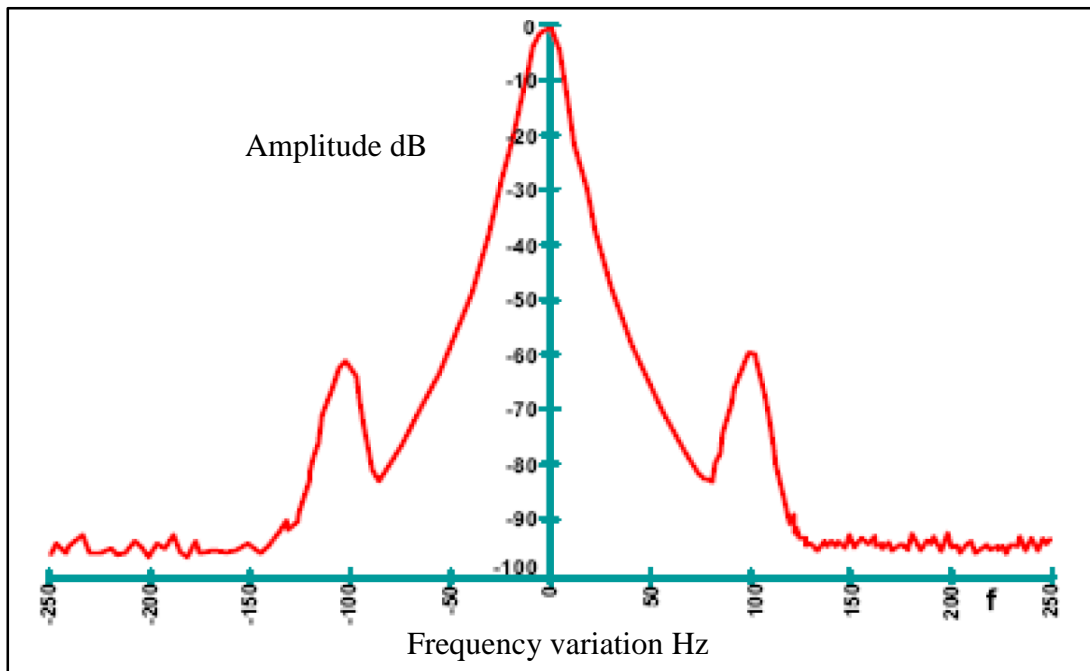


Fig. 2.28. Spectrum of phase modulated signal [2.39]

2.8 Optical Remoting

Optical Radio over Fibre techniques have been shown to be capable of providing direct range extension for microwave frequency wireless systems that rely on phase difference to provide high data rates [2.40]. Such systems have been shown to be capable of phase preservation over considerable lengths of optical fibre (13km) when operating with complex modulation schemes that require the use of multiple carriers and high level Quadrature Amplitude Modulation as shown in [2.41]. In this case a UWB wireless link using a frequency range of 3.168GHz to 4.752 GHz. Phased array clusters, such as those found in radar systems, require precise control of signal phase applied to adjacent antenna elements in order to achieve the required beam scanning function. An example of the use an optical fibre link to control phase in an antenna array is described in [2.42], this system demonstrates the use of an optically modulated signal and photodiode / amplifier combination to directly drive an antenna. Using this control method a two element array

operating at 4GHz with antennas spaced at 0.7 wavelength achieved a scan angle of +/- 21 degrees. Typically these approaches use external optical modulation schemes that require the use of optical amplification [2.43] leading to complex architectures. Distortion of the analogue signals and “matching errors” introduced by the electrical – optical – electrical (EOE) conversion process is also a cause for concern. Direct modulation of optical components would simplify any system, so reducing the potential for anomalies related to component matching and non-linearities. Remote positioning of key optical components can further improve the situation, as demonstrated in [2.44]. Here an Electro Absorption Modulator is used in close proximity to the antenna. This provides the necessary EOE conversion directly, at the site of the antenna, so the maximum use of optical interconnection is possible. It is still necessary, however, to provide a +/-ve bias to switch the device between transmit and receive modes. Reflective technologies, such as those used in [2.41], gives the possibility of optical “full duplex” operation as dual optical wavelengths can be utilised simultaneously. Achieving this mode of operation in the RF domain though has still to be demonstrated.

2.9 Polarisation

The use of antenna polarisation diversity, ie. the orientation of the Electrical “E plane” and the Magnetic “H plane” of an antenna has been shown to be a useful technique in telecommunications. In particular the property of being able to isolate the orthogonal polarisation planes of linearly polarised radiators is widely used to permit the re-use of common frequencies, for example in the transmit and receive paths of a wireless link. In determining the shape or dimensions of a hidden object, polarimetric methods such as those described in [2.45][2.46][2.47] indicate useful methods for any short range detection system. Key to any polarimetric microwave system, whatever the application, are

antennas that possess a high degree of polarisation plane isolation so as to minimise crosstalk between the diverse channels. Preservation of the polarisation state of the signal in the presence of clutter and varying dielectric conditions has been the subject of a large number of atmospheric and satellite communication studies. The depolarising effects described (irregular shaped objects, raindrops etc) could well cause the sensing signals to lose some degree of polarisation purity. Such conditions could then mask any results as polarisation plane isolation could be compromised. As these effects are likely to be specific to a particular set of circumstances this will be separately investigated experimentally under conditions that are explicit to the application and the operating environment.

2.10 Conclusions

A number of studies have been examined, focussing on the areas of medical imaging, ground penetrating radar and non-destructive evaluation. A large number of these studies were based on simulation and used delay and sum, averaging and invert and add techniques to demonstrate the potential data recovery methods associated with imaging techniques that will not be further pursued in this work. These post processing methods were necessary to negate the effects of dielectric mismatching, clutter and to produce a zero calibration condition but serve to illustrate the potential uses and limitations of the relatively long wavelength systems. Use within a homogenous medium greatly aids these methods as they rely on reflection from areas of dielectric contrast. Variations in this are a principle cause of phantom reflections and clutter. A number of antenna configurations were investigated in these studies including the monostatic MIST, bistatic and multistatic MAMI, the most accurate results being obtained from either multistatic or multi bistatic configurations. Most studies used time of flight measurements and pulsed

UWB methods of signal generation. Pulsed UWB provides a convenient signal for time of flight analysis and the wide bandwidth enables high resolution. Signal penetration however may not be uniform across the entire frequency spectrum as the higher frequencies generated may suffer absorption in some applications. Phase estimation APES was shown to offer the possibility of improved accuracy. Here the phase of the signal was estimated from the recovered signal amplitude (post process), this may not be practical as it is necessary to have accurate information about the signal at the point of launch. Practical implementations mostly use the pulsed UWB format and employed a variety of antenna types depending on the application. Propagation of UWB signals of this type poses a number of problems relating to the design of the antennas. Generally antennas capable of supporting these wide bandwidth signals fall into two categories, small printed devices and large horn antennas. Being small, antennas printed on a high dielectric constant substrate are particularly suited to medical applications. Demands of the high bandwidth requirement in these cases often lead to low antenna gain and associated omnidirectional radiation patterns. Whilst a wide area of illumination is desirable to provide adequate coverage back radiation leads to the reception of unwanted reflections and low gain leads to poor dynamic range. A stacked patch design addresses these issues but is difficult to manufacture and does not readily lend itself to use with polarisation diversity. Horn designs, being relatively large are more suited to ground survey type applications. Having gain and back radiation characteristics that are superior to printed designs they are however complex and difficult to implement, there may also be an issue related to the arrival times of signals within the horn structure. Building elements into arrays gives the advantage of increased gain and offers the possibility of beam steering by control of the phase of the signals applied to each element. Such phased array designs are used in radar systems to produce the required scan without the need for

mechanical movement. Stability of signal phase is critical for accurate scan control. A major problem exists in constructing these arrays, in that conventional cable interconnects can introduce phase inaccuracies induced by mechanical deformations in their dielectric layer under vibration and movement. Optical remote connection provides a solution to maintaining integrity the of phase information essential to the operation of these systems. External modulation of lasers and the associated need for optical amplification leads to inherent difficulties with device matching (Mach-Zehnder bias). Direct modulation would simplify any system if devices are sufficiently linear. The fragile nature of optical components could be to some extent overcome by the use of reflective modulation techniques. This enables remote positioning of these devices and enables any control of bias conditions to be localised. Polarisation, that is the use of antennas that radiate with their E plane in one direction, may be useful in recording the size and orientation of an object. Preservation of this information within the transmission medium will be necessary for this technique to be successful. This may be dependent on the uniformity of the material under examination and will be investigated separately.

References

- [2.01] Chao-Hsiung Tseng, Tah-Hsiung Chu. "An Effective Usage of Vector Network Analyzer for Microwave Imaging". IEEE Transactions on Microwave Theory and Techniques. Vol, 53, No.9 Sept. 2005 pages 2884-2891.
- [2.02] Jeongwoo Han and Cam Nguyen. "Development of a Tunable Multiband UWB Radar Sensor and Its Applications to Subsurface Sensing". IEEE Sensors Journal, Vol.7, No.1 Jan 2005, pages 51-58.
- [2.03] Preece, A.W. Green, J.L. Potheary, N. Johnson, R.H. "Microwave imaging for tumour detection". IEE Colloquium on Radar and Microwave Imaging, 16 Nov 1994 Pages 9/1 - 9/4
- [2.04] Staderini, E.M. "UWB radars in medicine". IEEE Aerospace and Electronic Systems Magazine, Volume 17, Issue 1, Jan. 2002 pages 13-18.
- [2.05] Fear, E.C. Meaney, P.M. Stuchly, M.A. "Microwaves for breast cancer detection". Potentials, IEEE Volume 22, Issue 1, Feb-Mar 2003 Pages 12 – 18.
- [2.06] Paul M. Meaney, Margaret W. Fanning, Dun Li, Steven P. Poplack, and Keith D. Paulsen. "A Clinical Prototype for Active Microwave Imaging of the Breast". IEEE Transactions on Microwave Theory and Techniques, Vol48, No.11, Nov. 2000, pages 1841-1853.
- [2.07] Xia Xiao, Kikkawa, T. "Study on the breast cancer detection by UWB microwave imaging". International Conference on Microwave and Millimeter Wave Technology, 2008. ICMMT 2008. Volume 4, Issue , 21-24 April 2008 Pages 1707-1710.
- [2.08] Beibei Zhou, Wenyi Shao, Gang Wang. "On the resolution of UWB microwave imaging of tumors in random breast tissue". IEEE Antennas and Propagation Society International Symposium 2005. Volume 3A, Issue, 3-8 July 2005 Pages 831- 834 vol. 3A
- [2.09] Yao Xie; Bin Guo; Jian Li; Stoica, P. "On Multi-Static Adaptive Microwave Imaging Methods for Early Breast Cancer Detection". IEEE International Conference on Acoustics, Speech and Signal Processing, 2006. ICASSP 2006 Proceedings. 2006 Volume 2, Issue, 14-19 May 2006 Pages 573-576
- [2.10] Xu Li, Shakti K. Davis, Susan C. Hagness, Daniel W. van der Weide, Barry D. Van Veen. "Microwave Imaging via Space-Time Beamforming: Experimental Investigation of Tumor Detection in Multilayer Breast Phantoms". IEEE Transactions on Microwave Theory and Techniques, 2004. Vol.52, No.8. Pages 1856-1865.
- [2.11] Yao Xie, Bin Guo, Luzhou Xu, Jian Li, Petre Stoica. "Multistatic Adaptive Microwave Imaging for Early Breast Cancer Detection". IEEE Transactions on Biomedical Engineering. Vol.53. No8, August 2006, pages 1647-1657.

- [2.12] Xu Li and Susan C. Hagness. "A Confocal Microwave Imaging Algorithm for Breast Cancer Detection". IEEE Microwave and Wireless Components Letters. Vol. 11, No.3, March 2001, pages 130-132.
- [2.13] Craddock, I. J. Preece, A. Leendertz, J. Klemm, M. Nilavalan, R. Benjamin, R. "Development of a hemi-spherical wideband antenna array for breast cancer imaging". First European Conference on Antennas and Propagation, 2006. EuCAP 2006. 6-10 Nov. 2006 Pages 1 – 5.
- [2.14] Craddock, I.J. Klemm, M.; Leendertz, J. Preece, A.W.; Benjamin, R. "An Improved Hemispherical Antenna Array Design for Breast Imaging". The Second European Conference on Antennas and Propagation, 2007. EuCAP 2007. 11-16 Nov. 2007 Pages 1 – 5
- [2.15] Nilavalan, R. Craddock, I.J. Preece, A. Leendertz, J. Benjamin, R. "Wideband Microstrip Patch Antenna Design for Breast Cancer Tumour Detection. IET Microwave Antennas Propagation, 2007,1, (2). Pages 277- 281.
- [2.16] Klemm, M, Craddock, I.J, Leendertz, J. Preece, A.W, Benjamin, R. "Breast Cancer Detection using Symmetrical Antenna Array". The Second European Conference on Antennas and Propagation, 2007. EuCAP 2007. 11-16 Nov. 2007 Pages 1 - 5
- [2.17] Klemm, M. Craddock, I. Leendertz, J. Preece, A. Benjamin, R. "Experimental and clinical results of breast cancer detection using UWB microwave radar". IEEE Antennas and Propagation Society International Symposium 2008, 5-11 July 2008 Pages 1 – 4.
- [2.18] Maciej Klemm, Ian J. Craddock, Jack A. Leendertz, Alan Preece, and Ralph Benjamin. "Radar-Based Breast Cancer Detection Using a Hemispherical Antenna Array Experimental Results". IEEE Transactions on Antennas and Propagation, Vol. 57. No 6. June 2009. Pages 1692-1704.
- [2.19] B. Guo, Y.Wang, j.Li, P. Stoica, R.Wu. "Microwave Imaging via Adaptive Beamforming Methods for Breast Cancer Detection". Journal of Electromagnetic Waves and Applications. Vol.20, No.1, 2006. Pages 53 – 63.
- [2.20] Raphael Lençrerot, Amélie Litman, Hervé Tortel, Jean-Michel Geffrin. "A microwave imaging circular setup for soil moisture information". IEEE Geoscience and Remote Sensing Symposium, 2007. Pages 4394 - 4397
- [2.21] Traian Dogaru and Lawrence Carin. "Time-Domain Sensing of Targets Buried Under a Rough Air-Ground Interface". IEEE Transactions on Antennas and Propagation, Vol. 46, No. 3, 1998. Pages 360-372.
- [2.22] Elena Pettinelli, Paolo Burghignoli, Anna Rita Pisani, Francesca Ticconi, Alessandro Galli, Giuliano Vannaroni, Francesco Bella. "Electromagnetic Propagation of GPR Signals in Martian Subsurface Scenarios Including Material Losses and Scattering". IEEE Transactions on Geoscience and Remote Sensing. Vol. 45, No.5, 2007. Pages 1271- 1281.

- [2.23] Olga Duran, Kaspar Althoefer, Lakmal D. Seneviratne. "State of the Art in Sensor Technologies for Sewer Inspection". IEEE Sensors Journal, Vol.2, No.2, 2002. Pages 73-81.
- [2.24] Tegan Counts, Ali Cafer Gurbuz, Waymond R. Scott, James H. McClellan Kangwook Kim. "Multistatic Ground-Penetrating Radar Experiments". IEEE Transactions on Geoscience and Remote Sensing, Vol. 45, No8, 2007. Pages 2544 – 2553.
- [2.25] Alexander G. Yarovoy, Timofey G. Savelyev, Pascal J. Aubry, Pidio Ekoue Lys, Leo P. Ligthart. "UWB Array-Based Sensor for Near-Field Imaging". IEEE Transactions on Microwave Theory and Techniques, Vol.55, No.6, 2007. Pages 1288-1295.
- [2.26] Sandra E. M. Dudley, Terence J. Quinlan, Stuart D. Walker. "Ultra broad-band Wireless Optical Transmission Links Using Axial Slot Leaky Feeders and Optical Fiber for Underground Transport Topologies". IEEE Transactions on Vehicular Technology, Vol.57, No.6, 2008. Pages 3471-3476.
- [2.27] Fu-Chiang Chen, Weng Cho Chew. "Microwave Imaging Radar System for Detecting Buried Objects". Geoscience and Remote Sensing, 1997. IGARSS '97. Remote Sensing - A Scientific Vision for Sustainable Development., 1997 IEEE International Vol. 4, 1997. Pages 1474-1476.
- [2.28] Vladimir Semenchik, Vasil Pahomov, Sergey Kurilo. "Some Peculiarities of Microwave Imaging in Concrete". MISMW'07 Symposium Proceedings. Kharkov' Ukraine, 2007. Pages 449-451.
- [2.29] Terence Quinlan, Sandra Dudley, Tony Jordan, Stuart Walker. "Improved Radio Frequency Imaging Resolution using Phase Contrast Interferometry". Loughborough Antennas and Propagation Conference, 2009. Pages 105-108.
- [2.30] David A. Imel. "Accuracy of the Residual-Delay Absolute-Phase Algorithm". IEEE Transactions on Geoscience and Remote Sensing. Vol. 36, No 1, 1998. Pages 322-324.
- [2.31] Paul M. Meaney, Keith D. Paulsen, Brian W. Pogue, Michael I. Miga. "Microwave Image Reconstruction Utilizing Log-Magnitude and Unwrapped Phase to Improve High-Contrast Object Recovery". IEEE Transactions on Medical Imaging, Vol. 20, No. 2. 2001. Pages 104-116.
- [2.32] Amin M. Abbosh and Marek E. Bialkowski. "Design of UWB Planar Antenna for Microwave Imaging Systems". IEEE International Conference on Signal Processing and Communications 2007. Pages 193 – 196.
- [2.33] Iwasaki, H. Kawabata, K. Yasukawa, K. "A circularly polarized microstrip antenna using a crossed-slot feed". Antennas and Propagation Society International Symposium, May 1990. vol.2 Pages 807-810.

- [2.34] U. Schwarz, M. Helbig, J. Sachs, F. Seifert, R. Stephan, F. Thiel, M.A. Hein. "Physically small and adjustable double-ridged horn antenna for biomedical UWB radar applications". IEEE ICUWB 2008, Hannover (Germany); May 13, 2008
- [2.35] Amin M. Abbosh. "Directive Antenna for Ultrawideband Medical Imaging Systems". International Journal of Antennas and Propagation Volume 2008, Article ID 854012.
- [2.36] Y. Yang, Y. Wang, A. E. Fathy. "Design of Compact Vivaldi Antenna Arrays for UWM See Through Wall Applications". Progress in Electromagnetics Research, PIER 82, 2008. Pages 401–418.
- [2.37] Jeongwoo Han, Cam Nguyen. "Development of a Tunable Multiband UWB Radar Sensor and Its Applications to Subsurface Sensing". IEEE Sensors Journal, Vol. 7, NO. 1, 2007. Pages 51-58.
- [2.38] Wu T., King R. "The cylindrical antenna with non-reflecting resistive loading". IEEE Transactions on Antennas and Propagation. May 1965. Pages. 369–373.
- [2.39] Hati,A., Nelson, C.W., Howe, D.A., Ashby, N., Taylor, J., Hudek, K.M., Hay, C., Seidef, D. Eliyahu, D. "Vibration Sensitivity of Microwave Components". IEEE Frequency Control Symposium, 2007 Joint with the 21st European Frequency and Time Forum. 2007-June 1 2007. Pages 541-546.
- [2.40] Sandra E. M. Dudley, Terence J. Quinlan, and Stuart D. Walker "Ultrabroadband Wireless–Optical Transmission Links Using Axial Slot Leaky Feeders and Optical Fiber for Underground Transport Topologies". IEEE Transactions on Vehicular Technology , Vol. 57, No. 6, Nov 2008. Pages 3471-3476.
- [2.41] Manoj Prasad Thakur, Terence James Quinlan, Carlos Bock, Stuart Walker et al. "480- Mbps, Bi Directional, Ultra- Wideband Radio-Over-Fibre Transmission Using a 1303/1564 Reflective Electro-Absorption Transducer and Commercially Available VCSELs". Journal of Lightwave Technology. Vol. 27, No. 3, Feb 2009. Pages 266 -272.
- [2.42] Deal, W.R. Jung, T. Wu, M.C. Itoh, T. "All-optically controlled beam-scanning array for antenna remoting applications". IEEE. Jun 1998 Vol.3, Pages 1383-1386.
- [2.43] Esman, R.D. Frankel, M.Y. Matthews, P.J. "New array capabilities by photonic beamforming". IEEE Microwave Symposium Digest, Jun 1998 vol.3. Pages 1363-1366.
- [2.44] Heinzelmann, R. Stohr, A. Groz, M. Kalinowski, D. Alder, T. Schmidt, M. Idger, D. "Optically powered remote optical field sensor system using an electro absorption-modulator". IEEE Microwave Symposium Digest, Jun 1998 Vol.3. Pages 1225-1228.

- [2.45] Yamaguchi, Y.; Nishikawa, T.; Sengoku, M.; Boerner, W.M. "2-D polarimetric imaging by an FM-CW radar". Antennas and Propagation Society International Symposium, 1994. AP-S. Digest, Vol.3, Issue , 20-24 Jun 1994 Pages 1998 - 2001
- [2.46] Yamaguchi, Y.; Moriyama, T. "Polarimetric detection of objects buried in snowpack by a synthetic aperture FM-CW radar". IEEE Transactions on Geoscience and Remote Sensing, Vol. 34, Issue 1, 1996 Pages 45 - 51
- [2.47] Yamaguchi, Y.; Nishikawa, T.; Sengoku, M.; Boerner, W.M. "Two-dimensional and full polarimetric imaging by a synthetic aperture FM-CW radar". IEEE Transactions on. Geoscience and Remote Sensing, Vol. 33, Issue 2, 1995 Pages 421 - 427

Chapter 3 Initial Experimental Work

3.1 Aims and Objectives

It has been seen in the previous chapters that conventional microwave frequency detection methods have a limit of resolution due to both wavelength and pulse rise times. The rate of attenuation in a given medium affects signal to noise ratio as well as reducing the high frequency component of fast pulsed systems such as UWB as used in the Bristol studies by Craddock et al, discussed in the previous chapter. Clutter due to material inconsistencies leads to scattering that can result in further degradation in the accuracy attained in size and position location systems. A detection system that utilises both phase and amplitude information mostly removes this dependence on fast edges, making it possible to increase accuracy. With the constraints of the need for high frequencies removed, it should now be possible to use “lower end” microwave frequencies, say below 10 GHz yet still obtain resolutions far better than would conventionally be expected at these wavelengths. Such a scheme then facilitates a higher degree of penetration, improved SNR and a consequential lowering of power level requirement when used with many commonly encountered materials. As indicated by Fig. 1. 1 and shown in numerous studies of the dielectric properties of many frequently encountered constituents, at higher frequencies problems associated with conductivity and absorption start to become apparent [3.01][3.02][3.03][3.04][3.05]. In addition to these losses, frequency dependant permittivity effects can contribute towards dispersive effects at higher frequencies. This will be particularly problematic for pulsed signals where the high frequency component will become attenuated or completely removed causing further pulse “spreading” to that of the antenna based dispersion discussed earlier to occur. Again by using a phase / amplitude based detection method this permits the use of a single frequency and so can

facilitate the use of a frequency that can be tailored to that of a specific application; flexibly catering for variables such as material properties and frequency defined antenna separation. By combining these properties for use in a short range detection system, of the type used for non-destructive evaluation of objects with a known or homogenous structure, the aim is to improve on the dimensional resolutions currently demonstrated. Using a priori knowledge such as that available in most NDE applications, the following experimental work will seek to establish the bounds of phase and amplitude measurements at frequencies up to 6GHz, the upper limit of available resources. In the first instance an investigation will be carried out into the properties of a single frequency in the detection and location of an object placed between the transmission paths of two antennas. The objective being to establish if the relationship of phase and amplitude can be practically applied to location and detection scenarios at the frequencies of interest. Based on the outcome, a sensing antenna array will be developed. The properties of both the antenna elements and overall properties of the array structure will be investigated. When optimised, the resulting sensing structure should form a self-contained unit capable of remote operation. In order to take advantage of this it will then be necessary to develop a bi-directional signal delivery method that will preserve phase integrity and signal clarity. So as to allow the possibility of using this technique for remote inspection purposes a target distance of 1km was chosen. As standard electrical interconnects exhibit phase instabilities even over short distances as discussed earlier, a phase preserving optical delivery system would seem ideal to facilitate remote operation of the microwave sensing equipment. Phase relationship preserving optical systems that are normally associated with antenna array control and information retrieval are usually associated with highly complex systems containing expensive optical components of the type sometimes found in military systems. The objective of the optical system to be used here

was that it should not only be accurate but also possess the minimum component count and be of low cost in order to complement a viable measurement system. Overall the objective will be to explore experimentally the properties of the combined short range detection system and its associated optical, remote signal delivery scheme. In particular, attention will focus on low power minimum component count optical transmission.

3.2 Radio Frequency System (proof of concept)

In order to assess the viability of taking measurements using a microwave frequency radio signal, a basic bistatic transmit and receive arrangement was constructed. This consisted of two Omron WXA-N1SF (Figure. 3.1.) Ultra Wide-Band (UWB) antennas simply connected to an Agilent 8753ES 6GHz Vector Network Analyser (VNA).



Fig. 3.1. Omron UWB antenna

These antennas in standard form have a useable frequency range between 3 GHz and 5GHz and a reported dipole like omnidirectional, toroidal, radiation pattern. A specified gain of around 2dBi confirms the stated radiation pattern. A simple antenna rotation test using a network analyser and two antennas suggested that these devices were also linearly polarised. Whilst these antennas have an excellent working bandwidth, the omnidirectional radiation characteristics and inherent low gain meant they may be compromised for the purposes of detection. The wide RF distribution angles leading to extraneous reflections from outside the area of interest and the low gain leading to poor system dynamic range. Nevertheless, the small size of these devices represented a distinct

advantage for use in a short range “sensing head” arrangement where multiple antennas are to be deployed. Preliminary experiments indicated that measurable and distinct variations in the phase and amplitude of a single frequency signal transmitted between two antennas could be obtained when a reflecting metallic target is introduced. These variations were thought to be due to cancellation effects at the receive antenna. Due to differences in the path length between the directly received and reflected signals, a phase difference is present. On recombination of the two signals at the antenna, the two interfering signals can either constructively or destructively add, giving a phase / amplitude signature that is unique to a point in space as shown in Figure 3.2. This behaviour is similar to the Fresnel Zone fading effect that is experienced by wireless signals operating in highly reflective, multi path rich environments.

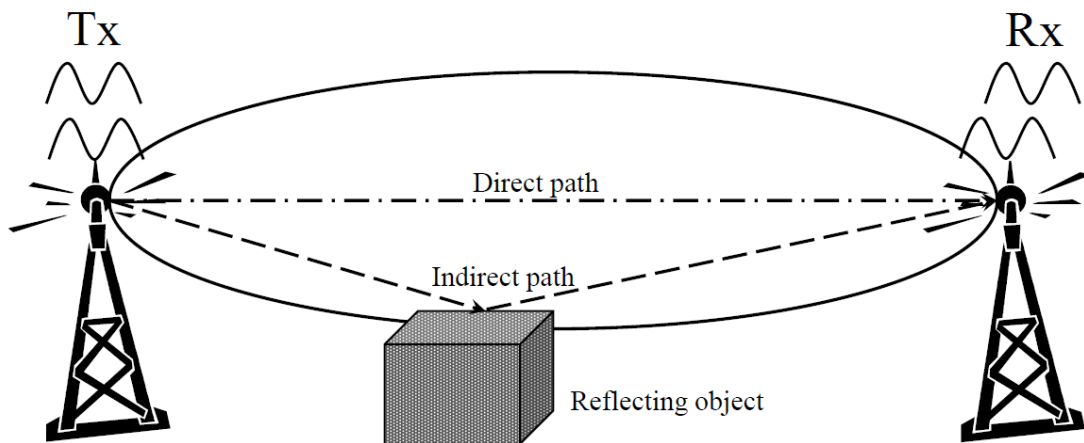


Fig. 3.2. Multi path phase cancellation

As mentioned in the previous chapters this “phase contrast” technique has been exploited for long range imaging and ranging purposes by the InSAR / IFSAR satellite imaging concepts. Here an adaptation of this technique was used at short ranges using the phase difference generated by the differing path lengths of the direct and reflected signal bouncing from a reflecting object. The initial proof of concept, experimental measurements were conducted using two Omron WXA-N2SL antennas mounted 9cm

apart on a 1cm spaced measurement grid, this equated to slightly more than one wavelength of the frequency to be selected. Each antenna was then connected to a Agilent 8753ES Vector Network Analyser (VNA), that was configured to measure the S_{21} (transmission loss) between the antenna pair. A “zero” calibration procedure was then performed providing a reference condition for the unimpaird signal path, the analyser would now only measure changes in the received signal due to the summation of direct and reflected transmission paths . With the VNA set to operate in Continuous Wave (CW) mode, simultaneous phase and amplitude readings could then be taken. A nominal frequency of operation of 3.5GHz was selected so as to be well within the frequency range of the antennas.

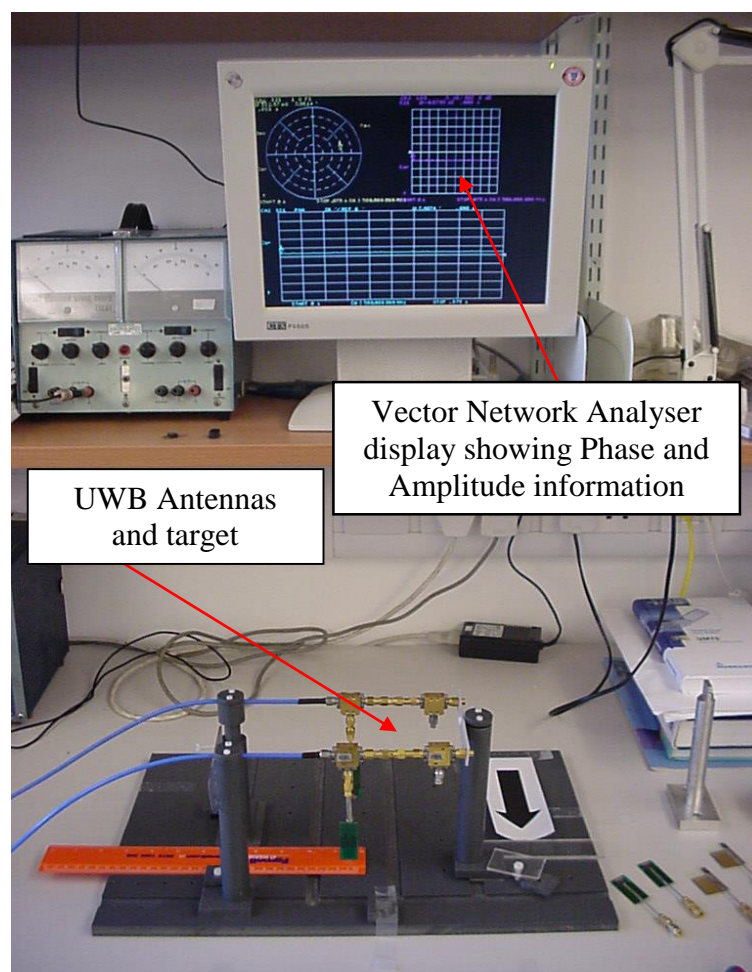


Fig. 3.3. Proof of concept experimental arrangement

As can be seen in Figure 3.3, a 2mm diameter metallic target was then introduced using a slider arrangement that permitted repeatable movements within the grid at 1cm intervals. As established earlier these antennas were linearly polarised and so were arranged so as to have a co-polar orientation with the framework. This procedure established the existence of easily discernable phase and amplitude values that were unique to each location on the grid as shown in Fig. 3.4. Here the vertical dotted lines indicate the target position distance between the two antennas placed at 1cm and 9cm on the grid. The distance from the sensing antenna pair is indicated on the solid horizontal lines and the corresponding values of phase and amplitude are shown on the X and Y axis of the plot. The representative antenna positions are indicated to the left and right of the plot.

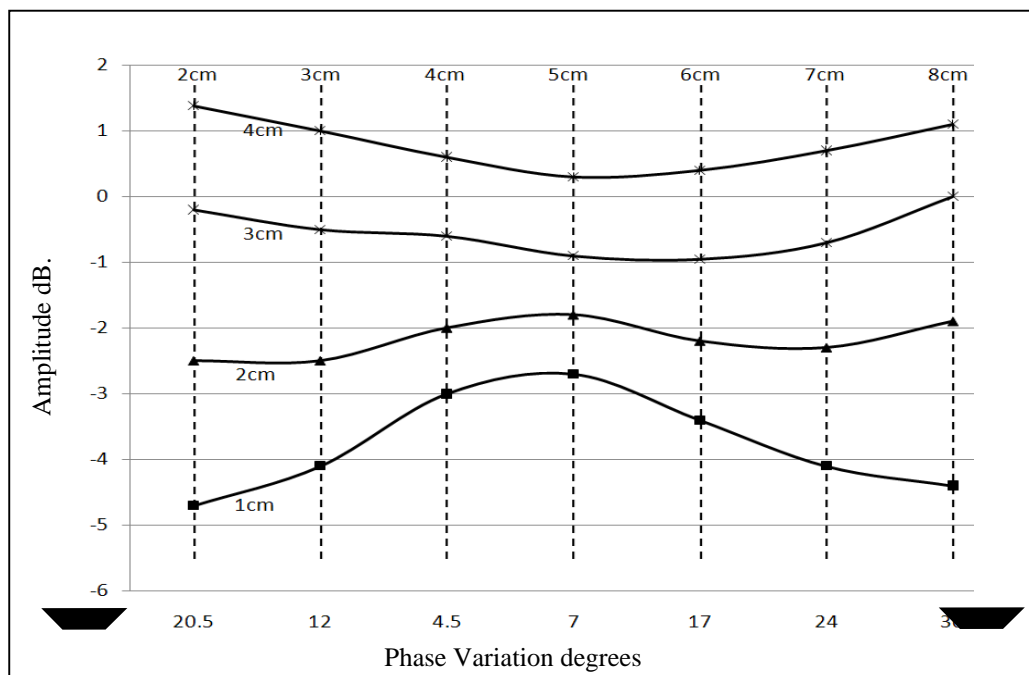


Fig. 3.4. Phase and Amplitude variation

This established a symmetry of values about the antenna pair axis, as well as indicating areas where a high rate of amplitude and phase variation occurred, possibly related to wavelength periodicity. Amplitude reduction being apparent around the 4.25cm half

wavelength centres. Figure 4. shows plots of phase against amplitude, with the target lateral distance up to 4cm and over a range of 2cm to 8cm between the antennas. At target to antenna distances closer than 1cm, measurements became corrupted, as in close proximity the target disrupted antenna function, also activity drops away towards 4.5cm minima. Changes in the frequency of operation could be used to optimise these regions of minimum activity. Discrete combinations of phase and amplitude values were recorded within the grid, indicating an area of reliable operation at a frequency of 3.5GHz. This could be used to advantage in the tailoring of antenna spacing and frequency choice to the size and material character of the object under investigation. Based on the above results, a triangulation-based mapping technique can be implemented to establish the sensitivity of the system. An example of such a relationship is shown below where the superposition of two cosine waves having relative amplitude and phase A and θ respectively, is given by:

$$y(t) = \cos(\omega t) + A \cos(\omega t + \theta) = A_1 \cos(\omega t + \theta_1)$$

Where: $A_1 = \sqrt{(1 + 2A \cos(\theta) + A^2)}$ and $\theta_1 = \tan^{-1}\left(\frac{A \sin(\theta)}{1 + A \cos(\theta)}\right)$

Referring to Fig. 3.5 below

$$\theta \cong \frac{\pi h^2 (x_1 + x_2)}{\lambda x_1 x_2} \text{ where } \lambda = \text{wavelength}$$

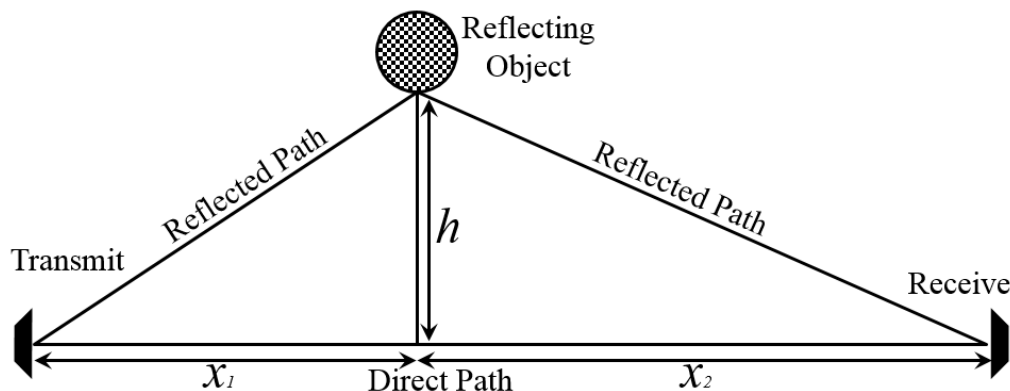


Fig. 3.5. Phase variation

Using such a method, in conjunction with a phase unwrapping algorithm and processing techniques [3.06][3.07] it may be possible to draw conclusions as to both the size and position of an object in the transmission path.

3.3 Tri – Antenna Array

Based on these results, a switched three antenna array was then constructed. Continuing to utilise the Omron UWB antennas, these were then mounted vertically around a 12cm circular, polycarbonate material, mount (Fig. 3.6.). Three polycarbonate support legs were arranged so as to hold the mount at 17cms above a baseplate that was engineered to allow repeatable target placement. RF connections to the antennas were via “Rhoflex” semi rigid cables and the use of right angled SMA connectors. Final antenna positions were measured as 7cm above the base plate and with a spacing of 9cm apart from each other. Using this structure, the characteristics and behavior of objects placed within the array will be further examined as will the interactions between the active antenna elements. Antenna Polarization / E plane orientation will be confirmed and target interaction within antenna E and H planes will then need to be proven. An operating procedure to establish optimal signal frequency and power levels will need to be established as will an optimised configuration for the VNA. Finally the purpose of this experimental stage will be to confirm the validity of the triangulation technique by obtaining identical readings between each of the three antenna pairs. With this relationship confirmed, the performance of the system with respect to object size and resolution could be evaluated. The VNA was then used as before to measure the forward transmitted values of both phase and amplitude values between each of the antenna pairs in turn, that would then form a three way bistatic antenna array. At this stage it was decided that for results to be repeatable, that a degree of system automation would be

necessary to enable signals to be switched around the system and also to allow the VNA to both generate and process the RF signal. Essential to this process was a method of switching the selected signal to be transmitted (and received) between each of the three antenna pairs as required. To facilitate this, a switching matrix was devised based around two models of Hittite Single Pole Double Throw (SPDT) RF switches. One type, (HMC536LP2E) being reflective, so un-terminated when open circuit, with an upper frequency limit of 6 GHz. The other (HMC270MS8GE) being non- reflective, terminated when open circuit, with an upper frequency limit of 8 GHz.

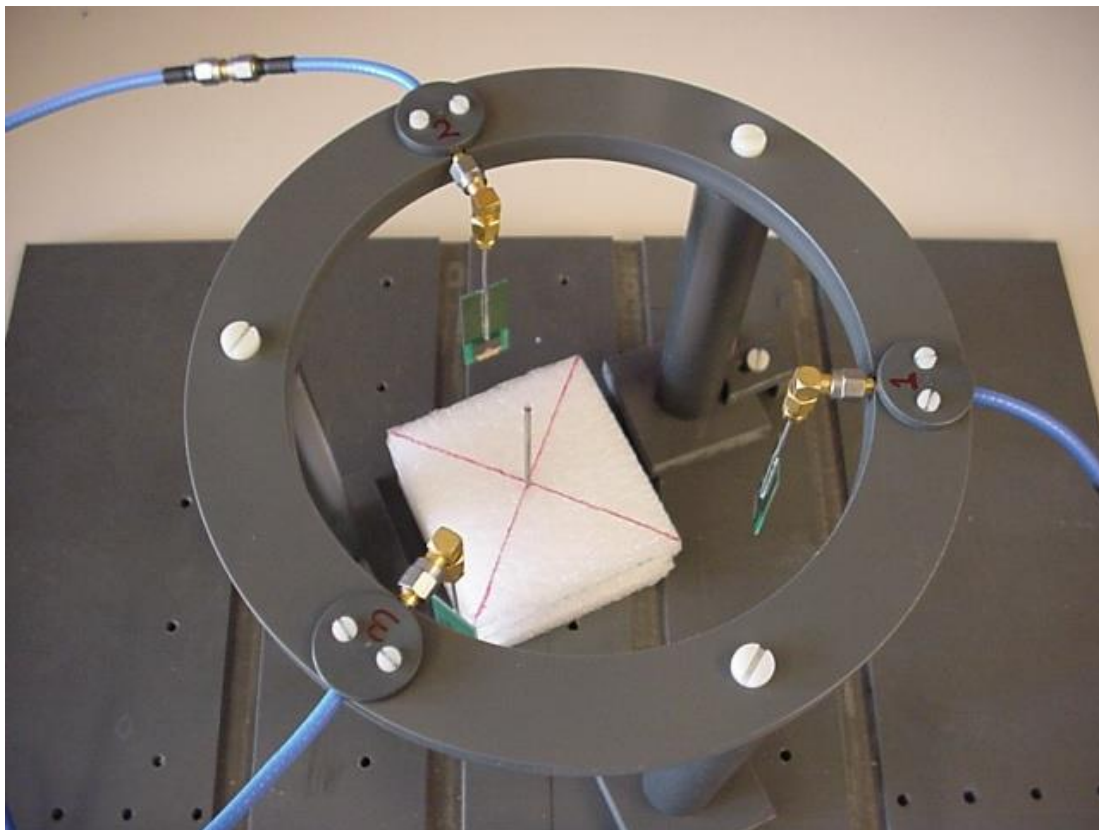


Fig. 3.6. Prototype antenna array

These switches were controlled by standard TTL logic levels, the required sequences for each mode of operation are shown in Figures. 3.7 a, b & c. Using un-terminated switches at this point in the circuit was not ideal, but was necessary as non-reflective switching

with this arrangement would lead to some of the RF paths being loaded when the switches were in the open circuit position. In the switching configurations shown throughout Figure 3.7, the area of most concern was at the “rf2” terminal of switch 3 where reflections may occur from Sw2 due to the open circuit created in mode 3. A Wilkinson type RF splitter (Mini Circuits ZX10-2-71S) with a frequency range of 2.95GHz to 7.1 GHz was used here to provide better than 40dB port to port isolation and so reducing any reflected power to a minimum. The completed switching sequencies for all three modes of operation, the antenna pair selection and signal paths are shown in Figures 3.7a, 3.7b, and 3.7c. together with the VNA connection operating in S_{21} mode. This did, however, lead to a 1dB imbalance in radiated power levels at the antennas. In practice it was found that this is easily compensated by the VNA channel calibration procedure.

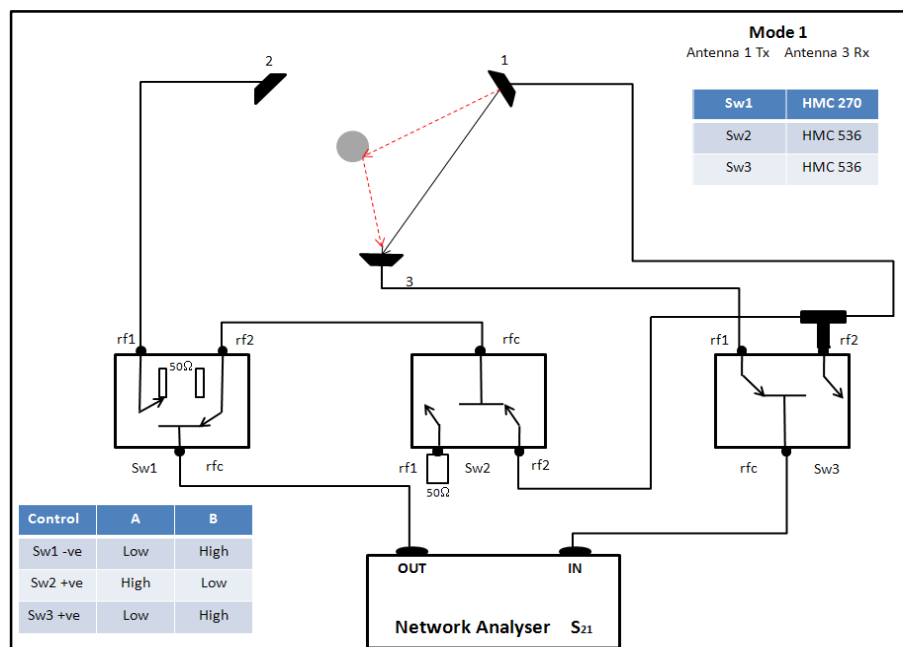


Fig. 3.7a, Mode 1. Antenna and RF switching arrangement

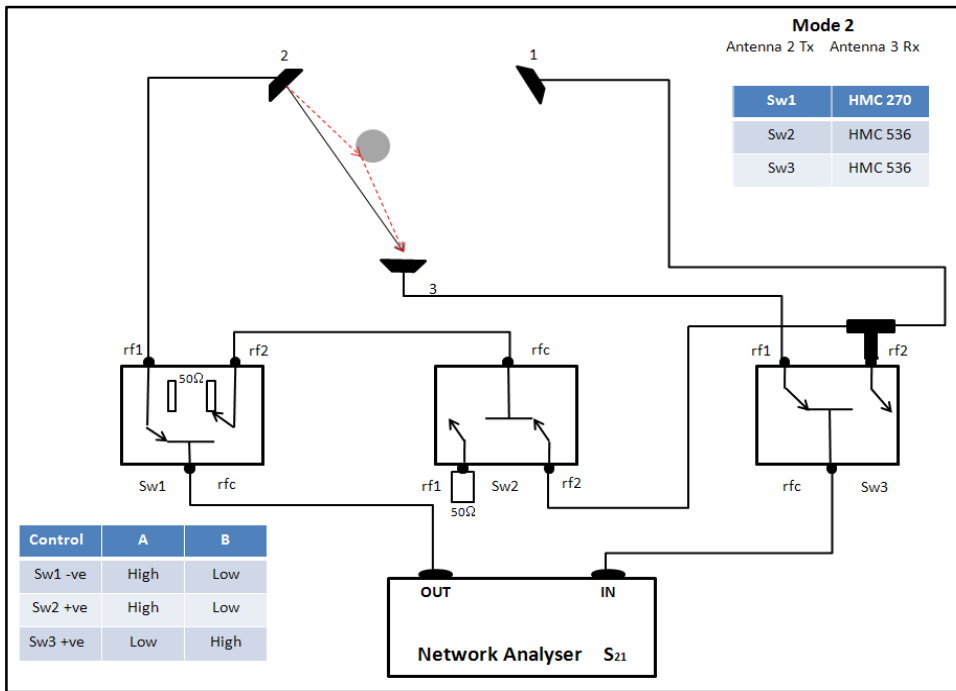


Fig. 3.7b, Mode 2. Antenna and RF switching arrangement

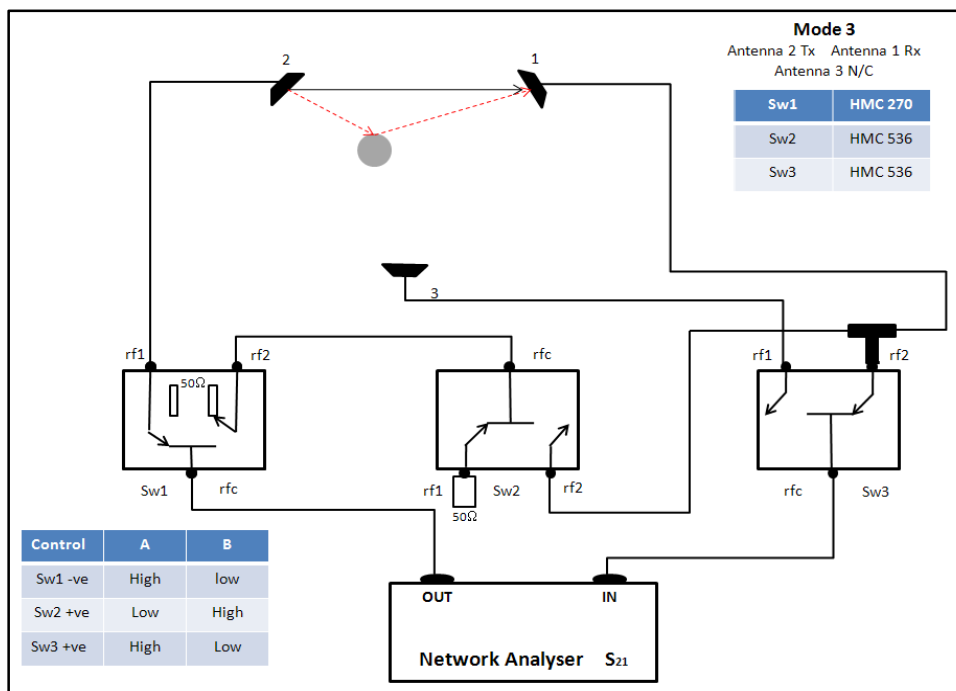


Fig. 3.7c Mode 3. Antenna and RF switching arrangement

With the antenna array and switching system design established it was then necessary to integrate this into the measurement system that could control both the VNA and the switch matrix sequentially. The overall system block diagram is shown in Figure. 3.8.

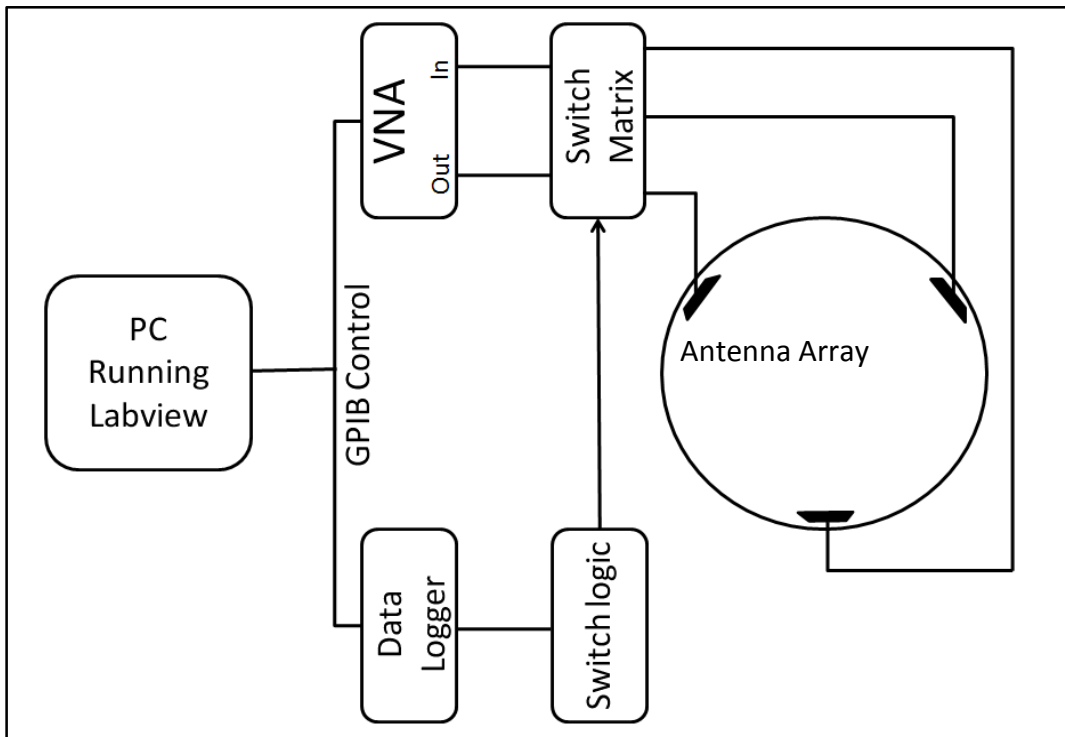


Fig. 3.8. Overall system diagram

Here the antenna array was directly interfaced with the switch matrix such that common input / output connection with the VNA is maintained in modes 1 to 3. Logic control circuitry as shown in Figure 3.9. provided the differential levels necessary for the switches to operate and also acts as an interface to the Agilent 34970A data logger. The purpose of the data logger was primarily to act as an interface that will allow computer control of the RF switching network. The desired sequences to select the appropriate RF switch settings were then pre - programmed into data logger in advance. Similarly the VNA was pre-programmed with frequency, power, span and display settings so that only these pre-set conditions needed to be recalled. This simplified the Labview program and speeded up the measurements. Both the VNA and the data logger are connected via their GPIB bus to a PC that is that is running National Instruments Labview software. In this way, both instrument control and synchronisation were established.

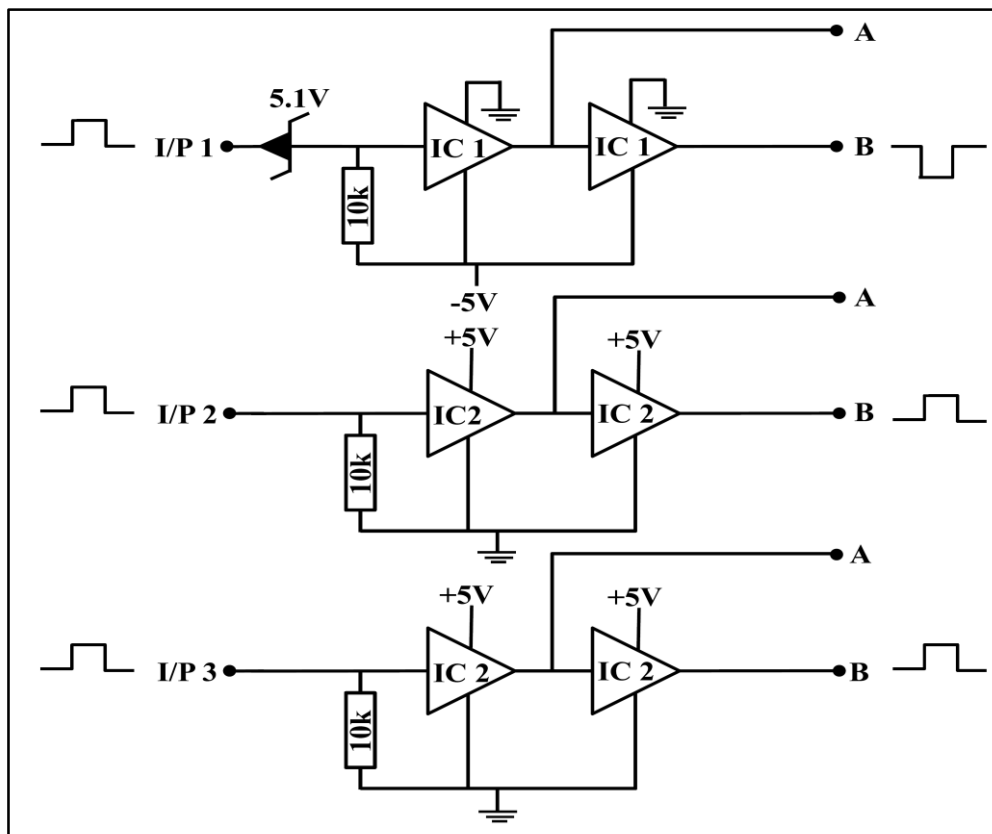


Fig. 3.9. Logic switch control circuitry

Two Labview sequences were devised, the first, to calibrate the VNA in each of the three measurement modes with the target absent, this was necessary to zero the “through path” between antenna pairs. The second sequence being designed just to take phase and amplitude measurements with the target in place.

3.4 Initial Investigations

The intention now was to use the information between each of the three antenna pairs to obtain values that would relate to the diameter of a centrally placed metallic (reflective) target. Ideally all three values would be the same and would vary identically as the target diameter is varied. A number of metallic targets were prepared, varying in diameter but all of 2.4cm in length. This length was chosen to avoid any possible resonance effects at

the chosen 3.5GHz operating frequency. These were then to be mounted in turn on a centrally positioned pillar made of a material with low dielectric constant so as to minimise any parasitic interference. In any case the calibration procedure would minimise any effects of the mount. Whilst positioning the mount it was noted that system sensitivity increased within a well-defined height range; this was consistent with the torroidal nature of the radiation pattern of a dipole antenna. With the targets positioned centrally to all three antennas and within the high sensitivity zone, measurements were taken over a range of 2.98mm dia. to 5.78mm diameter. Shown in Figure 3.10 are the resulting plots of phase and amplitude information taken between each of the three antenna pairs. As can be seen an acceptable match was obtained between all three modes with similar variations being indicated across the measurement range. However, a maximum phase variation of 0.4 degrees and a similarly small amplitude variation of around 0.15dB indicated very poor system sensitivity and an associated lack of resolution.

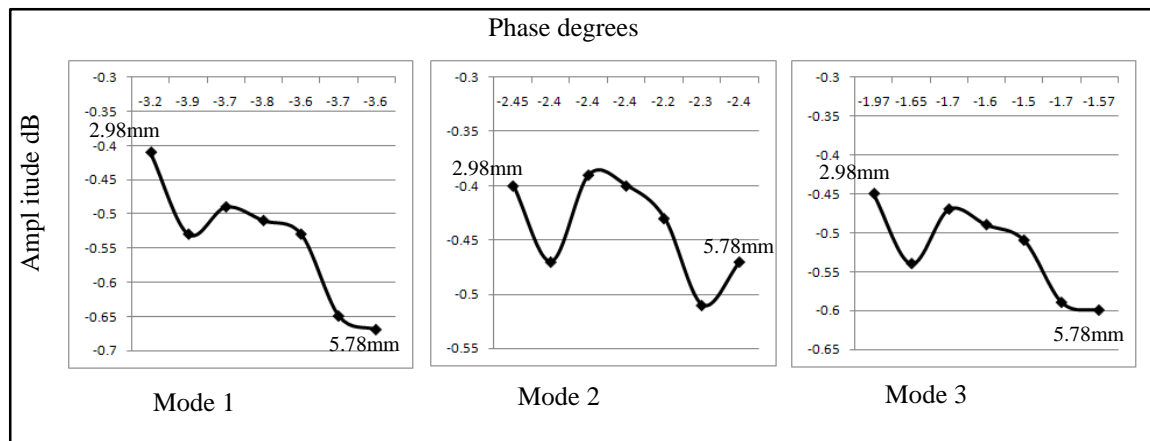


Fig. 3.10. Phase and amplitude variation with target diameter

It was decided to increase the frequency to 5GHz. This would have two effects. Any phase variation would be increased due to the shorter wavelength and the target at 6cm range would fall into a region of maximum amplitude slope variation as indicated in Fig.

3.11. With the increase in slope and the shortened wavelength a corresponding improvement in sensitivity could then be expected.

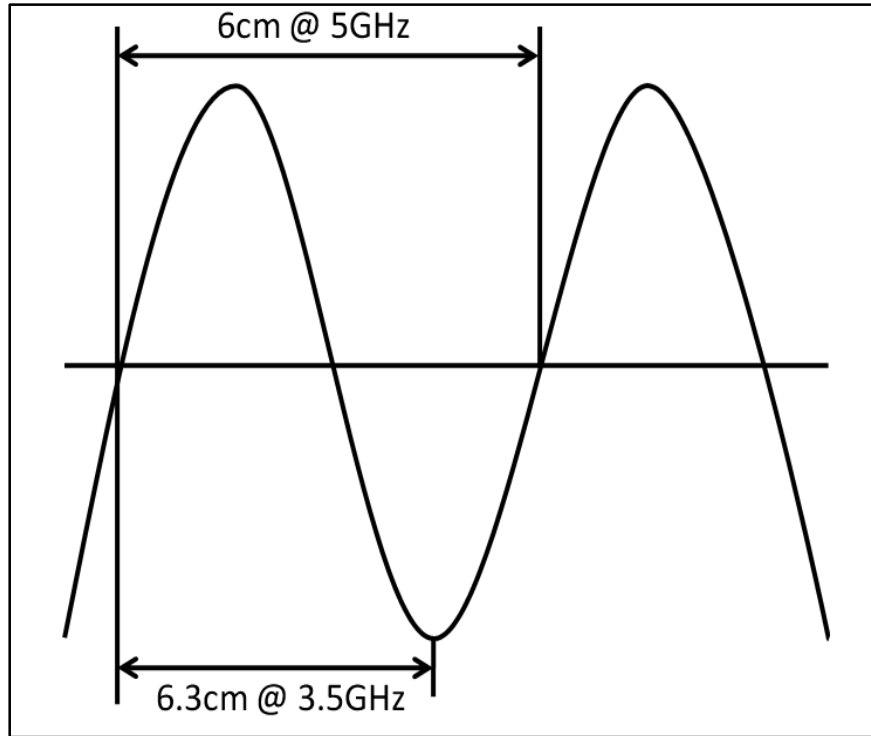


Fig. 3.11. Region of maximum amplitude slope

Figure 3.12. Shows the resulting plot in one mode of operation. A change of phase variation of 1 degree to 7 degrees over the target size range can be seen together with an amplitude change range of 0.4dB. This sensitivity increase was useful in confirming that the frequency of operation can be used to optimise the spacing of the sensing antennas as outlined above. However to show any practical improvement over current studies detection and resolution of objects significantly below 3mm - 5mm is necessary [3.08]. It was then decided to add a cylindrical reflecting ground plane around the outside of the antenna ring. This consisted of a Copper / Laminate material covering the entire sensing range of the antenna array. For practical reasons this was initially positioned about 5cms

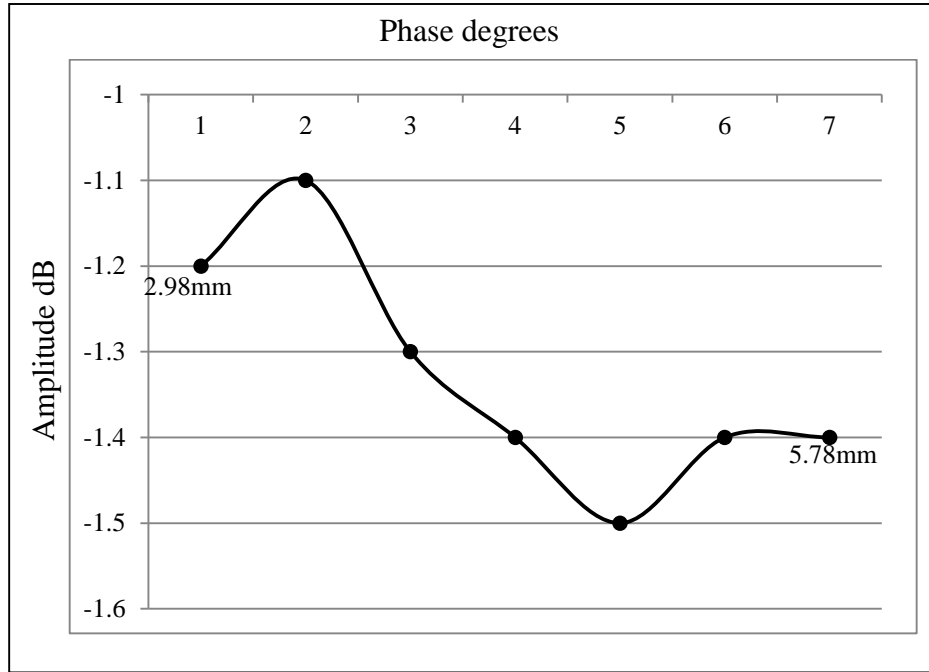


Fig. 3.12. Increased sensitivity at 5GHz

behind each antenna. This reflector would have two effects, firstly to prevent any unwanted radiation from the rear of the antennas producing spurious variations caused by the movement of nearby objects. Secondly, the resulting constraint of the RF field would change the radiation patterns within the shielding structure and so effectively increase the gain within the array. In this way it was hoped to further increase the effect. Figure. 3.13. shows that this gain increase resulted in an increase in the overall amount of phase shift and amplitude level but the amount of variation over the target range remained little improved at 5 degrees of phase and 1.2 dB in amplitude. At this point it was observed that even a 0.5mm x 24mm target placed in a vertical orientation in the central sensitive region of the antenna array produced 21 degrees of phase shift. Also if the target was then rotated to a horizontal orientation in the same area within the field there is little activity. This would suggest that sensitivity is at a maximum when confined to activity and

variations in the vertical plane. If the antennas have a dipole like radiation pattern then this would be consistent with the antenna E plane.

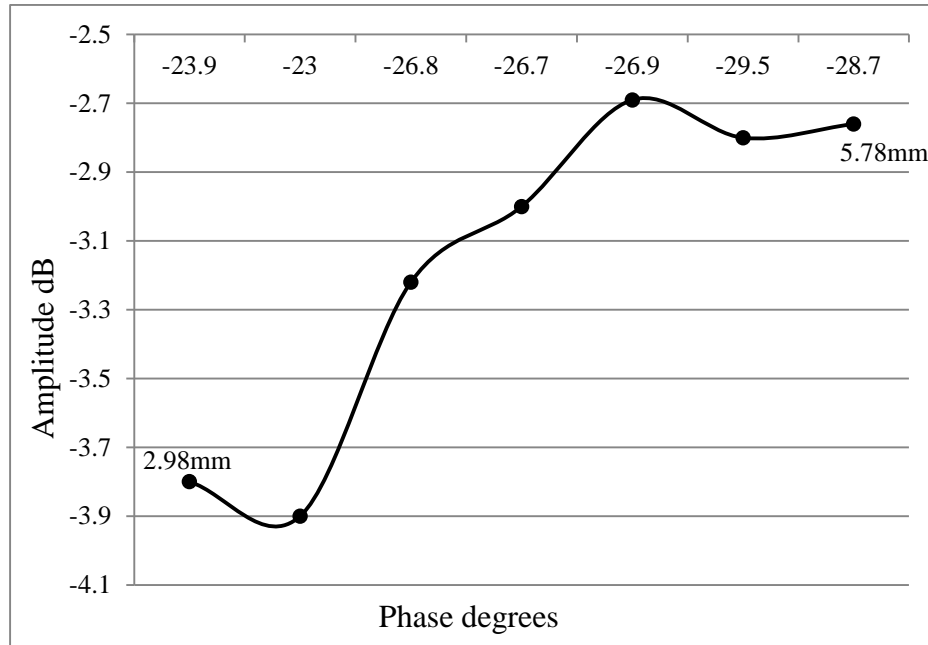


Fig. 3.13. Effect of the ground plane added 5cms from antennas

It also suggested that the antenna is strongly linearly polarised with the E plane confined to a vertical alignment in this configuration. In order to confirm this, two of these antennas were aligned so as to be co-polar, that is having identical alignments. One antenna was then connected to a Hewlett Packard 83711A signal generator running at a frequency of 5GHz. The other was then connected to a Rhode and Schwartz FSU spectrum analyser and the signal strength noted. One of the antennas was then rotated through 90 degrees so as to be cross polar. A 12dB drop in signal level was recorded indicating a corresponding degree of polarisation isolation. If this was the case, then the measurements so far were conducted across the antenna array H plane. In trying to measure target diameter variations, in this horizontal orientation H plane (cross polar) measurements were effectively executed. Such variations would be less sensitive than

those made under co- polar E plane conditions. In order confirm this assumption and also to ascertain the effectiveness of the ground plane addition, the structure was now moved into close proximity with the antennas in the array. Figure 3.14. shows the completed structure with the shielding ground plane in place. In doing this a further increase antenna directivity by further reducing back radiation could be expected. Any disparities in the shape or positioning of the shield relative to each antenna element would be more likely to produce differences in the performance between each antenna pair, as proved to be the case. Overall performance was enhanced, but considerable differences in sensitivity were now apparent between antenna pairs.

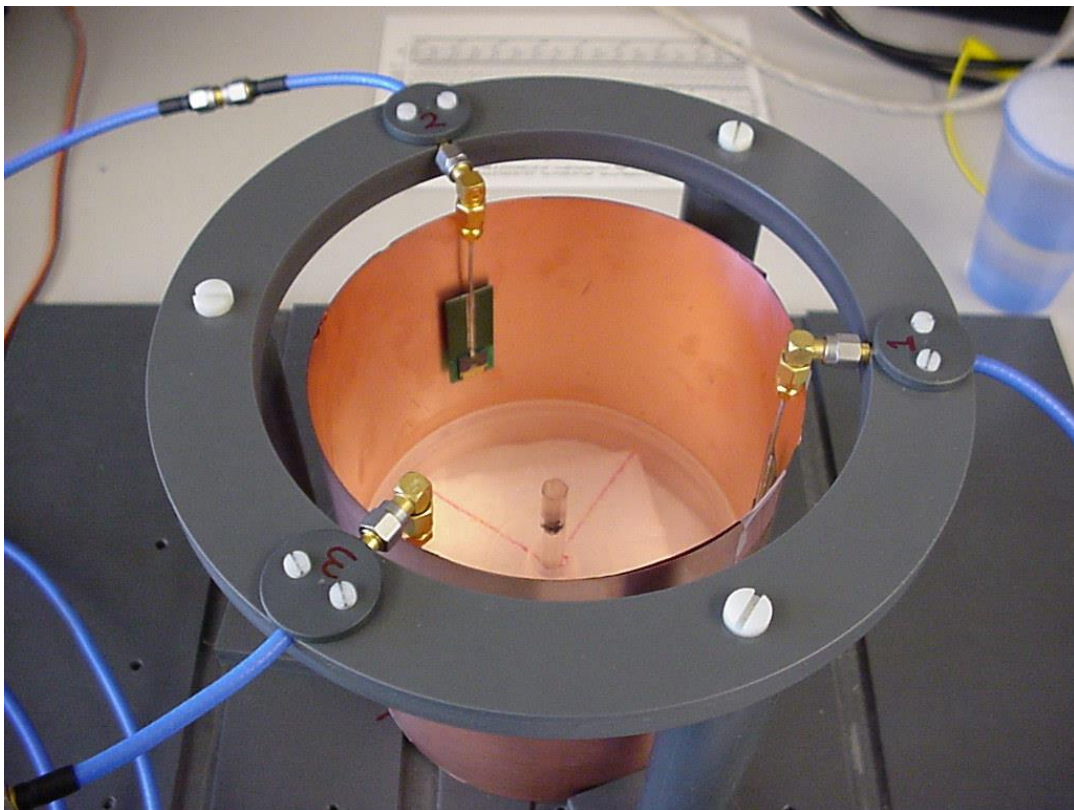


Fig. 3.14. Showing the position of the ground plane

Figure 3.15. shows the performance of the system in that of the most sensitive mode. On insertion of the target, an impressive 46 degrees of phase shift and over 4.5dB of amplitude variation was recorded. Although these changes were larger than those

recorded previously, this configuration was extremely sensitive to ground plane position, which in turn led to repeatability problems and so was abandoned. With such large initial changes when the target was inserted, it then seemed clear that the sensing array is indeed more sensitive in the vertically oriented E plane. Also that the array system gain would strongly influence the dynamic range and so the overall system performance. If so, measurements of target length, in this case, in the antenna E plane, would offer an acceptably improved measurement range and resolution characteristics.

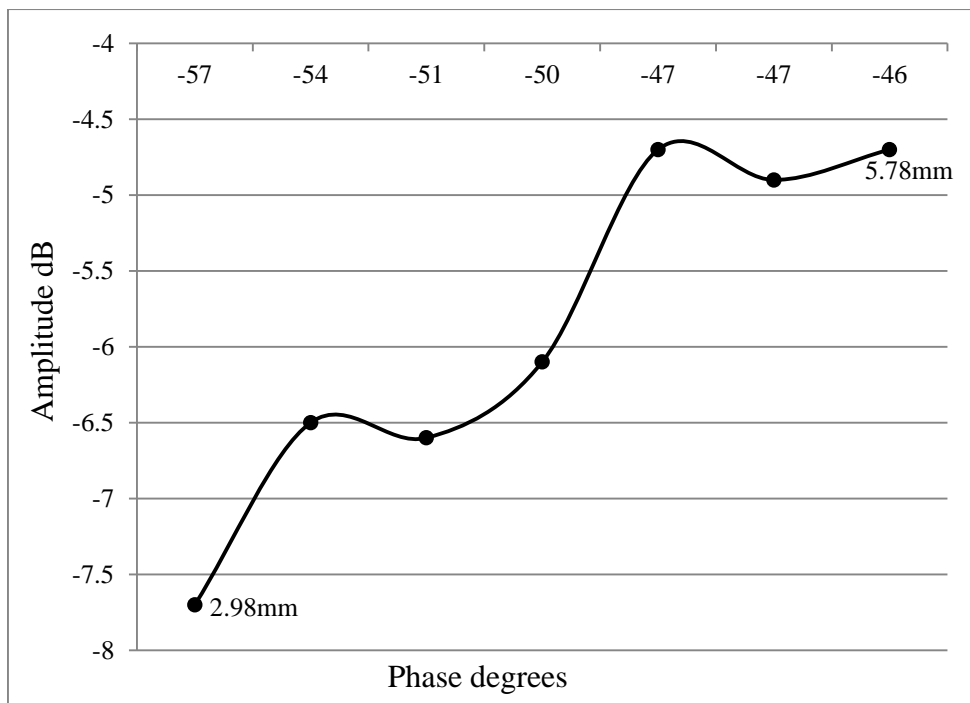


Fig. 3.15. Maximum sensitivity of target diameter measurements

3.5 E Plane Measurements

The shielding ground plane was then re-positioned to the outside of the supporting mount to a position 4cms behind the antenna array. This was determined so as to provide optimal gain advantage whilst not adversely affecting the sensitivity of array antenna positioning. A number of 3mm dia metallic targets were then prepared, varying in length

from 7mm to 20mm, in 1mm increments. These were to be mounted centrally to the antenna array as before, but this time on an improved PTFE ($\epsilon_r = 2.2$) mount. After adjusting the mount for maximum system sensitivity, these targets were then introduced, in turn and amplitude and phase variations recorded, this time in the now established, vertically orientated E plane. As can be seen in Fig. 3.16. clearly discernible data points are visible over the target size range with millimetre changes in size. Whilst amplitude varied by a little over 1dB, there was a credible phase variation of more than 40 degrees over the range measured, enabling a resolution potentially better than 1mm.

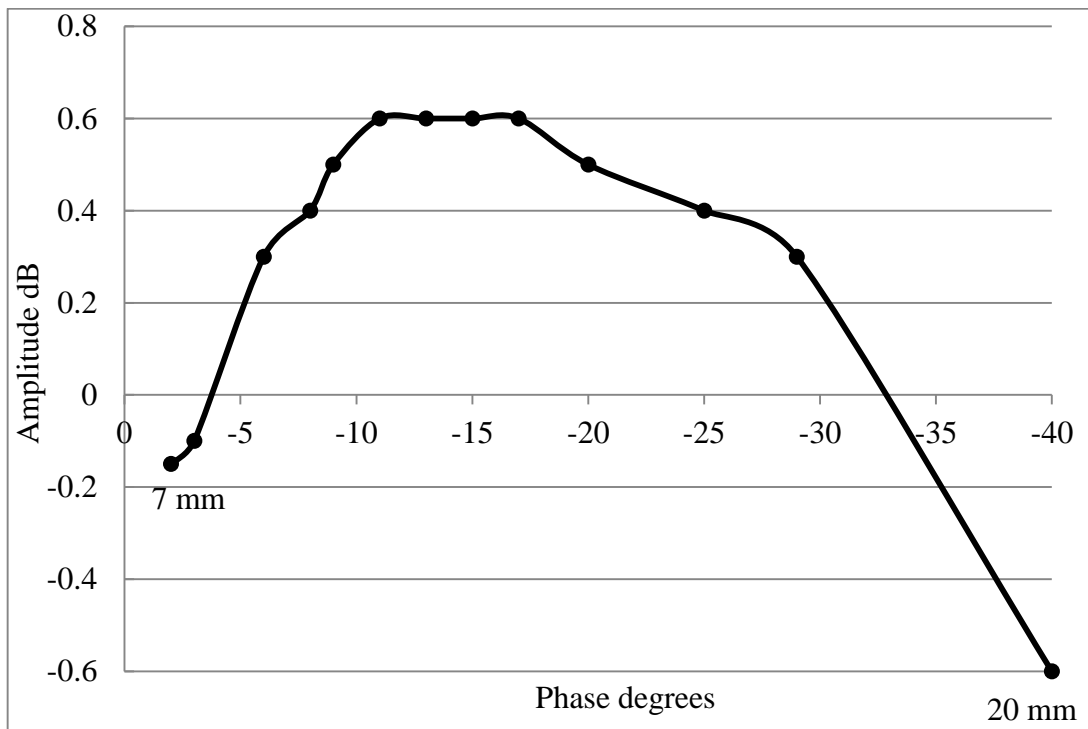


Fig. 3.16. E Plane, length measurements at 5GHz

3.6 Conclusions

Initial, proof of concept experiments indicated that the phase / amplitude relationship created when an object was introduced between two antennas could be used to determine information as to the objects position. It was established that measurable effects were

observable at dimensions far below that of the wavelength attributed to the sensing signal. Building on these observations a switched, bistatic, three way sensing array was constructed and optimised. Characterisation of the commercial UWB antennas indicated that they were linearly polarised and with a stated gain of 2dBi had a toroidal radiation pattern that produced a well-defined area of sensitivity within the array. The addition of a shielding screen both reduced the effects of external reflections as well as confining the radiated signals to effectively increase the antenna array gain. This in turn increases the dynamic range of the overall system and so leads to an increase in system resolution. Further system performance was found to be available by optimising the antenna spacing to coincide with areas of maximum waveform slope. This in fact also corresponded to an increase in operating frequency that inherently led to an increase in phase shift activity. Establishing the linear polarisation characteristic of the antenna introduced the ability to operate the system in the more sensitive E plane field of the array. Such polarisation dependence could then be used to advantage in that it opened up the possibility of using orthogonally separated measurement planes, so obtaining measurements in two dimensions. Such a measurement method lends itself for use where some prior knowledge of the materials under investigation is available. In particular, structures of a clutter free, homogeneous nature, where the electrical properties are known would be appropriate. In the fields of non-destructive evaluation and remote inspection these systems may prove a useful tool and would also be suitable for use in hazardous or difficult to reach environments. For this to be a viable proposition it will be necessary to develop a phase preserving method of connection between the sensing antennas \ switch matrix and the equipment used for analysis.

References

- [3.01] "Advanced Microwave Circuits and Systems", book edited by Vitaliy Zhurbenko, ISBN 978-953-307-087-2, Published: April 1, 2010. Radim Zajiček and Jan Vrba. "Broadband Complex Permittivity Determination for Biomedical Applications". Pages 365 to 385.
- [3.02] Ahmad Safaai-Jazi, Sedki M. Riad, Ali Muqaibel, and Ahmet Bayram. "Ultra wideband Propagation Measurements and Channel Modeling". DARPA NETEX Program. Report on Through-the-Wall Propagation and Material Characterization. Time Domain and RF Measurement Laboratory. Bradley Department of Electrical Engineering, Virginia Polytechnic Institute and State University, Blacksburg, Virginia 24061-0111. November 18, 2002
- [3.03] James Baker-Jarvis, Michael D. Janezic, Bill Riddle, Christopher L. Holloway. NIST Technical Note 1520, "Dielectric and Conductor-Loss Characterization and Measurements on Electronic Packaging Materials". July 2001 U.S. Department of Commerce.
- [3.04] Constantine A. Balanis. "Measurements of Dielectric Constants and Loss Tangents at E-Band Using a Fabry-Perot Interferometer". Langley Research Center, National Aeronautics and Space Administration. December 1969.
- [3.05] Sung-Mao Wu , Chi-Chang Lai, Hung-Hsiang Cheng, Yu-Che Tai, Chen-Chao Wang. "Frequency Dielectric Constant and Loss Tangent Extracting of Organic Material Using Multi-length Microstrip". International Conference Electronic Packaging Technology & High Density Packaging, 2008.008. July 2008 Page(s):1 –4.
- [3.06] T.Quinlan, S Dudley, T Jordan and S. Walker. "Remote, non-contact, radio frequency phase contrast detection using CWDM and directly modulated VCSELs". Antennas and Propagation Conference (LAPC), 2011 Loughborough. 2011 , Page(s): 1- 4.
- [3.07] Paul M. Meaney; Kieth D. Paulsen; Brian W. Pogue;and Michael I. Miga. "Microwave Image Reconstruction Utilizing Log-Magnitude and Unwrapped Phase to Improve High-Contrast Object Recovery". IEEE Transactions on Medical Imaging. Vol. 20, No 2, Feb 2001, pages 104 – 116.
- [3.08] Gibbins, D. Klemm, M, Craddock, I.J, Leendertz, J.A, Preece, and R A,Benjamin. "A Comparison of a Wide-Slot and a Stacked Patch Antenna for the Purpose of Breast Cancer Detection". Antennas and Propagation, IEEE Transactions on Volume: 58, Issue: 3, 2010 , Page(s): 665 - 674.

Chapter 4 Radio-over-Fibre, Phase Preservation

4.1 Introduction

Concurrent work conducted into the transmission of digitally modulated wireless formats over optical fibre (Radio over Fibre) being carried out in parallel with the antenna measurements described in the previous chapter suggested a potentially ideal solution to the signal phase preservation problem. This work focussed on the simultaneous delivery of Quadrature Amplitude Modulated (QAM) wireless formats that require accurate recovery of phase and amplitude information for the preservation of data integrity and continuity. Because the chosen wireless formats, by necessity are widely spaced in terms of frequency allocation and required relatively high operating bandwidths, this puts a significant strain on the optical transmission components. To further complicate matters these types of wireless signals use Orthogonal Frequency Division Multiplexed (OFDM) carrier generation with high peak to mean power ratios. Also by necessity these wireless formats require phase stability in the transmission medium. Such signals are widely used for wireless transmissions as they are resistant to multi path fading and so can work well in cluttered indoor environments. A principal difficulty exists here for the use of these signals in conjunction with optical transmission devices in that by their nature quadrature amplitude modulated OFDM signals require transmission systems with a high dynamic range. This was due to the fact that such signals inherently operated with peak to mean signal level ratios as high as 20dB. This would invariably stress optical devices and if not carefully managed can introduce distortion products that are in band to the wireless signals as well as surrounding formats. These distortion effects would lead to incongruities that would manifest themselves as unwanted deviations and collisions in

recovered data points that then lead to errors in recovered data. Whilst these commercially developed wireless formats rely on techniques such as error correction and adaptive data distribution, they represent a significant challenge to transmission over optical systems. A number of experiments were conducted, and described here, that demonstrated the suitability of directly modulated VCSELs and a Reflective Electro-Absorption Transducer (REAT) in the transmission of these signals up to a distance of 20 km. The development of the techniques that allow transmission of phase dependant wireless over fibre can then be applied to the delivery of similarly phase sensitive sensor signals. The following chapter describes the rationale and development of two optical transmission systems that would be adapted for use with the sensor system described in the previous chapter.

4.2 Quadrature Amplitude Modulation

Digitally modulated wireless signals in their most basic form can be represented as a signal where the phase of a carrier signal is altered by the application of a digital baseband sequence. If this phase shifting is arranged such that it is either 0 degrees or 180 degrees depending on whether the modulating signal is a logic “zero” or a “one” then a binary phase shift keying (BPSK) signal is said to result [4.01]. In this case the signal can also be referred to as a 2-QAM (Quadrature Amplitude Modulated) signal. These signals are usually represented using a Constellation Diagram. An example for a BPSK signal is shown in Fig. 4.1. If a carrier is now split and phase shifted by 90 degrees, it can be independently modulated so as to provide a further two data points and create a Quadrature Phase Shift Keying (QPSK) or 4-QAM signal. Figure 4.2a shows the constellation diagram of a 4-QAM signal.

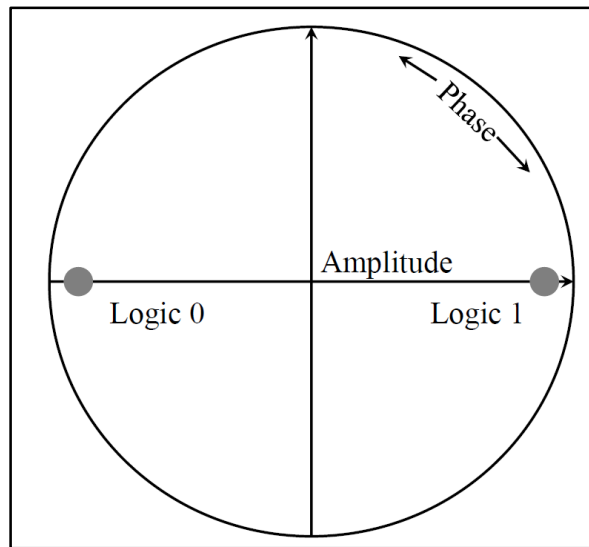


Fig. 4.1. BPSK Constellation Diagram

If further phase points are added the system can be expanded and with the addition of multi-level data sequences both phase and amplitude modulation produce the well-known 16-QAM constellation diagram shown in Fig.4.2b [4.02]. The differing data amplitude levels are represented by the dashed circles.

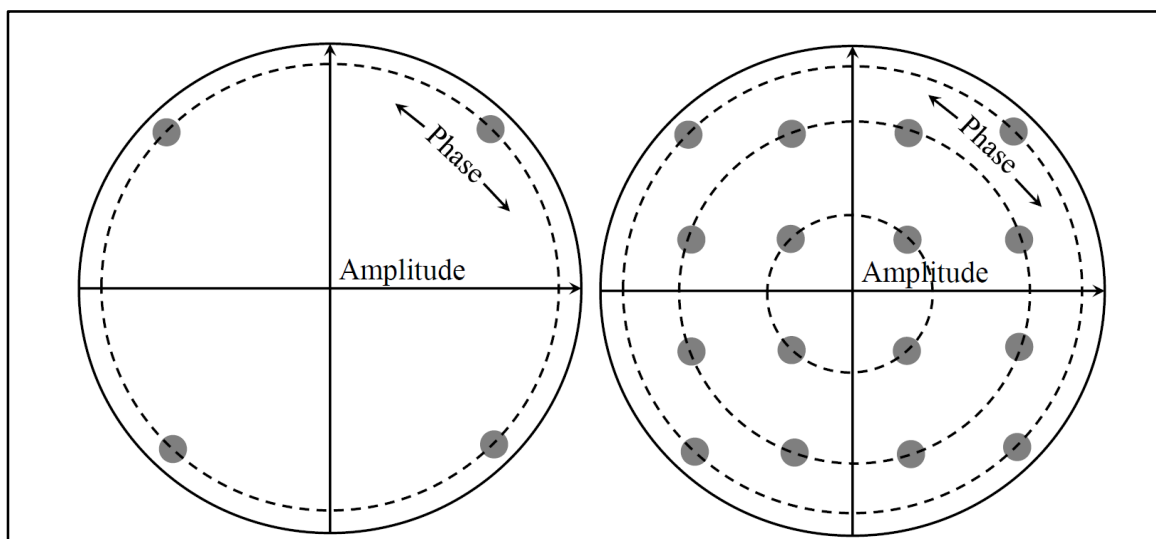


Fig. 4.2a. QPSK /4-QAM Constellation

Fig. 4.2b 16 QAM Constellation

In this way increasingly complex schemes can be constructed so as to improve data rates and transmission efficiencies. Increasing levels of modulation schemes and higher data rates lead to tighter constellation point densities, making it more and more difficult to recover information. A limit is reached when factors such as signal to noise ratio cause sufficient variation in the amplitude and phase stability to cause the points in the constellation to spread and collide. The constellations shown in Figs. 3a. and 3b are real examples of a Wimedia UWB constellation taken during the Radio over Fibre experiments to be outlined later. Here this process is clearly visible with distinct, individual, constellation points in Fig. 4.3a. and indistinct and merged data points in Fig. 4.3b.

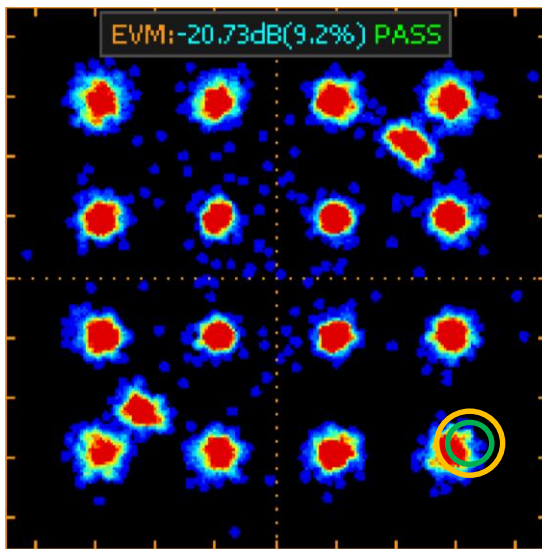


Fig. 4.3a Viable 16-QAM constellation

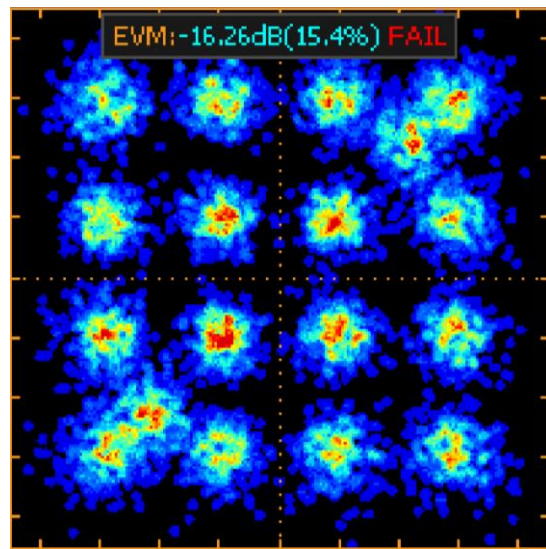


Fig. 4.3b Errored 16QAM constellation

4.3 Error Vector Magnitude (EVM)

Relevant to this work error Vector Magnitude (EVM) is recognised as the principal measure of quality of these complex, digitally modulated formats [4.03]. As can be seen in the above figures the degree of deviation from the ideal level experienced by each data

point is expressed in terms of EVM. As can be seen from Fig. 4.4. the error vector is derived from two components, one due to symbol magnitude variation and the other due to variation in the phase. Here the quadrant shown in the diagram relates to the real data point circled in Fig.3a. Normally expressed in dB terms and using the RMS power of each term EVM can then be defined as;

$$EVM(dB) = 10\log_{10} \frac{\text{Power,Error vector}}{\text{Power,Perfect magnitude}} \quad (1)$$

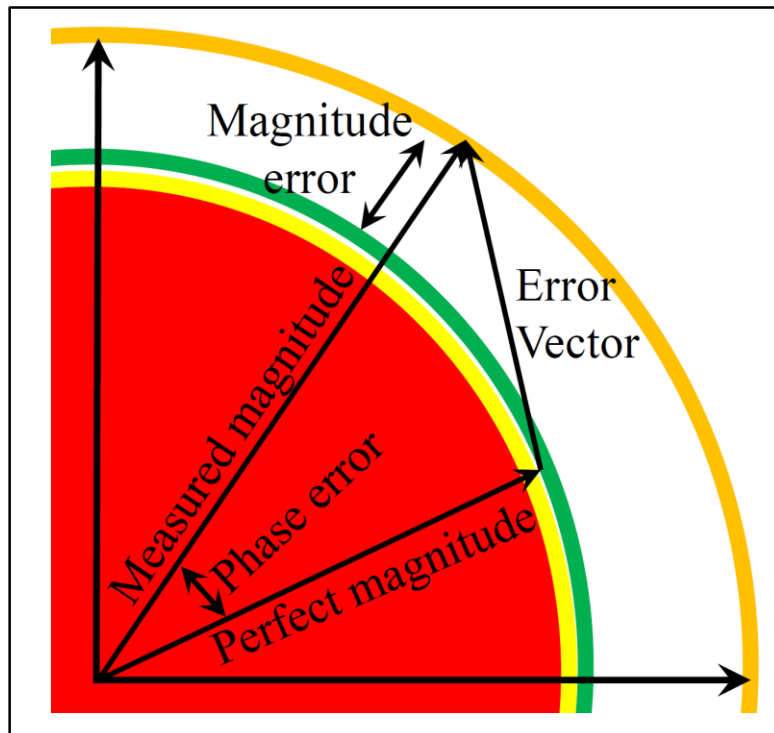


Fig. 4.4. Derivation of Error Vector

EVM measurement is the principal system quality indicator in these digitally modulated transmission schemes. If EVM is to be kept within acceptable levels, then any optical transmission system will rely heavily on phase and amplitude stability for optimal data delivery.

4.4 Reflected Modulation Method

Early work using VCSEL and a R-EAT [4.04] indicated that these devices used in combination were capable of delivering viable Wimedia UWB signals in a half-duplex format over a distance of 1km. This device had the property of behaving as a photodiode at 1300nm wavelengths (absorption mode) and as a reflective modulator (reflective mode) at 1500nm wavelengths. Taking advantage of this property, a CWDM optical transmission technique was employed. Whilst this early work was quite limited in scope it gave a good indication as to the capabilities of these types of optical transmission systems in relaying phase sensitive information. Reflective transducers used in bi-directional transmission systems offer the advantage of being able to place sensitive laser devices and users at risk. Later work that sought to use this R-EAT device at greater distances indicated that this device could be effective at distances up to 20km [4.05]. In order to attain this range, relatively high power lasers were used and the optical launch power adjusted to -1dBm at 1500nm and 5dBm at 1310nm to achieve minimum EVM at the respective receivers.

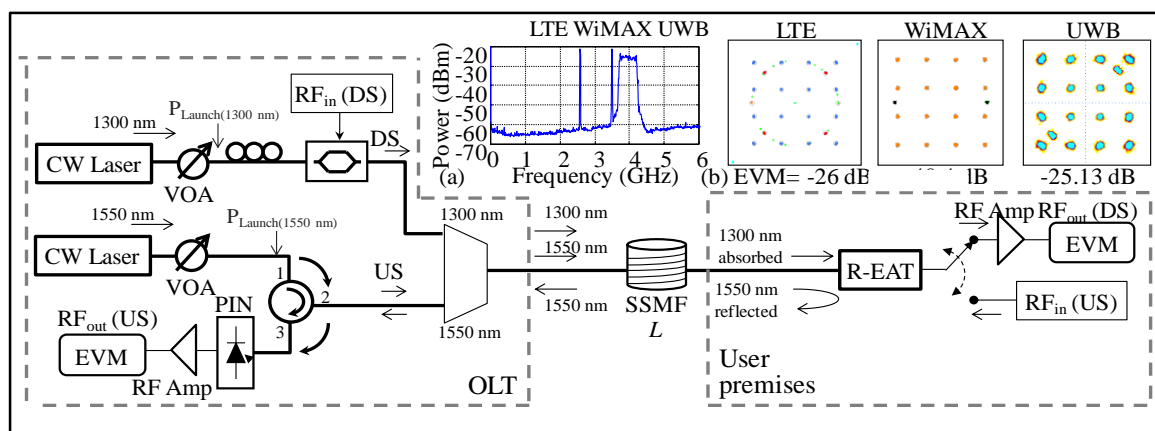


Fig. 4.5. Reflective transducer system diagram [4.05]

Figure 4.5. shows the experimental setup for the bi-directional optical transmission system. Here it can be seen that the 1300nm, absorbed path consisted of a continuous wave 1300nm laser (DFB-1310-BF-31-CW-FC-537) capable of a 15dBm power output. This was followed by an optical attenuator and a polarisation controller to facilitate the use of the Mach-Zehnder modulator (Covega LN-058) that was used to apply signal information to the downstream optical path. From this point the now modulated optical signal was applied to a CWDM splitter. This had the function of providing a connection to the single fibre pathway for both the 1300nm and 1550nm wavelengths. Following the splitter, 20km of single mode optical fibre delivers the downstream signal to the R-EAT device which performed the necessary optical to electrical conversion. In the upstream direction, a CW 1550nm, 15dBm power output laser (Fitel FOL15DCWD-A8119270-B) followed by an optical attenuator was applied to port 1 of a 3 port optical circulator. *(This device was crucial to the overall functioning of the upstream signal path as it separated the unmodulated forward signal from the modulated return signal from the R-EAT).* At port 2 the unmodulated optical carrier was passed on to the 1550nm port of the CWDM coupler and from there through the single mode fibre to the R-EAT. At this point the upstream signal from the user was applied to the now reflective device in order to modulate the returning 1550nm optical signal. This now passed through the system in the reverse direction and enters port 2 of the circulator. Following this the signal emerged from port 3 and is converted into electrical form by a photodiode (Discovery DSC-R402-AC). It should be noted that a switch is required at the common RF port of the R-EAT in order to separate the upstream and downstream signals; this limits operation to a half-duplex mode only, in this configuration. It was now possible to assess the signal degradation over the signal path. The triple format wireless placed considerable stress on the optical devices and so careful adjustment of levels was required for peak

performance. Shown in Fig. 4.5a. is the RF spectrum and Fig. 4.5b. the constellation diagrams of the generated signals at source. To establish the extent that noise and non-linearities generated from within the optical devices would contribute to any degradation of the transmitted signal, “back to back” measurements were taken with the fibre link being replaced by a 1 metre patch cord. Figure 4.6a is measured in the 1300nm absorptive mode, it can be seen that there was a linear increase in signal quality as optical power is raised. In the case of the reflective path a trade-off between SNR and saturation occurs as the properties of the photodiode / amplifier combination also came into play. In Fig. 4.6b. it can be seen that relatively poor EVM’s at the lower optical power of -8dBm improved linearly as the power was increased past -1dBm. Until this point system noise was the dominant mechanism for degradation of signal quality. Past this point as the optical power was increased signal quality again begins to deteriorate, this time due to the onset of device saturation.

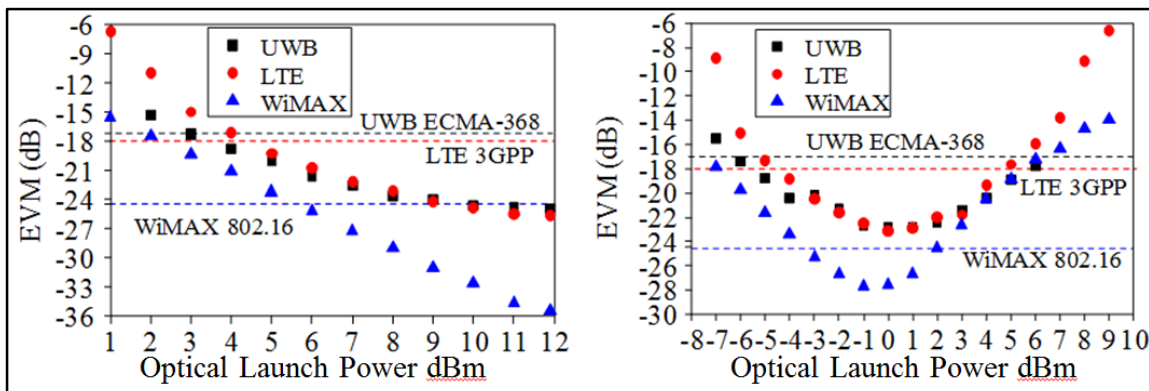


Fig. 4.6a. EVM / dBm at 1300nm

Fig. 4.6b EVM/dBm at 1550nm

Back to back performance indicated that at 1310nm the device contributed around 4dB to EVM degradation, whilst at 1550nm the figure was higher at around 12dB. EVM readings were then taken at optimal optical powers for differing fibre lengths. In Fig. 4.7a and 4.7b. it can be seen that in both the upstream and downstream cases signal decay is

fairly proportional to fibre length, deterioration being straightforwardly due to fibre attenuation. Figures 4.8a and 4.8b depict the received corresponding constellation plots for all three wireless formats at both wavelengths.

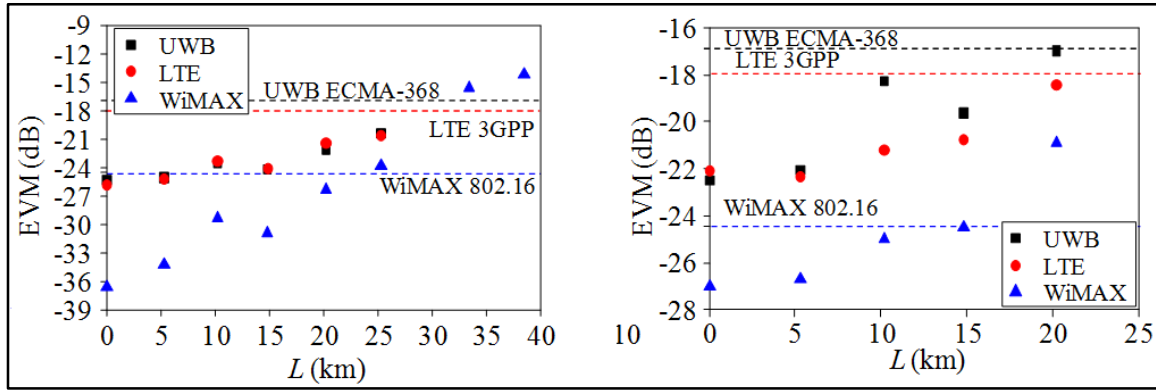


Fig. 4.7a. EVM / km at 1300nm

Fig. 4.7b EVM / km at 1550nm

It should be noted that the reflected 1550nm signal travels twice the distance, this may account for some of the increased signal deterioration. Also it can be seen that the WiMax signal is particularly sensitive to degradation. This is due to its close proximity to the UWB spectral component; any device induced distortion (due to non-linearity) may produce intermodulation products that will impact on the neighbouring Wimax EVM.

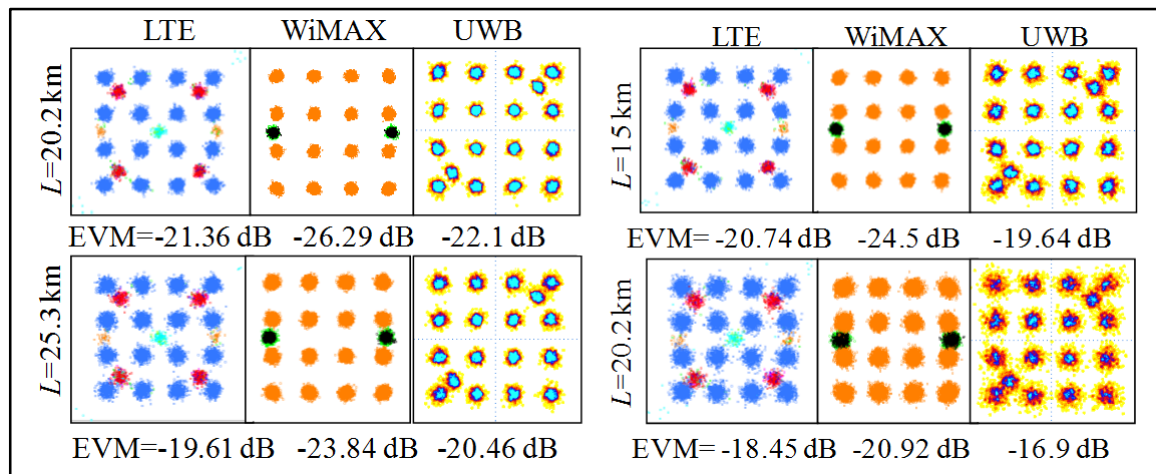


Fig. 4.8a. 1310nm Received signals

Fig. 4.8b 1550nm Received signals

4.5 Coarse Wavelength Division Multiplexing Method

The use of reflective transducers offered ease of remote deployment but raised concerns over full duplex deployment and as well as upstream / downstream isolation; these will be experimentally investigated later. A simpler and potentially more effective approach is to use the dual wavelengths to create individual signal paths. Each path can then be directed through a single optical fibre with the use of the CWDM splitter / combiners [4.06].

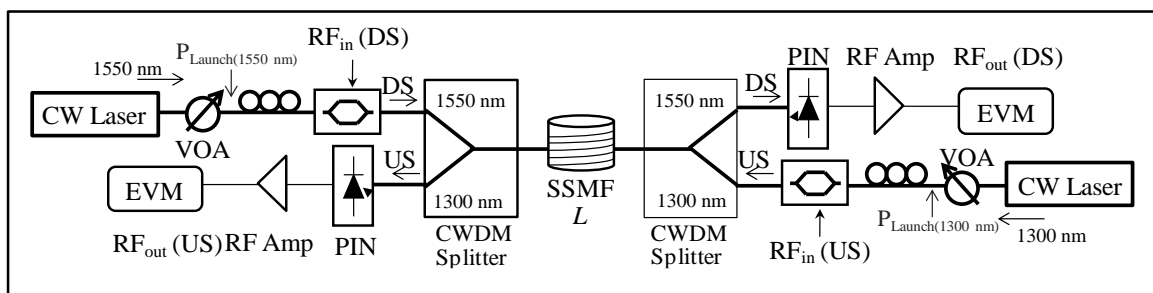


Fig. 4.9 CWDM experimental system [4.06]

Figure 4.9. shows the experimental arrangement deployed, as before the optical carrier was modulated using a Mach Zehnder (MZM) device, this time both at 1310nm and 1550nm wavelengths. Demodulation was also identical at both ends using a standard photodiode and amplifier combination. Each wavelength was then multiplexed / demultiplexed through the LAS-10-086 CWDM splitter / combiners to give upstream / downstream isolation of 40dB. With such isolation full duplex simultaneous transmission was readily accomplished.

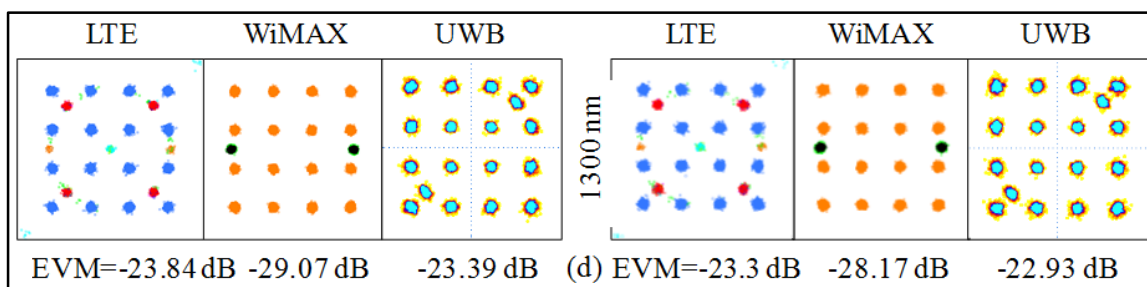


Fig. 4.10a. EVM for 1550nm (left) and 1310nm (right) at launch

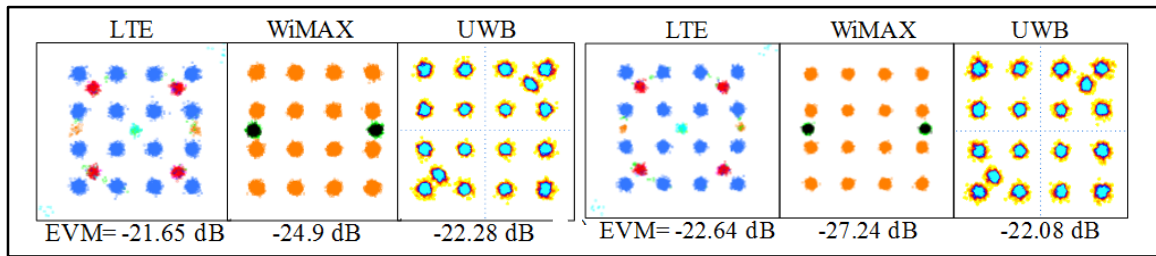


Fig. 4.10b. EVM for 1550nm (left) at 101km and 1310nm (right) at 50 km

EVM for each format was recorded at launch and at a distance where signal degradation was still at an acceptable level. The constellations shown in Fig. 4.10a are for a “back to back” 0km condition with a short patch chord replacing the fibre channel and as previously described with the optical power adjusted for optimum results. Due to the higher attenuation coefficient at 1310nm signals at this wavelength suffered signal degradation faster than the 1550nm optical channel. As can be seen in Fig. 4.10b a distance of 50km was covered at 1310nm with a signal deterioration of less than 2dB. At the 1550nm wavelength 100km was covered with similar results, the WiMax signal suffering most as before. This approach delivered greatly improved performance over the reflected method with less signal degradation and high upstream / downstream isolation due to the CWDM splitters.

4.6 Directly modulated VCSELs?

The CWDM technique provided improved performance and enabled a full duplex format but required the placement of active optical devices at the user site. As a result this environment presents many unknown factors and hazards that may affect device operation and lifetime. Ideally, remotely sited transducers will need to be simple, robust and low power. Conventional methods that use MZM’s that have bias variable phase characteristics and lasers that require cooling for stability lead to system complication and

consequently also have cost implications. An alternative was to use direct modulation, with the RF signal now being directly applied to the laser. As discussed earlier VCSEL's in particular lend themselves to this technique and also can be operated with a low power requirement at safe levels without the need for cooling. This makes these devices ideal for use with both the CWDM and R-EAT system architectures as outlined provided that sufficient bandwidth / frequency response and range can be supported. A critical consideration with directly modulated laser devices is that of matching the drive impedance of the VCSEL to that of the RF device supplying the signal (50Ω). This will affect not only the depth of modulation of the VCSEL but also can be used to shape the frequency response of the device to some extent as will be shown later. Direct modulation was facilitated by the use of a bias tee inserted between the RF signal sources and the anode of the VCSEL. Great care was taken to ensure that the signal path was kept as small as possible so as to minimise the introduction of stray inductances. Also when grounding the device it was found to be essential that any resonant effects due to induced currents in the ground path were avoided. Figure 4.11. shows a device mounted to a microwave tab SMA socket with the device anode connection kept very close to the SMA tab and. Device grounding was both through the body and via the cathode connection which was kept critically short. Resonance effects quickly appeared with variation from this layout. The assembly was adjusted whilst being monitored using an Anritsu 37397D Lightning VNA connected to the laser optical output via a Discovery DSC-R402AC photodiode assembly. *(whilst the effect of the bias tee and connecting cables could be removed during calibration, this was not possible for the photodiode)* In this way both forward transmission S_{21} , its corresponding reflection characteristics S_{11} and the structure impedance could be monitored up to a frequency of 10GHz. As can be seen in Fig. 4.12. this procedure was carried out for both devices, at a current of 12mA and produced

optical wavelengths of 1344nm and 1544nm respectively. With the exception of an increase in bandwidth with current these plots remained relatively unchanged down to a bias current of 5mA and up to a current of 15mA where the measurement was stopped. Whilst mounting these devices it became clear that a trade-off became necessary between upper frequency roll off and the integrity of a 50Ω impedance match across the frequency range. By sacrificing flatness across the occupied bandwidth it was possible to some extent to boost the high end of the frequency range. In the example shown in Fig. 4.12. the maximum frequency requirement was 4.8GHz; after that, an even amplitude across the frequency range was the priority. Final impedance match and bandwidth measurement results are shown with markers indicating coincident measurement points so indicating impedance variation with frequency. Figures 4.12a. and 4.12b. show the power reflected (not admitted) by the structure, the sharp dip in the trace indicates a probable resonance effect. The marker positions indicate a coinciding loop in the Smith chart trace, again indicating a resonant effect. This may open the possibility of introducing a narrow band signal beyond the normal VCSEL range as indicated by the dashed circles. In Fig. 4.12c and 4.12d. it can be seen that conservative -3dB bandwidths of 5GHz for both the 1547nm and 1344nm devices was accomplished. Shown in Fig 4.12e. and 4.12f. impedance was well matched at 44Ω to 45Ω across the range in the case of the 1547nm VCSEL. Less so in the 1344nm case, with impedance varying from 34Ω to 18Ω at the -3dB point as shown in Table 4.1. The selected devices (Vertilas VL-1310G-10G and VL-1550-10G) comfortably operate in 8mA to 12mA bias current window producing approx. 1mW optical power output in the 1300nm range and 0.6mW in the 1500nm range with a frequency response up to 5GHz.

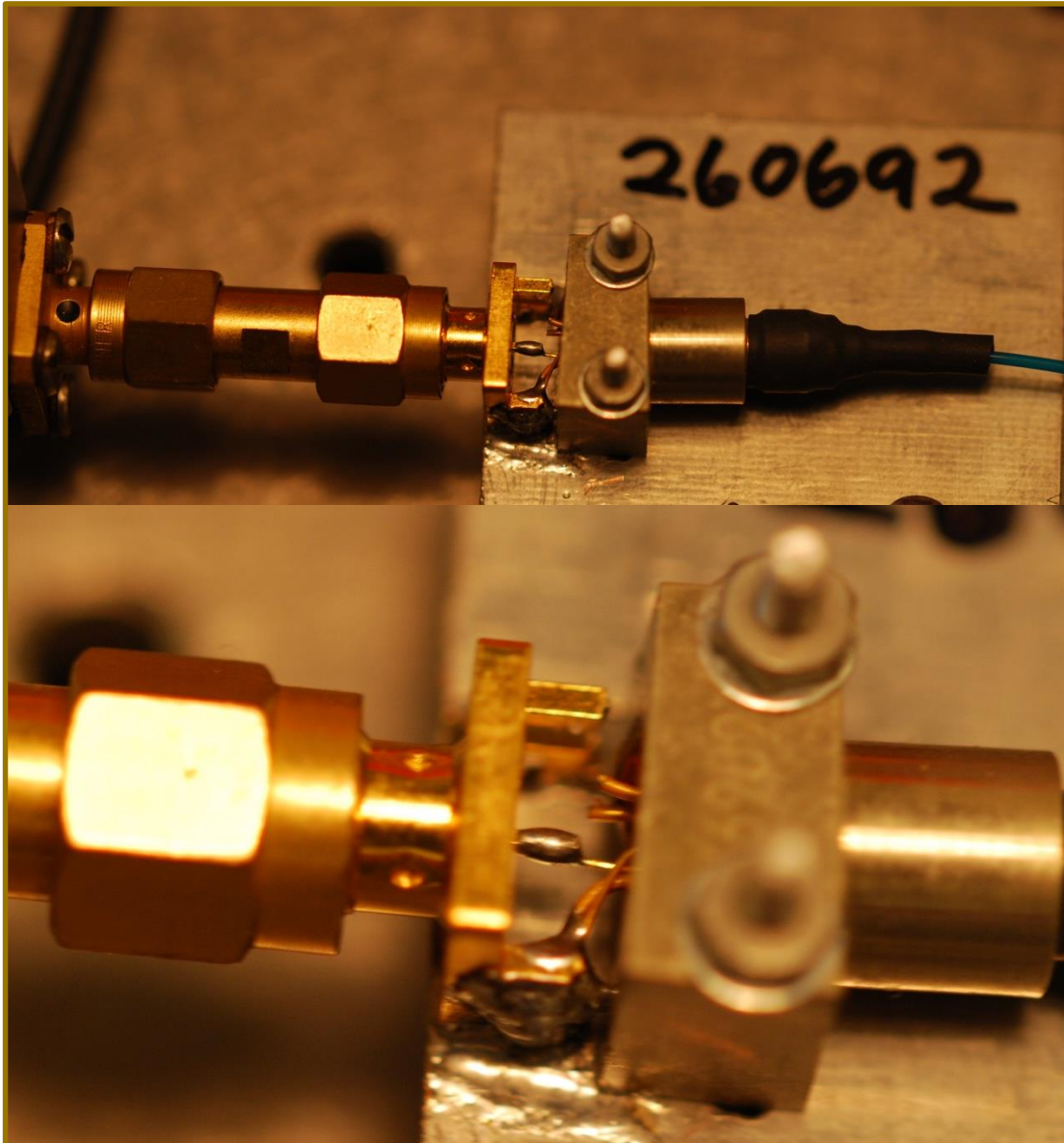


Fig. 4.11. Detail of mounted VCSEL

These devices are specified to vary in wavelength by less than 1nm over this range of current, making them ideal for uncooled operation in this type of application. With the suitability and behaviour of both VCSEL devices established a CWDM network was constructed with the initial aim of providing a low power high bandwidth solution for remote home access [4.07] [4.08]. In using a Wimedia UWB wireless signal this would also establish the suitability of this low power CWDM technique to deliver phase stable bi-directional information to distant destinations.

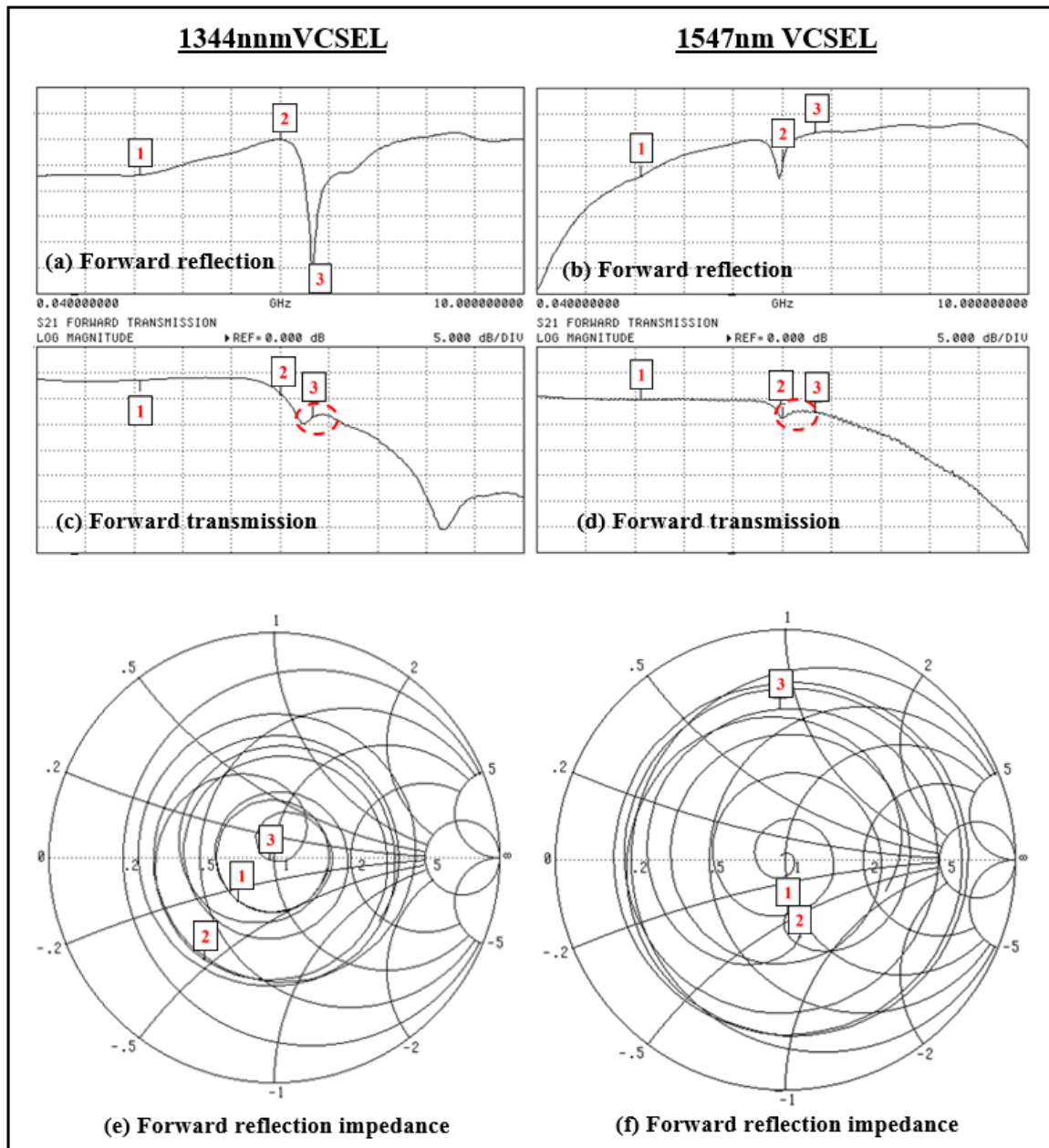


Fig. 4.12 Transmission and reflection bandwidth and impedance plot

Table 4.1. Mounted VCSEL performance parameters

Wavelegnth		1344nm	1547nm
Marker 1	2.1 GHz	(a)-17dB (c)-6.5dB (e)34Ω	(b)-17dB (d)-10.3dB (f)45Ω
Marker 2	5.0GHz	(a)-10dB (c)-9.2dB (e)18Ω	(b)-14dB (d)-13.8dB (f)44Ω
Marker 3	5.7GHz	(a)-37dB (c)-13.8dB (e)48Ω	(b)-8dB (d)-12.9dB (f)20Ω

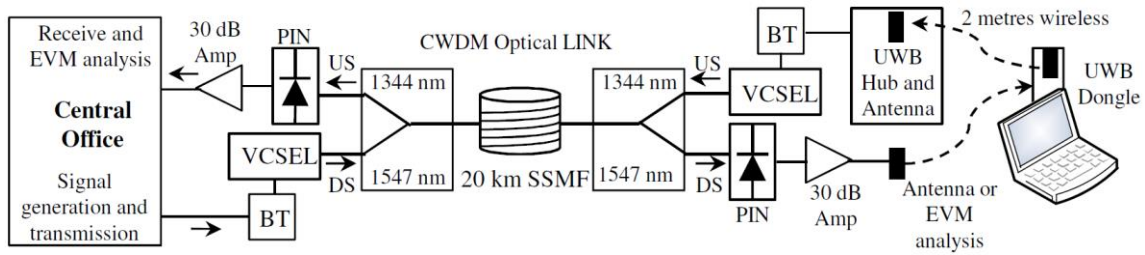


Fig. 4.13. VCSEL based CWDM experimental system [4.07] [4.08].

The experimental setup is shown in Fig. 4.13, at the core are the CWDM splitter / combiners and optical fibre as in the previously described method. The principal difference now was the much simplified optical delivery and low power requirements albeit at a shorter range. As with the previous investigations measurements were first taken at 0km so signal degradation over distance could be established. Figure 4.14. Shows the constellation diagrams and EVMs that were measured, also at this point RF spectrum plots were acquired as it was thought that a deteriorating signal to noise ratio would play an important part in understanding EVM degradation.

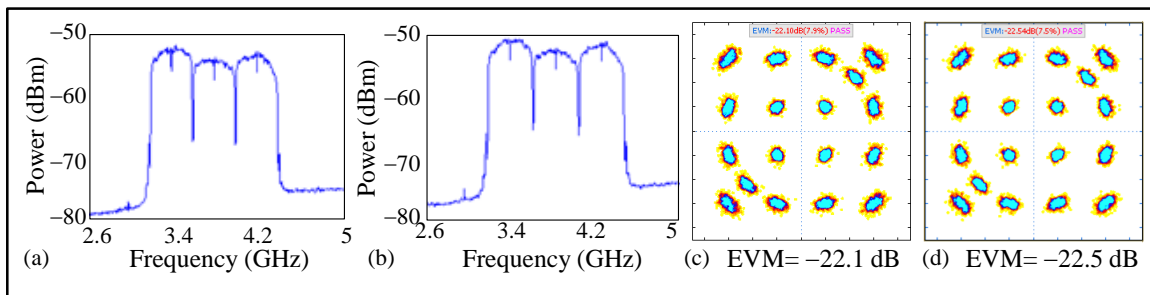


Fig. 4.14. RF Frequency spectrum and constellation at launch

With the modulating signal obtained directly from the UWB equipment it can be seen that EVMs of just over 22dB were obtained with an SNR of around 30dB. It was then decided to measure EVM performance against RF drive level for a fixed bias current, 12 mA was chosen as this was established as a safe maximum current.

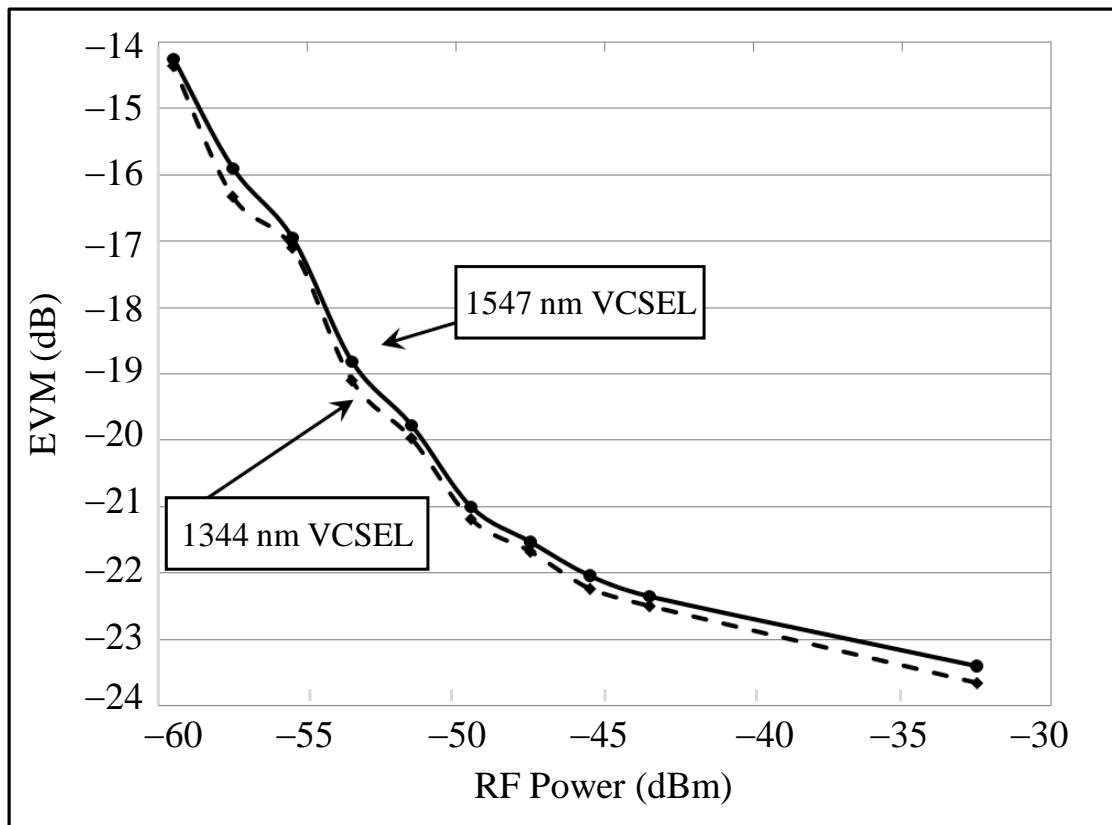


Fig. 4.15. RF power vs EVM a comparison of both devices (12mA bias)

As can be seen in Fig. 4.15, the EVM ranged from a poor -15 dB level at -60 dBm drive through to an acceptable -20 dB value further improving to approximately -23.5 dB at -30 dBm drive level. Interestingly both the 1344 nm and 1547 nm VCSELs gave similar results, suggesting that drive signal level was not particularly critical. Furthermore, little further enhancement in EVM was achieved with increasing drive level past this point as nonlinear contributions began to appear. From this it can be seen that either side of the -30 dB drive level EVM can be expected to deteriorate due to either poor SNR or distortion products related to device non-linearities. Two experiments were then conducted with the setup as shown in Fig. 4.13. In the first experiment the VCSELs were biased at 8 mA using the output directly obtained from the UWB device at a power level -44 dBm. At these levels a received SNR in the region of 25 dB was recorded at a range of

12.5km for the signals on both wavelengths as can be seen in Fig. 4.16a. (1344nm) and Fig. 4.16b (1547nm). This resulted in an acceptable signal EVM degradation of between 1.5dB to 4dB as can be established by comparing fig. 4.14.c with Fig. 4.16c. (1347nm) and Fig. 4.14d. with Fig. 4.16d. (1547nm).

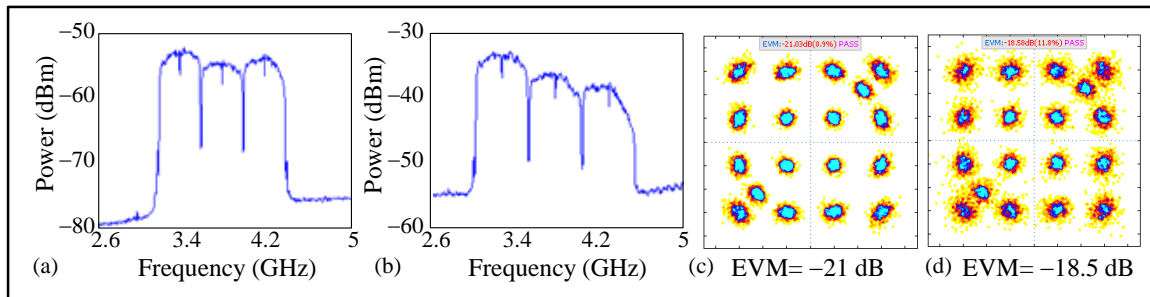


Fig. 4.16. Received signal plots at 12.5km 8mA bias current

In the second experiment the bias current was increased to the device safe maximum of 12mA and the RF drive level amplified to the -32dBm optimum identified in Fig. 4.15. Changing these parameters enabled the range to be increased to 20km and the increased bias also led to an extending of the upper frequency response limit in the 1547nm device. This effect can be seen when comparing the RF spectra shown in Fig. 4.17b. with that shown in Fig. 4.16b. where the consequence of the high end roll off can be clearly seen with the amplitude sloping off towards the high frequency end of the plot. Of more interest under these conditions was the apparent reduction in dynamic range in both the 1344nm (20dB) and 1547nm (15dB) associated spectra. It was likely that this was as a result of a combination of fibre attenuation and the production of in band distortion products. This was evident in the 1547nm case (Fig. 4.17b.) where clear signs of spectral re-growth were indicated. Even so signal degradation was maintained at around 4dB in both cases. These results probably represent the range limit of these devices with this type of signal as the safe operating optical power limit for the VCSEL would define

the signal SNR over the link and signal level will define the degree of distortion generated due to device non-linearity effects.

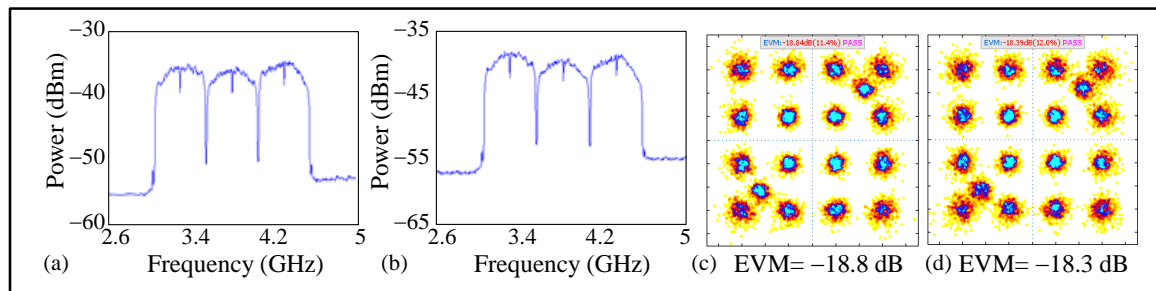


Fig. 4.17. Received signal plots at 20km 12mA bias current

This work was then expanded to further exploit the linearity of these devices across their available bandwidth by including two more wireless formats as before and a 2 Gbps baseband signal added [4.09]. Finally a detailed comparison of both the four format CWDM and reflected techniques was conducted [4.10].

4.7 Outline of some devices used

The following section provides brief descriptions of the optical devices used for the purposes of functional clarity only.

R-EAT: In this case the device used was a commercial development prototype produced by CIP, Ipswich, and as such the construction details were not available. It was essentially a Reflective Electro-Absorption Modulator (EAM) that had increased linearity. Early analysis inferred that this linearity was accomplished at the cost of device sensitivity and so was possibly operating in the more linear Franz-Keldysh effect region (Fig. 4.19. Below). A high degree of linearity was required so as to avoid the generation of in band intermodulation distortion in the spectrum of the wireless used. Due to the possibility of incursions from outside wireless sources it is also a desirable property to

protect the RF sensing signals to be used later. This device had two modes of operation, it is a photo-receiver at 1300nm wavelengths and a reflective modulator at 1500nm wavelengths. The functioning, electrical sensitivity, bandwidth and crosstalk properties of the R-EAT are characterised in detail chapter 5.

EAM: This is an active, semiconductor based device used for superimposing an electrical signal onto a laser generated light beam so producing a modulated optical signal. In these devices a variation in the strength of an electric field produces varying degrees of optical absorption by the semiconductor. This can be achieved by the application of a modulating voltage or signal. An example of a commercial EAM is shown below in Fig. 4.18.



Fig. 4.18. Example of a commercial EAM

There are two effects that make this possible, these are outlined in Fig. 4.19. As can be seen in the blue trace the Franz- Keyldish effect is the weaker of the two but produces a more linear progression to the absorption effect. When there is no electric field, minimum absorption takes place, absorption increases roughly in proportion as the electric field becomes more intense. In contrast the red trace showing the much stronger quantum-confined Stark effect (QCSE) shows little absorption with zero bias followed by a rapid

increase in absorption for very little increase in electric field strength [4.11] [4.12]. Such behaviour lends itself to the transmission of “baseband” digital signals but could present difficulties for wideband, modulated carrier and analogue formats.

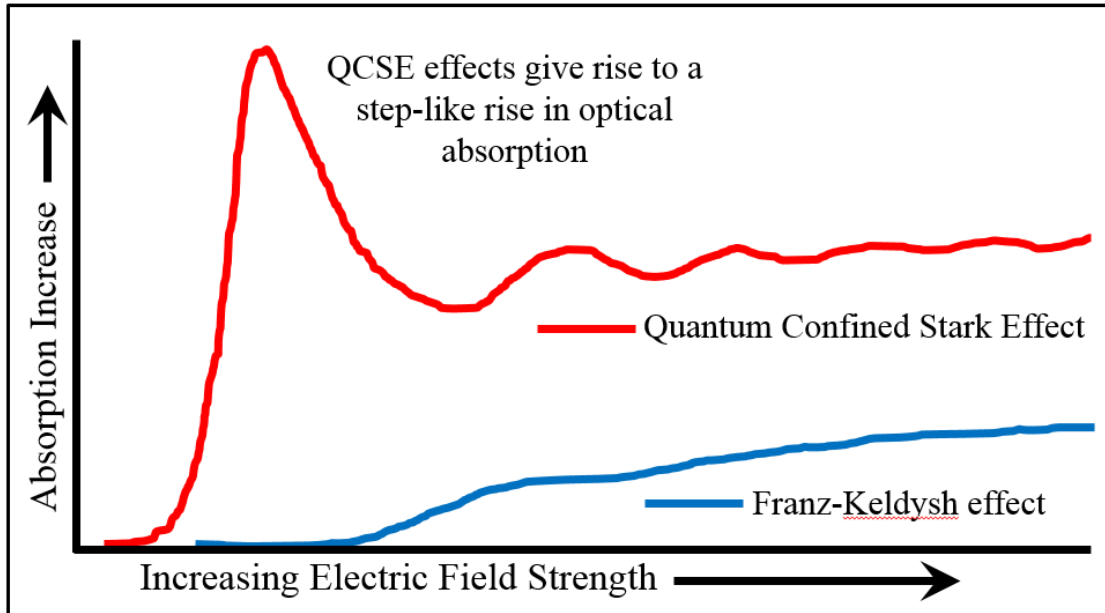


Fig. 4.19. Absorption Effects in an EAM [4.13]

MZM: Mach Zehnder Modulators (MZM) form the principal method of modulation used in many optical data transmission systems. These devices use electro-optic effects that can be induced in a crystalline structure. They typically consist of a device constructed of Lithium Niobate (LiNbO_3) whereby a laser light source is split at the input to the device and can then travel through two equal length paths. One of the paths however contains a length of LiNbO_3 crystal, after passage through this both legs are then recombined [4.14]. The essential functionality of an MZM is shown in Fig. 4.20. below. A feature of the LiNbO_3 material is that it is possible to vary the refractive index of the

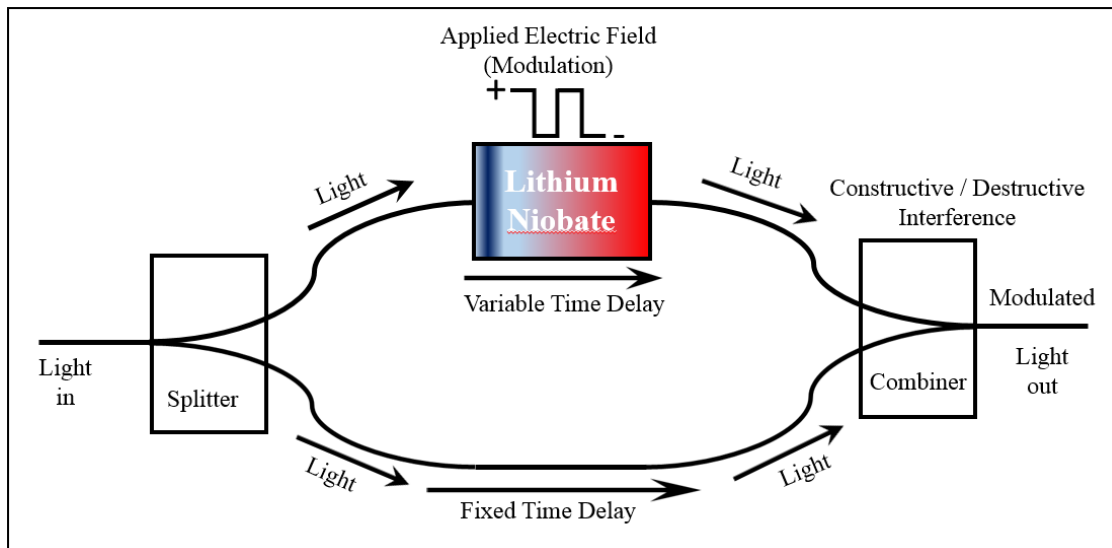


Fig. 4.20. Essential functionality of an MZM.

material by changing an electric field that is applied across the device. This may take the form of a DC bias or that of a data carrying signal, or both. By varying the refractive index the speed of propagation of the light can therefore be manipulated to produce interferometric effects on the combined output signal. This will result in either constructive or destructive interference in the light levels and so results in a modulated optical signal. In practice a combination of DC bias and data signals are necessary to produce symmetrical zero crossings of the data signal. Whilst this device is the modulator of choice in many instances it suffers two major shortcomings for use in this application. Firstly the phase variability with bias will almost certainly lead to system anomalies and secondly, MZM devices are also very sensitive to the polarisation of the optical carrier. This will inherently vary greatly with movements in the fibre so removing any advantages that would have been gained over cables by the use of optical remoting in the sensing system.

CWDM splitters: The devices chosen for this work were simple 1500nm / 1300nm splitters. These were low cost and gave an inherent isolation between wavelengths of up to 40dB. These are often constructed using a fused fibre technique [4.15] whereby two optical fibres are melted, fused together and twisted to form two wavelength specific passband regions. This technique is favoured for CWDM splitters of this type as it is a very low cost process and as can be seen in Fig. 4.21. (Taken from a commercial device) produces two distinct pass band regions having high isolation from each other.

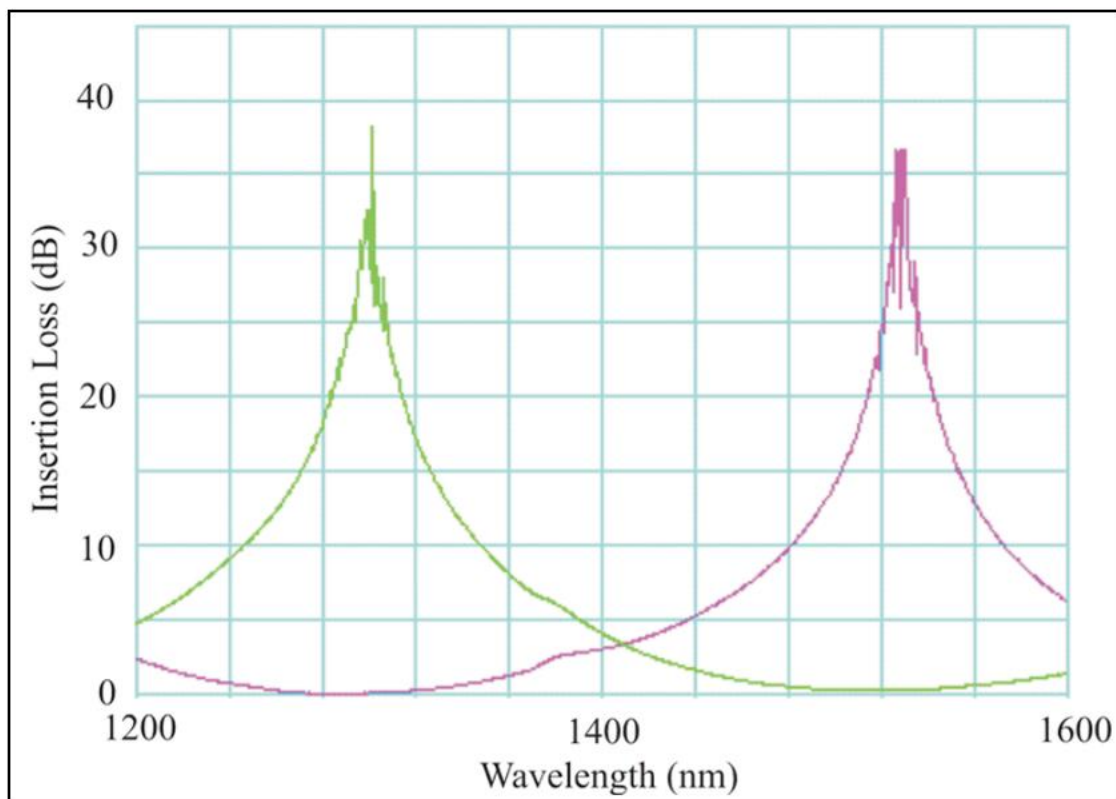


Fig. 4.21. Optical pass bands in a typical CWDM coupler [4.15]

Optical Circulator: Used here to facilitate reflective modulation with the REAT these devices are now a commonly used passive optical networks component. The device used here was a three port device and was used in a configuration that would allow a

modulated reflected signal to be routed to a sensing photo-receiver. This meant that as shown in Fig. 4.22. unmodulated light entering port 1 would exit at port 2 only.

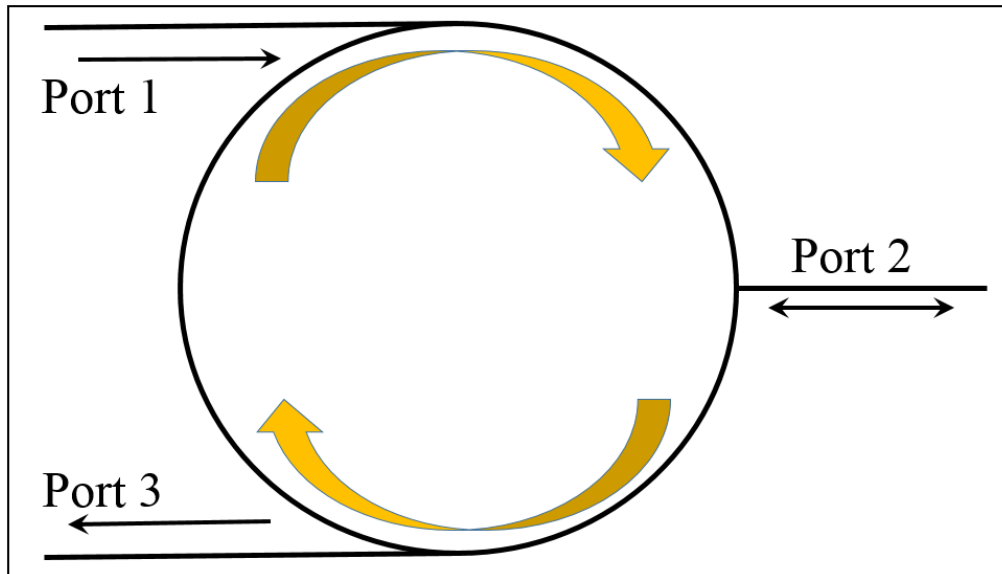


Fig. 4.22. Circulator layout

The reflected and now modulated light entering at port 2 is isolated from port 1 and only exits at port 3 for detection purposes. The light does not travel in the reverse direction within the circulator [4.14]. Developed in the early 1970's [4.16] these early devices used a combination of split prisms (to facilitate ports) and a Faraday rotator (to produce opposing polarisation planes and give isolation) to obtain port isolation. Later refinements that used Yttrium iron garnet (YIG) lenses to produce the Faraday rotation effect and single mode optical fibre resulted in more compact devices and [4.17]. Later devices that used birefringent crystal garnet crystal sections instead of lenses [4.18] and laser welded fabrication techniques resulted in the compact devices are seen today.

“Birefringence is the optical property of a material having a refractive index that depends on the polarisation and propagation direction of light.” [4.19].

VCSEL: As discussed previously these devices were preferential as they possess a number of electrical and physical features that make them especially suitable for the required short to medium range transmission purposes outlined. Also the low power requirement, direct modulation characteristics and temperature stability made them ideal devices for the applications discussed. VCSELs differ from the more traditionally used “edge emitting” devices in that the active components of the device are arranged vertically, in layers through the fabricated wafer. Fig. 4.23. shows the vertical nature of these active parts of the structures [4.20] and also a comparison of the construction of the Vertilas and Raycan VCSEL devices used in this work.

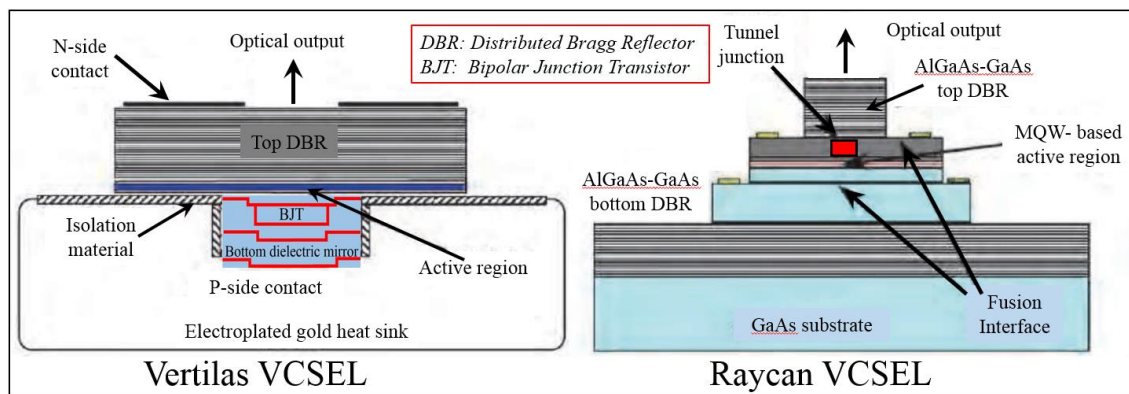


Fig. 4.23. Vertilas and Raycan VCSEL structures

It can be seen that the electrical contacts are separated vertically through the wafer and the optical output emits through an aperture in the top contact. Such a structure means that individual devices can be probe tested, assessed and graded before any cleaving is carried out so greatly aiding the manufacturing process. The Vertilas device also incorporates a transistor that aids in the controllability of the device.

4.8 Conclusions

Error Vector Magnitude uses phase and amplitude measurements to assess how far a QAM data point is moved from its ideal position as the result of factors due to a transmission medium. This measurement was used to provide a representative guide to the suitability of an optical transmission system to deliver phase sensitive information and affords a definitive indication of the preservation and integrity of the information delivered over such a link. Phase / amplitude plots passed through an optical transmission link can be used to display sensing information in the same way as an individual data point shown in an EVM constellation diagram. Optical transmission was shown to facilitate an ideal method for the delivery of phase and amplitude sensitive information as fibre does not suffer the limitations of copper coaxial cables as touched on earlier. Several options were investigated, each with differing properties, requirements and attributes. Initially a method using a reflective transducer showed promise. Limitations of this system were principally centred around the necessity to switch input and output functions, making the device used in this configuration only capable of half duplex transmissions. This will present a difficulty if used with a network analyser in the sensing system shown in the previous chapter as this requires simultaneous two way transmission. A significant advantage with this device is that it allows remote placement of optical devices. Such properties make the device highly desirable and so alternative component arrangements with the R-EAT will be investigated in the next chapter. CWDM architectures can facilitate high upstream / downstream isolation and give long range were found also to support full duplex operation. Unfortunately such performance also required the use of powerful lasers and polarisation sensitive MZMs at both ends of the transmission path making for a less than ideal solution. Directly modulated VCSEL devices used in combination with a CWDM architecture and a benign photo-receiver

provided a robust and stable platform for the shorter range use that would be ideal for these purposes. VCSELs used in this way required careful mounting methods so as to provide good impedance matching characteristics. Using resonance effects at the input also appeared to facilitate a limited frequency range extension which would be useful when using narrowband signals where flatness of response is not so critical.

References

- [4.01] Jeffery F. Beasley and Gary M. Miller. Modern Electronic Communication (Eighth Edition). Pages 469 - 476.
- [4.02] I.A. Glover and P.M. Grant. Digital Communications, Prentice-Hall Europe 1998. Pages 392 – 395.
- [4.03] Rene Schmogrow, Bernd Nebendahl, Marcus Winter, Arne Josten, David Hillerkuss, Swe Koenig, Joachim Meyer, Michael Dreschmann, Michael Huebner, Christian Koos, Juegen Becker, Wolfgang Freude and Juerg Leuthold. “Error Vector Magnitude as a Performance Measure for Advanced Modulation Formats. Photonics Technology Letter, Vol. 24, No. 1, Jan 2012. Pages 61 – 63.
- [4.04] Manoj P. Thakur, Terence Quinlan, Carlos Bock, Stuart D. Walker, Mehmet Toycan, Sandra Dudley, David W. Smith, Anna Borghesani, David Moodie, Moshe Ran, Yossef Ben-Ezra. “480Mbps, Bi-directional, Ultra-Wideband Radio-over-Fibre Transmission using a 1308/1564nm Reflective Electro-Absorption Transducer and Commercially-Available VCSELs”. JLT 2008. Vol.27,No.3.Feb 2009. Pages 266 – 272.
- [4.05] Maria Morant, Terence Quinlan, Stuart Walker and Roberto Llorente: “Transmission of Triple-Format OFDM Radio Signals in Reflective Passive Optical Networks Avoiding Brillouin Scattering Effect”. OFC 2011
- [4.06] Maria Morant, Terence Quinlan, Stuart Walker and Roberto Llorente: “First Demonstration of Triple-Play Bi-directional Full-Duplex CWDM Transmission in Passive Optical Networks”. OFC 2011
- [4.07] Terence Quinlan, Maria Morant, Roberto Llorente and Stuart Walker: “Ultra-Low Cost and Power VCSEL-Based 480Mbit/s UWB Radio over a Bi-Directional CWDM PON”. ECOC 2011.
- [4.08] Terence Quinlan, Maria Morant, Sandra Dudley, Roberto Llorente and Stuart Walker. “480Mbit/s UWB bi-directional radio over fiber CWDM PON using ultra-low cost and power VCSELs”. Optics Express 2011. Vol 19, issue 26, page b197.
- [4.09] Terence Quinlan, Sandra Dudley, Maria Morant, Roberto Llorente and Stuart Walker. “First Demonstration of Cooler-less, Bi-Directional, Format-Agnostic, Wireless and Gigabit Ethernet Network Provision using Off-The-Shelf VCSELs”. OFC 2012.
- [4.10] Terence Quinlan, Sandra Dudley, Maria Morant, Roberto Llorente, and Stuart Walker. “VCSEL-based, CWDM-PON systems using reflective technology for bi-directional multi-play service provision”. Optics Express 2012. Vol 20, issue 15, pages 16726 – 16734.

- [4.11] Jasprit Singh, Songcheol Hong, Pallab K. Bhattacharya, and Rajeshwar Sahai. “Quantum confined Stark effect of excitonic transitions in GaAs/AlGaAs MQW structures for implementation of neural networks: basic device requirements”. *Applied Optics*, Vol. 27, Issue 21, pp. 4554-4561 (1988)
- [4.12] Hazra, P. Bhattacharya, S. and Pal, S. “Effect of noise on Electro Absorption Modulator (EAM) and optimization - Used for optical communication”. *Conference on Emerging Trends and Applications in Computer Science (ICETACS)*, 2013 1st International. 2013 , Page(s): 52 – 56.
- [4.13] R. B. Welstand, J. T. Zhu, W. X. Chen, A. R. Clawson, P. K. L. Yuand S. A. Pappert. “Combined Franz–Keldysh and Quantum-Confined Stark Effect Waveguide Modulator for Analog Signal Transmission”. *Journal of Lightwave Technology*, Vol 17, No 3, March 1999.
- [4.14] *Fibre Optic Reference Guide, A Practical Guide to Communications Technology*, third edition. David R Goff. Pages 96-99, 121 and 123.
- [4.15] Olson Technology data sheet.
http://www.olsontechnology.com/ds/Standard_WDM.pdf
- [4.16] Shibukawa, Atsushi and Kobayashi, Morio. “Compact optical circulator for near-infrared region”. *Electronics Letters*, Volume: 14, Issue 25, 1978 , Page(s): 816-817.
- [4.17] Yokohama, I. Okamoto, K. Noda, J. “Polarisation-independent optical circulator consisting of two fibre-optic polarising beam splitters and two YIG spherical lenses”. *Electronics Letters* , Volume: 22, Issue: 7, 1986 , Page(s): 370- 372.
- [4.18] Yoji Makiuchi and Hiroshi Matsuura. “Development of a Low-Loss Optical Circulator”. *Furukawa Review*, No. 22 2002, Pages 1-4.
- [4.19] <http://en.wikipedia.org/wiki/Birefringence>
- [4.20] The Vertical-Cavity Surface Emitting Laser (VCSEL) and Electrical Access Contribution. Angelique Rissons and Jean-Claude Mollier, Institut Supérieur de l’Aéronautique et de l’Espace (ISAE), Université de Toulouse, France.
<http://cdn.intechopen.com/pdfs-wm/20484.pdf>

Chapter 5 Optical Transmission System

5.1 Introduction

As previously identified, for a phase reliant detection system such as that described in Chapter 3 to operate over even short distances, a method of transmission must be devised that preserves the integrity of that phase information. As outlined in chapter 2.7 most coaxial electrical signal cables will be affected by motion related variations in their dielectric layer that will lead directly to phase instabilities [5.01]. This will increase with mobility of the cable and the length of cable used in the connection. Such an impairment will severely inhibit the deployment of any network analyser based, phase sensitive measurement system [5.02][5.03]. Optical transmission schemes such as those described in the previous chapter appears to tackle this problem successfully achieving signal recovery over considerable distances. Recently marketed (2013) commercial solutions from Agilent [5.04] would also appear to suggest optical transmission methods for remote VNA connection, but these are costly and complex devices. An EVM performance commensurate with, or exceeding that required for accurate transmission and recovery of data will be necessary for the measurement system. To address this, a key challenge for any such sensing setup using these relatively low frequencies will be that of resolution and accuracy. The system here will operate at a target distance of 1km which should be suitable for most remote site operations. As the principle source of signal degradation was identified as attenuation induced reduction in signal to noise ratio, this shorter distance than previously used should also provide an improvement in received signal quality over that already shown in chapter 4. Two likely approaches were now to be investigated to ascertain their suitability for use with the already outlined RF measurement equipment

discussed in chapter 3. To further investigate their remote device placement advantages, in the first instance the existing RF system will be coupled to a modified R-EAT architecture. Following this the standard CWDM approach will then be evaluated and compared.

5.2 Reflective Transducer Approach

As shown in the previous chapter the use of reflective transducers offered some valuable advantages, a major problem with the device here, was that it had by necessity, a single common RF input / output port that served both upstream (US) and downstream (DS) signals. In this configuration it was not possible to support a simultaneous bi directional (full duplex) transmission. In the previously described function, an RF switch and power sensing arrangement separated the signal the US and DS signals so as to provide a time switched (half duplex) signal path. In order for the RF sensing section to function via the VNA a full duplex link was required as the measurement requires a forward transmission from one VNA port to the other. To accomplish this a signal needed to be generated at the output port of the VNA and converted to an optical signal, it can then be transmitted through the DS optical path and converted back into an electrical form before application to an antenna. After being received by its complementary antenna in the sensing head the now US signal is returned to the VNA receiving port in a reciprocal manner. Any signal switching between the optical paths would consequently disrupt the signal path. The optical transmission system was constructed as outlined in Fig. 5.1. In this arrangement the system was divided into two distinct sections, the remote sensing head and the laser / analyser end. Both sections being joined by 1km of single mode optical fibre. This arrangement offers the advantage of locating the majority of the optical components close to the VNA. Any necessary component interconnections can then be established over

very short distances using phase stable RF semi rigid cable and / or direct connector to connector interfacing. Due to device availability this system was initially constructed using Raycan RT3X031-FS2-40003 (1335nm) and Raycan RT23031-FFP-20031 (1550nm) VCSELs, both with an upper frequency limit of 4.25GHz these were not ideal and limited the frequency of operation to 4GHz. It should be noted that only the 1335nm VCSEL is modulated in this configuration. In order to provide a continuous US /DS signal path it was decided to add an RF circulator to the signal port of the R-EAT. This would separate the two signal paths in the same way as the optical circulator isolates the transmitted and reflected signals in the 1550nm wavelength section [5.05] [5.06]. With this frequency limitation it was then possible to select an RF circulator with a 20dB isolation frequency between 3.4GHz and 4.2GHz the RF circulator (Atlantec ACC 20070). This component was chosen solely because it offered maximum port to port isolation of the components available. In combination with the 1335nm VCSEL, this defines the maximum frequency of operation of the overall system. As can be seen in Fig. 1. at the remote, sensing end of the system, the transmitted and returned signals from the switch matrix are amplified and fed to the RF circulator ports. These amplifiers were necessary to provide sufficient level for the receiving antenna to modulate the R-EAT in the 1536nm reflective modulator mode and for providing sufficient drive level (0dBm) to the transmitting antenna in the 1335nm detection mode. As with the RF system described previously the sensing signal is generated at the output port of the VNA (in S_{21}) configuration and is applied directly to the 1335 VCSEL via a bias tee. A current source at this point provided the necessary bias. The now modulated 1335nm optical signal was then passed to the appropriate arm of a CWDM coupler and from there on to 1km of single mode optical fibre to the R-EAT. On reaching this device the signal undergoes optical to electronic conversion and is applied to the “common” port of the RF circulator.

On emerging from the next circulator port the signal was amplified and passed to the switch matrix as outlined previously. After passage through the switch matrix this signal was radiated by the selected antenna and received by its counterpart in the array and directed to another amplifier and on to the remaining port of the circulator. This signal, now travelling in the opposite direction, was re-applied to the R-EAT, where it now modulated the 1536nm optical signal.

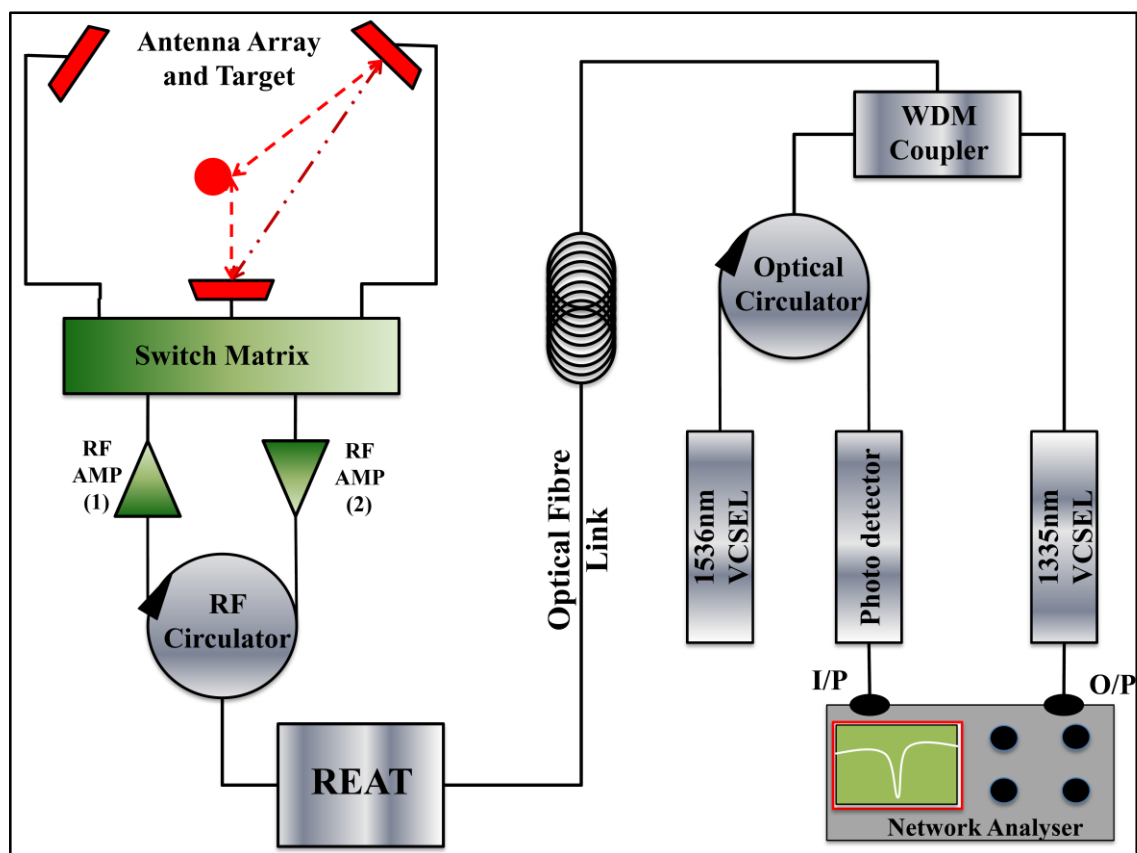


Fig. 5.1. Reflective optical transmission system diagram

In this path the optical signal was first generated by a stand-alone VCSEL. This unmodulated optical carrier is applied to the optical circulator and passed on to the 1550nm arm of the CWDM coupler, through the 1km of single mode fibre to the R-EAT. At this point the carrier was both modulated by the amplified signal from the switch matrix and reflected back through the optical fibre and the CWDM coupler. From here

the modulated signal passed through the optical circulator in an opposing direction to the original unmodulated optical carrier and on to the photodetector for optical to electrical conversion. At this point after suitable level adjustment the signal was returned to the VNA for analysis. For these reasons system frequency response was limited by the upper frequency limit of the 1335nm VCSEL / RF circulator combination to a maximum of 4.2GHz; the REAT has a bandwidth of around 10GHz. Phase variation will increase proportionally with the frequency of operation and so will also define the sensitivity of the system. However all the optical components other than the R-EAT have been sited remotely. In this way the function of the VNA can be remotely sited from the “device under test”, in this case the antenna array. Any disparities introduced by the optical transmission components, electrical amplifiers and the circulators both optical and electrical can be removed by through calibration of the VNA. It was now necessary to establish the performance of the active optical components. A Discovery DSC 402 HR photo-diode was used to measure the frequency response and distortion levels of these devices. The manufacturers published frequency response of this device is shown in Fig. 5.2. With a -3dB point of 10GHz, this is adequate for the frequencies likely to be required and has a smooth and predictable response. As part of the complete component package this device has an integrated amplifier with a gain of 20dB.

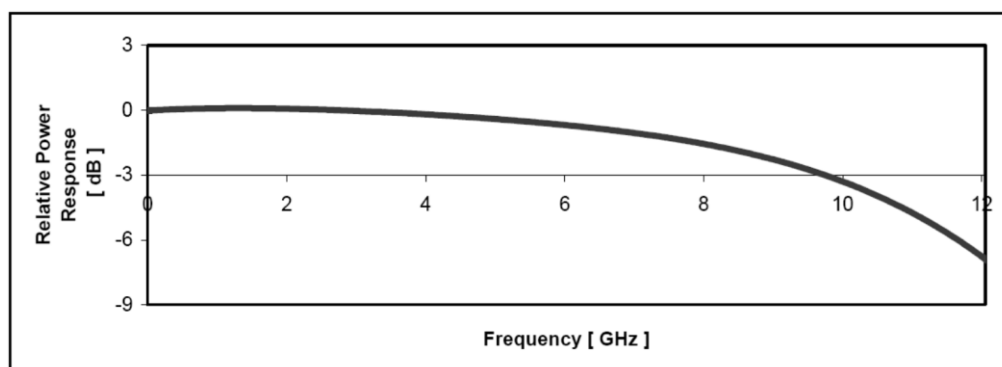


Fig. 5.2. Published S_{21} of Discovery Photodiode

This device was also used in the return path of the system as outlined above. As the 1335nm VCSEL was to be directly modulated by the VNA attention to the mounting detail would be necessary to obtain the maximum frequency response and account for any possible frequency range extension in the future. A similar approach to that outlined previously was adopted, a network analyser and photo-receiver being used to obtain the device characteristics as can be seen in Fig. 5.3. The resulting S_{21} plot of the VCSEL and photodiode in combination shows the frequency response between 1GHz and 6GHz. Two significant dips are apparent where the device would be relatively unresponsive to modulation, the lower frequency dip is probably due to grounding effects and the upper to the natural roll off of the device. The introduction of the lower dip was the result of a trade-off to obtain some response at the high 5GHz frequency for later use. A significant roll off of 10dB is also observed over the range of 1GHz to 4.2GHz, it is likely that this can be improved with further development of the mounting method and will be investigated later.

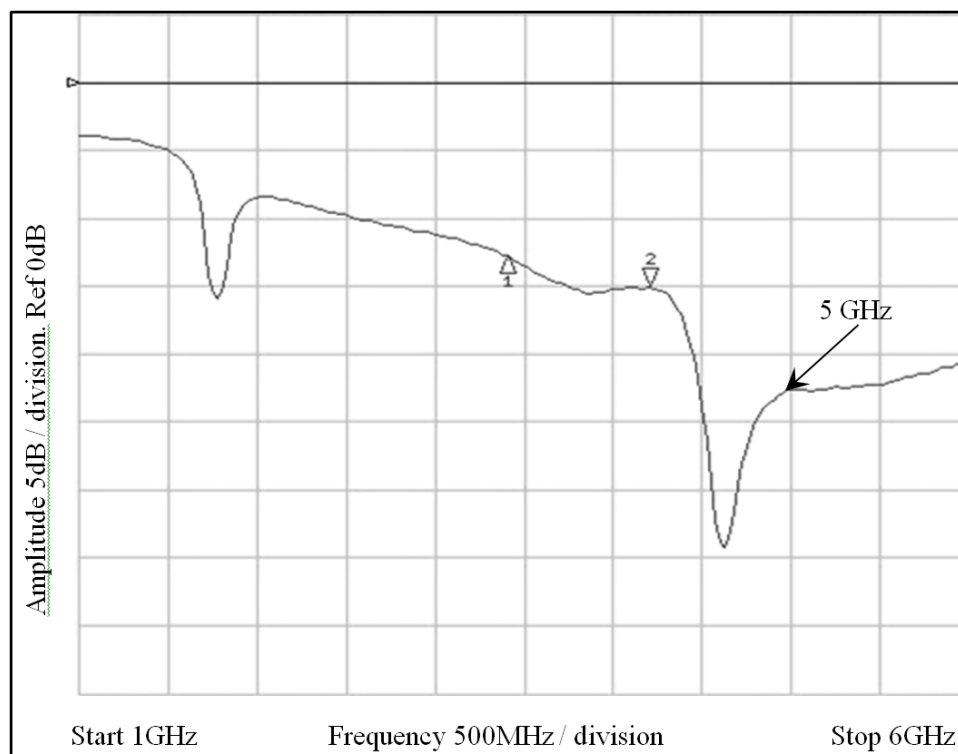


Fig. 5.3. Measured S_{21} of 1335nm VCSEL and Discovery Photodiode

Within the range of the circulator, 3.4GHz to 4.2GHz (markers 1 & 2) the response device was reasonably flat. Optimal bias current for the 1300nm VCSEL was found to be 7mA. At this current the device

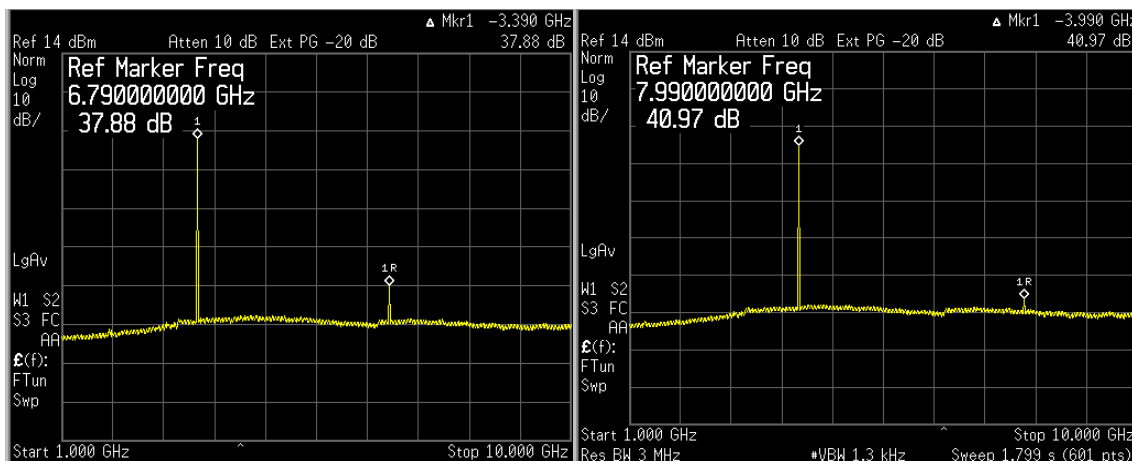


Fig. 5.4a.

Fig. 5.4b

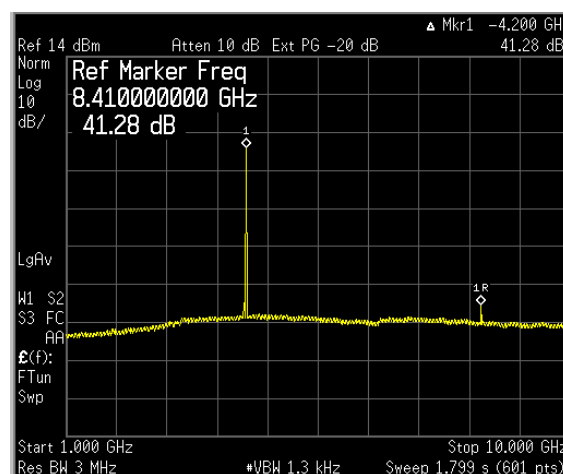


Fig. 5.4c.

2nd Harmonic distortion of 1300nm VCSEL over circulator range.

was within safe operating limits yet produced a useable optical output that also supported a low distortion RF signal. With a direct modulating power of -10dB from the VNA spectral plots were taken at three useable frequencies across the range as defined by the

circulator limits. At these levels only 2nd harmonic distortion at levels below the fundamental frequency of -37.8dB at 3.39GHz, -40.97dB at 3.99GHz and -41.28dB at 4.2GHz were recorded as shown in Fig. 5.4a-c.

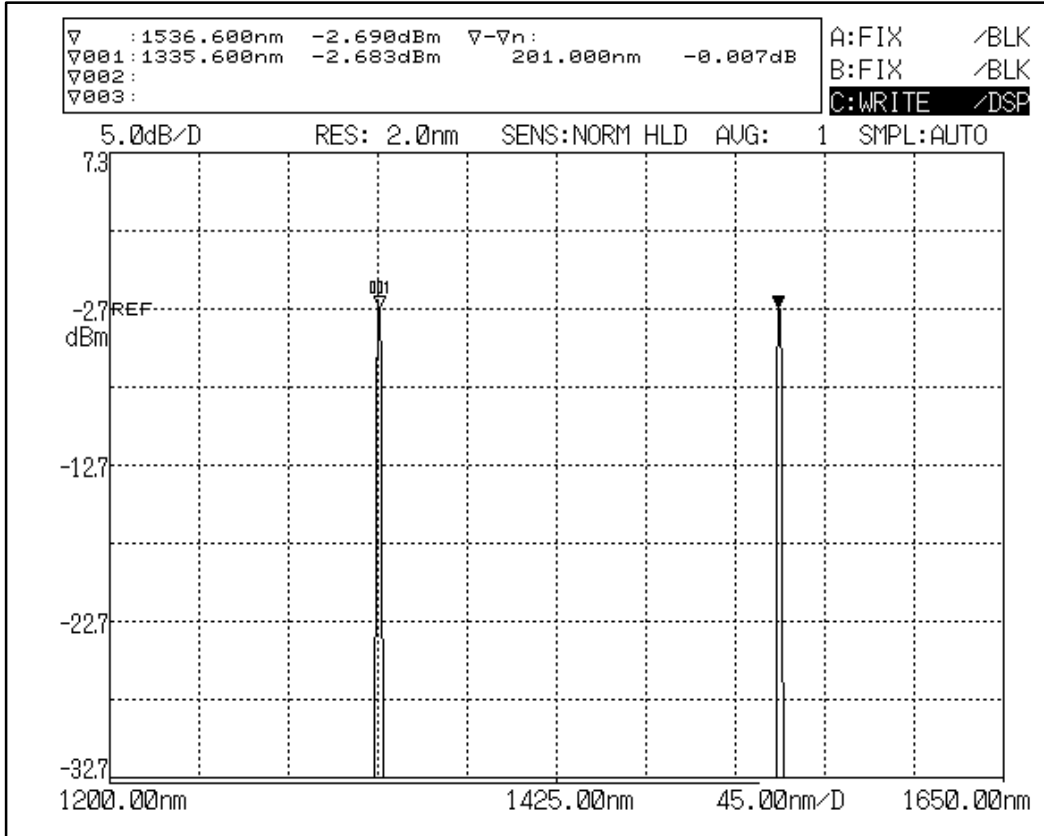


Fig. 5.5. Optical power levels of 1335nm and 1536nm VCSEL

High levels of distortion may be of concern due to possible mixing effects with external signals that could introduce in-band intermodulation products. This would be undesirable as it could lead to a loss of system definition due to the generation of uncorrelated signals that would probably appear as noise like effects across the signal of interest. With the bias current set to 7mA the 1300nm range VCSEL provided an optical power level measured at -2.68dBm with a wavelegnth of 1335.6nm. As modulation of the 1500nm device is accomplished by reflection (R-EAT), only power and optical wavelegnth needed to be considered for the return path. It was found that a bias current of 7mA was

necessary to provide an optical power of -2.68dBm, comparable to the now 1335.6nm VCSEL, with a wavelength of 1536.6nm. An ANDO Optical Spectrum Analyser (OSA) was used to record these levels as shown in Fig. 5.5. This shows the operating wavelength and power of both devices when combined. Both of these wavelengths being within the specified working range of the R-EAT at 20 deg. C. Final parameters and settings for both VCSELs are shown in Table 5.1.

Table 5.1. Power levels and wavelengths of VCSELs

Power levels of 1335nm VCSEL	Power levels of 1536nm VCSEL
bias current 7mA	bias current 7mA
Optical power -2.68 dBm	Optical power -2.69 dBm
Actual wavelength 1335.6nm	Actual wavelength 1536.6nm
RFsignal into VCSEL -10dBm @ 4GHz	Reflective modulation

The next step was to characterise the response of the REAT at both its operating wavelengths. As this device was sensitive to both optical wavelength and bias voltage that are interdependent to each other, plots were taken to establish optimal bias conditions for both VCSEL wavelengths. Such a procedure would aim to identify a setting that was acceptable for the device to operate in both its photo-detective (1335.6nm) and reflective (1536.6nm) modulation modes concurrently. The first task was to characterise the device sensitivity at differing wavelengths for varying bias conditions. With the R-EAT connected to a Hewlett Packard tuneable laser via a circulator, a 0dBm, 4GHz RF signal was applied to the input / output port. An optical power level of -2.69dBm was selected at the tuneable laser so as to be comparable with that of the power of the VCSEL. A range of wavelengths was selected in 5nm increments to cover the range of likely / possible lasers that may be used in future experiments. A Discovery DSC 402 photo-receiver with a built in amplifier of 20dB gain was then used to detect the RF power level of reflected signal.

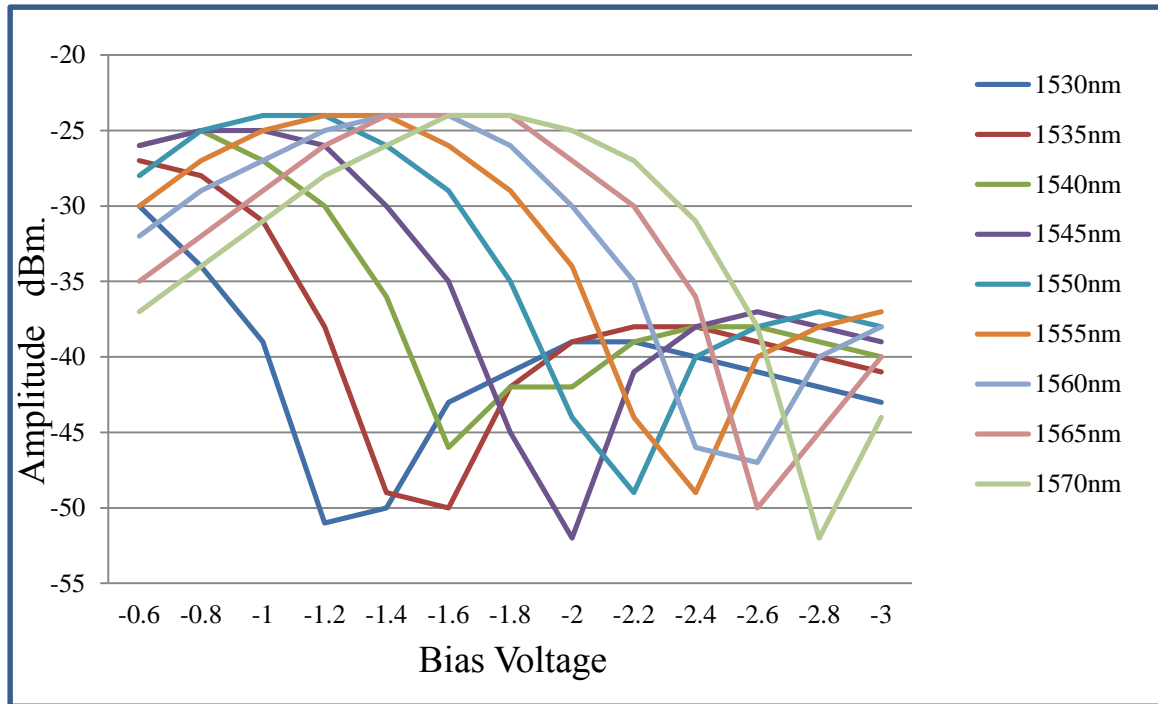


*Fig. 5.7. R-EAT Reflected signal / wavelength power Vs bias voltage**

* Measured using Discovery DSC 402 HR photodiode, sensitivity 0.8 Amps/watt with approx. 20dB gain TIA.

Figure 5.7. Shows the resulting plots indicating that at the VCSEL wavelength of 1536nm a bias voltage of between -2V to -1.8V would give maximum response and largest reflected signal amplitude. It should be noted that the signal levels shown in Fig. 7. include the 20dB amplification due to the photo-detector amplifier. Still in the same configuration, a VNA was now substituted into the system and the tuneable laser replaced with the 1536nm VCSEL. With the VNA in S_{21} configuration the output port (port 1) was connected to the R-EAT port and the input port (port 2) was connected to the photo-receiver. At this point a 20dB attenuator was used to remove the effect of any amplification and give a true power level reading. Using the S_{21} measurement function of the analyser, frequency response readings were taken across the range of 3GHz to 5GHz,

the useful range of the antenna system and likely useable frequency range of the system. The output power level of the VNA was held at 0dBm for consistency with the results shown in Fig. 5.7. Plots were taken between bias levels of -1.8V to -2.4V as shown in Fig. 5.8. This revealed a variation of around 1dB across the range 3GHz to 5GHz at all bias levels, this was consistent with the photo-receiver response shown in Fig. 5.2.

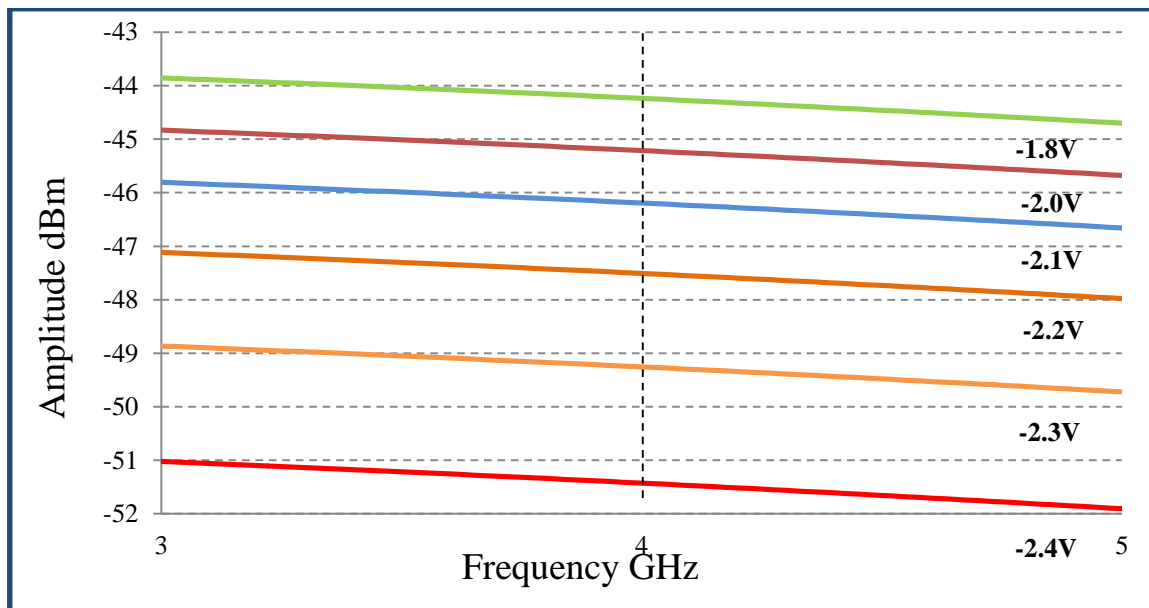


*Fig. 5.8. S_{21} of REAT in reflective mode at 1536.6nm** true levels 20dB gain subtracted
**Trend lines shown for clarity*

It can also be seen that a variation over the bias range of around 8dB is in agreement with the roll off indicated in Fig.5.7. As can be seen from these plots the ideal bias level is -1.8V at the 1536.6nm wavelength although there was clearly some room for bias variation but this comes at a penalty of 1dB loss in sensitivity across the range for 0.1V variation in bias.

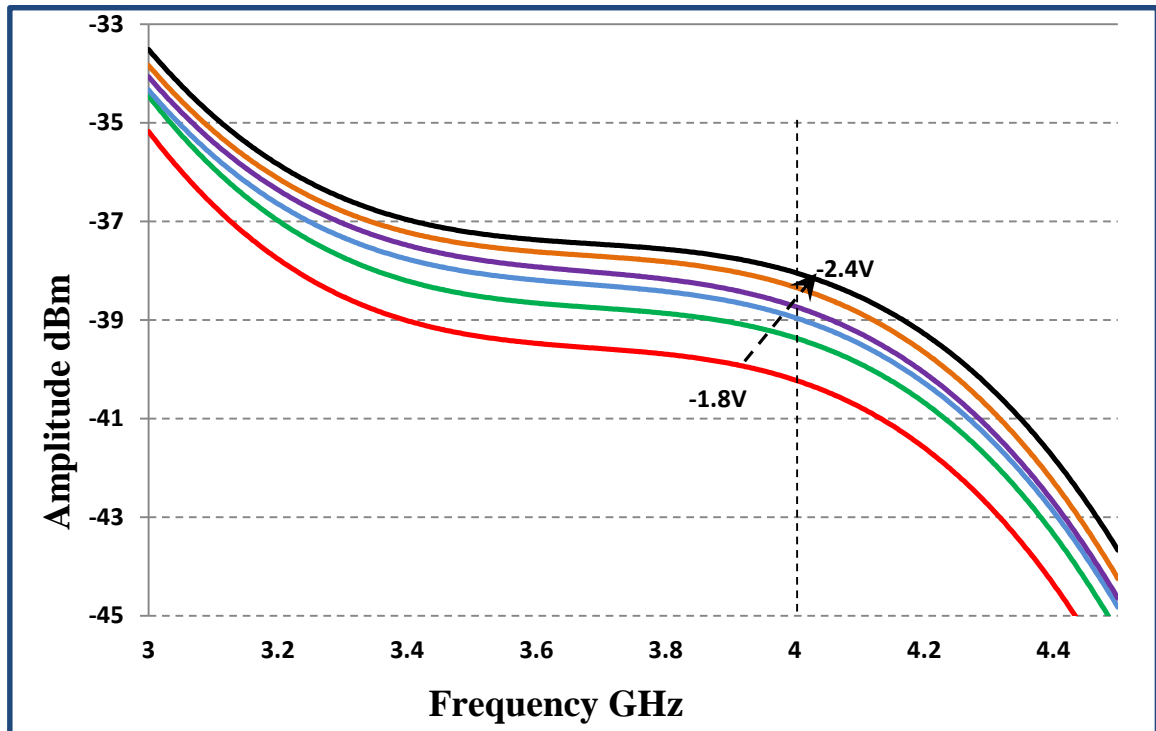


*Fig. 5.9. S_{21} of combined REAT and 1335nm VCSEL** true levels 20dB gain subtracted
**Trend lines shown for clarity*

With this range established the behaviour of the combined 1335nm VCSEL and the R-EAT in photodiode mode could then be established. With the VNA power level set to -10dBm and the VCSEL bias current was set at 7mA S_{21} measurements were taken between the VCSEL and the output of the REAT. This was carried out over the frequency range of 3GHz to 4.5GHz over the same bias condition range as in the previous reflective mode measurements. As the R-EAT was now in its photo-detection configuration direct measurements were possible and no further signal amplification was applied. This combination was found to be insensitive after a frequency of 4.6GHz was reached due to the rapid roll off in the VCSEL response as can be seen in Figure 5.3. Shown in Fig. 5.9. is the resulting series of frequency response curves, these are limited in range by the VCSEL and would seem to approximate the results shown in Fig. 5.3 over this frequency range. As can be seen in Fig. 5.9. the R-EAT was relatively stable in its photo-detection

configuration. With bias variation over the -1.8V to -2.4V range, a level difference of around 2dB at the selected 4GHz modulation frequency is indicated. From these results it was concluded that a bias voltage level of -2.2V would be optimal for both the 1536nm and 1335nm paths. With the system now configured as in Fig. 5.1. Forward (1335nm) RF power levels were measured as -43dBm after the REAT with the VNA drive level of -10dBm. This signal was then amplified to -3.5dBm into the switch matrix. At this level harmonic distortion was un-measurable but some low level (-40dB) RF peaks were occasionally present. These would be in band but at this level should not present a problem. RF input power to the VCSEL was now increased to -6 dBm to give the desired 0dBm power level into the RF switching matrix. At this level some spurious second harmonic distortion occurred due to the increased level of VCSEL modulation. This distortion was however 30dBs below the fundamental frequency as can be seen in Fig. 5.10a; spectrum of the signal at the input of the switch matrix and Fig. 5.10b showing second harmonic production at -32.85dB below the fundamental. At this level the distortion can probably be tolerated. If necessary a modest increase in amplifier gain at this point would allow the laser modulation to be decreased so reducing the distortion. At this power level the received signal at the output of the switch matrix is around -30dBm. Isolation due to the RF circulator is specified as 20dB. After the R-EAT the upstream signal level was measured as -40dBm at the port of the circulator, with the above level adjustment. To maintain isolation the return, downstream signal can be no more than 20dB above this level. This required that the signal power level presented to the 1536nm downstream path to be a maximum of -20dBm. Such a low power signal gives very low modulation in the reflected 1536nm signal, as shown in Fig. 5.8.

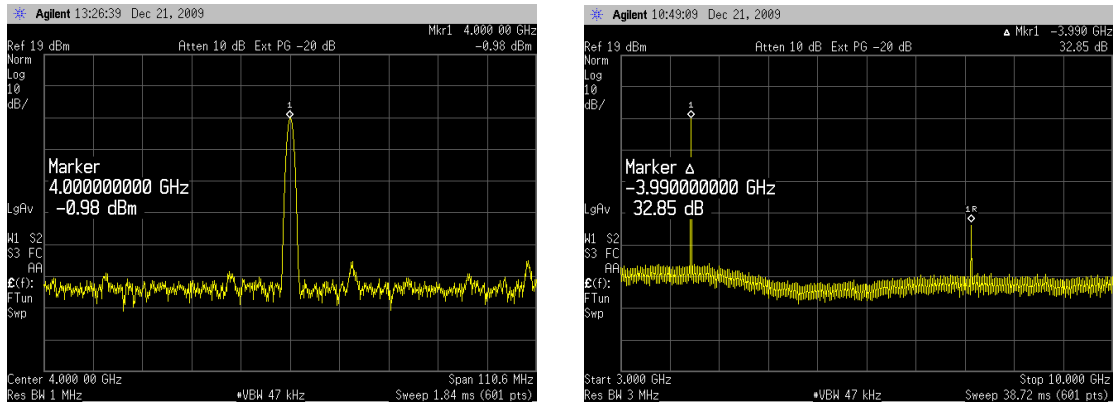


Fig. 5.10a. Upstream signal power level and Fig. 5.10b 2nd harmonic distortion level

The amplitude of this signal increases with a reduction of R-EAT bias. Unfortunately at the same time such bias reduction reduces the amplitude of the signal generated by the R-EAT in PD mode. With careful adjustments of all these parameters it was possible to detect phase and amplitude variations. However it was necessary to use large amounts of averaging to make discernible measurements. This made measurements both precarious and very slow and difficult to repeat. Further investigation also revealed that at these levels of modulation significant crosstalk levels within the R-EAT were present (-60 dB), approaching that of the recovered return signal -56dB. As a result the recovered signal would in any case be seriously compromised. To confirm this, another 1335 VCSEL was prepared in such a way that a “flat” response was possible up to 4.25GHz. This was again directly modulated from the VNA in S₂₁ mode. Using similar levels to those used in the measurement system, this was then applied to the device whilst the output of the circulator was monitored with a photo-receiver that returned any detected signal to the VNA. Fig. 5.11. shows the signal transfer between the 1300nm and 1500nm optical paths. The RF terminal of the R-EAT is terminated at 50Ω to avoid any possibility of reflections. Whereas this system would initially seem an elegant solution, the insensitive nature of the R-EAT and limited isolation of the RF circulator combine to produce a low

level signal with a poor SNR. The significant presence of crosstalk in the R-EAT necessitates the use of external switching to preserve signal integrity. This was not an option for a system that uses a network analyser that requires full duplex availability. With this in mind it was now decided to use a different approach based around the well-known 1500nm / 1300nm CWDM technique.

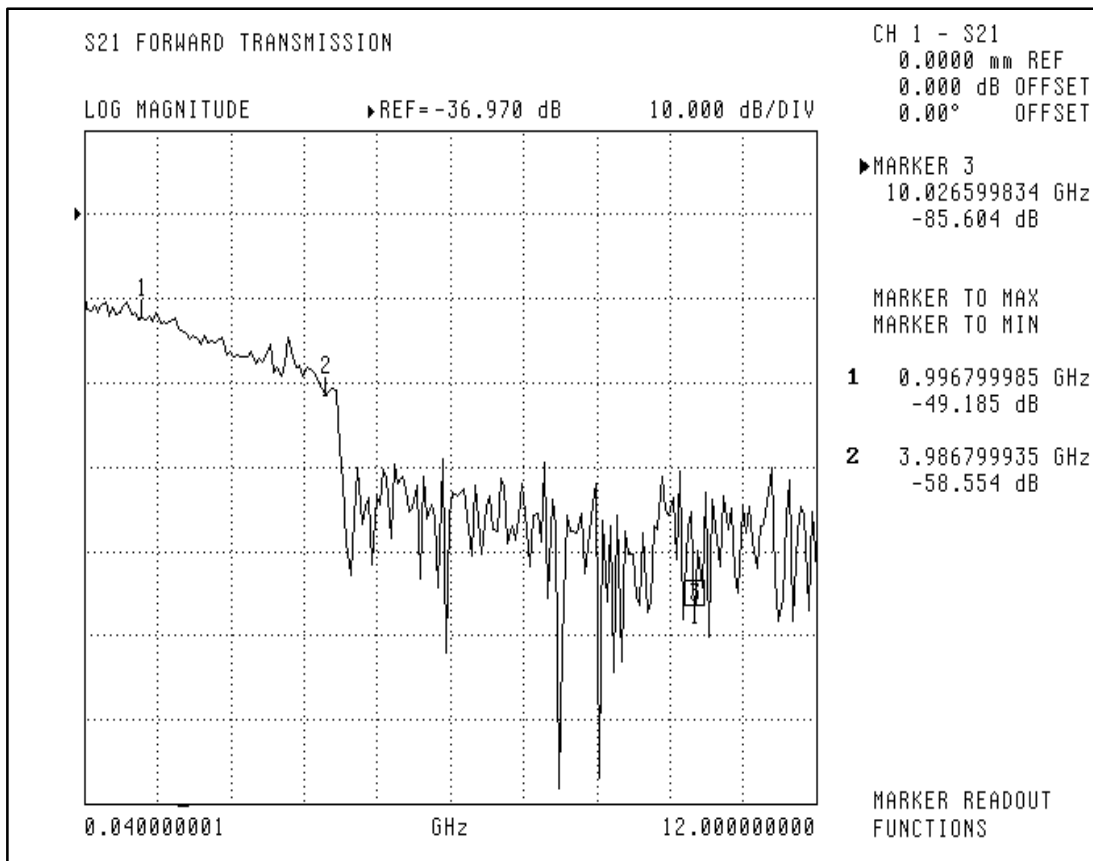


Fig. 5.11 optical path crosstalk within REAT

5.3 Coarse Wavelength Division Multiplexing Approach

Forgoing the advantage of remote optical component placement, this architecture offers a much simpler, symmetrical and robust approach. CWDM delivers significant potential gains in terms of signal isolation, control of signal levels and bandwidth availability. Bandwidth of the optical system was now only limited by that of the VCSELs. Also

without the losses introduced by the R-EAT there is much greater flexibility over signal levels, allowing an easier execution and delivery of the desired power levels within the RF sensing antenna array. Figure 5.12. illustrates the CWDM layout, at this stage this was essentially the same as that described in the previous chapter.

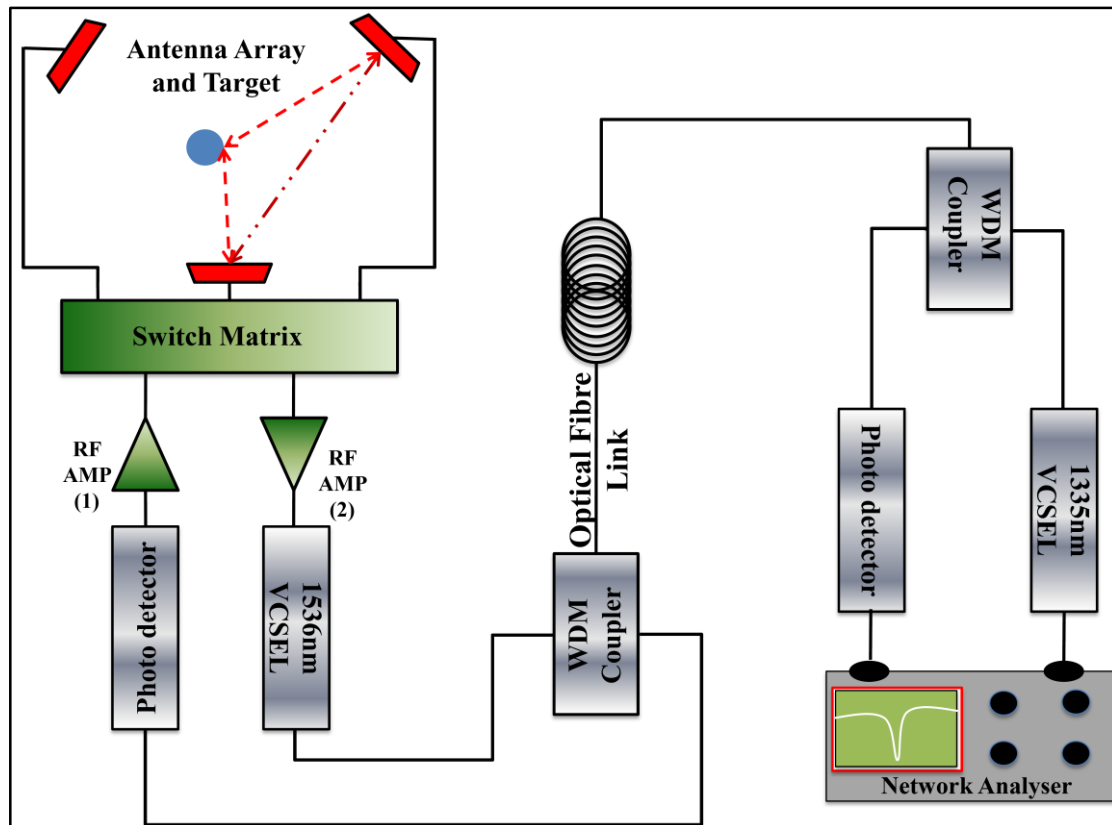


Fig. 5.12. CWDM optical transmission system diagram

Once again the 1335 VCSEL is directly driven from the VNA in S_{21} mode, but now was connected directly into 1300nm arm of a CWDM coupler. This provided isolation of up to 40dB between the 1335nm upstream and the 1536nm downstream paths. From the “common” connector of the coupler the modulated optical signal is transmitted over the 1km Single mode optical fibre directly into the “common” connector of the second CWDM coupler. From here the upstream signal was fed directly to a photo-detector via the 1300 arm of the optical coupler. The now electrical signal was then appropriately

amplified and applied to the input of the switch matrix and on to the selected antenna. The return, downstream path, was fed from the appropriate antenna directly into the switch matrix. It was then suitably amplified so as to directly modulate the 1536nm VCSEL with minimum distortion. From here the now optical signal follows the reverse 1500nm path through the CWDM couplers to a photo-detector and on to the input of the VNA. As with the previous design the 1335nm VCSEL was biased at 7mA and directly modulated from the VNA. A suitable power level of -10dBm and a frequency of 4GHz was established previously and so will provide a suitable starting point. To ensure the suitability of the 1536nm VCSEL and establish suitable RF drive levels, distortion and frequency response measurements were now carried out, as before, using the Discovery DSC 402 HR photodiode in combination with the VCSEL.

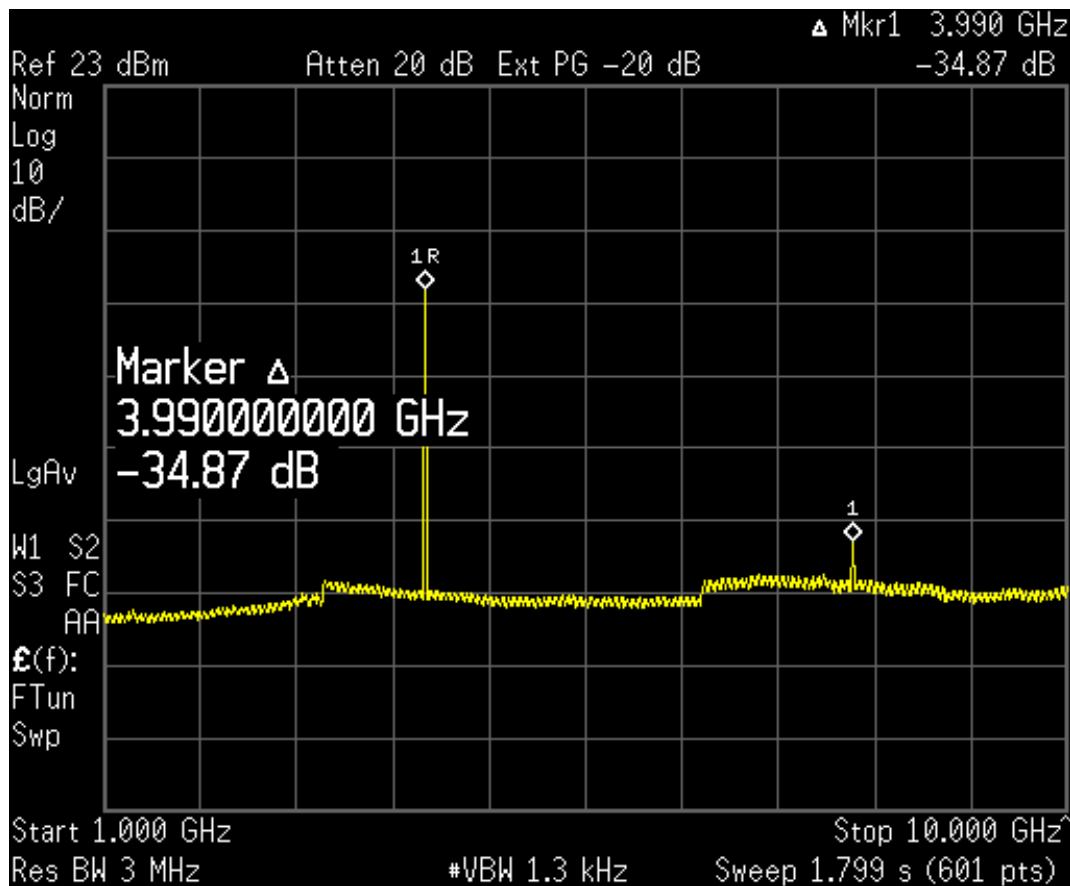


Fig. 5.13. 1536nm modulation and 2nd harmonic distortion level

This was carried out at a bias current of 7mA so as to match the optical power level of the 1335nm device as shown in table 1. The 1536nm VCSEL was then modulated with a 4GHz signal at a power level of -15dBm to produce a measured RF signal power level of -5.2dBm using the Discovery DSC 402 HR photodiode as before. Shown in Fig. 5.13. is the resulting plot, here it can be seen that second harmonic distortion is nearly 35 dB below the fundamental frequency of modulation. At this level of distortion and with the indicated SNR of the fundamental frequency shown to be in excess of 40dB a good quality signal can be expected.

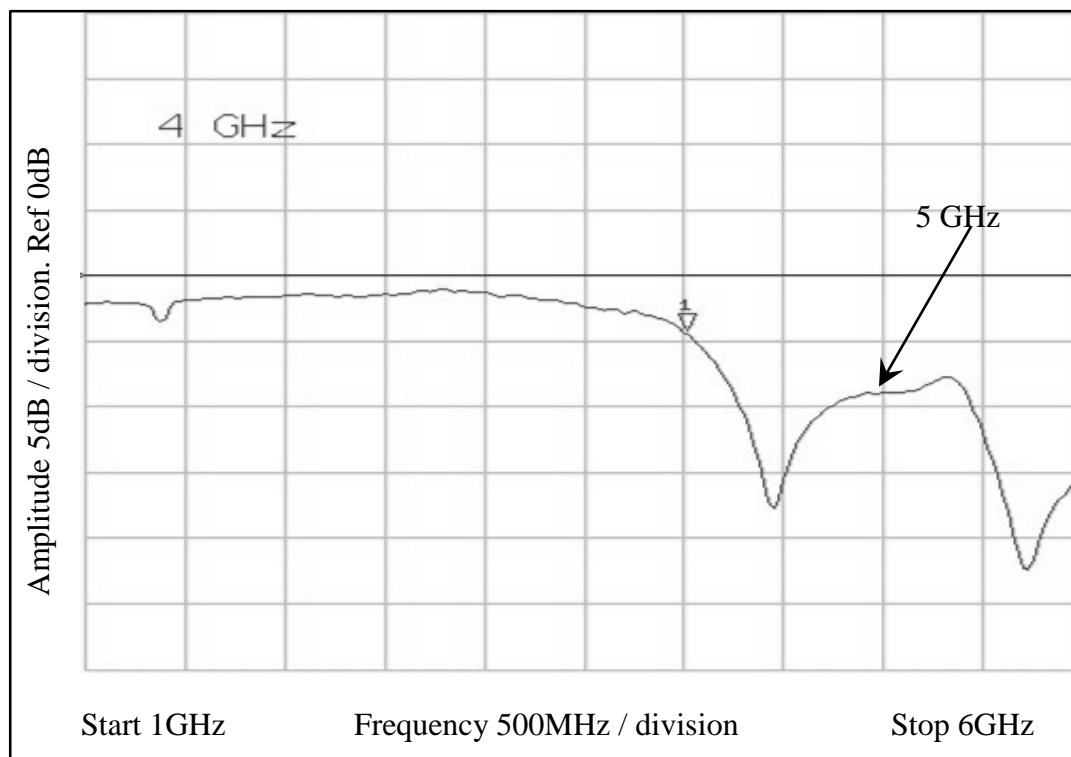


Fig. 5.14. Measured S_{21} of 1536nm VCSEL and Discovery photodiode

With the power level set to -15dBm the VNA was again used in conjunction with the photodiode to measure the frequency response of the 1536nm VCSEL. As can be seen in Fig. 5.14. this was similar to that of the 1335nm device with an initial high frequency roll

of at 4GHz. Also in common with its counterpart there is a reduced but pronounced recovery in the frequency response trace centred around the 5GHz region. Upstream / downstream isolation is dependent on the optical isolation within the CWDM couplers. This was measured at 1335.6nm / 1536.6nm by looking for crosstalk between the common input of the coupler and the opposing arm. (ie looking for 1335nm at the 1500nm arm). Using an Ando Optical Spectrum Analyser (OSA) optical isolation was found to be in excess of 40dB, with a typical insertion loss of 0.5dB. these Pirelli, WD1315U, CWDM couplers seem ideal for this purpose. The system was now connected as shown in Fig. 5.12. with the 1km optical fibre link between the two CWDM couplers. Electrical amplification was provided, as before, at the switching interface, this time to provide RF power level adjustment to the transmitting antenna in the array (approx. 0dBm) and to boost the signal from the receiving antenna to provide the optimal (approx. 15dBm) signal to the 1536nm VCSEL. In practice these levels varied a little due to RF amplifier specifications.

Table 5.2. Optical and RF power levels

Power levels of 1335nm VCSEL	Power levels of 1536nm VCSEL
bias current 7mA	bias current 7mA
Optical power -2.68 dBm	Optical power -2.69 dBm
Actual wavelength 1335.6nm	Actual wavelength 1536.6nm
RF signal level into switch matrix -1.4dBm	RF signal level from switch matrix -13dBm
RF signal level into 1335nm VCSEL -10dBm	RF signal level into VNA -32dBm

Measured optical and RF power levels were recorded as shown in Table 5.2, the RF signal levels being comparable to that obtained in the system when connected directly to

the VNA without the optical interface. As the aim of the optical transmission system is to provide an effectively “transparent” link between a “device under test” and the VNA for the purposes of phase and amplitude sensitive information transfer, level preservation represents a significant step towards achieving this goal. It then remained to verify that the system was capable of end to end transmission of the phase / amplitude information associated with the insertion of the metallic targets as used in the initial RF system experiments. As this system was currently operating at a lower frequency of 4GHz, a new set of measurements were now taken at 1mm increments from 20mm downwards as previously outlined. Measurements would be taken both before and after the optical link and compared for similarity. Figure 5.15. shows the resulting plot obtained from the RF section at the output of the switch matrix. Measurement points are clearly discernible over the range of 7mm to 20mm but the range of phase variation has fallen from 40 degrees in the 5GHz case to a little over 25 degrees in this 4GHz system. Figure 5.16. is the corresponding plot obtained through the optical system at 1km range. Although this provided a credible recovered signal plot with clear phase and amplitude variation and similar to those at source the considerable presence of noise and drift necessitated the heavy use of 16 averaging within the network analyser. Again this made the measurement procedure slow and cumbersome. At the lower end of the scale noise tends to mask the readings making accurate recording of the data points difficult. Overall the shape of both curves was similar and at the higher end there was good agreement of outcomes on the before and after plots. As expected the reduction of operating frequency to 4GHz resulted in a reduced phase change range.

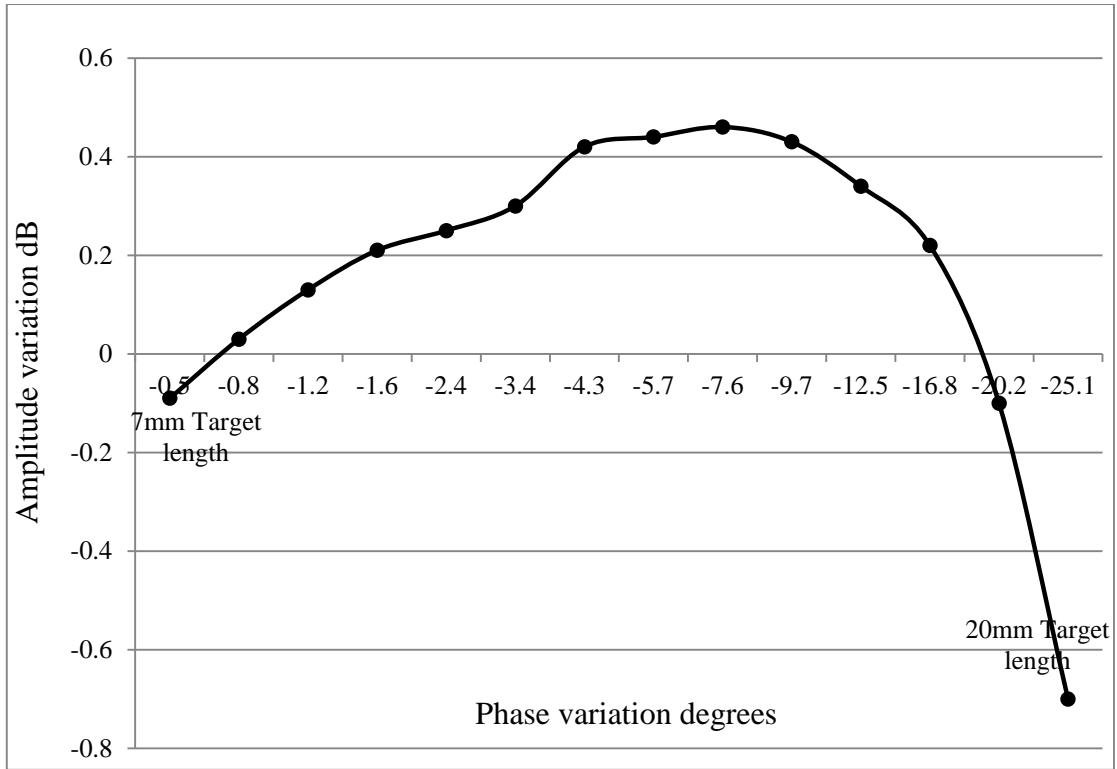


Fig. 5.15 Phase / amplitude variation before transmission

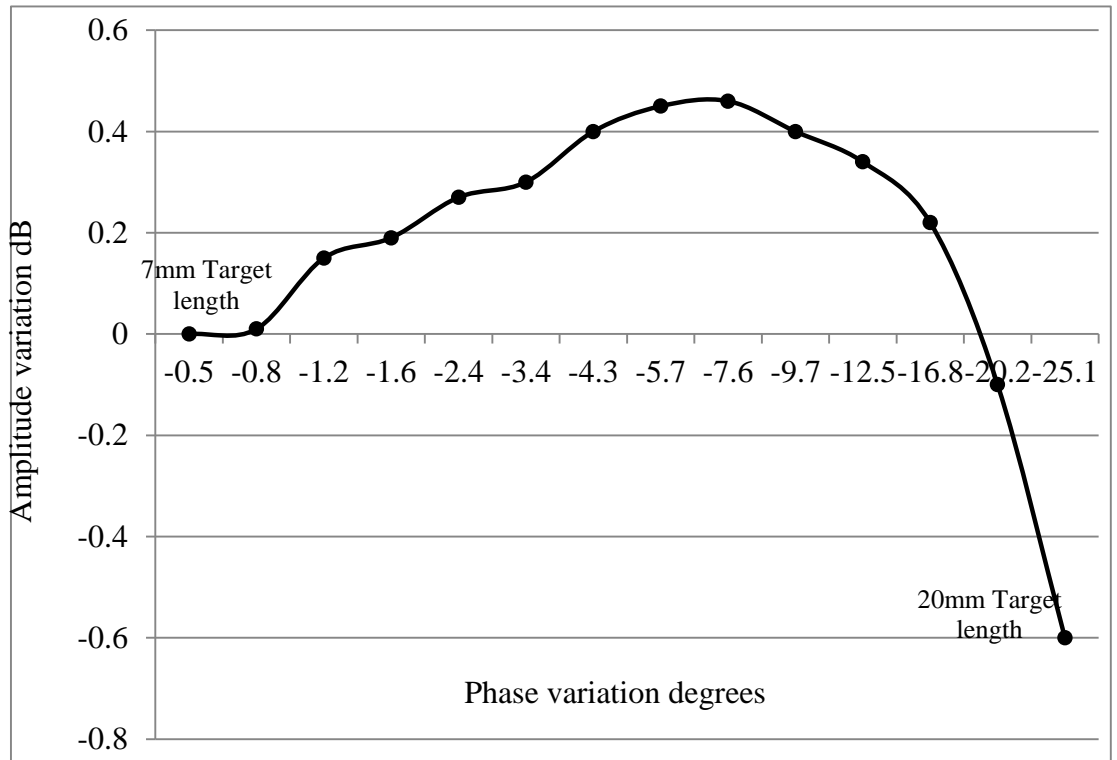


Fig. 5.16 Phase / amplitude variation after transmission

There were two clear challenges to the improvement of the transmission system now: Firstly to reduce the level of noise as this particularly effects the lower level readings and will ultimately reduce system resolution and secondly to increase the rate of phase change by restoring the operating frequency to 5GHz. In the first instance it was decided to investigate the radio frequency environment as any “pollution” around the frequency of operation would be detected by the array receiving antenna, amplified and directed to the 1536nm VCSEL. To do this an Agilent PSA 4440 spectrum analyser was fitted with a similar UWB antenna to that used in the array, this antenna had a gain of a little below 2dBi and was capable of operation up to a frequency of 10GHz. The antenna was then positioned within the array and revealed the presence of high levels of signals capable of generating noise like interference. Shown in Fig. 5.17. is the spectrum of received RF signals up to 10GHz. Since some of these signals seemed spurious and pulsed in nature, measurements were taken using the peak hold function of the analyser, over a period of 30 mins. As a result four principle frequencies emerged as being of concern, their frequencies and levels were measured and recorded as shown in Table 5.1 below:

Table 5.1 RF interference levels

Marker number	Frequency	Power	Source
Marker 1	833MHz	-23.65dBm	[mobile phone]
Marker 2	1.767GHz	-23.52dBm	[3G mobile phone]
Marker 3	2.433GHz	-22.94dBm	[wireless router]
Marker 4	3.783GHz	-41.3dBm	[spectrum analyser]

As can be seen these signals are present at high enough levels to impact strongly on the laser modulation and are in some instances comparable in level to the sensing signal. As a single frequency is used this is not a problem in the RF only section as the VNA operates at “zero span”. If however these signals are allowed into active optical devices

they can become problematic causes of harmonic and intermodulation distortion. As these may be unrelated to the sensing signal it is likely that they will appear as random variations in the signal of interest. Listed above are the measured levels with the likely sources shown in brackets.

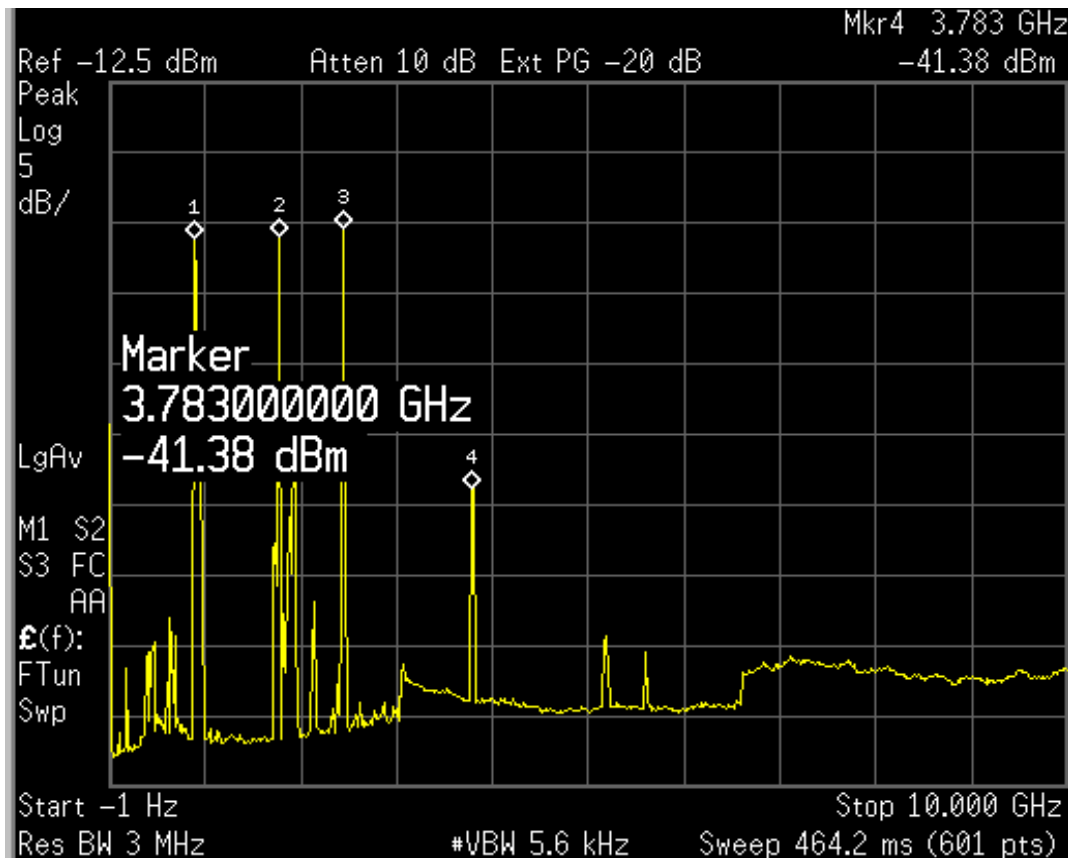


Fig 5.17 Spectrum of RF interference

Contamination from IEEE 802.11 (WiFi) wireless routers and laptops is commonplace, as are emissions from mobile phones and a plethora of mobile devices. The 3.7GHz peak was positively identified as emanating from the network analyser. In this case the noise free spectrum is above 4GHz only. Any useful practical system is needs to be capable of operation in an RF environment such as that outlined above. To compound the problem, as was shown in Fig. 5.3. the 1536nm VCSEL is at its most responsive at the frequencies

where these unwanted signals are present. As a first step it was therefore decided to insert a high pass filter at the input of the amplifier that drives the 1536nm VCSEL. This will allow free operation at 4GHz and above. A suitable filter was identified as a Mini Circuits VHF-3800 for this purpose as it has a high insertion loss across at the frequencies of most concern and a fairly steep roll off outside the stop band as shown in Fig. 5.18. Phase linearity was not considered an issue with this filter as only single frequency operation is required. Also repositioning the sensing head also helped to reduce interference from the 3.7GHz peak due to the network analyser to an acceptable level.

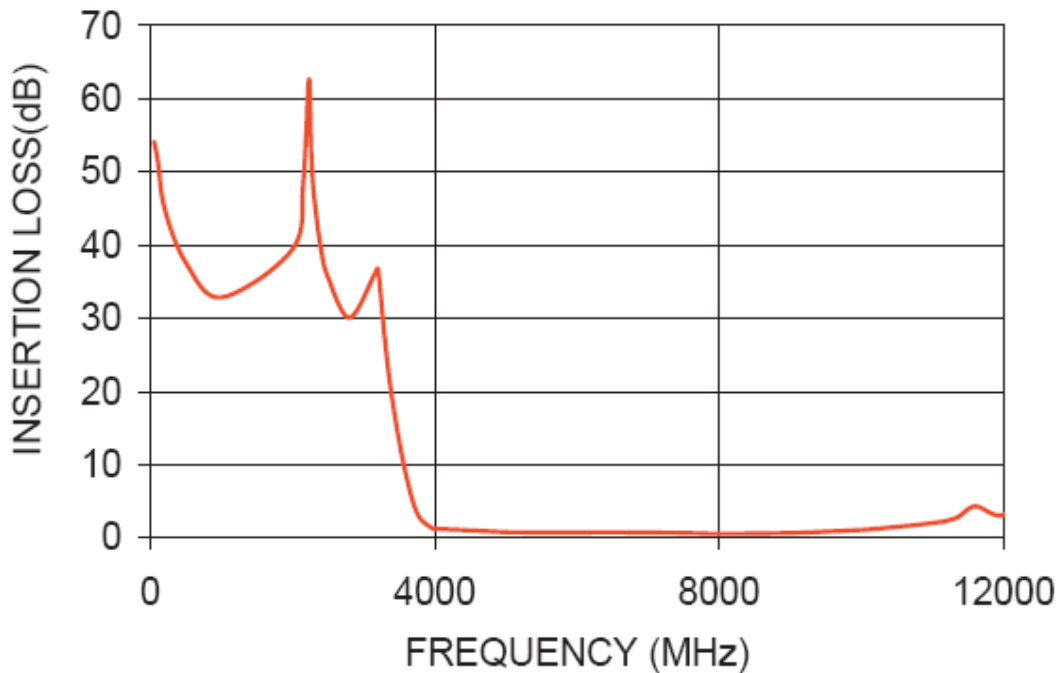


Fig. 5.18 Insertion loss of VHF-3800 filter [5.07]

Attention was now turned to raising the frequency back to 5GHz. This problem was to some extent anticipated when mounting the VCSEL devices as discussed earlier. As can be seen in the S_{21} plots shown in Fig. 5.3. and Fig. 5.14. the frequency response of both VCSELs has been extended beyond their specified range of 4GHz, albeit at a reduced sensitivity. This is indicated by the re-emerging peak marked at 5GHz in the plots, so

giving the possibility of operation at this higher frequency. In any case in order to draw a direct comparison with the original RF only system results it was decided to raise the operating frequency back to 5GHz. An added bonus is also that at this frequency the signal is located well away from the area that the filter begins to take effect. As can be seen in Fig. 5.3. and Fig 5.14. in this region both the 1335nm and the 1536nm lasers had a reduced sensitivity by around 7dB. To compensate for this the modulating power was increased to -6dBm in the 1335nm device, this made it possible to attain a radiated signal level of around 0dBm in the sensing antenna array. Such a drive level increase will inevitably lead to a rise in distortion attributed to the optical devices.

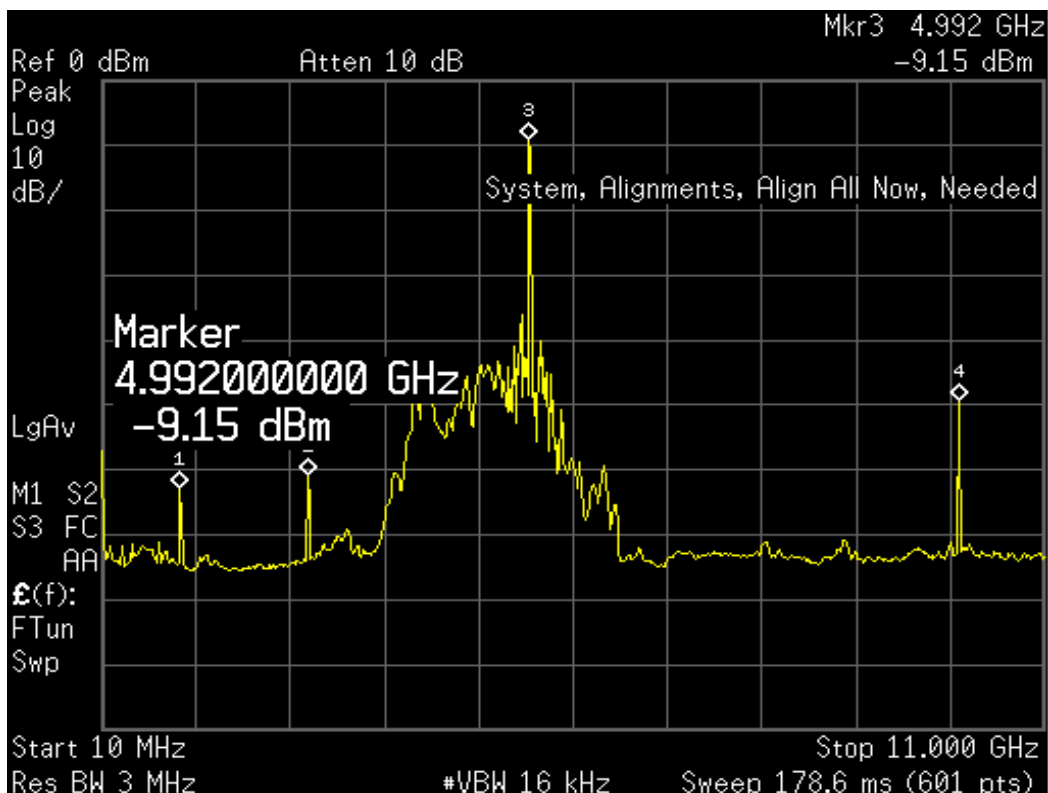


Fig. 5.19. Spectrum at input to 1536nm VCSEL

Figure 5.19. shows the RF spectrum presented to the input of the 1536nm VCSEL after the returning section of the switch matrix and passage through the associated amplifier.

Indicated here, is an acceptable final drive level of -9.15dBm into the 1536nm VCSEL, shown at marker 3. A Second harmonic distortion product can be observed at 10GHz indicated by marker 4. This was due to the high modulation level of the 1335nm VCSEL as mentioned earlier but this is nearly -40dB below the desired 5GHz signal and so is still at a viable level. Shown in Table 5.2 are the final RF signal levels, it can be seen that in the region below 5GHz

Table 5.2 Final RF levels

Marker number	Frequency	Power
Marker 1	926MHz	-61.6dBm
Marker 2	2.4GHz	-61.4dBm
Marker 3	4.99GHz	-9.15dBm
Marker 4	10GHz	-49.8dBm

(markers 1&2), the 926MHz (mobile phone) and 2.4GHz (WiFi) signals are now more than 60dB below that of the level of the 5GHz analysing signal. Although this represented a significant reduction in interference levels it can now also be seen in Fig. 5.19. that significant levels of spurious noise were now visible around the 5GHz frequency of optical modulation. System noise at this level was again reduced by using averaging in the VNA but at a reduced level to that required previously (4 averages). The principal cause of this noise was found to be optical reflections into the VCSELs. Replacing the optical PC connectors with angled APC connectors and the addition of optical isolators immediately after the VCSELs eliminated this problem. Figure 5.20. shows a screen plot of the resulting VNA traces with the analyser in the “zero cal” condition ie. with no object in the sense path. Amplitude is displayed in the top “square” plot, phase in the bottom “rectangular” plot and combined phase and amplitude in the top “polar” plot. As indicated by deviations from the central flat lines in both the phase and the amplitude plots there was still a significant amount of noise present at this stage. This

had the effect of causing random deviation from the ideal phase / amplitude position of the combined point in the same way as that of the data points displayed in the previously discussed constellation plots. The likely cause of this was now the effect of device noise becoming more apparent due to operation of the VCSELs in the less responsive 5GHz region and so represented the limit of the devices.

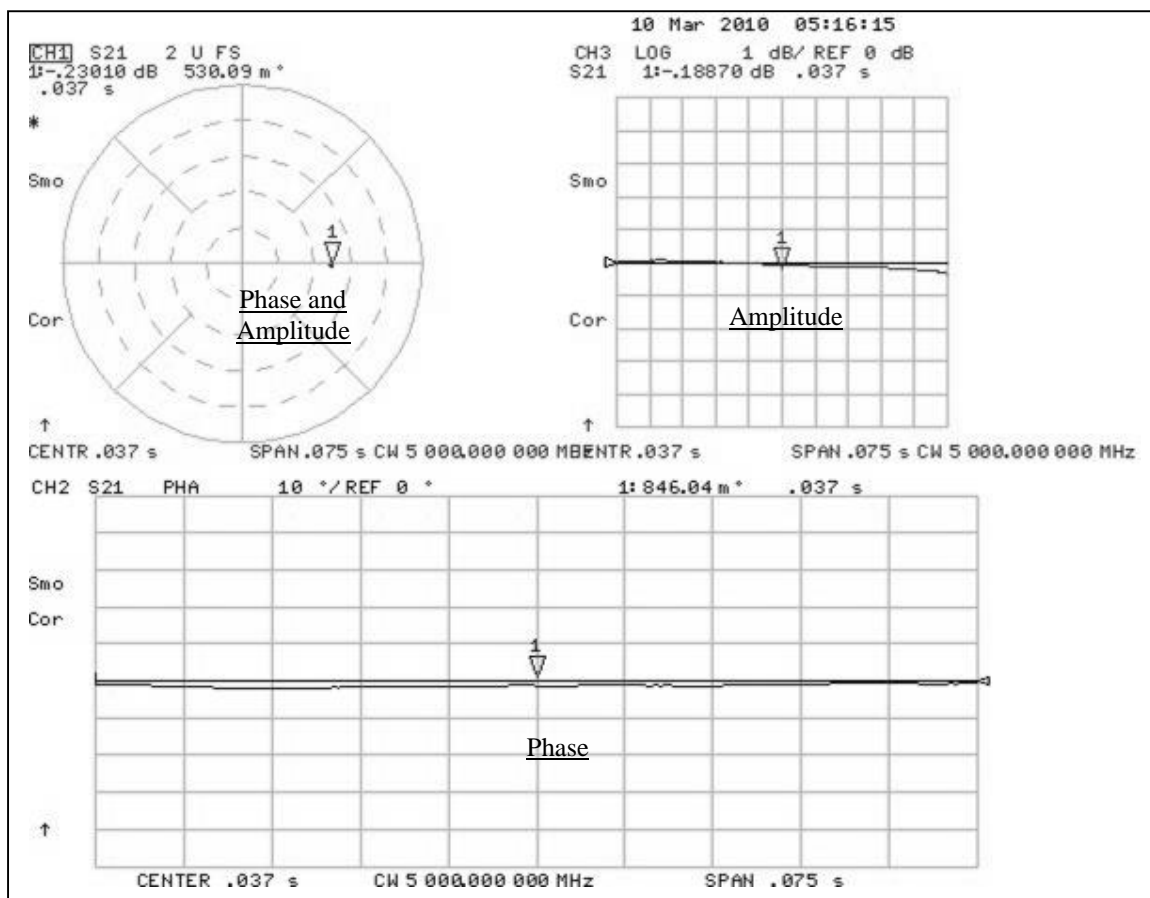


Fig. 5.20 .Screen plot of VNA after noise improving measures

With system noise reduced to this level it then became apparent that the system also suffered from a degree of temperature dependant drift. The causes of this problem were found to be due to two effects. Temperature dependence of VCSELs was initially confirmed as a contributory factor but by far the major contribution was shown to be due to temperature dependant variation of group delay due to the RF amplifiers. The use of

active temperature control was considered undesirable as it leads to increased system complication, power use, and cost. Currently this problem is being managed by providing insulation around the VCSELs to prevent sudden temperature fluctuations and increasing the mass of the RF amplifiers to provide thermal inertia. In this way the effects of temperature changes are to a large extent slowed down and are therefore manageable. A measurement sequence was then devised that incorporated a calibration immediately prior

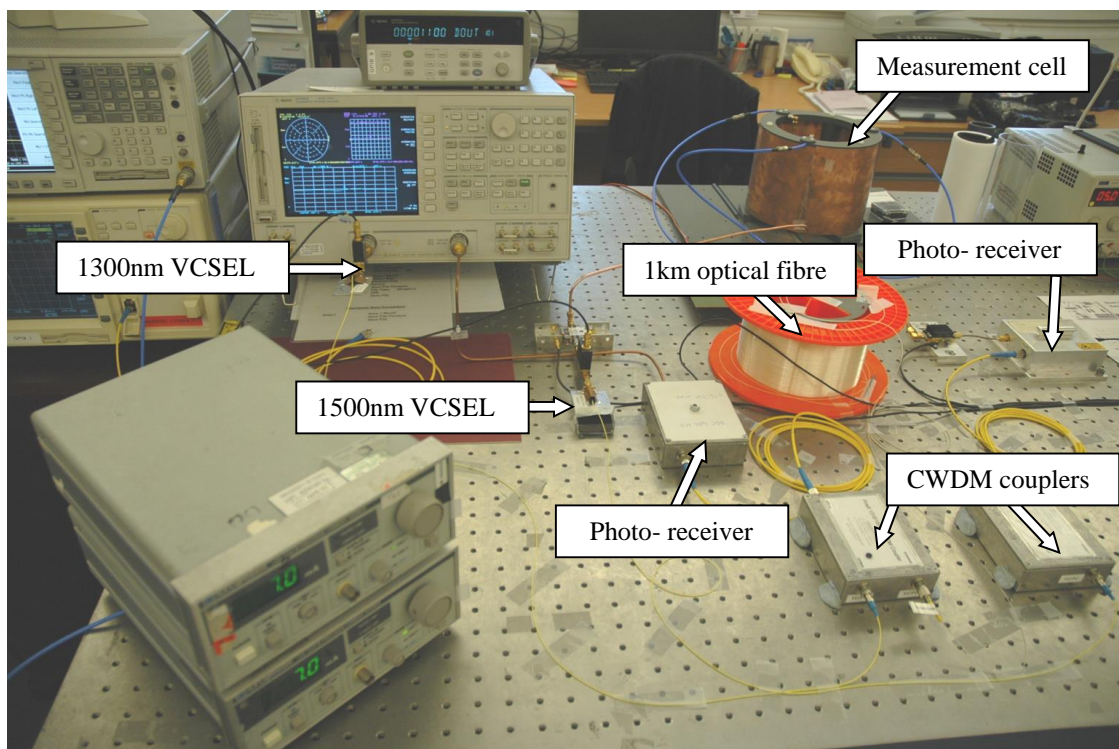


Fig. 5.21. CWDM based measurement system

to measurement, so minimising any effects of drifting. This could then be deployed either prior to every measurement or periodically as required. Figure 5.21. shows the complete system prior to the addition of the thermal protection measures for clarity. With the complete system now operating at 5GHz it was possible to compare readings through the optical channel with those obtained directly from the RF section of the antenna array (Fig. 3.15. Chapter 3). Following the same procedure as described earlier the series of

2mm dia. metallic targets were introduced to the sensing array oriented such that length variation occurred in the E plane of the antennas. As the measurement system was extremely sensitive to any movement in the surrounding screen and positioning equipment it was essential that these comparison measurements were taken under identical conditions. With this established phase and amplitude measurements were then recorded for a series of 2mm diameter targets varying in length between 7mm and 20mm at 1mm increments. Figure 5.22. Shows the resulting phase / amplitude plot after optical transmission over 1km of single mode fibre. It can be seen that the range of variation of both phase and amplitude parameters was comparable with those obtained prior to optical transfer (Fig. 3.15. Chapter 3.) but also it can be seen that there was difficulty in reproducing a smooth curve, due mostly to the effects of the noise mentioned earlier. A further cause for concern was that it was not possible to reliably attribute readings to the 7mm target, as noise effectively masked these readings, as well hence the lack of detail at this end of the plot. Whilst the interference reduction methods of filtering, the replacement of the optical connectors and the addition of optical isolators had been shown to improve the accuracy of the system, it would seem that the only way to further improve system performance was to now use wider bandwidth VCSELs and to increase the modulation depth of the devices so improving SNR of the sensing signal.

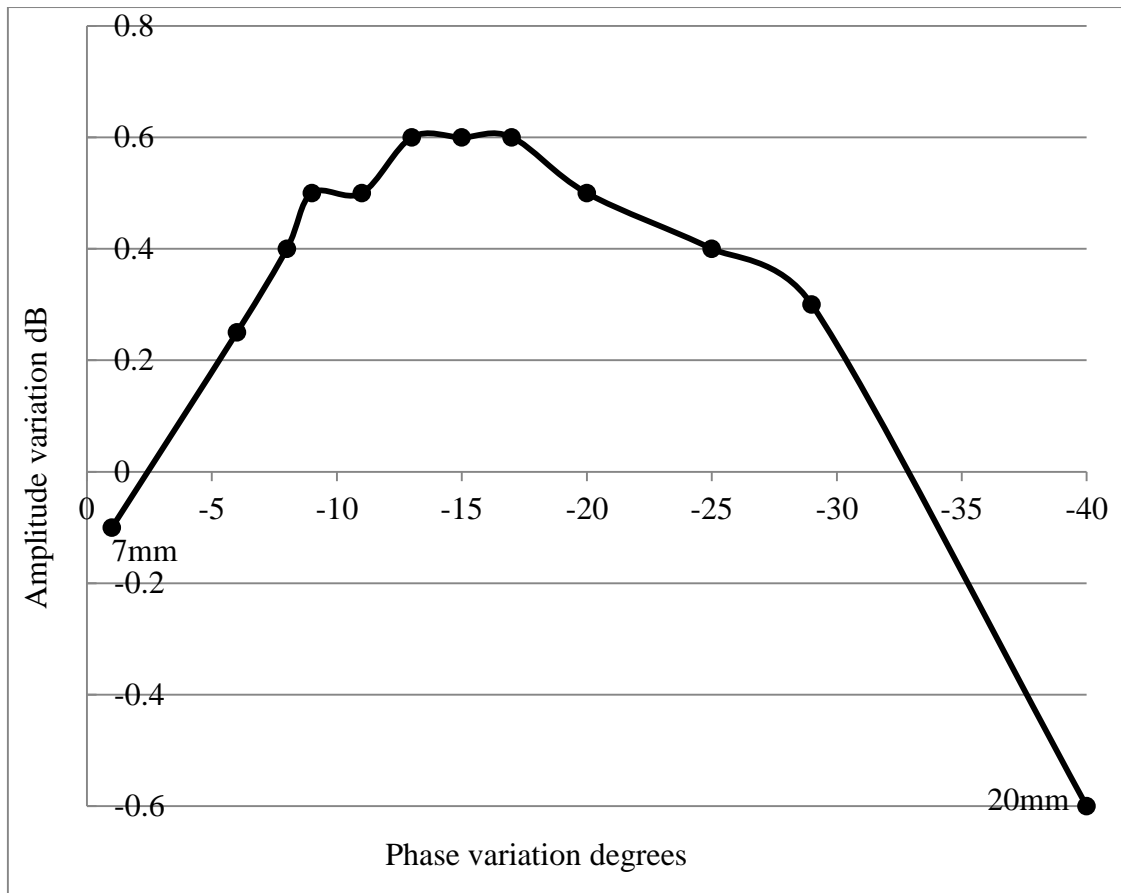


Fig. 5.22. Phase / Amplitude plot after 1km optical transmission

5.4 Final CWDM system

With the need for higher bandwidth devices now apparent it was decided to replace the Raycan 4.25GHz devices with the Vertilas 5GHz VCSELs as discussed in Chapter 4. The devices supplied were Vertilas VL-1320-10G-P2-H4 and VL-1550-1550-10G-P2-H4, these had specified maximum bias current levels of up to 20mA. Over this range optical wavelength varied from approx. 1343nm to 1346nm in the first case and 1546nm to 1551nm in the second so permitting a degree of wavelength selection if desired. These devices were also previously shown to be more sensitive to modulation than the Raycan VCSELs. Optimal signal drive levels and bias conditions for these applications would then need to be established in the first instance. This was carried out using the devices

mounted as described in Chapter 4. to produce an optimal 50Ω match across the range, whilst again being mindful of any range extension possibilities.

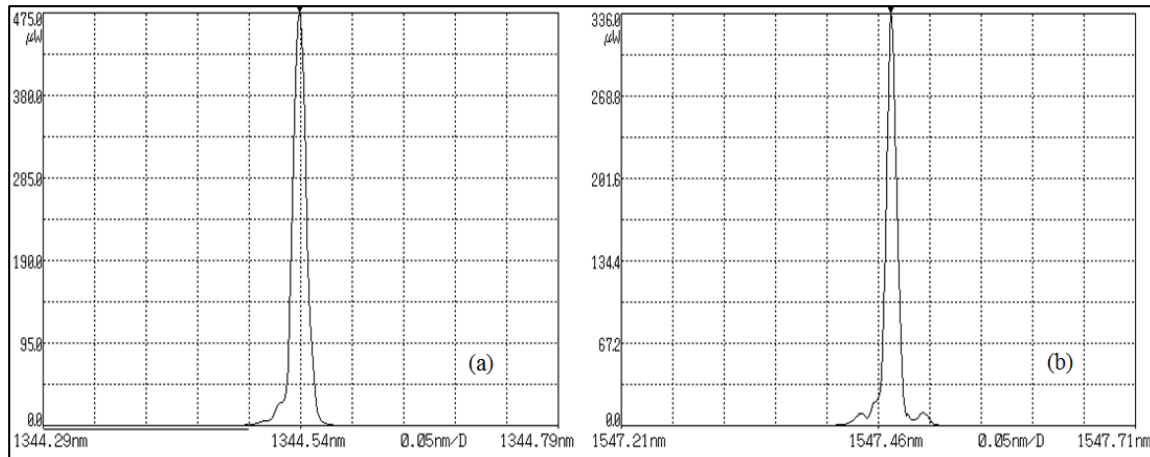


Fig. 5.23a. and Fig. 23b. VCSEL optical spectrums at 10mA bias current

A comfortable bias current level of 10mA was selected for both the 1300nm and 1500nm devices. Using an Ando Optical spectrum analyser, power levels of $475\mu\text{W}$ at an optical wavelength of 1344.54nm and $336\mu\text{W}$ at an optical wavelength 1547.46nm recorded as shown in Fig. 5.23a and Fig. 5.23b. These wavelengths and optical power outputs were now ideally matched for use with the finalised CWDM transmission system now fitted with the RF high pass filter, APC connectors and optical isolators as outlined previously. To facilitate possible future system development (using swept or broadband signals) and also to utilise the full potential of the VCSEL and antenna combination it was then decided to verify and if possible, match, the bandwidth performance of all devices. Both VCSELs were evaluated for drive level and bandwidth availability using a HP-83732B microwave signal generator driving directly into each device and a 10GHz Discovery DSC-402HR photo-receiver that provided electrical conversion for analysis by a Rhode & Schwartz 26GHz FSU spectrum analyser. As a result it was established that a suitable drive level was -20dBm for both devices. Figures 5.24a and 5.24b show the resulting

spectral analysis obtained for both devices at this -20dBm drive level over a frequency range of 2GHz to 11GHz, well beyond the specified range of operation. Modulation frequencies were selected at 100MHz intervals from 3.2GHz to 5.3GHz; this will give a good margin of frequencies over which detection could then be carried out. From these plots it can be seen that a signal to noise ratio in excess of 40db is obtained across this range for both the 1344nm and 1547nm VCSELs. Second harmonic distortion was however, significant but should not present difficulties in this narrow bandwidth application, provided no mixing effects occur with outside RF sources.

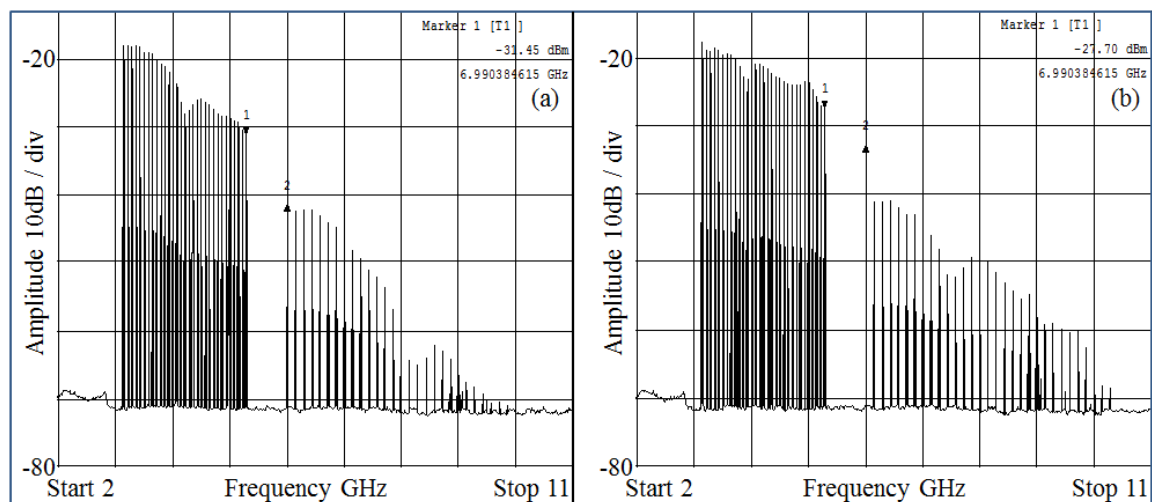


Fig. 5.24a. 1344nm frequency spectrum and Fig. 5.24b. 1547nm frequency spectrum

As the frequencies in question lie between 7GHz and 10GHz it was unlikely that any RF sources at levels high enough to present a significant risk existed in the current operating environment. Attention was then directed toward the Omron WXA-N2SL antennas described in Chapter 3. These antennas were originally designed for use in WiMedia UWB devices with a requirement for operation at frequencies between 3.1GHz and 5GHz. and so defined the limits over which the detection system could operate. It became apparent when measuring the S_{11} return loss of the antenna that whereas the device had sufficient bandwidth coverage there were significant variations across the range. Figure

5.25a shows the measured return loss of a standard device with markers placed 3GHz (marker 1) with a return loss of -5.8dB, 4GHz (marker 2) with a return loss of -15.1dB, 5GHz (marker 3) with a return loss of -13.1dB and 6GHz (marker 4) with a return loss of -2.3 dB. Such variations within the system would clearly introduce regions where there would be seriously reduced sensitivity due to signal reflection from the antenna feed. In order to remedy these defects it was decided to try to modify the device to produce a smoother frequency response.

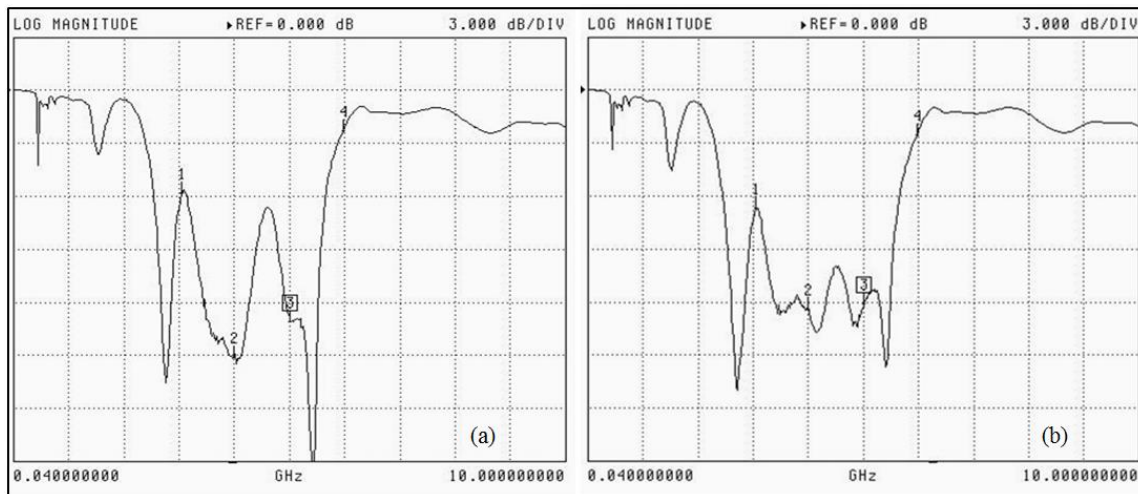


Fig. 5.25a. S_{11} of standard antenna and Fig. 5.25b S_{11} of antenna with Perspex tuning strip

This would be facilitated by adding a discontinuity to the dielectric layer of the antenna. It was determined empirically that the addition of a small Perspex strip, ϵ_r 3.0, to the top edge of the antenna produced a frequency shifting effect in the S_{11} return loss response. Careful adjustment of the size and position of this strip could therefore be utilised to alter the antenna resonance across its range and so tune the antenna. Using this effect it was shown to be possible to improve the S_{11} results across the range and most significantly in the region above 4GHz; where the chosen operating frequencies are allocated. Figure 5.25b. illustrates the S_{11} trace of the tuned antenna with markers placed at the same points

as previously selected. With Marker 1 at 3GHz a return loss of -6.7dB was measured, Marker 2 at 4GHz gave a return loss of -12.4dB, Marker 3 at 5GHz indicated -13.0dB and finally Marker 4 at 6GHz remained at -2.5dB. With the functional bandwidth of both devices now established the final CWDM measurement system was assembled as shown in Figure 5.26. Here the measurement cell is essentially the same as outlined previously, with the addition of a dielectric material screen surrounding the target when required as for the indirect measurements described later. It can be seen that optical isolators are inserted following the VCSEL outputs in both optical paths. The position of the Mini Circuits VHF-3800 high pass filter is shown, and to further reduce the impact of any RF system noise low power consumption and low noise amplifiers (LNA) were deployed. These consisted of a Hittite H392L LNA followed by an Atlantec AOX-010200 power amplifier used at amplification points 1 and 2 as shown on the system diagram. These changes led to total system power consumption of 6Watts. With these improvements in place the aim was to further reduce the noise problem, so leading to better resolution. In addition this would enable the reduction or preferably the elimination of the need for averaging at the network analyser, potentially leading to faster measurements. As discussed earlier the use of a tri-antenna array was to allow for the possibility of position location as well as size estimation. To this end three modes of operation were established for measurements between each of the antenna pairs. If all three modes of measurement between the antenna pairs were to be used it is important to establish parity of each mode (1,2 or 3) with that of its neighbour. After careful alignment of each antenna and each antenna pair, good agreement in phase and amplitude readings was obtained between each switched pair condition, this is shown in Table 5.3. Readings were initially taken at the RF switch matrix output at a frequency of 5GHz. As with the previous measurements

a series of 2mm cylindrical metallic targets of varying length were inserted centrally into the antenna array.

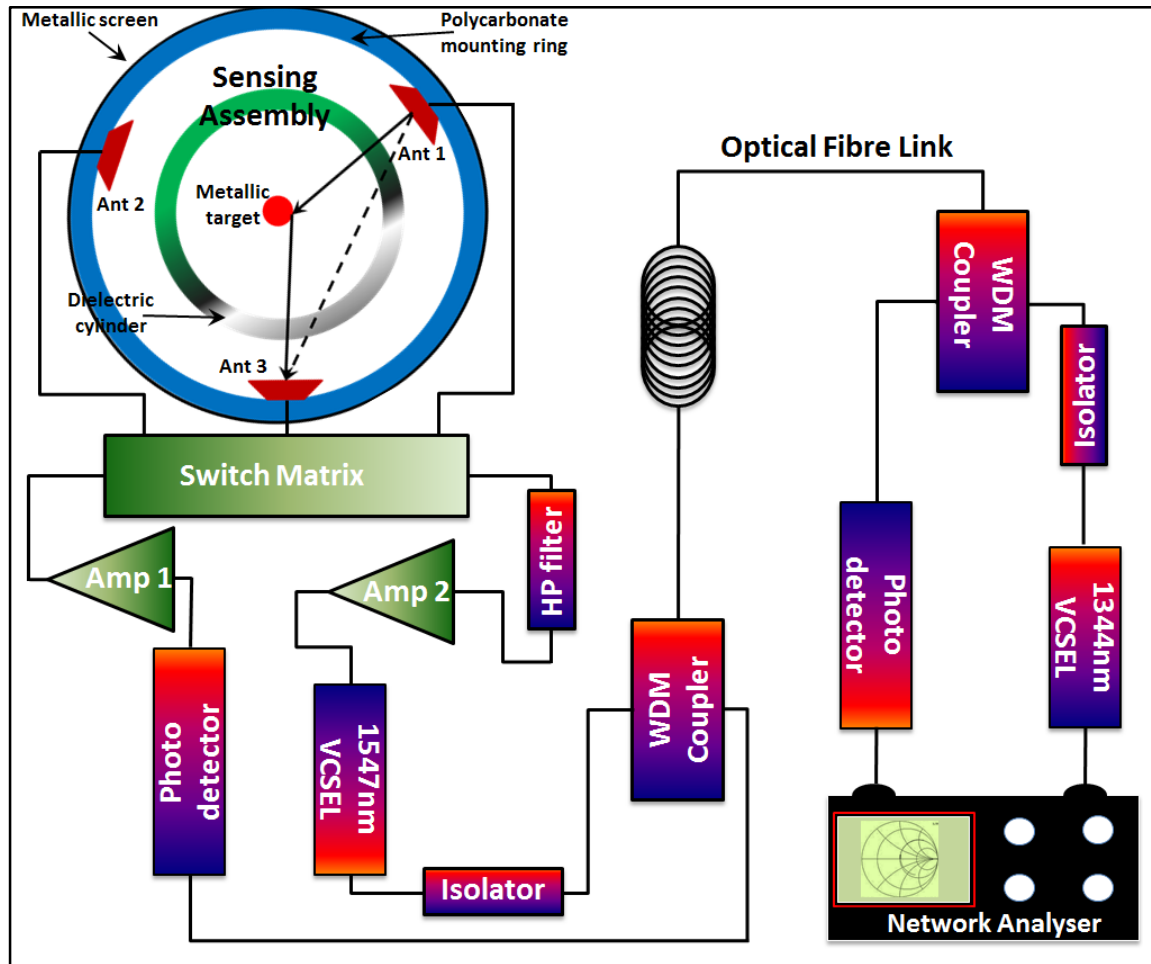


Fig. 5.26 Final system diagram

Phase and amplitude measurements were then taken in each of the three measurement modes. As can be seen from table 3 it was now possible to measure targets over a range from 20mm down to 6mm. Also there is a good degree of agreement between each of the antenna pairs and each of the millimetre steps is easily discernible. Figure 5.27a. shows the phase / amplitude plot of measurement mode 3. This shows a similar range to that previously recorded indicating that the RF tuning measures used to “flatten” the antenna

frequency response had no adverse effects on the radiation pattern and gain of the antenna.

Table 5.3. Comparison of phase (deg) and amplitude (dB) readings

Target length mm	Before Optics Mode 1		Before Optics Mode 2		Before Optics Mode 3		After Optics Mode 3	
	Phase	Amp 1	Phase	Ampl	Phase	Ampl	Phase	Ampl
20	-39.4	-0.13	-39.5	-0.15	-39	-0.2	-38	-0.2
19	-30.6	0.26	-30.7	0.36	-30	0.3	-30	0.3
18	-24.9	0.29	-25.1	0.4	-24	0.37	-23	0.5
17	-18.6	0.38	-19	0.42	-18	0.4	-18	0.5
16	-15.1	0.46	-15.9	0.48	-15	0.4	-15	0.5
15	-12.4	0.39	-13.1	0.41	-12	0.38	-12	0.43
14	-10.4	0.35	-10.5	0.4	-10	0.35	-10	0.39
13	-8.2	0.35	-8.5	0.35	-8	0.3	-7.8	0.33
12	-6.4	0.29	-7	0.28	-6	0.25	-6	0.27
11	-4.9	0.26	-5.1	0.24	-4	0.21	-4	0.2
10	-3.9	0.19	-4.1	0.2	-3	0.16	-3	0.14
9	-2.9	0.18	-3.1	0.16	-2.7	0.1	-2.8	0.1
8	-1.8	0.15	-2.1	0.11	-1.6	0.12	-2	0.08
7	-1.1	0.1	-1.7	0.09	-1	0.1	-1.2	0.1
6	-0.9	0.07	-1.1	0.05	-0.8	0.06	-0.8	0.05

The CWDM optical system was then connected and with the VCSELs biased at 10mA RF drive levels for both were adjusted to the pre-determined -20dBm. A phase / amplitude plot was then taken as previously described as shown in fig. 5.27b. As can be seen when comparing both, plots there was a good level of agreement at most data points, with a similar range of both phase and Amplitude variation. With these measures taken to reduce both the optically induced noise, the RF interference and the inherent system noise, a much improved signal to noise ratio resulted within the system, this, subsequently resulted in the EVM of each data point being reduced. In turn it was then possible to further reduce the need for averaging to four iterations and consequently speed up measurement times. Improvement in SNR / EVM was predictably most

noticeable at the lower end of the target range where conditions were more challenging and variations are at their smallest.

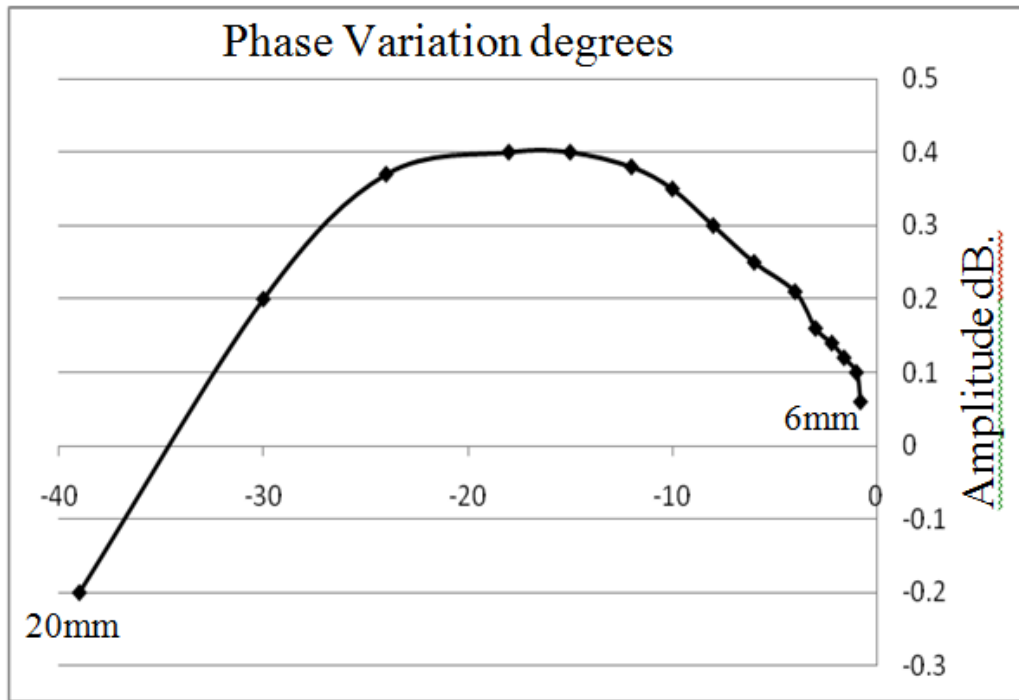


Fig. 5.27a. Mode 3 E-plane, length measurements before optical transmission

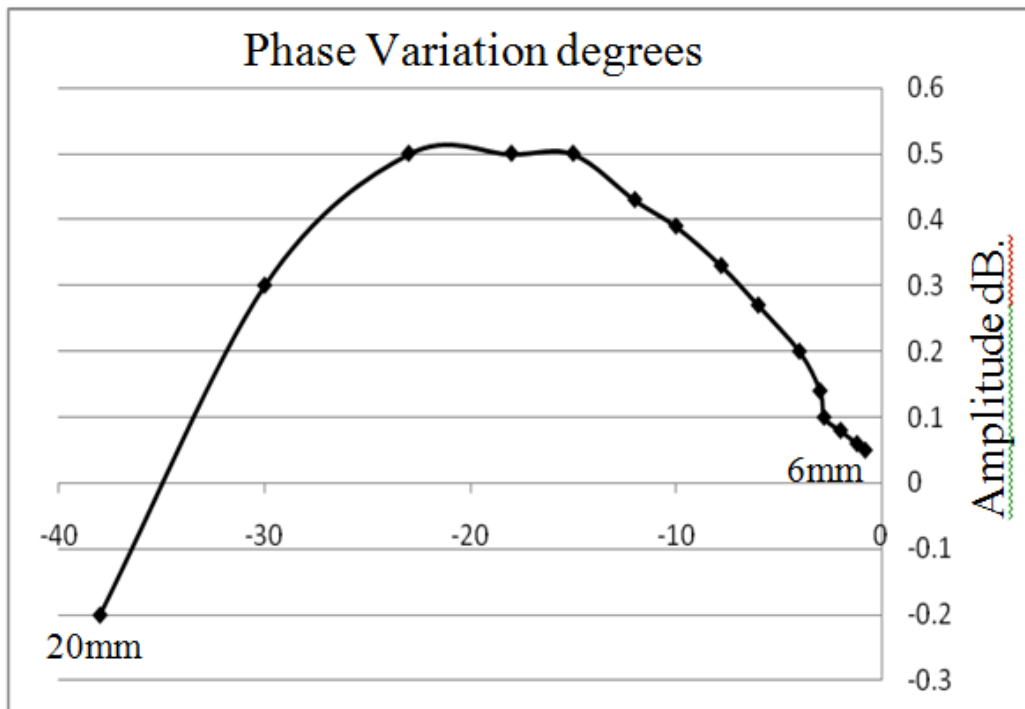


Fig. 5.27b. Mode 3 E-plane, length measurements after optical transmission

These results represented a clear improvement on those obtained previously with clearly discernible and well defined data points before and after optical transmission. Signal quality improvement can be seen in a comparison of the VNA screen plot shown in Fig. 5.28. below with the previous VNA plot (Fig. 5.18.). The “single spot” of the combined phase / amplitude polar readout (top left) signifies a low EVM which is confirmed by the improved flatness of the amplitude (top left) and phase (bottom) readout traces.

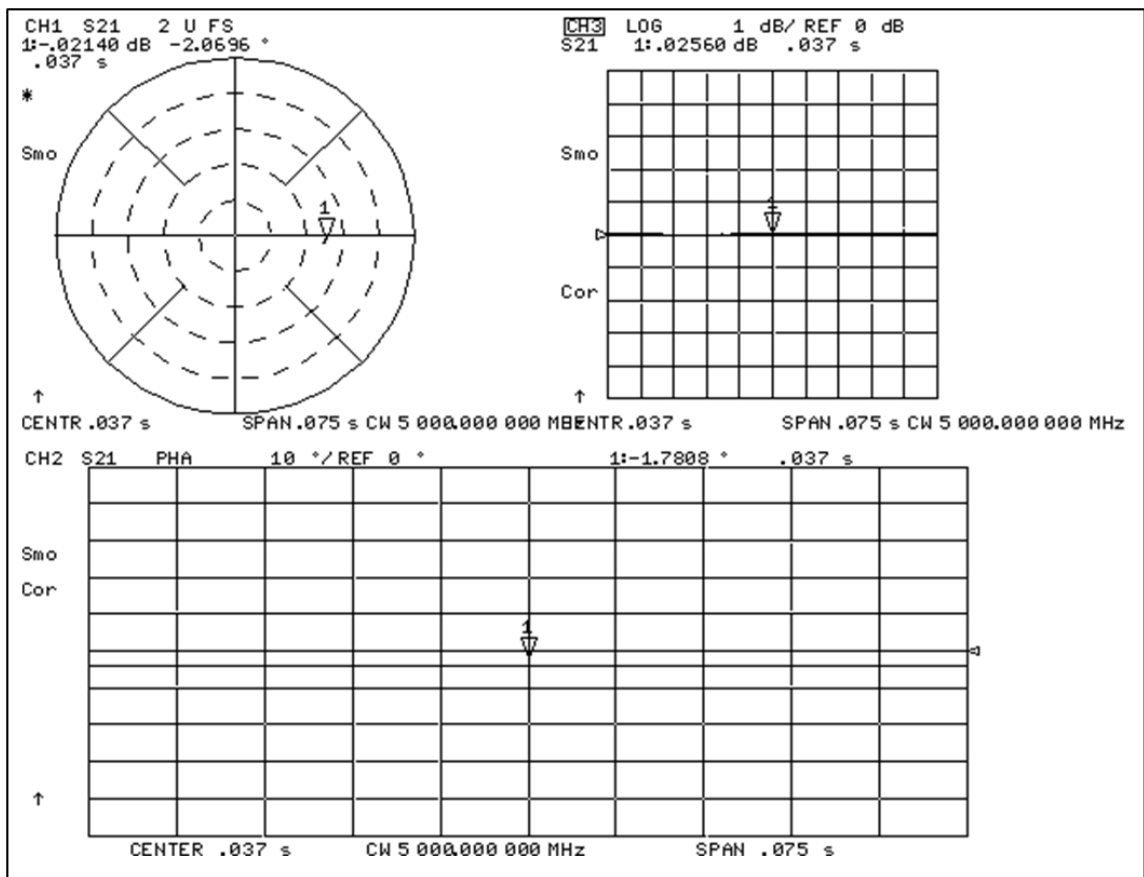


Fig. 5.28. VNA screen plot

It was then decided to explore the performance of this detection system with the target shrouded with a variety of non- conductive materials. Two such examples using materials with known dielectric properties are shown in Fig. 5.29. and Fig. 5.30. [5.08]. A Cylinder of each of these dielectric materials was then prepared, each measuring 16.5cm in length

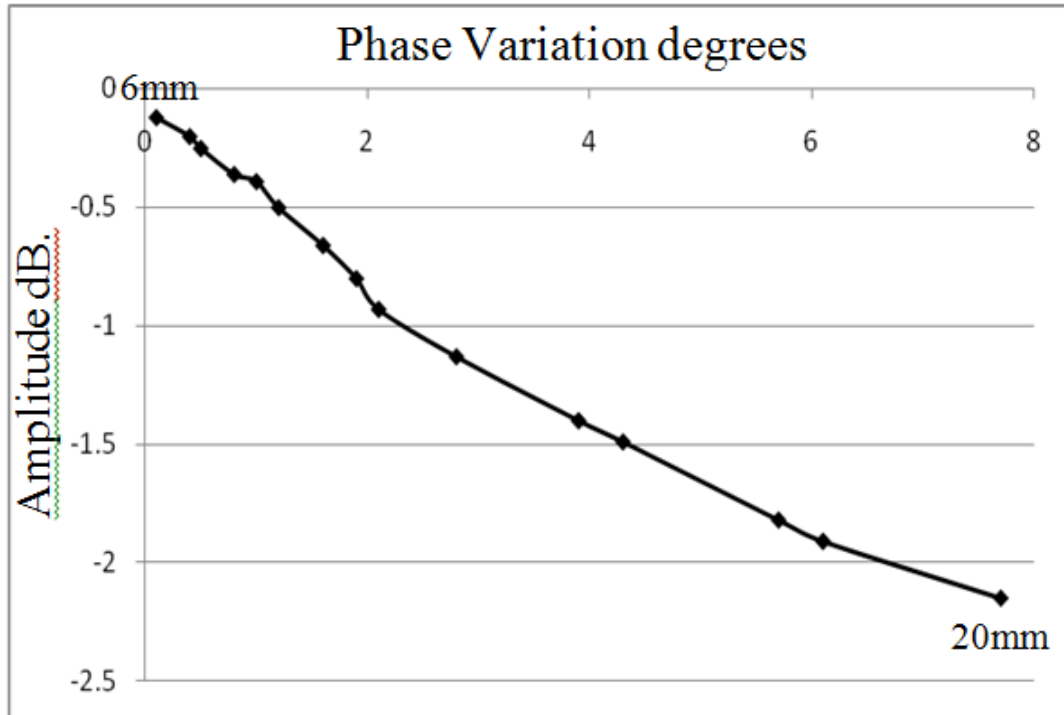


Fig. 5.29. Through PTFE tube

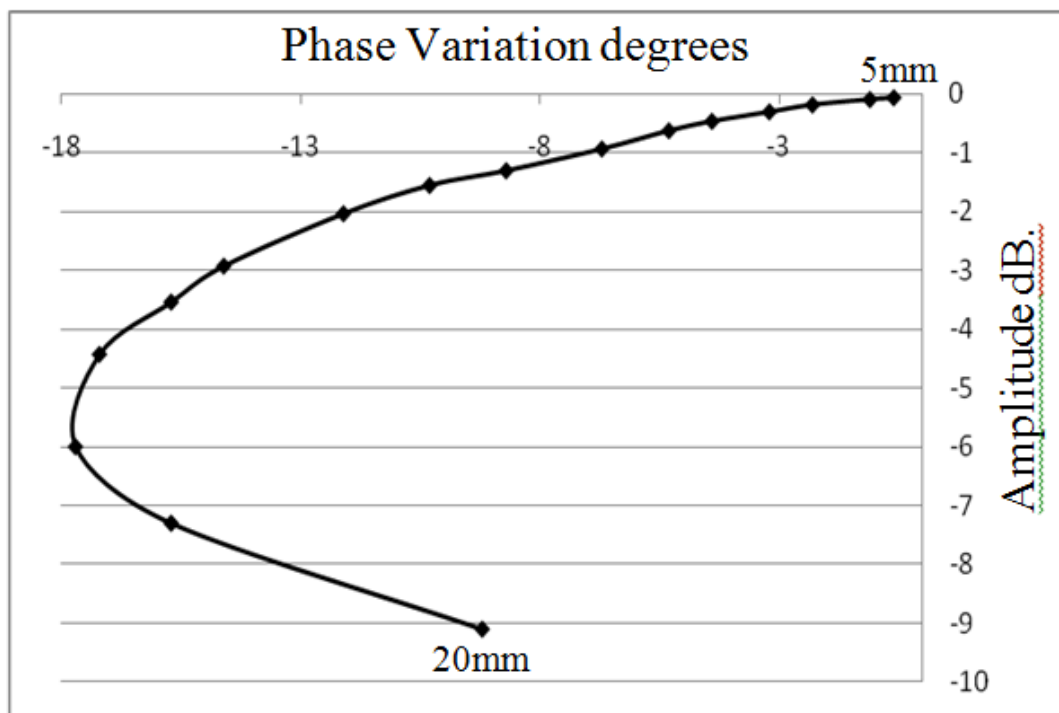


Fig. 5.30. Through perspex tube

and 7.5cm in diameter and with a wall thickness of 6.5mm. These were then positioned in turn so as to completely obscure the target area from direct illumination from the antennas and the same series of metallic objects inserted at the identical position as for the previously described set of results. The first cylinder, made of PTFE, (ϵ_r 2.2) was positioned centrally between the target area and the sensing antennas and the series of 2mm dia metallic targets were introduced. Figure 5.29 shows the resulting phase / amplitude plot indicating better defined and spaced data points with less phase and more amplitude variation than previously recorded. Data points were again clearly resolvable over a 20mm to 6mm target size range. The second example shown is for a perspex cylinder ($\epsilon_r=3.4$) which was now inserted in place of the PTFE one. Again using the same power level of 0dBm; the above procedure was repeated, with the resulting plot shown in Fig. 5.30. In this plot it can be seen that not only do the data points have improved definition spacing but also that the smallest target size identification range has been extended down to 5mm. These effects were possibly due to wavelength shortening due to the increased effective dielectric constant of the transmission path caused by the introduction of the non-conducting cylinders. Following this procedure target was again rotated through 90 degrees and the measurement procedure repeated. In this orientation the system was found to be unresponsive, confirming the earlier experimental assertion as to the polarisation sensitivity of the measurements and suggesting that polarisation was not affected by the introduction of the dielectric material.

5.5 Conclusions

It was established in the previous chapters that it was necessary to produce a system of transmission capable of preserving the phase and amplitude information carried by the single frequency unmodulated carrier used by the VNA for analysis. In order to facilitate

remote operation a target distance of 1km was selected, optical fibre and associated optical signal delivery systems were the ideal medium to accomplish this. Two approaches were investigated with the aim of producing a method that was simple and exhibited low power consumption, whilst being stable and accurate. The first approach employed a reflective optical transducer. Initially the use of this device was very attractive as it had very low power consumption and allowed sensitive laser and photodiode components to be remotely sighted away from the RF sensor head. Extensive characterisation of the transducer confirmed it's suitability as a device that could be operated within the parameters required but the device had a significant architectural flaw, in that it had a common upstream / downstream RF signal port. To overcome this problem it was decided to use an RF circulator so as to discriminate between the necessarily simultaneous sensing signals travelling in opposite directions to and from the VNA. It was found that due to the large disparity in upstream / downstream signal levels it was not possible to obtain sufficient isolation for the system to operate reliably. Some indistinct results were obtained but it was likely that these should be attributed to crosstalk within the reflective transducer and RF circulator; as a result this approach was abandoned, although some useful information was obtained. During the course of this investigation it was necessary to develop an understanding of how to directly modulate VCSELs and obtain an extended frequency response from these devices. This proved useful in the implementation of the second method to be investigated, the CWDM approach. The CWDM optical system allowed a high degree of directional isolation, this being due to the inherent 40dB optical isolation of the CWDM splitters. Such inherent isolation allowed accurate, crosstalk free transmission of phase and amplitude information. Accurate, bi-directional, full duplex, transmission was accomplished over 1km of single mode optical fibre. Using directly modulated VCSELs, carefully mounted,

the sensing frequency was raised from 4GHz to 5GHz and filtering added leading to increased measurement sensitivity and reduced noise effects from environmental RF interference. This technique allowed greatly simplified remote access to, and control of sensing multiple antenna arrays. Further noise reduction was made possible with the use of wider bandwidth VCSEL's . Using mounting techniques acquired from the previous experimental VCSEL use, improved 50Ω impedance matching was now possible, as was the frequency response that was now a good match to that of the antenna. These improvements combined to produce a system with an improved SNR which in turn reduced the need for averaging which would slow measurement speeds in a practical system. Building on this, the performance of the measurement technique was then evaluated when the same set of targets was completely obscured from direct view of the sensing antennas by non-conducting materials. Using these methods it was shown that viewing through these higher dielectric materials does not degrade the performance of the system for a given power level. Target identification was extended down to 5mm with clearly defined millimetre resolved data points. This indicated that detection through these high dielectric materials may to some extent increase the accuracy of phase based measurements. Such enhancement can be attributed to wavelength shortening in the higher dielectric constant material, which in turn leads to increased phase shifting. Such performance would potentially allow sub-millimetre resolution, but this would be limited by transmission material losses, which would decrease the SNR of the received signal. This ability to see through non-conducting materials allowed for sensing applications without the need for the antenna to be in contact with, or immersed in, the propagating medium. Using non-contact sensing methods can lead to simplified antenna design as the sensing antenna can be "air matched" as usual and there is no need for the use of matching fluids etc [5.09][5.10]. In turn greater system flexibility becomes possible, as

this allows the possibility of scanning array mobility, both along and around the object of interest, a desirable feature if image reconstruction is required. With the rotation of the target it was also shown that signal polarisation orthogonality was undisturbed by transmission through the dielectric material. With the integrity of the VCSEL based CWDM optical transmission link established, the development of a polarisation switchable detection system was then investigated. This would necessitate the design and fabrication of a suitable antenna that complements the current RF and optical transmission system. From the work carried out to this point, the physical attributes of the antenna, a desired radiation pattern, gain and bandwidth performance, as well as frequency choice, have been established. These parameters will dictate the choice of design, as described in the following chapters.

References

- [5.01] Jussi Säily, Pekka Eskelinen, Antti V. Räisänen. "Pilot Signal-Based Real-Time Measurement and Correction of Phase Errors Caused by Microwave Cable Flexing in Planar Near-Field Tests". IEEE Transactions on Antennas and Propagation, Vol.51, No 2, Feb. 2003 Page(s) 195-200.
- [5.02] Ronald D. Esman, Michael Y. Frankel, and Paul J. Matthews. "New Array Capabilities by Photonic Beamforming" (invited). Microwave Symposium Digest, 7th-12 June 1998, pages 1363 - 1366 vol.
- [5.03] I.J.Craddock, M, Klemm, J. Leendertz, A.W. Preece and R. Benjamin. "Development and Application of a UWB Radar System for Breast Imaging." Loughborough Antenna and Propagation Conference, 2008, p.24..
- [5.04] <http://cp.literature.agilent.com/litweb/pdf/5991-1828EN.pdf> Extending the Measurement Plane up to 1 km in Vector Network Analysis.
- [5.05] T.J. Quinlan, S.E.M.Dudley and S.D.Walker. "Radio-over-Fibre Phase Contrast Imaging using a Reflective Electro-Absorption Transducer and 1550/1310nm VCSEL's". OFC 2010.
- [5.06] Terence Quinlan Sandra Dudley, Tony Jordan, Stuart Walker "Improved Radio Frequency Imaging Resolution using Phase Contrast Interferometry". LAPC Nov. 2009.
- [5.07] Mini circuits data sheet
- [5.08] Terence Quinlan Sandra Dudley, Tony Jordan, Stuart Walker "Remote,Non-Contact, Radio Frequency Phase Contrast Detection using CWDM and Directly Modulated VCSELs". LAPC Nov 2011
- [5.09] Gibbins, D. Klemm, M. Craddock, I.J. Leendertz, J.A. Preece,A. Benjamin, R. A Comparison of a Wide-Slot and a Stacked Patch Antenna for the Purpose of Breast Cancer Detection. IEEE Transactions on Antennas and Propagation, Volume: 58 , Issue: 3 2010 , Page(s): 665 – 674.
- [5.10] Klemm, M. Craddock, I.J. Leendertz, J.A. Preece, A. Benjamin. R . "Radar-Based Breast Cancer Detection Using a Hemispherical Antenna Array Experimental Results". IEEE Transactions on Antennas and Propagation, Volume: 57, Issue: 6 2009 , Page(s): 1692 – 1704.

Chapter 6 Design and Modelling of a Polarisation Plane Switchable Antenna

6.1 Design Considerations

As was evident in Chapter 1 a multitude of antenna designs have been used for the purposes of radio frequency detection. Mostly these designs were non-specific, and also often compromised system performance in terms of size, practicality, cost and complexity. Using the knowledge gained from the work so far, it was then possible start with a clear picture of what is required. From this an antenna structure that encompasses as many of the desired features as possible and incorporates these in to a practical solution can be selected and designed. As with the commercial UWB design used in the current array, small size and a wide bandwidth are the first pre-requisites. This allows for a compact array design which is important in a short range detection system and wide bandwidth allows for flexibility of placement as discussed previously. Low back radiation is required to eliminate spurious external reflections and a high gain structure will aid an improved SNR and so enhance system resolution performance. If the design is to support polarisation diversity it must have two distinct polarisation states with high isolation between each state. Finally if the design is to be used to detect phase differences, emission from each polarisation state should be from the same point in space and exhibit identical and preferably symmetrical radiation pattern characteristics in both polarisation states. These conditions will be necessary to ensure that readings are directly comparable at the same point on the target for both polarisation planes. A number of schemes were considered, the simplest of these was to utilise two, wire dipole antennas, mounted orthogonally about the same axis. Whilst this would provide a solution that was easily simulated it would not meet the criteria outlined above in that the gain would be rather

low, the radiation pattern widespread and each element would be relatively large in size in comparison to the measurement cell. Two further fundamental issues make this option unattractive in that due to the dimensions, the far field condition is remote and it is difficult to construct a phase matched feed arrangement to both dipole elements. Printed dipole designs similar to that used initially can overcome some of these difficulties in that the antenna dimensions can be reduced but in common with the wire design the principal stumbling block lies in the feeding arrangement. If both antennas are to be located on the same plane then the feeds for both structures are coincident and therefore difficult to separate. Another design given consideration was that of a co-axial, wide bandwidth, axially fed leaky feeder [6.01]. In this case the feed for each of the orthogonally situated antenna structures is directly at the end of a length of radiating semi rigid co-axial cable. Several configurations were considered but either the antennas could not be easily positioned on the same plane or the necessary half wavelength spacing could not be accomplished without obstructing the feed arrangement. Similar slotted designs again suffer similar difficulties of geometry and deployment. All the options discussed so far will also tend to suffer with a low gain characteristics unless deployed as self-contained arrays. Other options considered were horn type antennas, both printed and flared Vivaldi designs and the familiar standard three dimensional horn. Whilst these designs possessed the desired gain, bandwidth and radiation pattern properties, they tended to be large devices that would be difficult to deploy in a compact sensing head. Also if polarisation diversity is to be exploited as desired, feed options and physical placement possibilities once again become limited. With the above options unlikely to provide an ideal solution it was decided to explore alternative patch antenna designs. Patch antennas offer the advantage of having a gain of up to 9dBi. and with careful design of the ground plane low back radiation is possible. In conjunction with a potentially compact design the planar

nature lends itself to common source emission with little side lobe generation. With careful placement of dual antenna feeds it is also possible to excite differing polarisation planes and states so allowing the possibility of switchable polarisation plane selection. A serious limitation to conventional designs however is that these devices only support narrow bandwidths and the extent of isolation between polarisation planes in a switched configuration is unclear [6.01]. The background, design procedure and modelling of a suitable polarisation switchable, linearly polarised patch antenna will now be described. This device will feature high isolation between polarisation planes, a wide usable bandwidth and an operating frequency of 5GHz so as to match the optical transmission system as described earlier.

6.2 Patch Antenna Background

A basic patch antenna consists of a conductive ground plane, a dielectric layer and a conductive radiating top layer which, when excited, forms a resonant structure. Excitation is established via a feeding arrangement to the top layer and can be accomplished in a number of ways. The specific nature of the feed is dependent on parameters such as bandwidth requirement, the structure geometry, impedance matching and radiation (polarisation) properties etc. Commonly used coupling methods include Probe, Stripline and Cavity methods, each having differing attributes which will be discussed later. Although the radiating top patch can be of almost any shape [6.02] for the purposes here a design that possesses clear radiation properties that are both orthogonal and symmetrical, is essential. To this end the simplest realisation of this, which was based on a square design was selected as a starting point. In a finished design, radiation will occur along selected edges which function in a dipole like manner this patch dimension is defined by approximately the half wavelength distance of the operating frequency. This

dimension will to some extent be defined by the effective dielectric constant (ϵ_{reff}) and thickness of the separating substrate. The thickness of the radiating metallic layer (patch) influences the electrical propagation across the face of the patch and so helps define a feed point and the impedance at a given point. Dependant on the placement of the feed, the electrical propagation on the patch face will behave in different ways and so can be used to define input impedance and areas of radiation at the patch edges. In this way it is possible to select electrical activity at either the vertical or horizontal edges of the square radiating element.

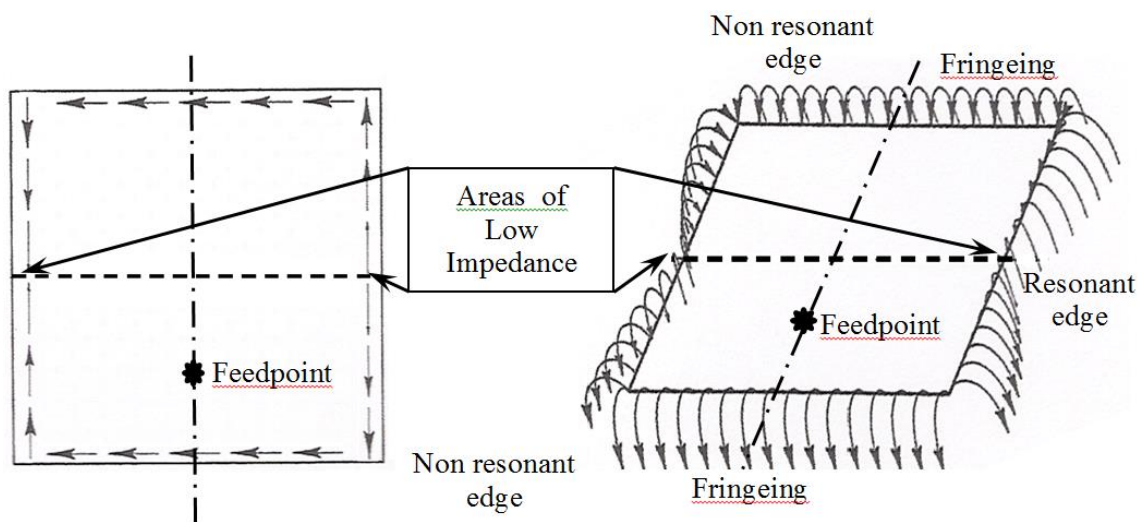
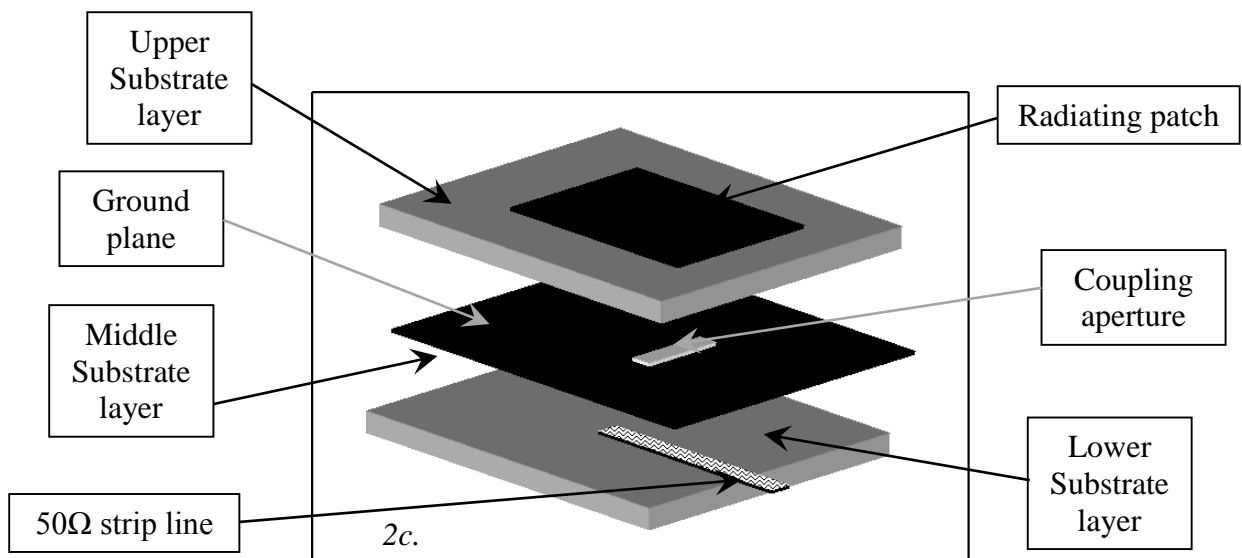
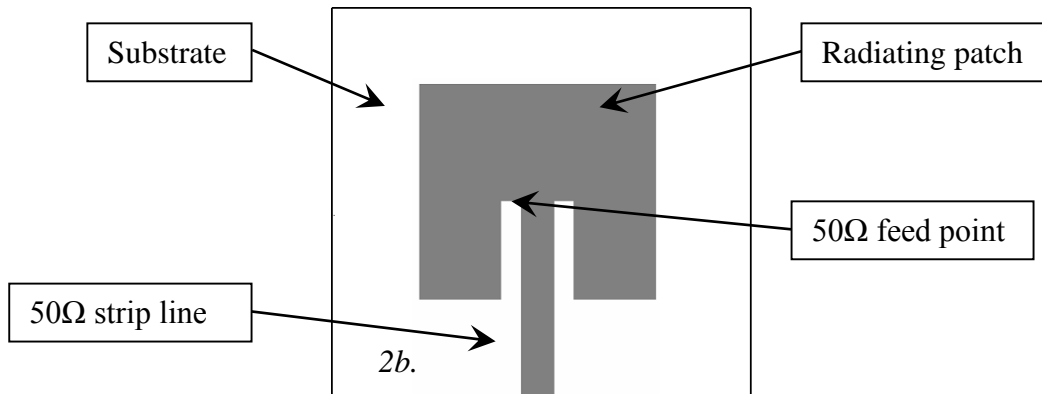
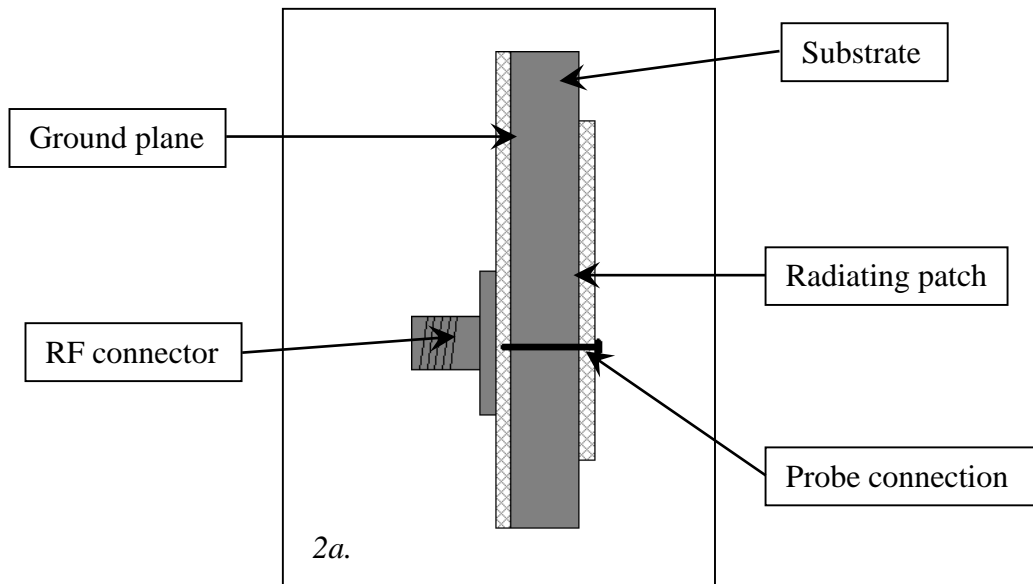


Fig. 6.1a. Voltage on patch face

Fig. 6.1b. Propagation at edges

In this way, the aim is to create an arrangement that exhibits dipole like properties on the two opposite edges of the square patch that will be a half wavelength apart without any excitation of the other two similarly resonant edges. In practice this edge spacing is usually closer to 0.4 of the chosen frequency wavelength to facilitate in phase coupling of the two dipoles formed whilst avoiding the formation of unwanted side lobes [6.03][6.04]. In order to create this situation, firstly it is necessary to identify an input point at which to couple to the two desired resonant edges in an identical manner. Also this area should permit a 50Ω impedance point to be established. In a square patch this

point is usually to be found along a centre line of the non-resonant edges. It should be noted that if a truly square patch were to be created it would probably be necessary to allow for some compromises away from the ideal dimensions for the reasons outlined above. Figure 6.1a. illustrates a typical, nominal placement region of a patch feed point, the arrows indicate areas of voltage activity magnitude. At the centre of the resonant edges there is a region of low voltage / high current activity, at this point the impedance is relatively low. These voltages increase, as does impedance up to the quarter wavelength limit of the edge of the patch, current distribution magnitude is the inverse of these activities. Figure 6.1b. shows the associated propagation due to this behaviour with a low impedance at the centre and high impedance at the extremities, mimicking that of a dipole antenna. Also shown here is the electric field at the non-resonant edges that produce the fringing effects. Whilst this effect plays no direct role in the antenna radiation it has a significant impact on the patch dimensions and will be discussed later. The position of the patch feed can deliver differing radiation properties; for instance a carefully placed feed on a diagonal face track can provide simultaneous orthogonal edge stimulation that produces circular polarisation. Circular polarisation can also be accomplished by using centrally placed feed points as shown in Fig. 1; these must be positioned orthogonally and then simultaneously exited through a 90 degree splitter. As two separate linear polarisations are required, these two independent feeds would be exited individually as needed. In the case of these dual feed polarisation selectable configurations the location of the feed points requires very accurate placement. In practice this can be difficult to achieve, but is necessary if polarisation purity is not to be degraded by unwanted coupling effects [6.05]. Positioning of this feed point is most readily accomplished by that of a probe feed of the type shown in Fig. 6.2a. Here the inner conductor of an RF



Feed methods: Fig. 6.2a. Co-axial probe. 2b. Stripline and 2c. Cavity / slot

connector is directly connected to a predetermined point on the radiating patch after passing through the antenna substrate layer. The outer, ground connection is mounted in contact with the assembly ground plane. A drawback of this method lies in that the connecting probe can possess unwanted inductance that leads to matching difficulties and a consequent narrowing of bandwidth. This situation worsens in structures that rely on the use of a thick substrate layer to reduce the “Q” factor due to the structure. Such situations can, to some extent be corrected by the use of a compensating capacitance placed within the substrate, or at the probe interface with the patch [6.06]. In practice this would however be hard to implement. An alternative is the use of an “open circuit” tuning stub placed along the non-radiating edge of the patch [6.07] [6.08] [6.09]. Due to energy being reflected from the stub, this has the effect of altering the current distribution on the patch face, so compensating for the inductive probe disparities. In a design that will require the use of all patch edges this approach would be inappropriate. Similarly, the stripline method shown in Fig. 6.2b, provides a well matched solution but typically suffers from extreme bandwidth limitation of between 2% - 5% [6.10]. Also the asymmetry introduced by this design renders it unsuitable, as with the stub solution. Described in Fig. 6.2c. is a simplified slot fed approach, this provides an elegant solution in that there is no direct connection between the radiating patch and feeding structure. In this case the structure is essentially made up of a radiator supported by a substrate, beneath which is a ground plane containing a slot. This ground plane is backed by a further substrate layer, underneath which is the feeding stripline. Antenna optimisation is achieved by varying the size and position of the slot and feeding stripline. Variations on this design using crossed slots [6.11] have been successfully fabricated to produce circularly polarised devices. These multi-layer designs are however difficult to fabricate reliably and again there would be difficulties with individual feed excitation of a crossed slot. With these

features in mind it was decided to adopt the coaxial probe feed approach. Using modelling techniques developed for mm wave circuit design [6.12] it is hoped that the coaxial probe inductance issue can be overcome using the inherent capacitance properties of the structure to tune out any deficiencies. To facilitate this parametric design optimisation feature in the modelling software will be used to fine tune the probe placements on the patch face.

6.3 Design Methodology

In sections 6.1 and 6.2 a number of antenna types and the possible design options available have been considered. Taking these options into account it was decided to initially develop a square patch antenna based on a thick substrate design for maximum bandwidth performance. At this stage it would be critical to optimise the feed characteristics for matching and bandwidth performance. Although not ideal it was decided to use the coaxial probe feed method for ease of construction. Such an arrangement also facilitates convenient connection to externally sited RF switches that will be required for polarisation plane selection. Any resulting parasitic inductance effects will then be compensated using the intrinsic capacitance due to the complete structure as outlined earlier. Once established, a second feed can then be added and both the effect of this, and the viability of polarisation switching and isolation properties and effects on the radiation patterns assessed. Preliminary calculations were to be based around the widely used transmission line modelling technique described by “Balanis” [6.13] as this provides a good starting point for this type of structure. As a first step it was necessary to decide the materials and components to be used in the device, as this will directly affect both the dimensions and performance of the finished design. As it was freely available the upper, radiating patch layer was to be constructed from FR4 printed circuit board material. This

would be of a substrate thickness of 0.75mm fibre glass material fronted by a Copper layer of 0.1mm in thickness. With a relative permittivity of 4.4 the thickness of this layer was kept to a minimum as it would be necessary to keep the electric field in the region below the radiating patch as weak as possible. Below this and providing the crucial space between the patch substrate and the ground plane is a 3.2mm layer of Eccostock PP-2 material. With a permittivity of 1.03 and a loss tangent of 0.00001 this substrate is ideal for reducing the strength of the electric field in the region between the ground plane and the radiating patch as discussed earlier. As a next step it was necessary to calculate the wavelength at the frequency of operation as this will be used to establish basic initial dimensions. Since this antenna is to operate a frequency of 5 GHz the wavelength in air was taken as 5.98cm for the purposes of the design calculations that follow. As the basic dimensions of the patch are also defined by the wavelength shortening (electric field concentration) effect due to the dielectric layer the next step is to calculate the effective dielectric constant (ϵ_{reff}) of the FR4 layer using equation (1) [6.13]. This is standard practice so as to compensate for any variation in dielectric constant (ϵ_r) due to the effect of the air layer above the patch. Here, the value of ϵ_r attributed to that of the FR4 substrate, was taken as 4.4, the thickness of the substrate, h , was taken as 0.75mm and W was the half wavelength distance at 5 GHz, then taken as 29.9mm.

$$\epsilon_{reff} = \frac{\epsilon_r + 1}{2} + \frac{\epsilon_r - 1}{2} \left[1 + 12 \left(\frac{h}{W} \right) \right]^{-\frac{1}{2}} \quad (1)$$

$$\epsilon_{reff} = \frac{4.4 + 1}{2} + \frac{4.4 - 1}{2} \left[1 + 12 \left(\frac{0.75}{29.9} \right) \right]^{-\frac{1}{2}}$$

$$\epsilon_{reff} = 4.18$$

The next step was to calculate the effective dielectric constant of the two combined FR4 and Eccostock layers. As the permittivity of the Eccostock material was given as 1.03, ϵ_{reff} was assigned a value of 1 and equation (2) [6.07][6.08] used to calculate the combined value for both layers.

$$\epsilon_{\text{reff}} = \frac{\epsilon_{\text{reff}1}\epsilon_{\text{reff}2}(h_1 + h_2)}{\epsilon_{\text{reff}1}h_2 + \epsilon_{\text{reff}2}h_2} \quad (2)$$

Where $\epsilon_{\text{reff}1}$ was the value for the Eccostock layer (1), $\epsilon_{\text{reff}2}$ was the value for the top layer h_1 was the thickness of the FR4 and h_2 was the thickness of the Eccostock.

$$\epsilon_{\text{reff}} = \frac{4.18(0.75 + 3.2)}{4.18 \times 3.2 + 0.75}$$

$$\epsilon_{\text{reff}} = 1.179$$

As previously outlined the dimensions of the patch are essentially linked to that of the half wavelength existing within the structure at the frequency of operation. As mentioned earlier, radiation occurs at the patch edges where a dipole like ‘‘slot antenna’’ condition should exist. So as to accommodate this, the aim now is to calculate this effective length (L_{eff}) using equation (3) [6.13]. Here c was the speed of light, f was the desired frequency of operation of 5GHz and ϵ_{reff} is as previously calculated.

$$L_{\text{eff}} = \frac{c}{2f\sqrt{\epsilon_{\text{reff}}}} \quad (3)$$

$$L_{\text{eff}} = \frac{2.99}{10\sqrt{1.179}}$$

$$L_{\text{reff}} = 25.36 \text{ mm}$$

Also as briefly discussed earlier the electric field associated with the radiating patch extends beyond the confines of the patch / substrate junction to form “fringeing fields” that extend electrical activity outside the area defined by the above calculations. This phenomenon has the effect of extending the influence of area of electrical activity beyond the physical confines of the patch. For the purposes of these calculations this must be taken into account, as if left uncorrected, this would have the consequence of effectively increasing the size of the patch and so changing the resonant frequency. An appropriate correction for this fringeing extension can be made using the formula (4) below [6.13]. Here this size reduction (ΔL) refers to the reduction in length to be made at one edge only, L was the effective length value calculated above and h was the distance between patch and ground plane.

$$\Delta L = 0.412h \frac{(\epsilon_{\text{reff}} + 0.3) \left(\frac{L}{h} + 0.264\right)}{(\epsilon_{\text{reff}} - 0.258) \left(\frac{L}{h} + 0.8\right)} \quad (4)$$

$$\Delta L = 0.412 \times 3.75 \frac{(1.179 + 0.3) \left(\frac{25.36}{3.75} + 0.264\right)}{(1.179 - 0.258) \left(\frac{25.36}{3.75} + 0.8\right)}$$

$$\Delta L = 3.03 \text{ mm}$$

The final patch antenna edge dimension for the square patch radiator is then given by

$$L_{\text{eff}} - 2\Delta L$$

$$19.3 \text{ mm}$$

[Equations taken from Antenna Theory Analysis and Design (Third Edition). Constantine Balanis pages 811-820.]

6.4 Linearly Polarised Square Patch

With a basic dimension for the square patch design calculated and the materials to be used assimilated into a basic design strategy, it was now possible to construct a model in order to assess functionality of the overall design. This was to be carried out using CST Microstripes software. As will be seen this software is capable of predicting the return loss due to the antenna feed and its position, current distribution on the patch face, expected radiation pattern and polarisation behaviour.

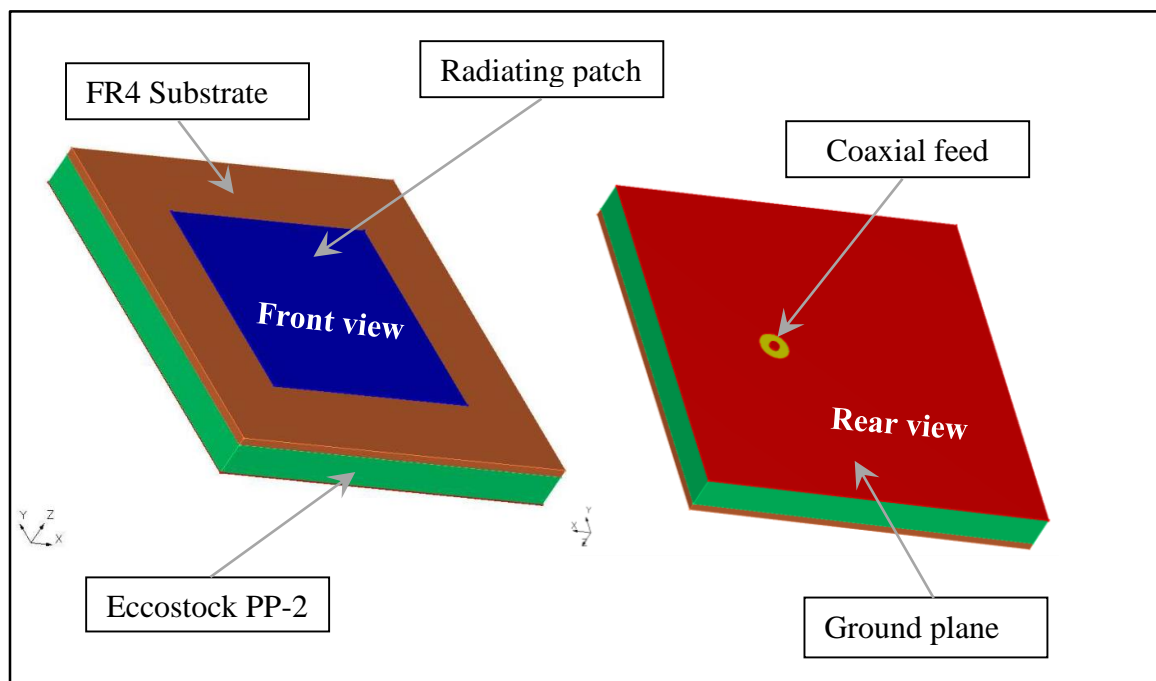


Fig. 6.3. Model layout and basic components of the square patch design

Before analysis can begin it was necessary to construct the model using the CST Microstripes electromagnetic modelling environment. This required that all component parts were defined in terms of physical size and relative position as well as in terms of their electromagnetic properties. Figure 6.3. shows front and rear views of the basic square patch assembly as created in the model environment with all component parts assembled as previously described. It was decided to feed the device directly via a length

of 3.5mm semi rigid coaxial cable. This was facilitated in the model with a 1mm diameter central copper core connecting directly to the radiating patch, this central core being surrounded by a 3mm PTFE sheath that passes through all layers except that of the radiating patch. A 50Ω port would then be set up in the model between the central copper core and the edge of the 3mm hole in the ground plane. Using this method reduces the connector count in this application as well as minimising disruptive interconnections between the probe and RF socket so reducing any spurious effects to a minimum. A ground plane size of 35mm x 35mm was chosen, although smaller than the recommended dimension, from past experience this was thought to be sufficient to limit back radiation to a minimum, ensure an acceptable antenna gain and yet importantly, allow a compact design. An initial feedpoint position was chosen along a centre line of the patch to facilitate symmetrical interactions with two edges. As the optimal position of this was uncertain, a parametric search facility was used that incrementally moved the feed position of the feed along this centre line.

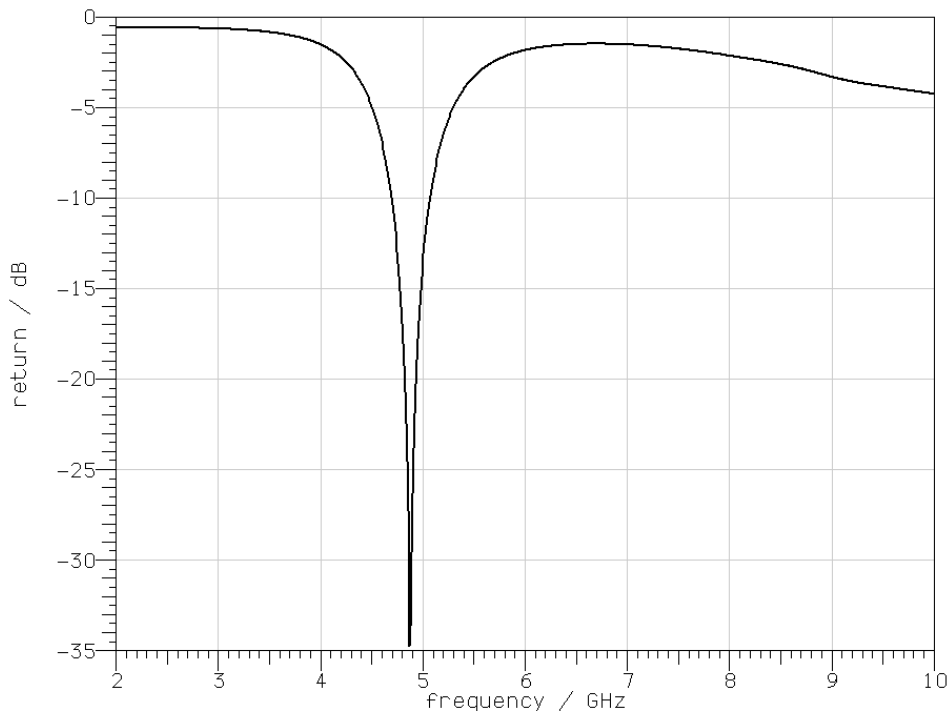


Fig. 6.4. Return loss plot of the 5 GHz square patch

Return loss plots for all these points were then compared in terms of coupling bandwidth and magnitude of signal loss and the frequency at which that loss occurred. A small adjustment of the patch size to 21mm resulted in the return loss plot shown in Fig. 6.4. with the feed positioned 6mm from the patch centre one axis (see Fig. 6.3.) A possible explanation for this was that fringing activity being less than expected. This may have been as a result of using the Eccostock material as a separating substrate instead of an air gap. As can be seen the frequency at which the best match occurs in this case is 4.9GHz with no higher order modes occurring up to the 10GHz model limit, this provides a good starting point for the design. With this low Q design the broad aspect of the trace also indicates that a wide device bandwidth can be expected, though as will be seen later with this type of structure a higher useable bandwidth than the 400MHz indicated at the 10dB point can be expected. Next the current distribution on the patch face was examined as shown in Fig. 6.5. A distinct difference in the levels of activity can indicate the likely characteristics that can be attributed to the final patch design. Relative activity amplitude is indicated as in the scale shown beneath the prediction plot. Shown in Fig. 5. is the current distribution on the conductive area of the patch and the ground plane beneath, the substrate areas have been removed for clarity. It can be seen that the red and yellow areas indicating high current concentration are confined to two opposing edges of the patch as required. These areas of activity are also mirrored in the ground plane below as might be expected and from the earlier patch function and fringing discussions. Importantly for this application it can be seen that there are significant differences in the current density behaviour on the two orthogonally opposed patch edges. The red / yellow areas indicating high surface current areas and the blue where there is little surface current activity present. Also it can be seen that the current distribution along these edges is not uniform, with high current regions being present towards the centre of each edge leading to a

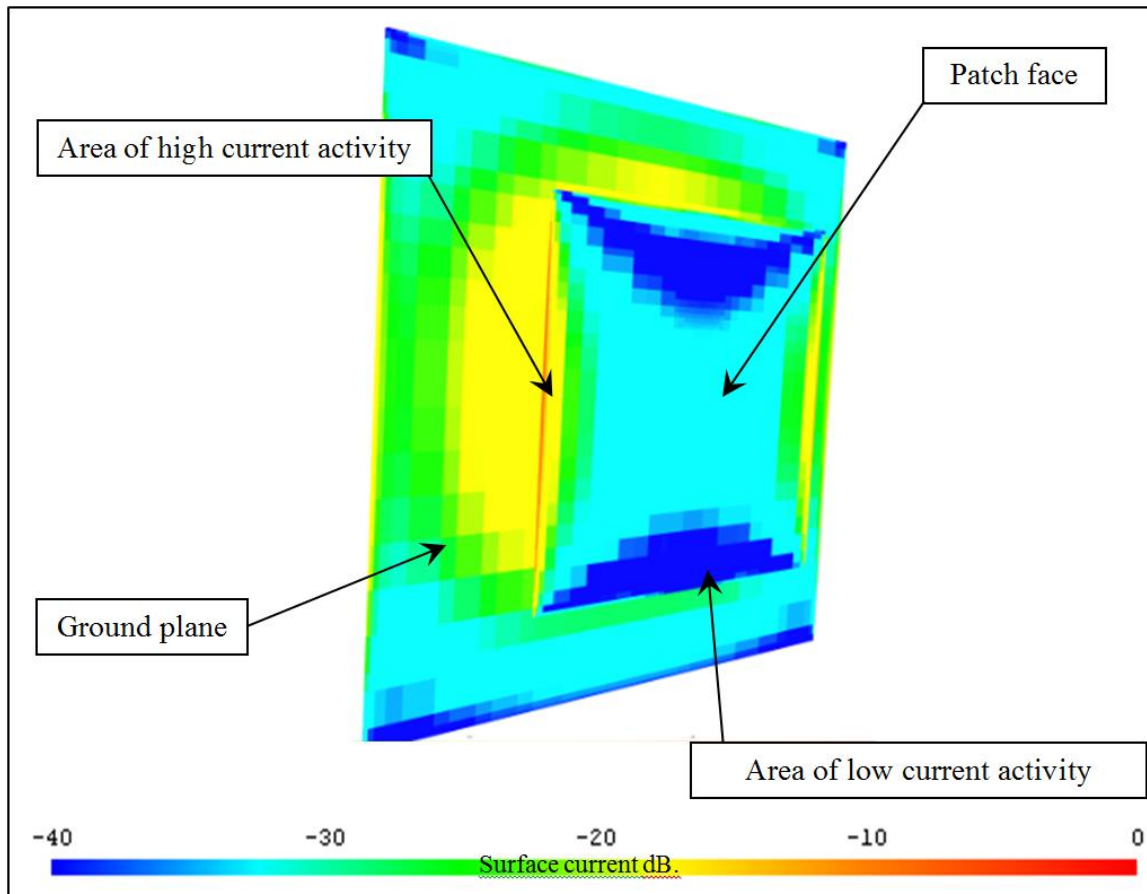


Fig. 6.5. Current distribution on patch face

dipole like condition as outlined earlier. This behaviour indicates that radiation will mostly occur at each of the two edges of high activity and so should combine to form a pattern of radiation with an E- plane aligned in one direction only. As a result it can be expected that this design will possess the strong linear polarisation characteristics that are required as an initial design feature. Figure 6.6. and figure 6.7. show the co-polar and cross polar radiation pattern predictions associated with the patch assembly. In Fig. 6.6. it can be seen that in a vertically polarised co-polar configuration an E-plane gain of 7.94 dBi can be expected, as shown in the lower left corner of the simulation plot.

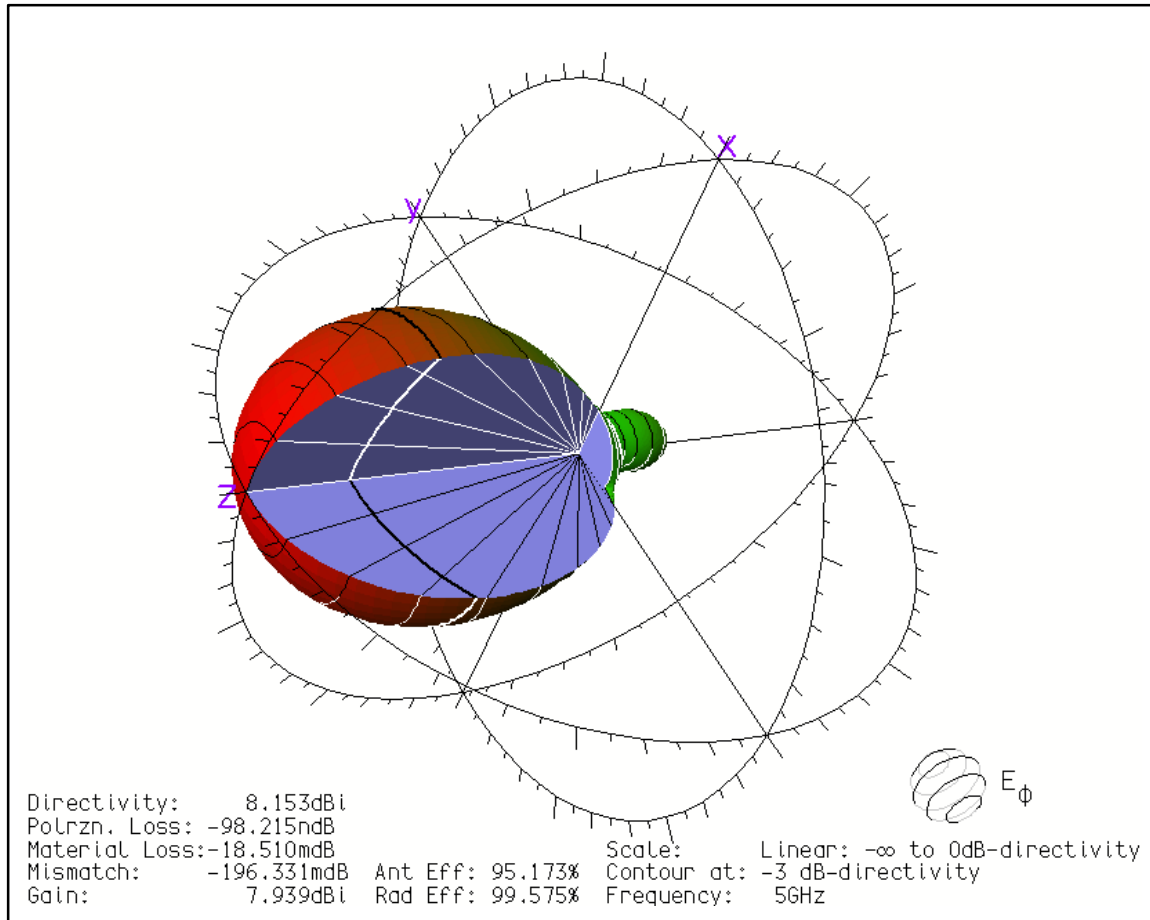


Fig. 6.6. Co- Polar plot

In the Fig. 6.7. cross polar prediction the radiation pattern plot is very different, with a forecast gain figure of just -68.52dBi. These results suggest that this structure will exhibit strong linear polarisation characteristics with little tendency to excite the unwanted orthogonal plane at this stage. Also as indicated by the low current density predictions at the edges of the ground plane shown in Fig. 6.5.very little radiation to the rear of the patch in indicated. Back radiation is of particular concern, as if it is present at significant levels, unwanted reflections may result from objects outside the sensing array as seen earlier.

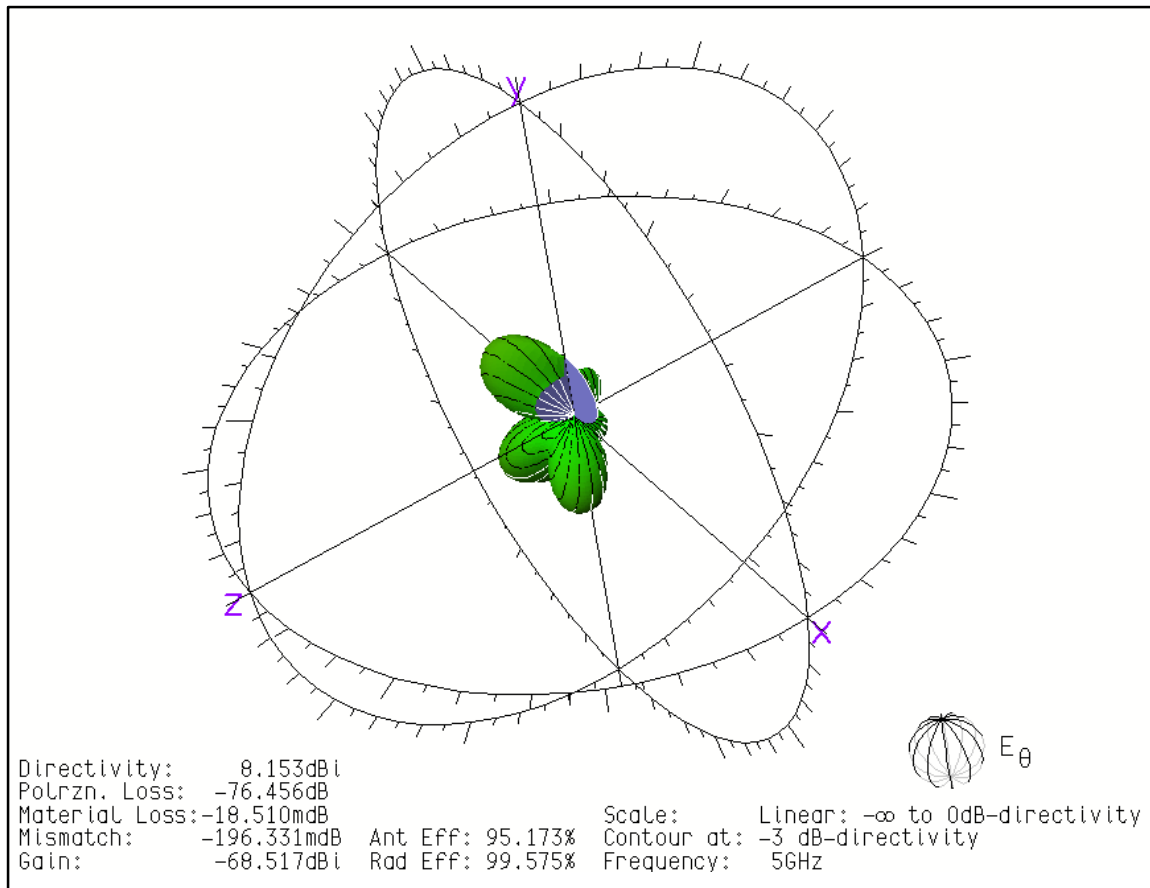


Fig. 6.7. Cross Polar plot

This would then require the addition of RF shielding which could influence the sensitivity and response of this application. In addition it can also be seen that it can be expected that the device will possess low side lobe and symmetrical radiation properties. If a sensing technique is to be used that relies on the use of both polarisation planes, these will be important features to ensure sensing symmetry.

6.5 Polarisation Switchable Square Patch

With the basic linearly polarised design modelled it was then possible to extend this to a dual feed design. Adapting the well-known dual feed technique used to obtain circularly polarised patches separately excited feeds placed orthogonally along the two central axes

of the square radiating surface were used. To implement this, a feed point was selected at the same 6mm offset position as before but this time an additional port was added on the orthogonal axis of the square patch face to create the dual feed configuration [6.14]. This would allow the possibility of stimulating emission at the two patch edges independently. The intention would eventually be to use an externally sited RF switch to select which port was to be excited and in this way select which polarisation plane would be activated. Such a switching arrangement avoids the use of PIN diodes that can be difficult to position and terminate correctly [6.15]. Commercially available connectorised RF switches couple readily with the 3.5mm semi rigid coax compatible port design and are

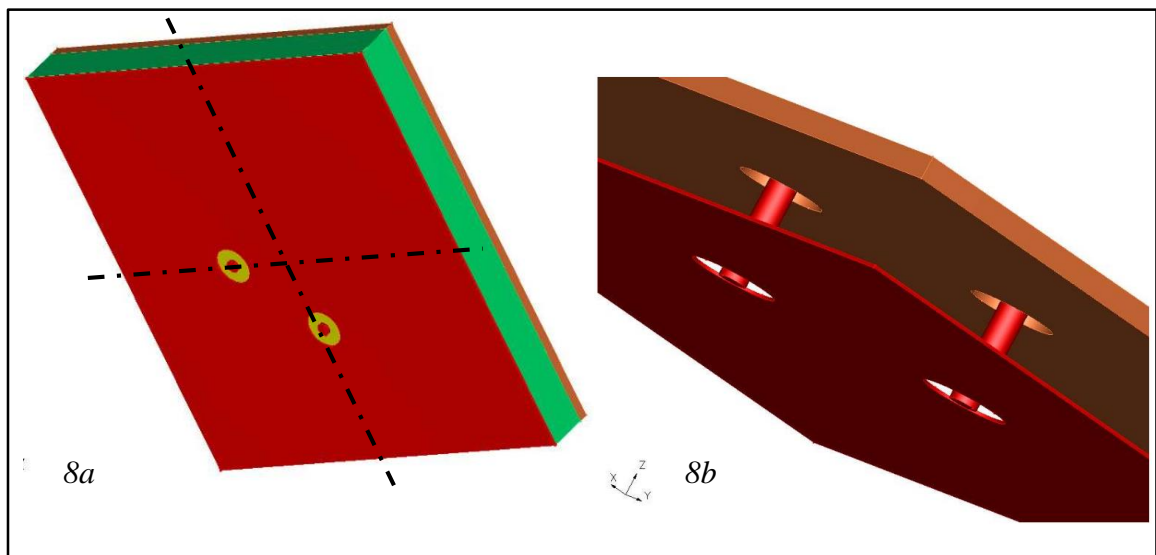


Fig. 6.8a. Dual feeding port placement and 6.8b. model construction

easily interfaced with standard logic integrated circuits for control purposes. In this way either vertical or horizontal edge excitation could be activated with a corresponding selectivity of polarisation plane being possible. Figure 6.8a. shows the model graphic with port placements at 6mm offset from their respective centre positions. Figure 6.8b. depicts the construction of the feed ports using the 3.5mm semi rigid coax, here some of

the non-metallic elements have been removed for clarity. Construction was the same as for the single feed patch with the bottom, red layer representing the antenna ground plane with clearance holes created that allowed direct contact with the semi rigid outer conductor. This outer conductor was terminated at the ground plane. The upper brown layer is the FR4 material that supports the radiating patch, this time with clearance holes created to allow passage for the PTFE insulating layer of the semi rigid coax. A similar approach was again adopted to allow passage through the Eccostock layer. Finally the central conductor of the feeding port was created as a 1mm cylindrical copper entity that was in direct contact with the patch located on the surface of the FR4 layer.

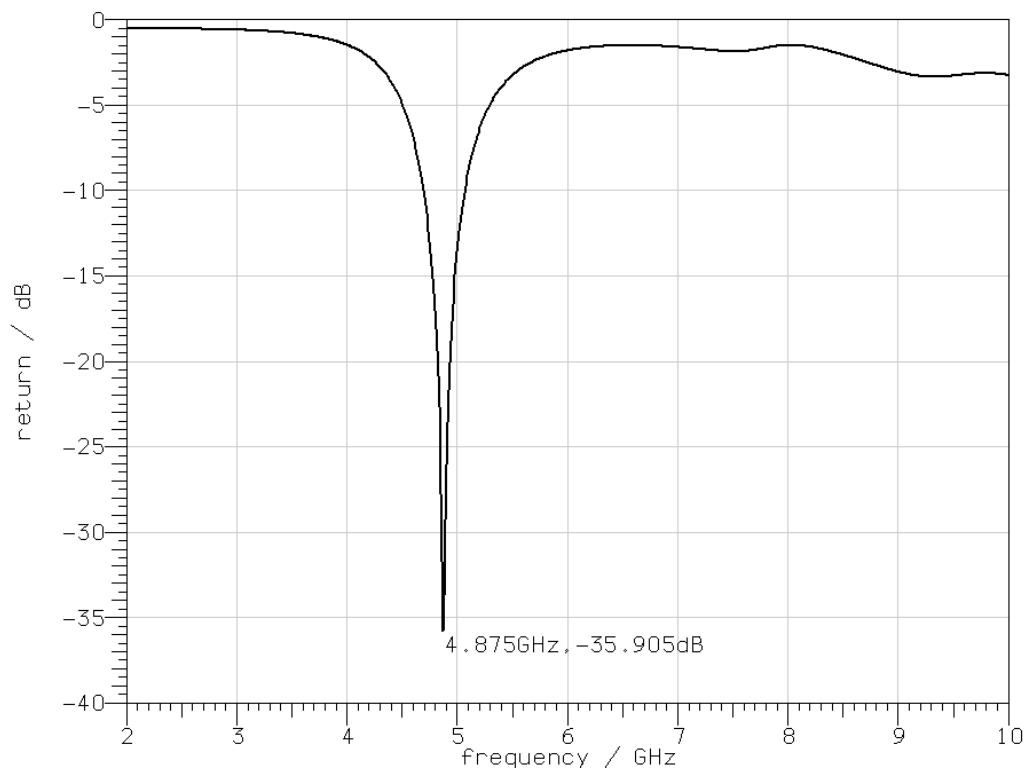


Fig. 6.9a. Port 1 excited

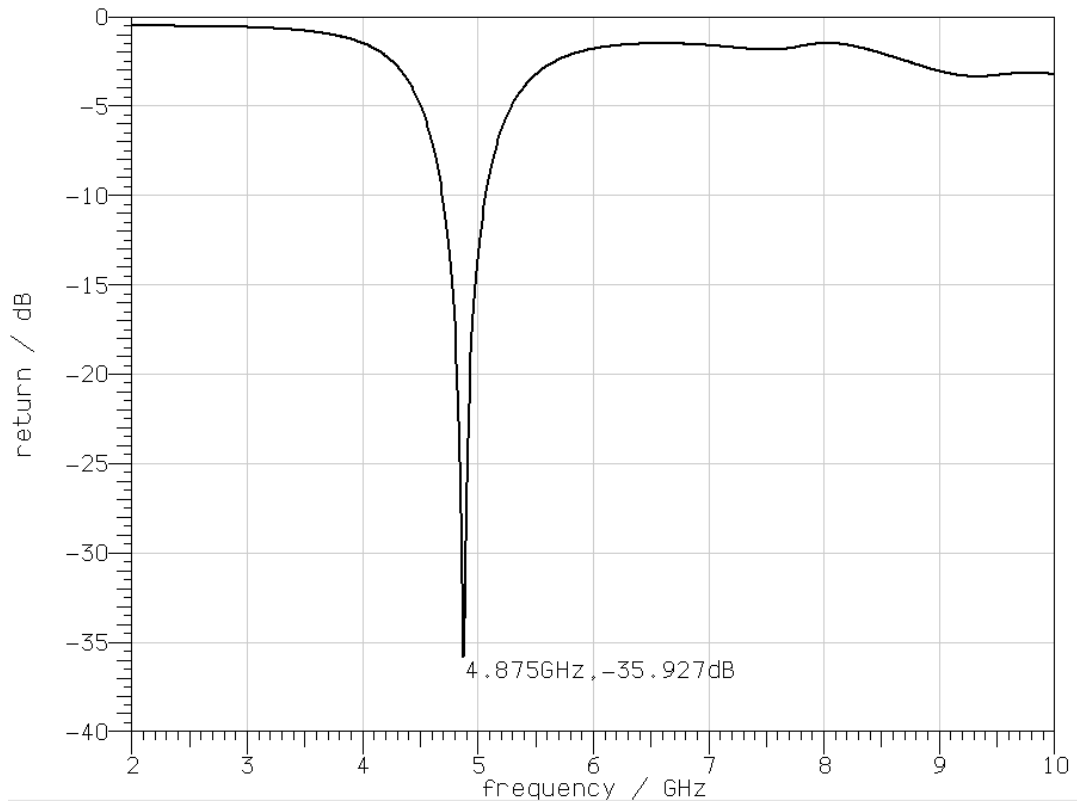


Fig. 6.9b. Port 2 excited

Using the port activation facility of the Microstripes software each antenna port was then excited in turn with the unused port terminated at 50Ω . This procedure simulated the action on a non-reflective RF switch being used to stimulate each polarisation mode in isolation. Initial analysis of the S_{11} return loss at each port is shown in Fig. 6.9a and Fig. 6.9b. Comparison of these plots showed virtually identical properties at each input and only minor variation from the single port return loss plot shown in Fig. 6.4. Both ports having a peak return loss in excess of -35dB at a frequency close to 4.9GHz . This indicated that there is little disturbance to the patch performance caused by the addition of the extra port and that good 50Ω impedance matching can be expected at both feeding points to the patch surface. In addition to the usual parameters of interest, with this dual input device it is also necessary to investigate the isolation properties between each mode

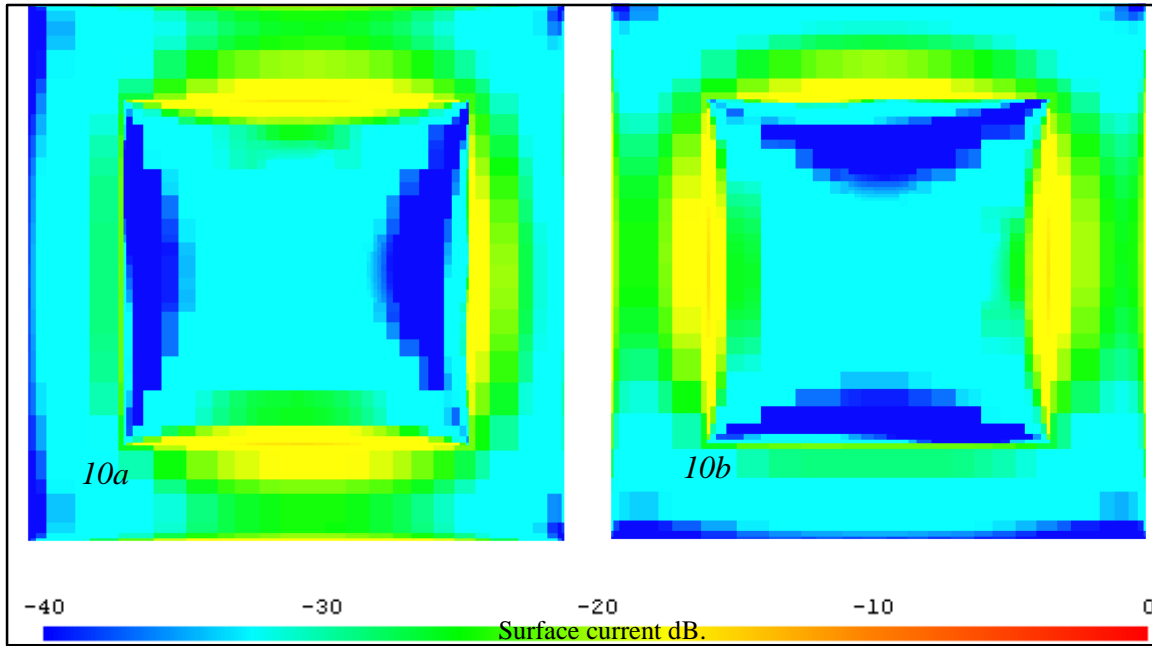


Fig. 6.10a. Port 1 excited

Fig. 6.10b. Port 2 excited

of operation. A high degree of isolation was essential if two independent modes of measurement were eventually to be established. Surface current distribution plots of the patch face were then examined as shown in Fig. 6.10a. and Fig. 6.10b; with, as shown previously current magnitude indicated in the scale beneath the plot. This is viewed from directly above the patch and so also shows some current activity occurring on the surrounding ground plane below. As formerly shown, this technique provides a good indication of probable areas where radiation will occur and so will suggest the expected polarisation behaviour of the antenna. Figure 6.10a shows activity when port 1 is activated and port 2 is terminated as the red and yellow colours indicate activity is predominantly confined to the horizontal patch edges. When port 2 is activated and port 1 terminated (Fig. 6.10b) this activity was then transferred to the vertical antenna edges. In both cases the orthogonally orientated edges exhibit areas of low current distribution activity as indicated by the blue colours displayed. Properties of this nature indicated that each edge pair can be activated relatively independently of each other so producing polarisation isolated outputs. As a high degree of autonomy between each polarisation

plane will be required to ensure that there is little interaction between readings, the next stage was to quantify the degree of isolation that can be expected. As a square patch has identically resonant surfaces in both polarisation planes and a non-ideal radiating edge separation (not 0.4λ) then this was of some concern.

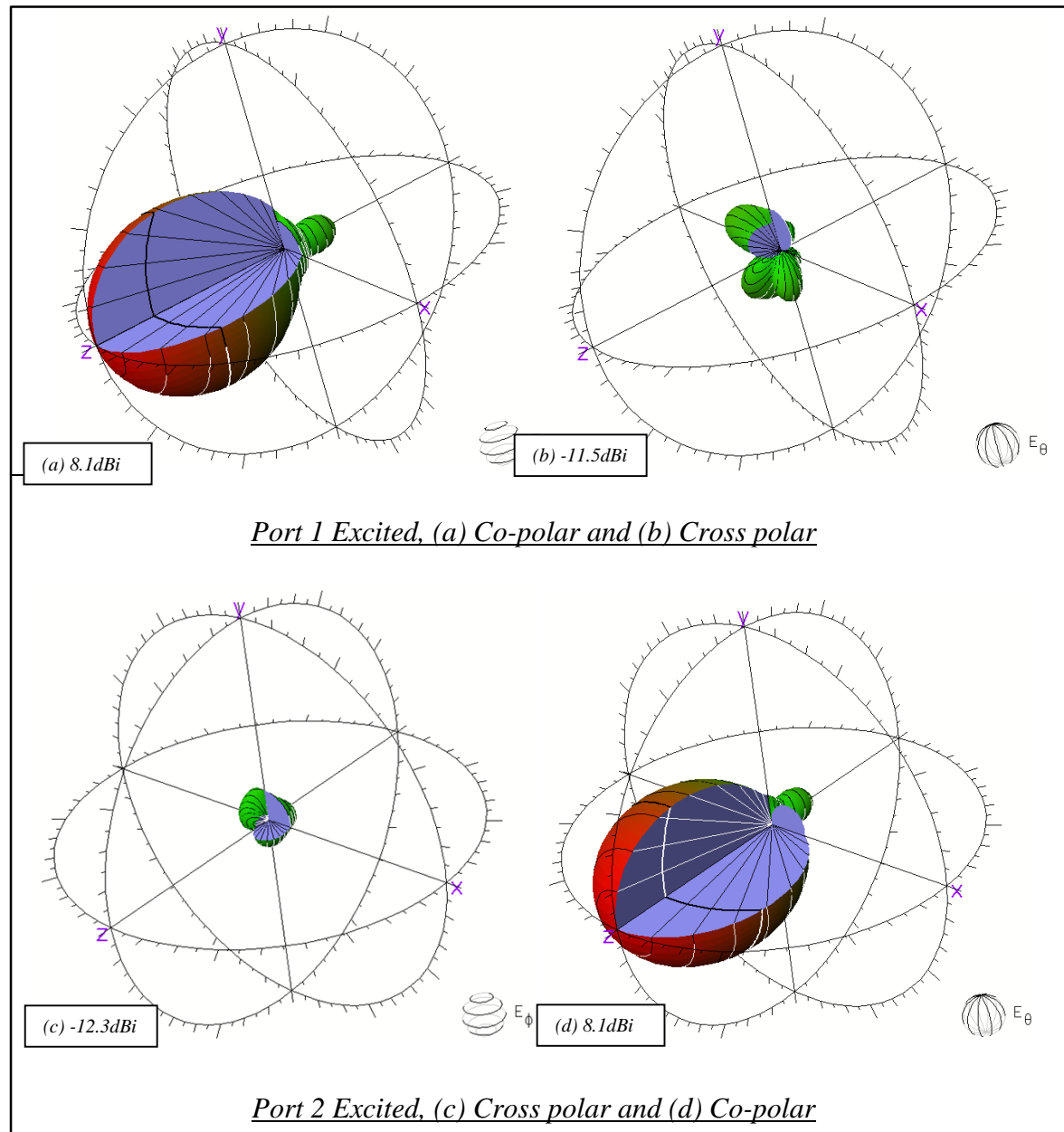


Fig. 6.11. Radiation pattern and polarisation indications

So as to assess the isolation performance radiation pattern predictions were then carried out for port activation conditions. Figure 6.11. shows the corresponding plots of radiation pattern and gain for co-polar and cross polar orientations with either port excited. With the excitation of port 1 co-polar gain was predicted to be 8.1dBi (Fig. 6.11a.) with a cross polar gain of -11.5 dBi (Fig. 6.11b.). Radiation pattern formation was unaffected with a strong single lobe being sustained as was the absence of any back radiation generation. A similar result was obtained with the stimulation of port 2 with a cross polar gain of -12.3 dBi (Fig. 6.11c.) and a co-polar gain of 8.1 dBi (Fig. 6.11d.) being predicted. This isolation of around 19dBi is comparable to a number of more complex designs that typically employ elaborate feeding methods [6.16] [6.17] but is still disappointingly low. Using complex feed and coupling arrangements an isolation of between 23 dBi to 25 dBi has been reported for a square patch design [6.18] but such devices would be very difficult to fabricate in practice and reportedly will still lack the likely bandwidth capability displayed in the design being developed here. Predicted results are frequently difficult to match in practice so achieving this degree of isolation is likely to be optimistic for a real device.

6.6 Linearly Polarised Rectangular Patch

It seems likely then that the cause of this lack of polarisation purity was due mutual resonance of the unstimulated edges. This will, most likely, be due to the dimensions being the same on all four of the patch edges. To test this proposition it was now decided to extend the patch length in one direction to form a rectangular patch. If this notion is correct a de-tuning of the lengthened edges should be seen that leads to an increase in the polarisation independence of the now linearly polarised rectangular patch over that of the initial square patch design. A model was created using the same design criteria as for the

square patch design but with a nominal patch extension of 2 mm either side of the central feed point. This created a patch of 21mm x 25mm and was thought to be sufficient to effectively detune the horizontal edges whilst preserving the positive coupling attributes of the spacing of the vertical edges. As before performance was optimised using the parametric search function of the software to find the 50Ω coupling point on the patch face. This was now found to be at 7mm from the shorter patch vertical centre point and as before placed centrally along the longer horizontal axis.

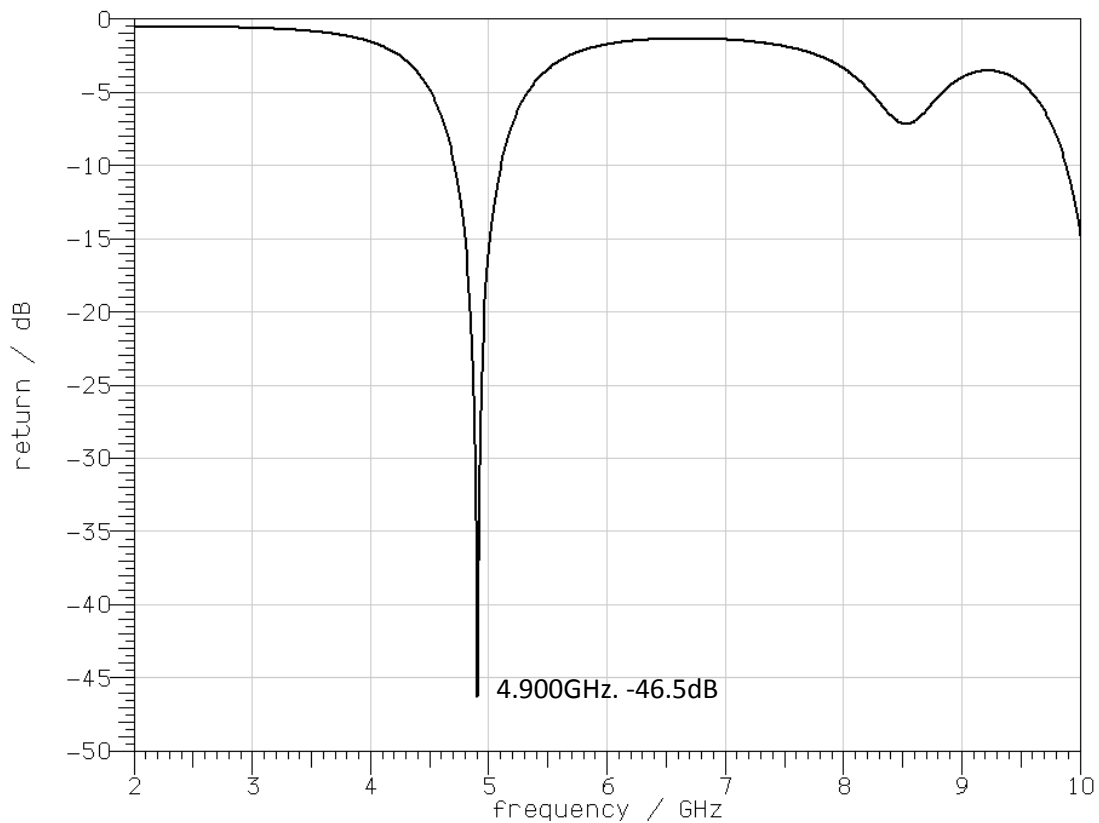
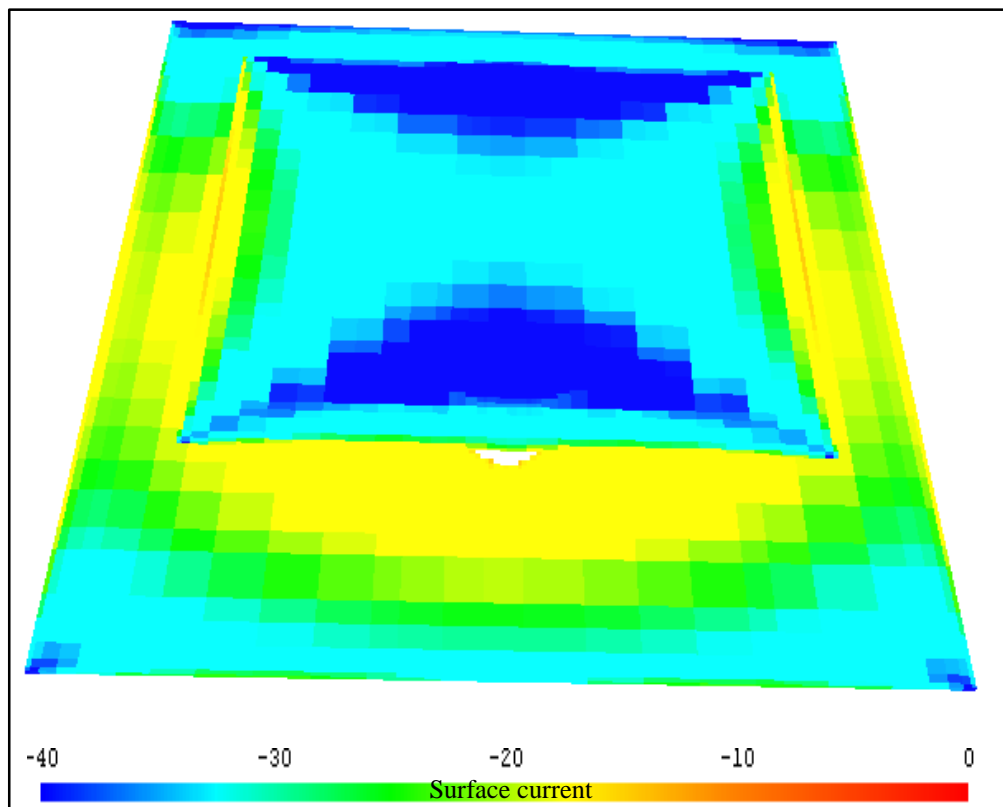


Fig. 6.12. Rectangular patch S_{11} return loss

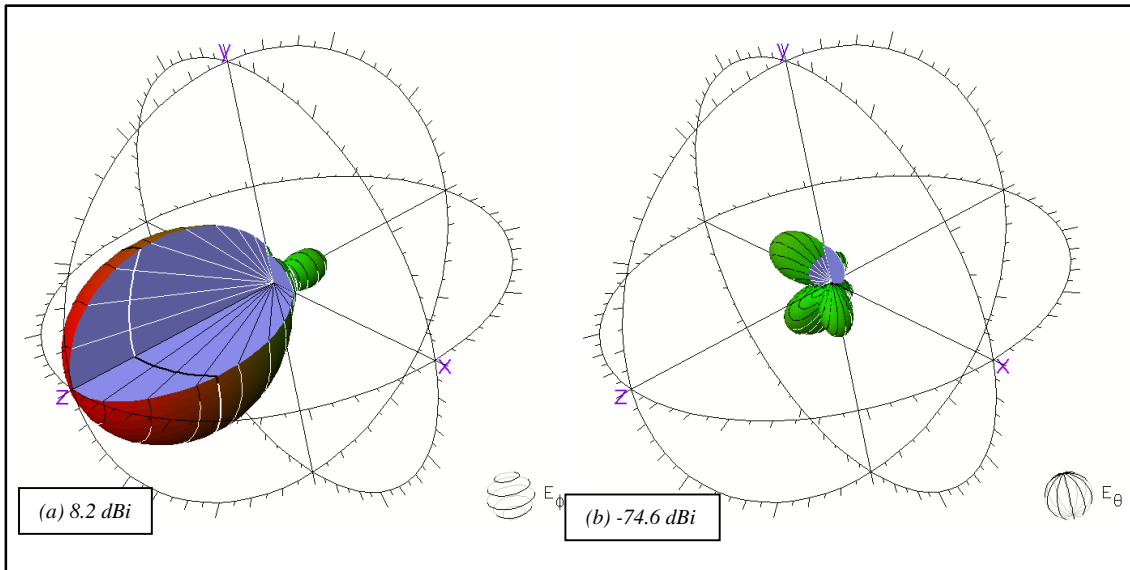
The resulting S_{11} return loss performance can be seen in Fig. 6.12; a dramatic increase in return loss to -45dB also became apparent, indicating greatly improved input impedance matching at the frequency of 4.9GHz. The associated current distribution plot shown in Fig. 6.13; as before depicted the current distribution magnitude on the radiating patch

face as well as the assembly ground plane. Indicated here was a high degree of activity along the two shorter resonant edges as indicated by the red areas with activity at levels far below this on the orthogonal, longer, non-resonant edges. Activity such as this would indicate a high degree of polarisation purity can be expected from this type of assembly. As set out previously this supposition can be verified from the radiation pattern predictions as shown in Fig. 6.14. Here it can be seen that the desired co-polar radiation properties of the square patch are preserved,



6.13. Current distribution of rectangular patch

(Fig. 6.14a.) with the antenna gain unaffected at around 8.2 dBi but the cross polar gain shown in Fig. 6.14b. was now indicated at -74.6 dBi. A significant improvement in isolation performance over the square patch can be expected, with the integrity of the radiation pattern remaining intact.



Co-polar, Fig. 6.14a. and Cross polar, Fig. 6.14b.plots of the rectangular patch

6.7 Polarisation Switchable Crossed Rectangular Patch

To further develop the design, the model was then constructed to combine the best attributes of the patches described above. Using the improved polarisation isolation due to the rectangular design, as well as the thick substrate and dual coaxial feeds of the square designs, the intention now was to orthogonally superimpose two rectangular patches to form a switchable crossed rectangular patch design. A similar approach was adopted by [6.19] [6.20], here cross shaped planar designs are suggested that enable independent polarisation planes. These designs however operate at very narrow bandwidths this being exacerbated by the stripline feed described in the first case and in the second a single coax feed cannot support switching. High isolation between polarisation planes is however reported. Unlike these designs the antenna being developed here needed to support symmetrical and identical radiation patterns in both planes as well as possessing a wide bandwidth. In addition also needed to maintain

polarisation isolation across the operating frequency range, meaning that both patch and feed symmetry were essential.

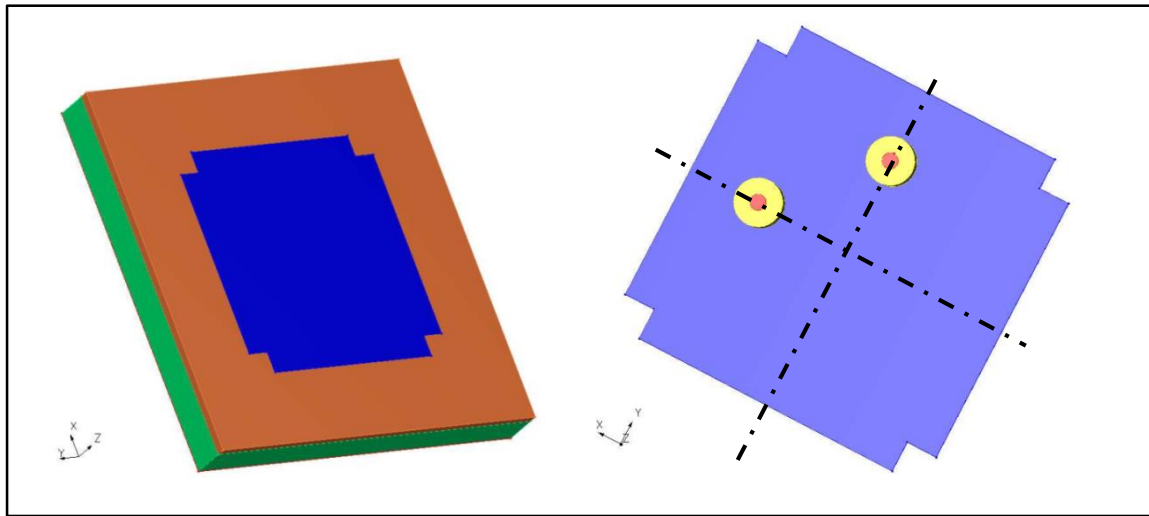


Fig. 6.15a. Antenna structure & Fig.15b. Patch feed points

The crossed rectangular patch shape was created in the model environment by taking the long dimension of the rectangular patch (25mm) as a basic square dimension and then removing 2mm x 2mm sections on each corner so as return to the 21mm resonant length dimension. With the information from the previous designs identical materials, properties and feed dimensions etc. were incorporated into this final design. On running the model it was found that a size reduction was necessary in order to attain the desired 5GHz frequency of operation. This produced a final patch dimension of 21.5mm x 21.5mm with 2mm x 2mm cut-outs at each corner. Figure 6.15a. shows the complete “structure stack” with the crossed rectangular radiating patch shown in blue, the supporting FR4 material shown in brown, the separating Eccostock PP2 layer in green and below that the patch ground plane. Figure 6.15b. shows the feed details from the model graphic as viewed from the underside of the radiating patch with all other material removed for clarity. Optimal feed positions were this time found to be once again at 6mm from the rectangle

centre lines. With these adjustments implemented each port was activated as before and analysed in turn with the unused port terminated to 50Ω .

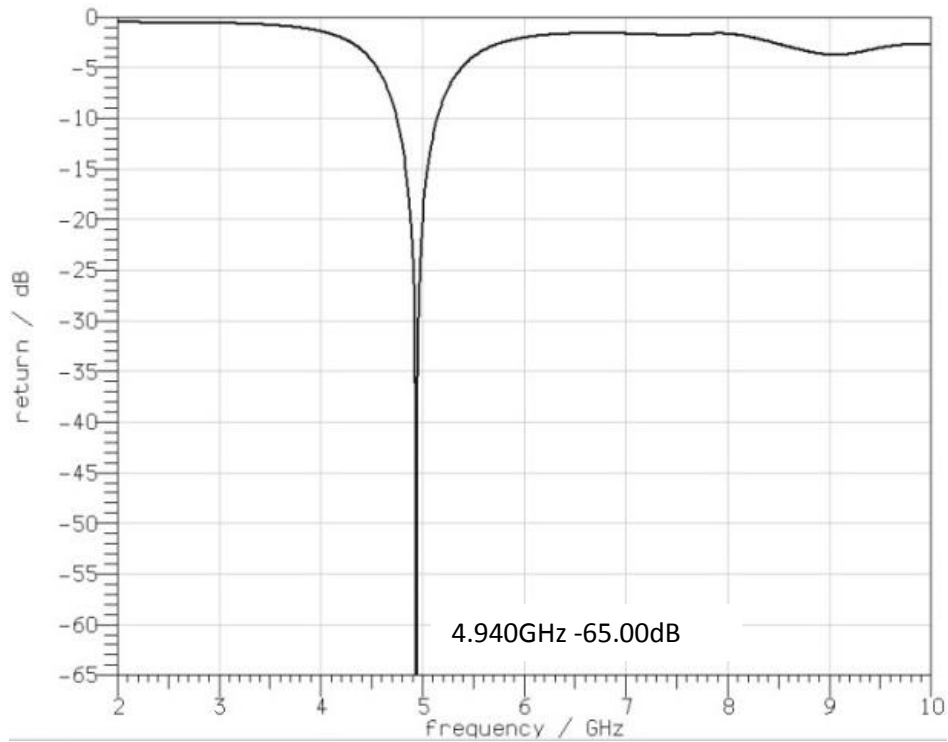


Fig. 6.16a. Port 1 Excited

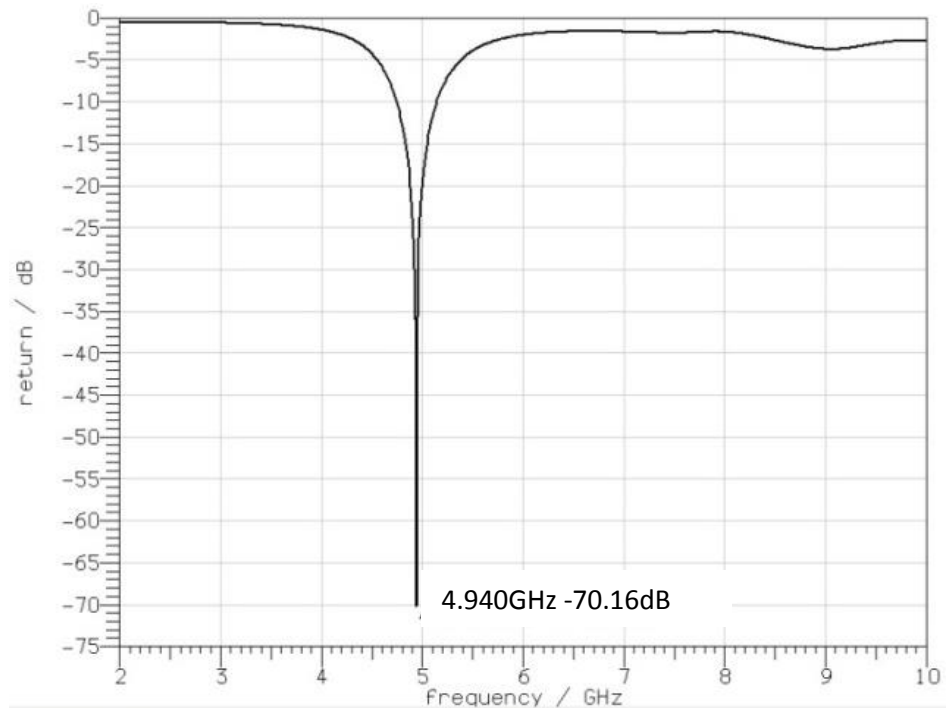


Fig. 6.16b. Port 2 Excited

Figures 6.16a. and 6.16b. show the predicted S_{11} return loss plots for the stimulation of each port. From these plots it can be seen that an optimal impedance match now occurs at 4.94 GHz in both cases, both ports behaving in a virtually identical manner. At this frequency there is now vastly improved matching. Figure 6.16a. indicated that an expected return loss of -65 dB for port 1 is likely and Fig. 6.16b predicted a return loss of -70 dB for port 2. Also the trace is now much flatter up to the 10 GHz model limit with much less indication of the high order mode formation that was becoming apparent in the case of the rectangular patch (see Fig. 6.12.). Figure 6.17 shows front and side views of the conductive areas of the structure indicating current activity distribution as with the previous designs discussed. In addition to the view from directly above the patch the corresponding side view is also now shown indicating which of the two ports was activated. It can now be seen that as each port is excited this is indicated by the red colouration of the pin (as seen in the lower, side view, illustrations).

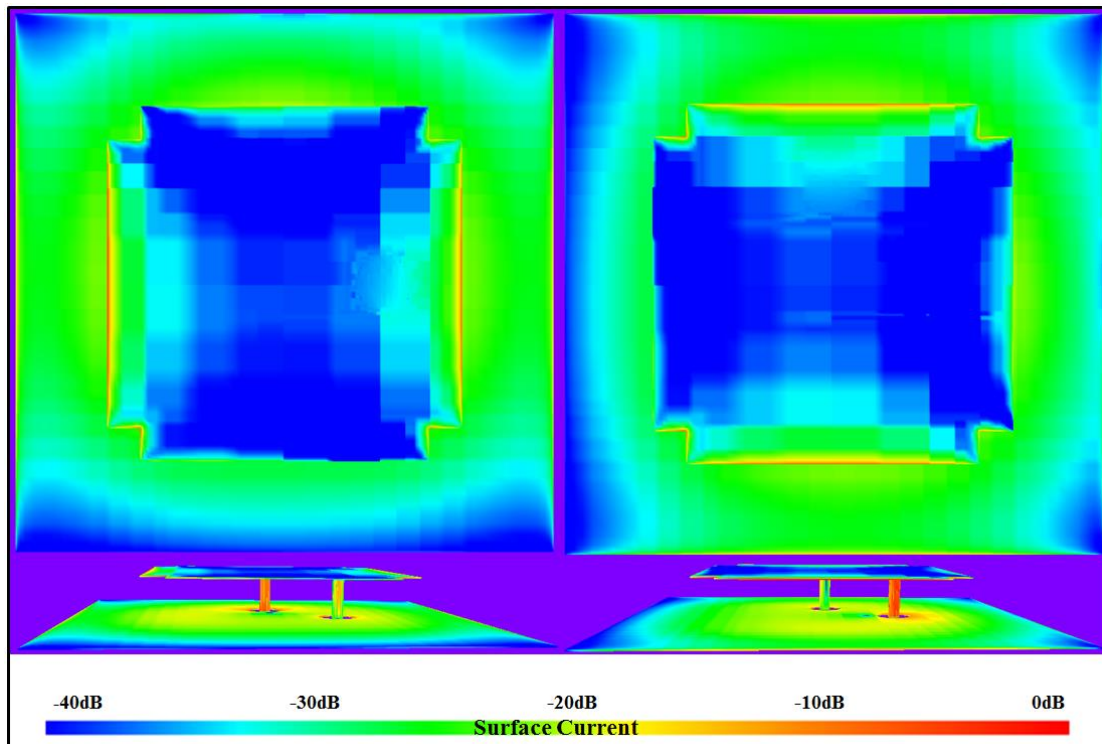


Fig. 6.17a. Port 1 Excited

Fig. 6.17b. Port 2 Excited

Corresponding current distribution plots clearly show that the selected edges are activated as before with very low activity in the cut out areas. It can now also be seen that there now exists a very distinct current gradient across the patch surface as indicated by the red – blue colour change. The dipole like behaviour of the current distribution mentioned earlier is now also much more visible. With such distinct differences occurring across the patch face it is likely that increased polarisation isolation can be expected. Verification of this is shown in Fig. 6.18 with the predicted co-polar and cross polar radiation patterns and gain figures of the final structure with either port stimulated. Despite the now irregular shape of the patch the co-polar radiation patterns remain symmetrical and both are identical in shape in both modes of operation. With predicted co-polar gains of 8.18 dBi and 8.21 dBi both polarisation planes are very closely matched as would be expected from the combination of the return loss and current distribution results shown in Figures 6.16 and 6.17. As with the previous designs very little back radiation or side lobe formation is evident indicating optimal edge coupling and ground plane efficiency. Importantly corresponding cross polar gains were closely matched and predicted at -20.1 dBi and -20.3 dBi respectively. As can be seen from these co-polar / cross polar gain predictions, polarisation isolation of around 28 dB can now be expected, giving an improvement over the square patch predictions of around 8 dB [6.21].

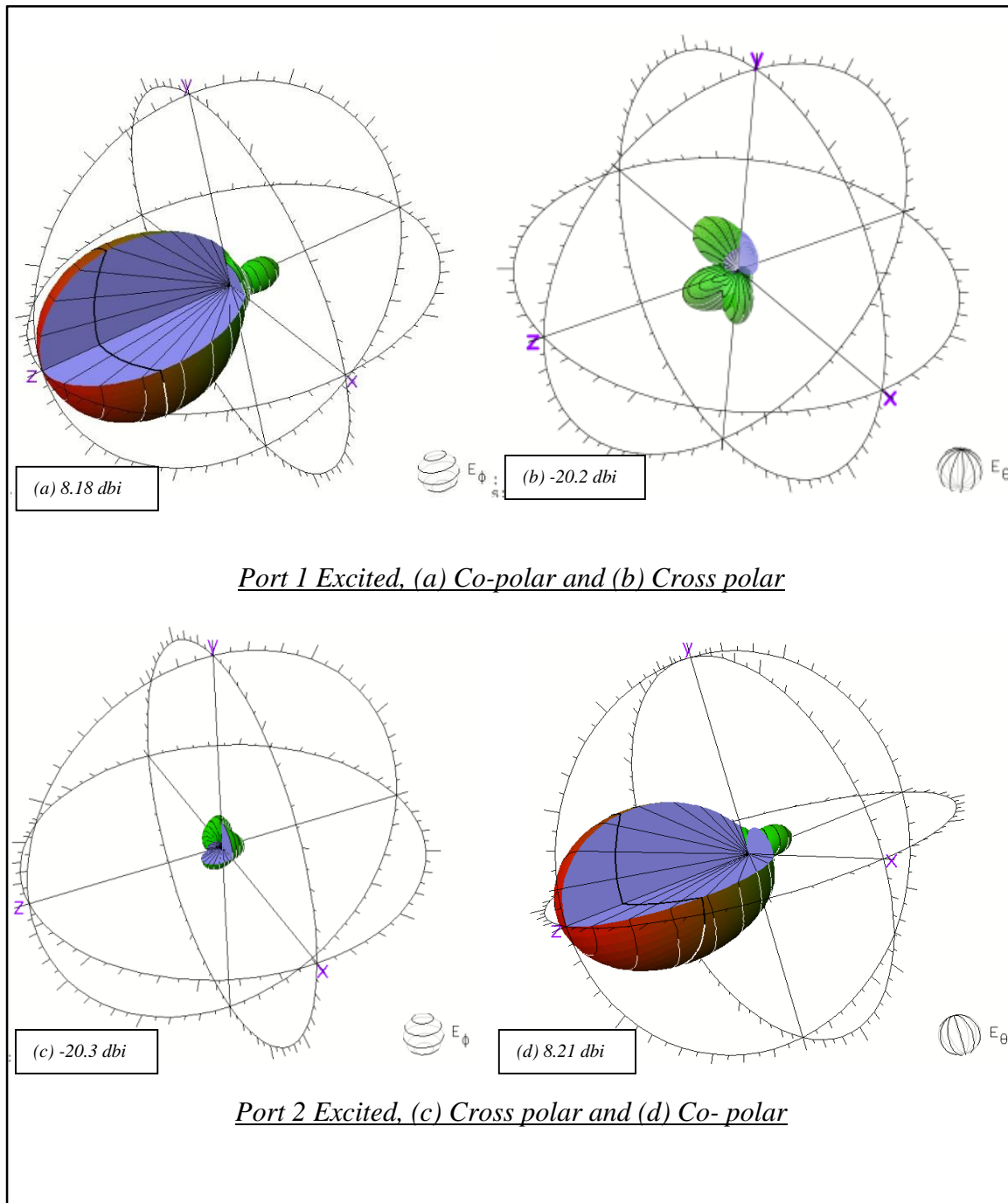


Fig. 6.18. Radiation patterns and polarisation indications

6.8 Conclusions

Primarily a number of antenna design options were considered, these being evaluated against criteria such as size, gain, bandwidth, polarisation characteristics and radiation pattern, feeding arrangements and practicality of construction. A patch antenna design

was thought to be the most suitable as it offered a compact structure, the possibility of generating well defined polarisation planes and could offer a well-defined radiation pattern with low back radiation. In addition the planar nature would have the advantage of offering a common point of emission in two polarisation planes. These designs also offer a considerable gain advantage over other small antenna designs but often suffer from a lack of bandwidth due to a combination of their inherently high Q nature and the required feed topography. It was decided to attempt to overcome these limitations by developing a low Q design that would inherently relax limitations imposed by the feed characteristics. This was to be accomplished by using a thick, low permittivity substrate between the ground plane and radiating patch. Such a design necessitated the use of a coaxial probe feed that would suffer from unwanted inductance issues but this could to some extent be overcome by careful placement within the structure. Four devices were modelled so as to establish the design parameters of a final optimised structure. The first of these was a linearly polarised square patch. Indications here were that the thick substrate design used in conjunction with the coaxial probe feed had the potential to support a wide bandwidth performance and still deliver maintain a gain figure commensurate with conventional patch designs. Building on this a dual probe version was then modelled that predicted that linear polarisation switching was viable and that near identical radiation patterns could be expected on both planes. Next, this was developed into a single feed rectangular patch which demonstrated that increased polarisation isolation could result from this type of structure. Finally, the crossed rectangular device that contained the best attributes of all three previous designs was shown to deliver a superior performance and was suitable for incorporation into a polarisation switchable detection system.

References

- [6.01] Sandra E. M. Dudley, Terence J. Quinlan, Stuart D. Walker. “Ultrabroadband Wireless – Optical Transmission Links Using Axial Slot Leaky Feeders and Optical Fibre for Underground Transport Topologies”. IEEE Transactions on Vehicular Technology. Vol 57, No 6 Nov 2008. Pages 3471 – 3476.
- [6.02] Antenna Theory Analysis and Design (Third Edition). Constantine Balanis. Page 811.
- [6.03] http://urbanmicrowave.com/portfolios/the-basics-of-antenna-arrays/#!/slide_1
- [6.04] http://urbanmicrowave.com/portfolios/the-basics-of-patch-antennas/#!/slide_1
- [6.05] R. K Mishra and T. Milligan. “Cross-Polarization Tolerance Requirements of Square Microstrip Patches”. IEEE Antennas and Propagation Magazine, Vol. 38, No. 2, April 1996 pages 56 – 58.
- [6.06] Broadband Planar Antennas Design and Applications, Wiley, 2006. Zhi Ning Chen and Michael Y. W. Chia. Pages 32 – 37.
- [6.07] Terence Quinlan, Sandra E.M. Dudley, Stuart Walker. “A High Throughput Short Range Transmission System Utilising Compact Patch Antennae”. Loughborough Antenna and Propagation Conference. April 2005.
- [6.08] Terence Quinlan, Sandra E.M. Dudley, Stuart D. Walker. “Towards a 10GHz bandwidth antenna array operating within the 2GHz to 11GHz frequency window”. Loughborough Antenna and Propagation Conference April 2006.
- [6.09] Terence Quinlan, Sandra E. M. Dudley and Stuart D Walker. “10.4 Gb/s Wireless Provision Featuring Linearly Polarised 802.16 Band Patch AntennaArrays.”I.E.E. Conference on Access Technologies 2006.
- [6.10] Antenna Theory Analysis and Design (Third Edition). Constantine Balanis. Page 813.
- [6.11] Hisao Iwasaki. “A Circularly Polarized Small-Size Microstrip Antenna with a Cross Slot”. IEEE Transactions on Antennas and Propagation, Vol. 44, No. 10, October 1996. Pages 1399 – 1401.
- [6.12] http://www.integrandsoftware.com/papers/DAC_2012_60G_workshop_integrand.pdf
- [6.13] Antenna Theory Analysis and Design (Third Edition). Constantine Balanis. Pages 816 - 818.
- [6.14] A. Habibzadeh Sharif and M. Soleimani. “Accurate Analysis and Design of Dual-Feed Circularly Polarized Microstrip Patch Antenna Based on Multiport Network Model”. Antennas Propagation and Microwave Conference 2005 Proceedings.

- [6.15] Tai-Un Jang, B. Y. Kim, Young-Je Sung, Y.-S.Kim. “Square Patch Antenna with Switchable Polarization using Spur-line and PIN Diode”. Antennas Propagation and Microwave Conference 2005 Proceedings.
- [6.16] Rui-Hung Chen and Jeen-Sheen Row. “Single-Fed Microstrip Patch Antenna With Switchable Polarization”. IEEE Transactions on Antennas and Propagation, Vol. 56, No. 4, April 2008 pages 922 – 926.
- [6.17] Stefano Maddio, Alessandro Cidronali, Iacopo Magrini and Gianfranco Manes. “A Design Method for Single-Feed Wideband Microstrip Patch Antenna for Switchable Circular Polarization”. 37th European Microwave Conference 2007. Pages 262 – 265.
- [6.18] Tzung-Wern Chiou and Kin-Lu Wong. “Broad-Band Dual-Polarized Single Microstrip Patch Antenna With High Isolation and Low Cross Polarization”. IEEE Transactions on Antennas and Propagation. Vol. 50, No. 3, March 2002, pages 399 – 401.
- [6.19] Ahad Tavakoli, Alireza Monajati, and Rouzbeh Moini. “A Wide Band Dual-Polarized Microstrip Patch Antenna”. Antennas and Propagation Society International Symposium, 1997. IEEE., 1997 Digest Volume: 2 1997, Page(s): 956 - 959 vol.2.
- [6.20] Ahad Tavakoli, Nader Damavandi, and Rouzbeh Moini Mazandaran. “Analysis of Cross-Shaped Dual-Polarized Microstrip Patch Antennas”. Antennas and Propagation Society International Symposium, 1995 , Page(s): 994 - 997 vol.2.
- [6.21] Terence Quinlan, Nick Warren and Stuart Walker. “A 1.5 GHz Bandwidth, Linear Polarisation Switchable, 5 GHz Crossed Rectangular Patch Antenna”. Loughborough Antennas and Propagation Conference, Nov 2012.
- [6.22] Antenna Theory Analysis and Design (Third Edition). Constantine Balanis. Pages 816 and 817.

Chapter 7 Implementation of Antenna Design

7.1 Introduction

The design and modelling carried out in the previous chapter defined all the parameters and material details necessary to now fabricate a viable high isolation switched polarisation plane antenna design. The next challenge was to assemble and test a number of structures that replicate and so confirm the modelled predictions. It will also be necessary to demonstrate that these results are repeatable and that a number of identical devices can be fabricated.

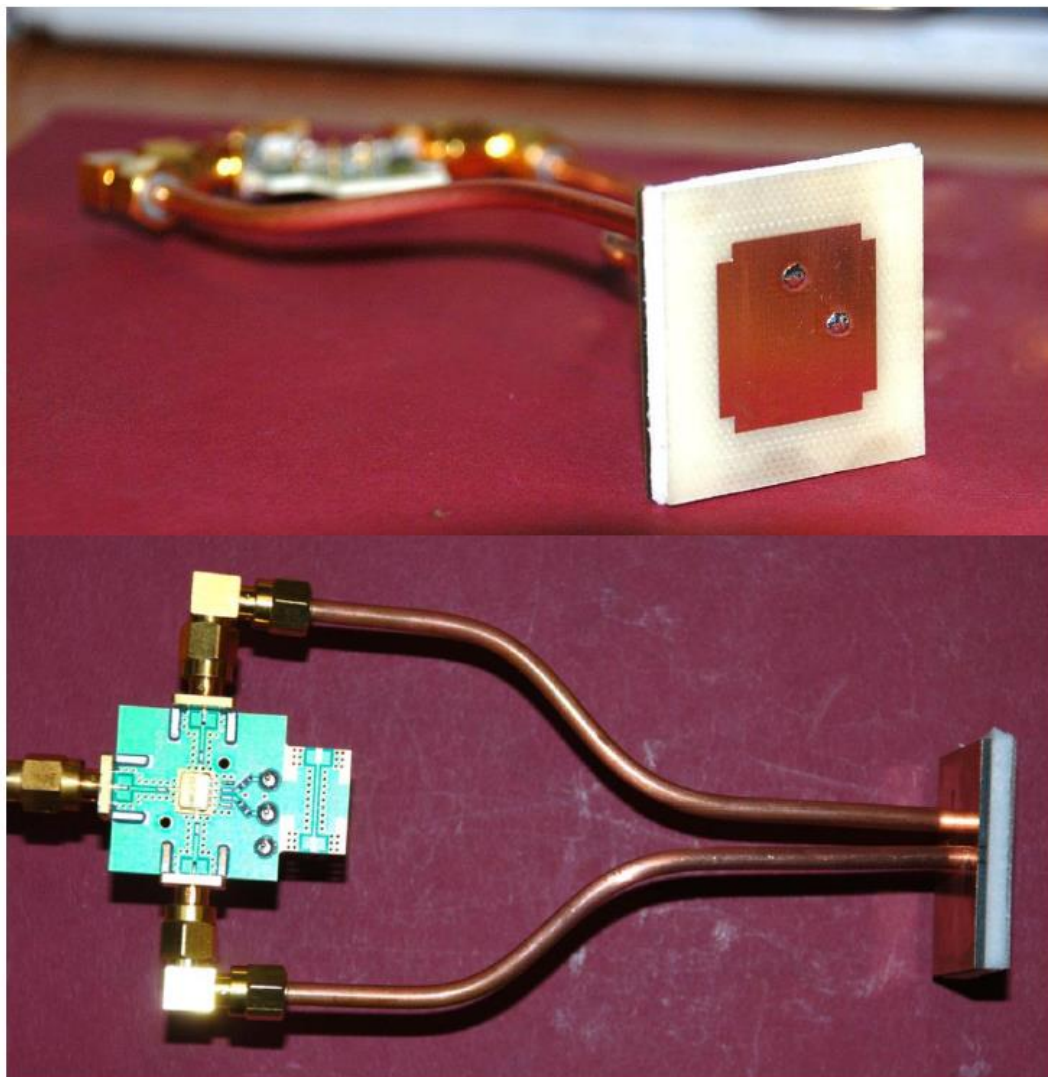


Fig. 7.1. Finished antenna assembly with RF switch attached

Using the information gathered from the modelling exercise three antennas were to be fabricated. Firstly it was necessary to pre-fabricate and form the semi rigid coax cable feeds. These were to consist of 12cm lengths of RG 402 cable with SMA connectors fitted to one end, the other end being stripped and prepared to form the coaxial probe feed. After preparing the ground plane from a 35mm x 35mm section of double sided FR4 material the outer conductor was soldered directly to the inner copper surface. At this point care was taken to ensure that there was no contact with the outer copper layer, as this was found to introduce some unwanted resonance effects. In this way the outer screen of the coax was incorporated into the ground plane on one face of the FR4 material only. These coax assemblies were then used for connection to a Hittite HMC 232 single pole double throw non-reflective (50Ω terminated) RF switch. This semiconductor type device was mounted on an evaluation PCB as can be seen in the lower half of Fig. 7.1. This assembly then provided a convenient former for the Eccostock foam material to be fitted, trimmed and fabricated. Once formed this material was then glued to the ground plane allowing the previously drilled and machined top layer and radiating patch to be accurately positioned, glued to ensure homogenous contact and soldered in place. The completed assembly with the patch and supporting layers front view is shown in the top section of Fig. 7.1. In all three devices were fabricated, all of which exhibited the properties outlined in the following sections with only minor variations.

7.2 Input / Feed Measurements

Modelling results suggested that a good impedance match could be expected at the design centre frequency of around 5 GHz, a broad S_{11} return loss indicating a wide useable bandwidth and little activity outside this frequency range. Initial assessment of the antenna performance was carried out using an Anritsu 37397D VNA over the

frequency range of 2GHz to 10GHz. Care was taken to calibrate the VNA to take account of the effect of the coaxial probe feed cable length as this could add misleading capacitive and inductance effects as well as introducing phase anomalies to the measurement. The effect of the semi rigid feed cable being approximated during the calibration procedure by the addition of a representative length of cable. S_{11} return loss measurements, were then taken on each input port of the antenna in turn with the remaining, unconnected port terminated at 50Ω . As with the simulation technique, this would mimic the action of the non-reflective RF switch and avoid any unwanted reflections from the unused antenna port.

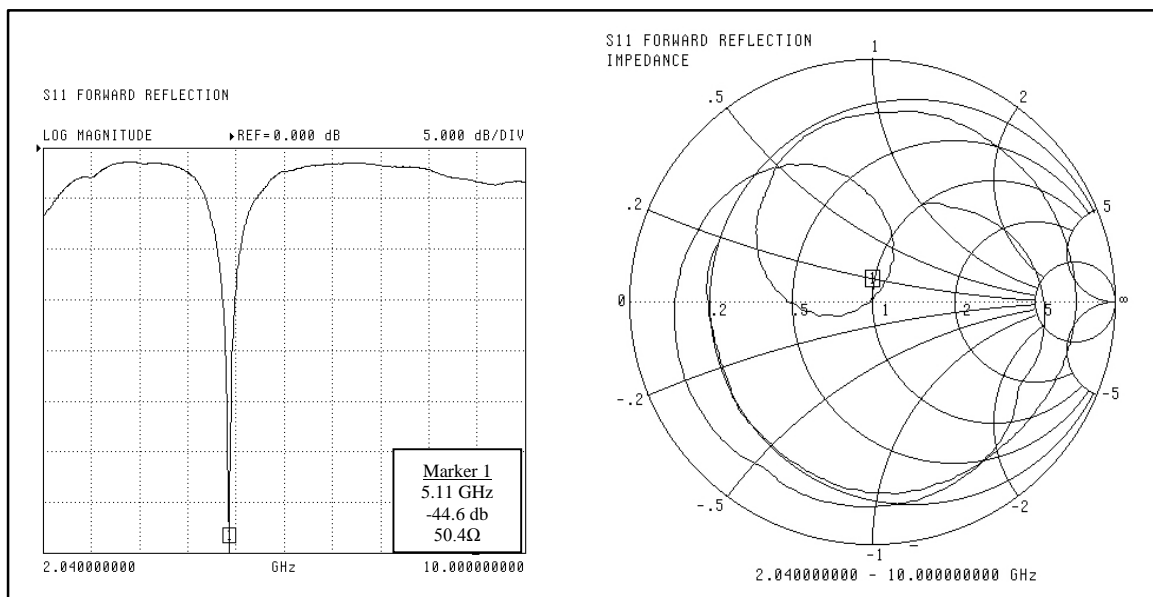


Fig. 7.2a S_{11} of Port 1 return loss Fig. 7.2b. S_{11} of port 1 impedance measurement

Figure 7.2a. shows the resulting return loss plot with port 1 stimulated. As can be seen this closely resembles the modelled result shown in Fig. 6.14. of the previous chapter. This revealed well matched input characteristics. with port 1 returning a respectable signal level of -44.6 dB at a frequency of 5.11 GHz. The associated impedance characteristics for port 1 are shown in the Smith chart displayed in Fig. 7.2b. Shown here

is a measured impedance of 50.4Ω at the acceptable frequency of 5.11GHz . Also as can be seen from the resonant loop in the Smith chart trace the structure showed little tendency to respond outside this region. Both ports were well matched with a similar result being obtained for port 2 as shown in Fig. 7.3a and Fig. 7.3b. As can be seen port 2 had a slightly lower return loss figure at -39.3 dB at a marginally different frequency of 5.14 GHz . With an input impedance of $49.1\ \Omega$ at that frequency again and with no tendency indicated of other resonances being present, this was considered a satisfactory result for both input ports.

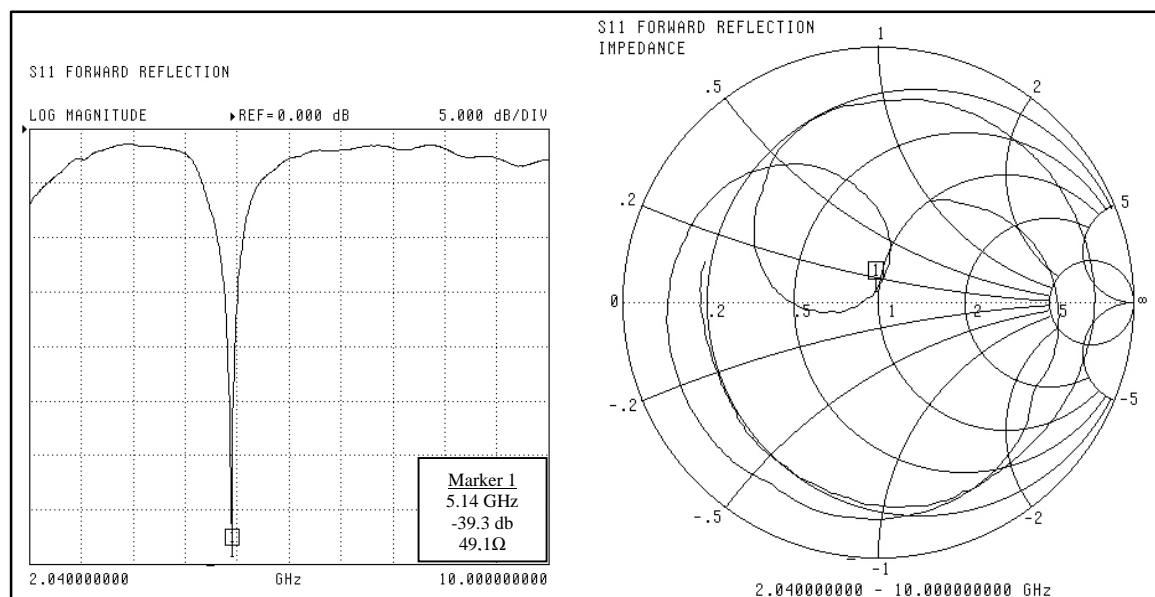


Fig. 7.3a S_{11} of Port 2 return loss Fig. 7.3b. S_{11} of port 2 impedance measurement

With these results being very similar to those predictions obtained with the antenna model, this was taken as primary evidence that the model is valid and that the other predicted parameters, including the radiation pattern predictions, are sound. If polarisation isolation and gain measurements are also found to be comparable to those predicted, this would further re-enforce this supposition.

7.3 Polarisation Isolation Measurements

As it was central to the validity and usefulness of the design, next it was decided to measure the polarisation plane isolation of the devices. Two identical antenna structures were now required. By measuring and comparing the co-polar and cross-polar behaviour of an antenna pair in this realistic situation the viability of the completed test cell would now be assessed. Any irregularities in the radiation pattern could drastically reduce polarisation plane segregation and would also degrade the accuracy of the mutual gain measurements to be carried out later. With the RF switches now connected as shown in the lower section of Fig. 1. each of the coaxial probe inputs could then be easily activated in turn to switch polarisation states. Using a pair of patch assemblies, one connected to each port of the VNA; these were then mounted approximately 0.75 metres apart and aligned to give maximum amplitude with the RF switches set so as to give a co-polar orientation of the devices. S_{21} , transmission loss measurements were then conducted over the transmission path between the antennas at the same frequency range used for the previous S_{11} measurements. Figure 7.4a. Shows the resulting co-polar response, indicating a useable -10dB bandwidth between markers 2 and 3 of 1.68 GHz and a centre frequency of 5.05 GHz. As well as confirming a peak resonant frequency close to that predicted by the modelling this result validates the “low Q” technique in obtaining wide bandwidth patch performance with coaxial probe feeds. Switching the port excitation on one antenna revealed the cross polar characteristics as shown in Fig. 7.4b. Measurement of the levels indicated a fall of 23.2 dB at 4.26 GHz, 24.6 dB at 5.05 GHz and 27.6 dB at 5.94 GHz, again suggesting reasonable agreement with the model. These results represent a significant improvement over the designs studied, in both available bandwidth and polarisation segregation across the operating frequency range.

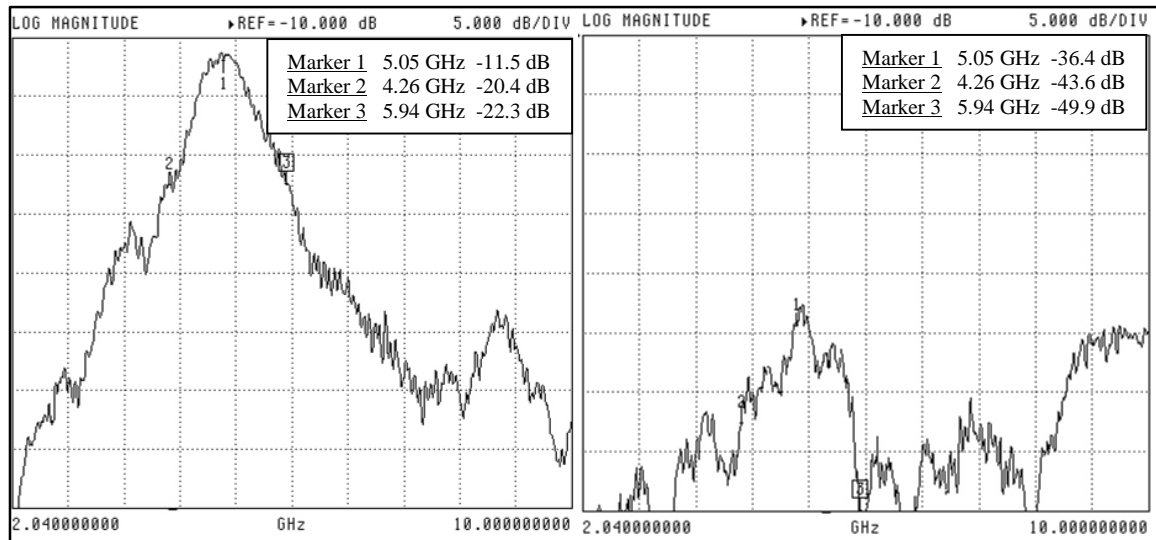


Fig. 7.4a S₂₁ of port 1 to port 1 co-polar plot *Fig. 7.4b. S₂₁ of port 1 to port 2 cross polar plot*

So as to confirm consistency of the devices and port characteristics, the ports on both antennas were then switched, identical results were obtained with this reciprocal port activation.

7.4 Gain Measurements

Finally the gain of the antennas was measured using two of the finished devices. One for transmission, connected to a Hewlett Packard 83711A RF signal generator set at the desired frequency of 5 GHz and a power level of 0 dBm. The second, receiving antenna was connected to a Rhode and Schwartz FSU spectrum analyser set to measure received power. Both antennas were then positioned one metre apart for ease of calculation with their co-polar ports activated and both antennas aligned for the maximum received signal strength. A power of -30.5 dBm was subsequently recorded. Free space path loss (FSPL) was then calculated using the (Friis) equation (1) below.

$$FSPL = 20\log_{10}(F) + 20\log_{10}(d) + 32.5 \text{ dB} \quad (1)$$

Where F was the frequency and d was the distance in metres giving a FSPL of 46.47 dB. This equated to an individual antenna gain of 7.98 dBi, again very close to that of the predicted value. For the purposes of these measurements and the future construction of the measurement cell a far field distance of 1.54cm for this device was calculated from the standard equation

$$d = \frac{2D^2}{\lambda} \quad (2)$$

Where d was the far field distance, D was the antenna dimension of 2.15cm and λ is the wavelength at 5GHz taken as 5.98cm.

7.5 Conclusions

Shown here was the implementation, construction, and experimental verification of a wideband, linear polarisation switchable, crossed rectangular patch antenna. The device exhibited a centre frequency very close to that of the design aim of 5 GHz with gain and polarisation isolation measurements taken at that frequency. A useable -10 dB bandwidth of 1.68 GHz. was also accomplished with polarisation isolation being maintained across that frequency range. The use of the thick substrate “low Q” technique coupled with coaxial probes was shown to be effective in achieving this wide bandwidth performance. This technique successfully compensated for any limitations introduced by the use of the dual coaxial probe patch feeds. Polarisation plane isolation was confirmed across the useable frequency range at levels close to those predicted for this crossed rectangular design strategy. These parameters were verified by far field S_{21} transmission loss measurements. Both input return loss characteristics and polarisation and gain measurements are very close to those predicted and so positively indicate the validity of the modelled results. With a measured antenna gain of 7.98 dBi being within 0.3 dB of

the modelled prediction the low back radiation and forward radiation pattern properties that were predicted can also be expected to be correct. Polarisation switching was accomplished via an on board RF switching arrangement and integral semi rigid coaxial cable / probe feed technique using off the shelf, commercially available materials and components. Using these methods of construction and measurement a number of closely matched devices were readily produced indicating that this device was both stable and consistently repeatable.

Chapter 8 Polarisation Switchable Measurement System

8.1 Final System Overview

With the development of the polarisation switchable sensing antenna complete and the VCSEL based optical transmission system finalised it was then possible to combine the two entities. Capable of functioning up to a distance of 1km this would then form “a polarisation switched, narrowband RF probe system using a VCSEL optical feed” [8.01]. As with the UWB based antenna based system the three patch antennas were mounted on a 120 degree pitch around a polycarbonate frame to facilitate the sensing head as shown in Fig. 8.1. below. Shown here is the completed sensing head assembled with the patch antennas orientated so as acquire orthogonal readings from a vertically aligned metallic target as described in the preceding chapters.

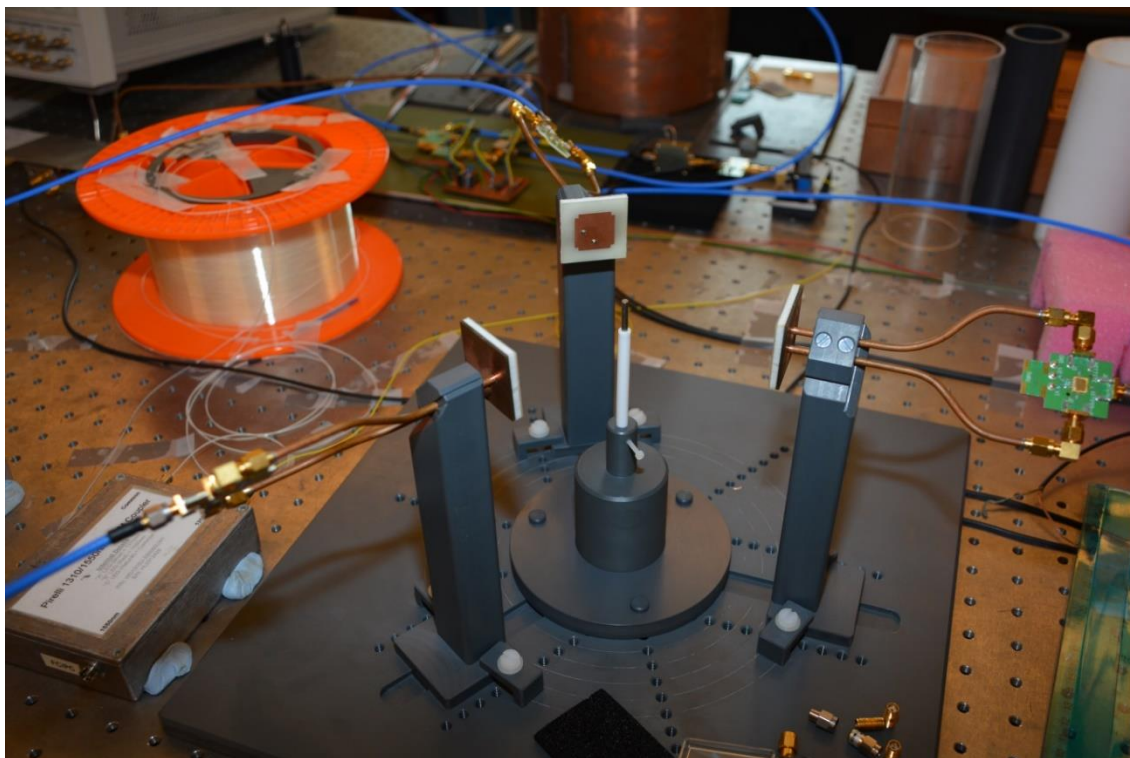


Fig. 8.1. Polarisation switchable sensing head.

As can be seen the semi rigid coaxial cable probe feeds were utilised to both accommodate the Hittite RF switches as well as aid in the alignment and mounting of patch antennas. Optimal horizontal placement of the antennas was frequency dependant and accommodated by a sliding arrangement in the mount. To ensure consistency with earlier versions of the system the frequency of operation was defined at 5GHz; as before, therefore the antenna spacing was arranged to be as for the previous UWB antenna design also. For this purpose the patch face was taken as a nominal reference point. So as to ensure that there was no interaction or coupling between the antenna and the target and that the now narrow radiation beam did not compromise the measurements, it was now necessary to ensure the measurements were taken in the far field. This far field distance was taken as 1.54cm from the calculation in the previous chapter, meaning that the 9cm spacing between antennas allowed a suitable target to antenna far field distance. Vertical positioning of the target into the peak antenna beam area was accomplished with a screw locked PTFE post as before. With the RF switches in place this now allowed a direct “drop in” replacement for the original sensing head. An additional control function was then required for polarisation plane switching that needed to be synchronised to the antenna pair selection function. This was easily accommodated using an extra bit on the data logger sequence to toggle between the input selection logic lines of the Hittite RF switches. As can also be seen from Fig.8.1. there is no longer any shielding material surrounding the sensing head structure. This was found to be no longer necessary as there was now very little influence apparent from the movement of outside objects, people etc. This was thought to be the result of the now tightly controlled and relatively narrow beam (no side lobes) characteristics due to the patch design. Also the absence of back radiation eliminated reflected interference from behind the patch structure. All these features gave

rise to a very stable sensing platform. As a result any concerns as to the negative effect of the screen on polarisation plane orthogonality and separation could now be allayed.

8.2 Antenna to antenna measurements

As suggested by the initial experimental work in chapter 3 antenna gain will affect the system dynamic range, higher gain leading to better SNR and so improved resolution. If this is the case then it may be expected that the patch antenna design with a gain in the order of 8dBi will show an improvement over the UWB antenna with a gain of 2dBi. To verify the performance of the antenna in the overall system firstly measurements were taken between two devices without the optical link in place as with the previous set of experiments.

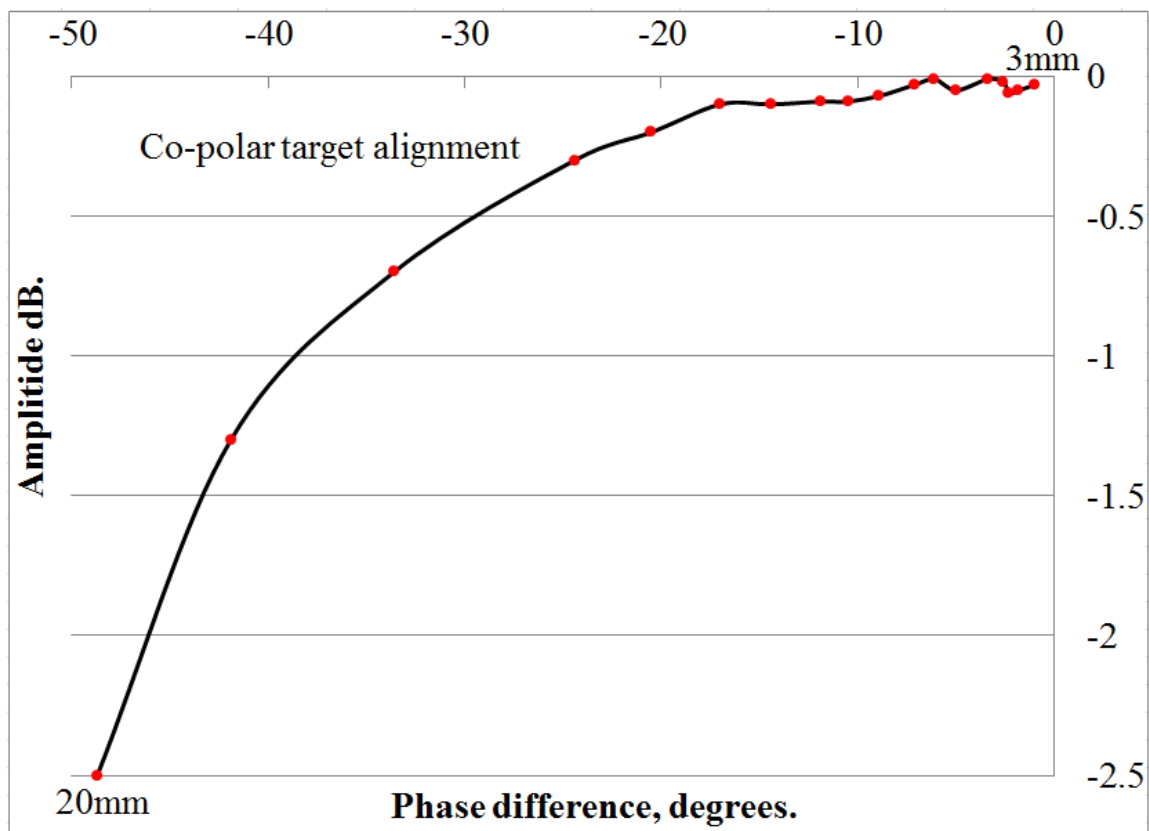


Fig. 8.2. Co-polar patch to patch to target measurements

Using the same set of targets as before and with the antennas adjusted to give maximum sensitivity a range of phase / amplitude readings were taken. Patch input ports were selected so that there was co-polar alignment between two patches as well as aligning the E-planes along the target. Figure 8.2. shows the plot of the resulting co-polar data series. From this it can be seen that target size identification has been extended down to 3mm and that data steps are still clearly discernible. The phase shifting range has also been extended at the higher (20mm) end of the measurements to 48.7 degrees. These results further indicate that the higher gain due to the patch antenna has increased the overall dynamic range of the measurement system.

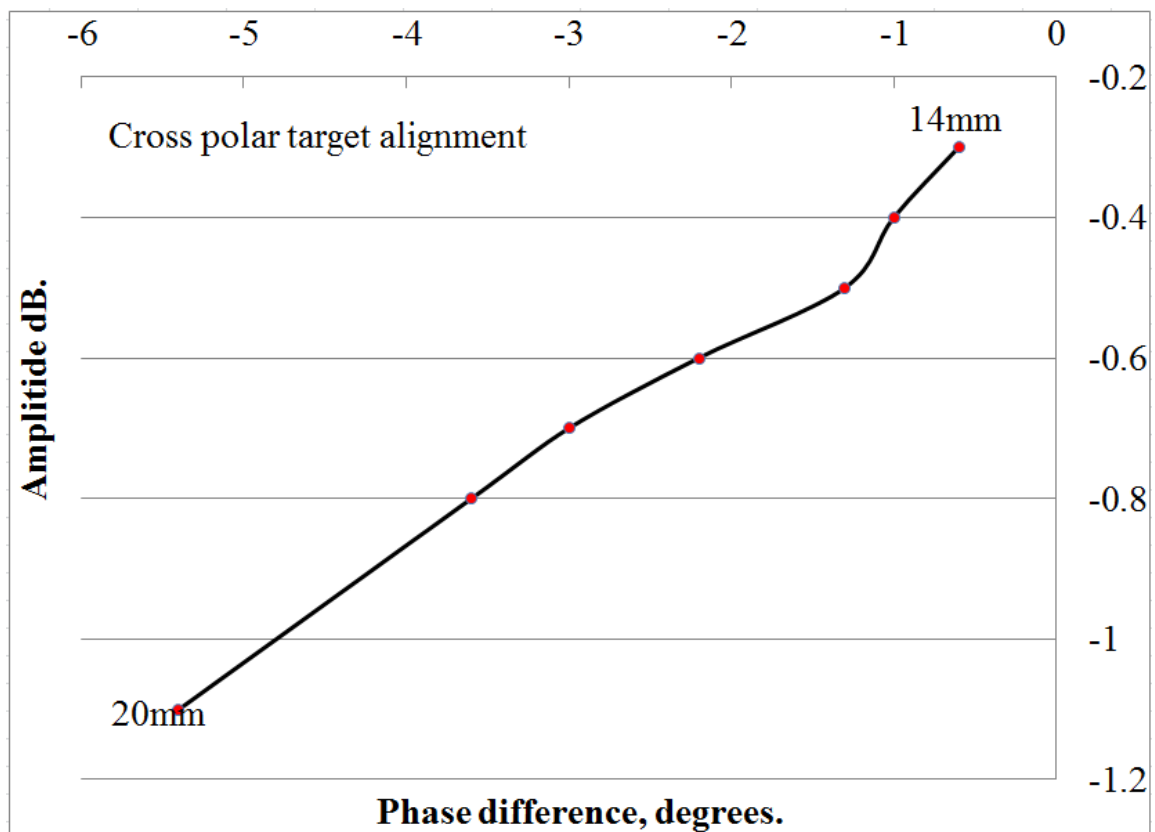


Fig. 8.3. Cross polar patch to patch, cross polar to target measurements

It was then necessary to evaluate an identical set of readings with the antennas polarisation planes switched through 90 degrees (cross polar). If these results are at a

reduced level then this will confirm the results obtained in the earlier chapters with the linearly polarised UWB antennas. Figure 8.3. shows the results obtained from the same set of targets from 20mm down to 14mm where readings became too small to register. As can be seen these results are far below those obtained from the co-polar measurements shown in Fig. 8.2. Such a result confirmed the possibility of acquiring isolated sequentially switched measurements on the two orthogonally opposed polarisation planes available to the antenna.

8.3 Radio over fibre comparison

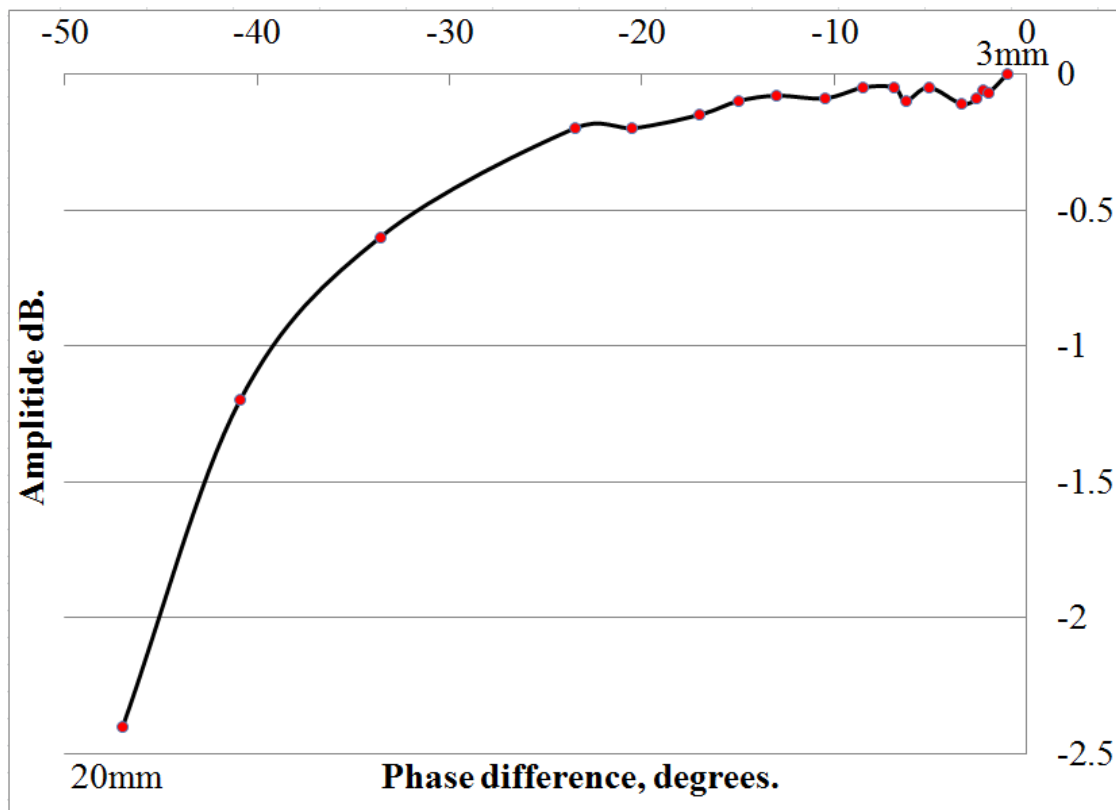


Fig. 8.4. Co-polar patch to patch to target measurements after optical transmission

As the VCSEL based optical delivery system was now proven, and transmission and reception levels could remain the same, the complete sensing head was now substituted and the co-polar measurements shown in Fig. 8.1. were then repeated. The resulting

readings are shown in Fig. 8.4. where it can be seen that the recorded levels after optical transmission closely resemble those prior to passage through the 1km of optical fibre. Again, as with the previous results this indicates that the optical system complements the antenna and is capable of preserving the nature of the phase / amplitude data acquired from the sensing head. Polarisation switching of the antenna produced similar results to those recorded in Fig. 8.3. For ease of comparison the complete set of readings is shown in Table 8.1.

Table 8.1. Comparison of readings

Target length mm	Before Optics		Before Optics Cross -Polar		After Optics	
	Phase deg	Ampl dB	Phase deg	Ampl dB	Phase deg	Ampl dB
20	-48.7	-2.5	-5.4	-1.1	-47	-2.4
19	-41.9	-1.3	-3.6	-0.8	-40.9	-1.2
18	-33.6	-0.7	-3	-0.7	-33.6	-0.6
17	-24.4	-0.3	-2.2	-0.6	-23.5	-0.2
16	-20.5	-0.2	-1.3	-0.5	-20.5	-0.2
15	-17	-0.1	-1	-0.4	-17	-0.15
14	-14.4	-0.1	-0.6	-0.3	-15	-0.1
13	-11.9	-0.09	-	-	-13	-0.08
12	-10.5	-0.09	-	-	-10.5	-0.09
11	-8.9	-0.07	-	-	-8.5	-0.05
10	-7.1	-0.03	-	-	-6.9	-0.05
9	-6.1	-0.01	-	-	-6.3	-0.01
8	-5	-0.05	-	-	-5.1	-0.05
7	-3.4	-0.01	-	-	-3.4	-0.11
6	-2.6	-0.02	-	-	-2.6	-0.09
5	-2.3	-0.06	-	-	-2.3	-0.06
4	-1.8	-0.05	-	-	-2	-0.07
3	-1	-0.03	-	-	-1	0

8.4 Conclusions

This final system encompassed the combination of the best attributes of RF sensing and optical delivery systems discussed in a number of respects. Firstly the planar antenna design described was small in size and so allows integration into a compact sensing head design. Such a patch configuration gives the advantage that both polarization planes are generated from the same point in space and at the same time possesses a gain in excess of 8dBi in both planes. This represented a significant advance over the previously proposed crossed dipole type designs for this sensing application as the higher gain inherently leads to an improved signal to noise ratio in the received signal and so an enhanced system sensitivity. The single lobe properties of the radiation pattern meant that orthogonal measurements can be performed about the same axis, enabling coincident readings of both polarisation planes, at any point within the illumination area. A high degree of separation between antenna measurement planes lead to low crosstalk / high isolation between coincident measurements. Such properties helped to ensure a high degree of independence between orthogonal readings. When operated in combination with the directly modulated, VCSEL based, coarse wavelength division multiplexed optical delivery system, accurate remote operation over a distance of 1km was accomplished. Phase contrast techniques used in this application again yielded measurements capable of enabling sub mm resolution using a narrow bandwidth, single cm wavelength, sensing frequency. With the benefit of the system noise reduction techniques discussed previously, combined with the increased dynamic range attributed to the antenna, the measurement range was extended down to an object size 3mm. Coupled with the polarisation switching capabilities of the antenna the system as a whole has now been shown to be capable of optically remoted single point dual axis measurements.

Reference

- [8.01] Terence Quinlan and Stuart Walker. "A Polarization Switched, Narrow Band, RF Probe System Using a VCSEL Optical Feed." IEEE Sensors Journal, Vol. 14, No. 12, Dec 2014, pages 4348 to 4353.

Chapter 9 Summary of Chapters and Further Work

Described in this thesis is the background, design methodology and practical implementation of a phase related, single frequency microwave detection system. An optical network that supports the remote operation of the sensing devices was also researched, devised and evaluated. The work shown here is divided into eight descriptive chapters prior to this summary. These chapters are intended to provide a description of the background reasoning, rationale and developmental steps that led to the experimental evolution of the final detection system.

Chapter 1: Sets the scene, introducing some basic concepts and applications relating to radio frequency detection. Initial notions of RADAR are introduced and some basic ranging and detection principles are described. Some limiting factors based around problems associated with signal quality limitations and radar cross section effects are then introduced. Signal attenuation and SNR are briefly discussed as is the influence of the permittivity (dielectric constant) of the transmission medium. Differing antenna configurations are then introduced as is the effect this can have on the performance of a detection system. Multiple antenna arrays and phase related inter-antenna and array effects are also briefly discussed. Stemming from this, methods of generating polarisation separated electromagnetic fields and how these may be used to extend and enhance microwave detection techniques are then introduced. Following this, the chapter goes on to briefly mention the bandwidth limitations of substrate based antenna designs, techniques that may be employed to overcome these limitations and their use in UWB detection. Finally the use of phase contrast is introduced with ifSAR satellite surveying given as an example.

Chapter 2: Expanded on some of the concepts outlined in Chapter 1. Particular emphasis is placed on the functional operation and performance of component parts within short range microwave detection systems. The chapter also examines studies carried out for specific applications. The first of these to be examined in this chapter was that of medical imaging. A number of extensive and comprehensive studies were examined so as to illustrate the degree to which this area has been explored. Many of these employed complex antenna arrays that were supported by comprehensive image reconstruction algorithms and techniques, all required a largely homogenous transmission medium to avoid problems of clutter. The most promising of these studies employed slot coupled, suspended patch type antennas to support a pulsed UWB “time of flight” radar technique. The next area to be explored was that of ground penetrating radar. This is an extremely challenging area as any system has to cope with unpredictable interface conditions as well as a transmission medium that is by its nature not homogenous. Again these studies used a number of differing antenna designs tailored to supporting signals that could provide adequate penetration and in addition employed “delay and sum” techniques to try to overcome the clutter issues. Although system resolution is not so much of an issue here this did illustrate a method that could be developed to overcome the issue of clutter to some extent. Following on from this the area of non-destructive evaluation was addressed and the area of phase based detection was introduced. Some issues relating to the advantages and disadvantages of the technique were discussed and an appropriate frequency range identified and the issue of “phase unwrapping” was briefly identified. Moving on from this Chapter 2 then examines a number of different antenna designs that have been used for detection purposes. Factors including the radiation characteristics, pulse response, bandwidth availability, ease of construction and antenna size are considered. As the antenna requirement for the system to be developed is

very specific in that it needs to be small in size, have a wide bandwidth and sufficient gain as well as controllable polarisation properties, the correct choice of design will become apparent in later chapters. Finally the problems associated with the preservation of phase properties in the transmission system are raised and the possibilities for optically remoting the sensing head are initiated. Throughout Chapter 2 a number of short range system studies were examined that go beyond the detect and ranging function previously discussed in Chapter 1. These studies debate methods that seek to not only locate an object but also to reconstruct and image of the subject. In all these studies a significant common problem with system resolution was identified that was associated with the time of flight methods employed coupled with the ratio of the microwave wavelength to that of the subject.

Chapter 3: Briefly recapped the findings of the previous chapter to identify a scheme that could be employed and developed to address the resolution issues associated with microwave detection systems. Aims and objectives were identified as well as some initial parameters and an outline methodology and strategy. An initial proof of concept experiment was described so as to establish the basic premise of the use of microwave frequency phase and amplitude related measurement use for short range detection methods. The use of a network analyser and commercial antennas was validated and produced some ground rules for detection that were to be expanded later. Based on these results the chapter goes on to describe the construction of a sensing head and the RF switching, electronics and software that would allow triangulation based measurements to be acquired. Using this setup a series of experiments were then described that established the optimum configuration of the measurement head. As a result it was concluded that using the linearly polarised commercial antennas allowed the possibility of making

measurements separated by the polarisation planes of the antennas. The chapter concludes by showing a series of E plane orientated, optimised, amplitude and phase measurements carried out on a series of targets of differing sizes. This procedure also confirmed that the technique was capable of much higher resolution than that previously shown in many of the studies discussed in Chapter 2.

Chapter 4: Described work that was carried out in parallel with the detection system study but was directly relevant to, and was used to, provide a solution to the problem of providing interconnects that could preserve phase information. The chapter begins with a description of the type of signals that were to be transmitted and identifies the optical fibre transmission techniques that were investigated. Two devices were identified, VCSELs for their low power requirements and an R-EAT device for its ability to enable remote deployment. As the type of Radio over Fibre signals to be used deployed various levels of QAM the phase and amplitude preservation requirement was directly comparable to the sensing application also. A brief description of these signals was given along with a short explanation of EVM for clarity. A detailed description of experiments that led to successful bi-directional optical transmission using both types of devices then followed. Constellation measurement methods confirmed the effectiveness of these methods over distances far in excess of that required for the sensing application (20km). As most accuracy deviations were as a result of signal to noise ratio effects this could only improve at the 1km target distance. Methods used to tackle the problems associated with the direct VCSEL modulation methods are described. The effectiveness of these measures was shown using a variety of VNA plots, frequency spectrum plots and constellation analysis. An outline description of some of the devices used is given towards the end of the chapter.

Chapter 5: This chapter described in detail the experimental procedures carried out in order to arrive at a satisfactory optical information delivery system suitable for use with the microwave detection system at this point of development. [A similar commercial system is also cited in this chapter, this post-dates (2013) the work carried out and published in this thesis.] Investigations into both reflective and CWDM optical systems are described and their attributes analysed. Firstly a system that utilised the reflective transducer was described. Adapting the system used for data transmission, a system is described that attempts a full duplex function by adding an RF circulator to the output port of the R-EAT. This section also contains much analysis of the electrical and optical characteristics of the device and associated VCSELs using a variety of techniques. Crucially R-EAT crosstalk was also quantified, this along with a lack of isolation in the RF circulator was shown to render this approach unsuitable but is included as it demonstrated some useful measurements that would also be relevant later. Secondly the evolution and refinement of the CWDM system into a viable option is described. At this point the only VCSELs available had a limited bandwidth but a matching technique is described that extends this sufficiently to obtain results. Before and after optical transmission results are shown that confirm the functioning of the CWDM system to be valid. Sources of system noise are identified and eliminated at this stage, also the need for optical isolators was identified (these techniques were incorporated into the RoF work at this stage also). Finally a CWDM system is described that uses the wider bandwidth VCSELs used for the RoF systems. In conjunction with the noise reduction measures and some response flattening of the antennas plots are shown that indicate much improved resolution with a reduced need for any signal averaging. Measurements are also shown for the system performance though some common dielectric materials that indicated

further resolution improvements may be possible and that polarisation is also not affected in these cases.

Chapter 6: With this established Chapter 6 focussed on the design of a polarisation switchable antenna. Design options were considered and the chosen configuration was that of a patch design as this gave a good gain performance a small size and a planar platform from which to launch the signal. Some design options and configurations were discussed that could increase bandwidth but overall it was decided to adopt a design based on a thick substrate square patch with a coaxial feed. This option was chosen as it provided a practical, realisable and repeatable design. Square patch dimension derivations are shown and calculations are described. The chapter then goes on to describe how these and the material parameters are used to construct a CST Microstripes model and shows the resulting analytical plots and diagrams. These indicated a well behaved linearly polarised square patch with a well formed single lobe radiation pattern and little back radiation. The next section describes the addition of a second port, so enabling excitation on two orthogonal polarisation planes and introduces the use of RF switches at the antenna feed points. S_{11} return loss predictions were shown for both ports and the predicted effectiveness of the technique indicated with both surface current plots as well as co-polar and cross polar radiation pattern plots. A discussion of the polarisation plane isolation then leads into a description of the development of the design into that of a rectangular patch antenna. The performance of this was then analysed using the same parameters as for the square design and an increase on isolation between radiating and non- radiating edges noted. A natural progression from this led to the final crossed rectangular patch design that possessed all of the desired characteristics for use with the sensing system. Predictions for the final device were then shown that indicated that both

input ports were well matched to the desired 50Ω impedance value and were very close in magnitude at 65dB and 70dB respectively. A comprehensive surface current analysis diagram indicated that edge excitation activity was confined to that selected by port excitation with little interaction. These properties were confirmed by the polarisation dependant radiation pattern plots that concluded the chapter that indicated polarisation plane isolation to be in the order of 28dB with co-polar gain in excess of 8dBi. If this could be translated into a practical structure this antenna is ideal for the sensing purposes of the system.

Chapter 7: Concentrated on the fabrication of the switchable antenna assembly and the measurement of the antenna parameters to confirm the performance of the design and so the validity of the modelled predictions. Detail of a completed antenna assembly is shown together with the port switching arrangement. Following on from this VNA measurements of both input ports were shown that concur with the model and also confirm acceptable 50Ω input impedances are present at the desired frequency ranges. Next, far field, polarisation isolation and gain measurements were shown that also closely matched the predicted results. With these measurements being commensurate with the model, it was concluded that the modelled results were both valid and credible.

Chapter 8: Chapter 8 then draws together all elements of work to form the complete optically remoted polarisation switchable phase contrast sensing system. A new antenna mount was described that accommodated the new devices, these being incorporated into the existing switching and optical transmission system. Initial experiments established that the low back radiation and tighter forward radiation pattern of the new antennas removed the need for any extra screening at the sensing head. An experimental procedure

that established the correct functioning of the antennas and increased sensitivity due to the higher gain of the patch configuration was then described. Next, measurements that confirmed the validity of the polarisation properties of the antenna and orthogonal sensing technique were described. Finally, just as for the previous system, a set of identical measurements were taken after optical transmission to confirm the transparency of the link. This showed detection down to 3mm with sub mm steps being clearly discernible.

Further Work: Whilst this work has focussed principally on the physical attributes and problems of microwave sensing, the integration of data gathering and image reconstruction techniques would represent a significant addition to the work. As seen in Chapter 1 and Chapter 2 many of these techniques already exist and have been the subject of a large number of studies. This could be used as a tool to allow further work that should include investigations into phase shifting behaviour within the measurement cell, factors such as the external screen position and the influence of the resulting measurement cell shape on sensitivity could then be assessed in more detail. As seen antenna design has a great influence here and there is potential for further development here also. Further assessment of the effect on system sensitivity in the presence of various dielectric materials and multiple permittivity's and how these may effect polarisation preservation of orthogonally separated sensing signals should be conducted. Of great interest would be how polarisation planes behave in the presence of dielectric materials of irregular shapes, also the associated propagation effects and limitations / enhancements this may introduce on the analysing signal. An example of this is the way rain drops affect propagation in mm wave satellite communication systems and weather radars. The relatively long wavelengths deployed in the proposed system may alleviate such

problems however, as seen, wavelength shortening can be expected. The development of a high density scanning multi antenna sensing array mount would greatly enhance the project, as this would allow large amounts of data to be gathered and analysed and would be essential if the system were to be used in any form of imaging. Noise reduction / cancellation techniques could be investigated to enhance the recovered signal SNR. This could use Digital Signal Processing techniques could facilitate filtering methods that would reduce “shrouding” due to noise and so further enhance system resolution. Such methods may be essential if the system is to be used in real world environments polluted by emissions from new generation mobile devices.

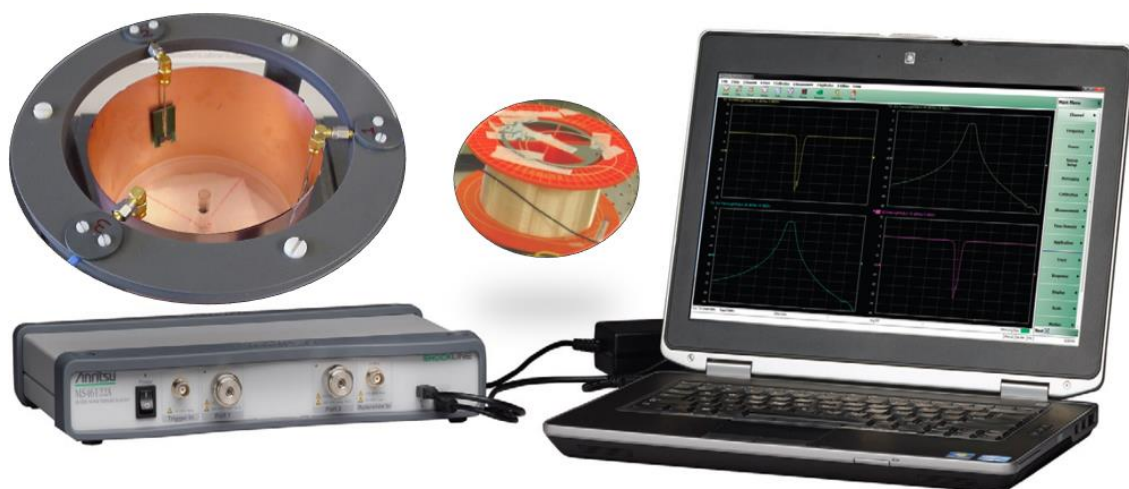


Fig. 9.1. Components of a potential complete system.

The original intention of the research was to produce a complete microwave imaging system. The full extent of this task soon became apparent and it was decided to concentrate on the issues of resolution and the accurate delivery of the data. With these problems addressed the ultimate future goal would be to implement these techniques in a fully functioning detection scheme. New generation VNA's that can interface directly with laptops are now available that will facilitate the highly portable and low cost analysis

and visualisation system that was initially envisaged. As shown in Fig 9.1 above, this, in combination with the use of multi antenna electronically switched arrays and uncomplicated low power, low cost optical data delivery systems mean that such a system is potentially attainable. Applications could then include medical imaging that would be available to younger clients, where conventional techniques fail due to higher density body tissues. Importantly, with the upcoming development and provision of widespread wireless networks, these facilities could then also be made available to those living in more remote and less developed regions of the world. In an NDE role, the potential for such a portable system has already been discussed and again, with suitable similar development this also becomes a viable proposition.

Authors Relevant Publications

Listed below are the authors publications showing abstracts as referred to in this thesis and listed in date order.

2005

Terence Quinlan, Sandra E.M. Dudley and Stuart Walker. "A High Throughput Short Range Transmission System Utilising Compact Patch Antennae." Loughborough Antennas and Propagation Conference. April 2005, pages 108-111.

"With the introduction of IEEE 802.16 Standard, frequencies in the 2GHz to 11GHz region will now become available for short range wireless local / metro area applications. Taking advantage of this, systems that offer a wider bandwidth within this frequency range will significantly enhance the potential of such networks. The proposed system is a high throughput, dual frequency, short range system, featuring wide bandwidth, suspended patch antennae and a phase locked loop data and clock recovery circuit."

2006

Terence Quinlan, Sandra E.M. Dudley and Stuart D. Walker. "Towards a 10GHz Bandwidth antenna array operating within the 2GHz to 11GHz frequency window." Loughborough Antennas and Propagation Conference April 2006 pages 201 to 204.

IEEE.802.16.3 has made the 2 GHz to 11 GHz frequency window available for exploitation, [1] with applications in the WiMAX / Metro Access Network [2] arena, maximising available bandwidth here is plainly highly desirable. Here we describe a linearly polarised, tri band; patch antenna array that combined with the use of a standard 4 QAM technique is capable of a data throughput in excess of 10 Gb/s. The design is based around a stub tuned, 4 GHz patch antenna. This is modelled using Agilent A. D. S. software and is then scaled both up and down to provide coverage at 2.4 GHz and 6 GHz.

Terence Quinlan, Sandra E. M. Dudley, and Stuart D Walker. "10.4 Gb/s Wireless Provision Featuring Linearly Polarised 802.16 Band Patch Antenna Arrays." I.E.E. Conference on Access Technologies 2006 pages 29 to 31.

"Wireless links are becoming an increasingly significant means of transferring data over short to medium distances. Systems such as WiMAX (Worldwide Interoperability for Microwave Access) have been developed with this in mind but would soon become congested if asked to cope with the demands of the latest generation of VDSL modems. Here we describe a 10.4Gbs wireless transmission system that operates within the frequency range of the I.E.E.E.802.16 standard. This system utilises a tri-band, wide bandwidth, linearly polarised antenna array to achieve this data rate.

2008

T. J. Quinlan, S.E.M.Dudley and S.D.Walker. "Time-Resolved Bragg Effects in an Ultra Wideband Leaky Feeder Antenna Array Based on Semi-Rigid Coaxial Cable". Loughborough Antennas and Propagation Conference March 2008 pages 125 to 128.

"We have investigated leaky-feeder, Ultra Wide Bandwidth antennas based on standard semi-rigid coaxial cable where axial slots are used to form a Babinet dipole antenna array. The slot function, array effect and slot spacing define both the radiation pattern and array bandwidth. Simulations based on Microstripes modelling software predicted the radiation characteristics whilst multi-GHz coherent time domain reflectometry was used to investigate slot size and spacing effects."

Sandra E. M. Dudley, Terence J. Quinlan and Stuart D. Walker. Ultrabroadband Wireless – Optical Transmission Links Using Axial Slot Leaky Feeders and Optical Fibre for Underground Transport Topologies. IEEE Transactions on Vehicular Technology. Vol 57, No 6 Nov 2008. Pages 3471 – 3476.

"This paper describes a hybrid leaky feeder / fiberoptic transmission system for use in underground transportation networks. The system has a 1.6-Gb/s throughput and features an ultrawideband axial slot leaky feeder, which is based on a standard semirigid coaxial cable as a fixed antenna. Patch antennas with a 4-GHz center frequency and a 1-GHz, –10-dB bandwidth are proposed for the rolling stock. This highest reported data rate was achieved by combining two 800-Mb/s in-phase and quadrature (I and Q) phase-shift keying (PSK) modulated data streams. A specially designed carrier and data synchronization system provided a convenient interface to a 1.3/1.5- μm duplex singlemode fiber-remoting network. The measured 2.4- to 6-GHz leaky feeder bandwidth allows multiradio multiband wireless mesh networking and, therefore, low-contention gigabit rolling stock data communications."

2009

Terence Quinlan, Sandra Dudley, Tony Jordan and Stuart Walker. "Improved Radio Frequency Imaging Resolution using Phase Contrast Interferometry. "Loughborough Antennas and Propagation Conference, 2009. Pages 105-108.

"Phase contrast techniques offer notable enhancement in resolution when used in optical microscopy. Microwave frequencies offer a high degree of penetration but resolution is limited in comparison to traditional imaging techniques. Application of this principle to centimetre wavelength radio frequency imaging can provide significant improvement in system accuracy. Using standard vector network analysis phase and amplitude measurements, dimensional resolution better than 1mm at a frequency of 5GHz was obtained. Signal integrity is maintained over a distance of 1 km using a novel optical transmission system that utilises a Reflective Electro Absorption Modulator and directly modulated Vertical Cavity Surface Emitting Lasers."

Manoj Prasad Thakur, Terence James Quinlan, Carlos Bock, Stuart Walker et al “480-Mbps, Bi Directional, Ultra- Wideband Radio-Over-Fibre Transmission Using a 1303/1564 Reflective Electro-Absorption Transducer and Commercially Available VCSELs.”. Journal of Lightwave Technology. Vol. 27, No. 3, Feb 2009. Pages 266 -272.

“We describe 480 Mbps, bi-directional ultra-wideband (UWB) radio signal transmission over 1 km of single-mode optical fiber. Key components are a highly linear, reflective electro absorption transducer (EAT) and commercially available 1308-nm and 1564-nm VCSELs with 4.8-GHz bandwidth. Detailed EAT and 1308-nm VCSEL distortion analyses and measurements are presented highlighting the low intermodulation and harmonic distortion necessary for typical 18-dB wireless channel error vector magnitudes (EVMS). Direct VCSEL modulation with Wimedia supported band group 1 (3.1–4.8 GHz) MB-OFDM UWB signals was modelled with VPI transmission Maker, suggesting a minimum EVM of 18.733 dB at 0.4502 OMI. This was confirmed by 480 Mbps upstream and downstream EVM measurements over fiber of 21.4 dB or better. Fully functional, half-duplex, bi-directional data transfer was achieved with interlocked RF switches.”

2010

T.J. Quinlan, S.E.M. Dudley and S.D. Walker. “Radio-over-Fibre Phase Contrast Imaging using a Reflective Electro-Absorption Transducer and 1550/1310nm VCSEL’s”. OFC 2010. JTHa57.

“Radio-over-fibre phase contrast imaging is a new technique for object characterization in hostile environments. Commercially-available 1550nm/1310nm VCSELs and a reflective electro-absorption transducer offer sub-mm resolution over 1km of SMF in a 3.1-5 GHz bandwidth.”

2011

Maria Morant, Terence Quinlan, Stuart Walker and Roberto Llorente. “Transmission of Triple-Format OFDM Radio Signals in Reflective Passive Optical Networks Avoiding Brillouin Scattering Effect.” OFC 2011, JWA72.

“Brillouin scattering is identified as a severe limitation in narrow line-width, bi-directional reflective systems. A spectrum management mitigation technique for triple-format OFDM signals is demonstrated over 15 km passive optical network using reflective electro-absorption transceivers.”

Maria Morant, Terence Quinlan, Stuart Walker and Roberto Llorente. “First Demonstration of Triple-Play Bi-directional Full-Duplex CWDM Transmission in Passive Optical Networks.” OFC 2011. OWB3.

“Bi-directional CWDM radio-over-fiber transmission of triple-format full-standard OFDM signals in coexistence (UWB, WiMAX and LTE) (1.178 Gbit/s full-duplex) is demonstrated over 50.6 km SSMF in passive optical networks without amplification or regeneration stages.”

Terence Quinlan, Maria Morant, Roberto Llorente and Stuart Walker. "Ultra-Low Cost and Power VCSEL-Based 480Mbit/s UWB Radio over a Bi-Directional CWDM PON." ECOC 2011.

"Ultra-low cost and power, -44dBm direct modulation of commercially-available 1344nm and 1547nm VCSELs by band-group 1 UWB signals is demonstrated over a 20.1 km, SSMF, CWDM optical network. EVMs < -18.3 dB were achieved."

Terence Quinlan, Maria Morant, Sandra Dudley, Roberto Llorente and Stuart Walker. "480Mbit/s UWB bi-directional radio over fiber CWDM PON using ultra-low cost and power VCSELs." OpEx 2011 Vol. 19 Issue 26, pages.B197-B202.

"Radio-over-fiber (RoF) schemes offer the possibility of permitting direct access to native format services for the domestic user. A low power requirement and cost effectiveness are crucial to both the service provider and the end user. Here, we present an ultra-low cost and power RoF scheme using direct modulation of commercially-available 1344 nm and 1547 nm VCSELs by band-group 1 UWB wireless signals (ECMA-368) at near broadcast power levels. As a result, greatly simplified electrical-optical-electrical conversion is accomplished. A successful demonstration over a transmission distance of 20.1 km is described using a SSMF, CWDM optical network. EVMs of better than -18.3 dB were achieved."

Terence Quinlan Sandra Dudley, Tony Jordan and Stuart Walker. "Remote, Non-Contact, Radio Frequency Phase Contrast Detection using CWDM and Directly Modulated VCSELs". LAPC Nov 2011. Pages 1 to 4

"Microwave imaging techniques using centimetre wavelengths gives benefits of low cost and high penetration coupled with low RF exposure. Non-contact methods such as that described here give the advantage that the antenna design procedure does not have to compensate for the electromagnetic properties of the medium under investigation. Surrounding material does not degrade the accuracy of the phase contrast based measurement technique described. The measurement system was complemented by the development of a Coarse Wavelength Division Multiplexed (CWDM) optical transmission system enabling remote operation over 1km. This technique achieves improved directional isolation over the previously reported reflective optical method. Target identification down to 5mm with sub-mm resolution was achieved at just 5 GHz carrier frequency."

2012

Terence Quinlan, Sandra Dudley, Maria Morant, Roberto Llorente and Stuart Walker. "First Demonstration of Cooler-less, Bi-Directional, Format-Agnostic, Wireless and Gigabit Ethernet Network Provision using Off-The-Shelf VCSELs." OFC 2012.

"We used cooler-less, directly-modulated, commercially-available, 1345.6 nm and 1541.9 nm VCSELs to deliver bi-directional, co-existing UWB, WiMAX, LTE and GbE capacity over 20.6 km of SSMF. Error-free GbE supported 65 nm SiCMOS 60 GHz pico-cell connectivity"

Terence Quinlan, Sandra Dudley, Maria Morant, Roberto Llorente, and Stuart Walker. "VCSEL-based, CWDM - PON systems using reflective technology for bi-directional multi-play service provision" OpEx 2012 Vol. 20 Issue 15, pp.16726-16734.

"Orthogonal frequency division multiplexing based on radio-over-fiber schemes allows the direct use of multiple, native format wireless platforms. In combination with standard baseband provision such as Gigabit Ethernet, this provides access to a wide range of services without requiring specialized end-user equipment. However, such signals have a high laser power-bandwidth requirement which may not be a good fit to the domestic environment. Here we explore the use of low-power optical components in customer premises which interface with an intermediate optical network node. Two solutions in the context of SSMF over a CWDM optical network are described, based on either reflective or direct modulation. EVMs of better than -35 dB were achieved."

Terence Quinlan, Nick Warren and Stuart Walker. "A 1.5 GHz Bandwidth, Linear Polarisation Switchable, 5 GHz Crossed Rectangular Patch Antenna." Loughborough Antennas and Propagation Conference, Nov 2012. Pages 1 to 5.

"Specifically designed for use with a centimetre wavelength, phase contrast, microwave detection system this antenna operates at a centre frequency of 5 GHz. The design utilises off the shelf RF switches for ease of implementation. The ability to be switched between two orthogonally separated polarisation conditions allows separate E plane measurements to be conducted. A wide bandwidth capability permits antenna placement optimisation and a swept measurement capability. Dual probe feeds ensure ease of construction whilst the low Q nature of the device enables a wide operating frequency."

2014

Terence Quinlan and Stuart Walker. "A Polarization Switched, Narrow Band, RF Probe System Using a VCSEL Optical Feed." IEEE Sensors Journal, Vol. 14, No. 12, Dec 2014, pages 4348 to 4353.

"Microwave detection techniques requiring high penetration are often reliant on the use of centimeter wavelengths. Systems such as these can also potentially be capable of being highly portable as well as being suitable for use in harsh and demanding environments. Further advantages of these systems are that they can also be cost effective, offer low levels of RF exposure and are of potential use in short range non-destructive evaluation applications. Lack of resolution is overcome by the use of a phase contrast technique. Using antennas specifically developed for this purpose the use of polarization adds a further measurement plane. The 5GHz. crossed patch design described here utilises commercially available RF switches for ease of implementation and exhibits typically 22dB isolation between each orthogonal - linearly polarised plane. This allows independent E-plane measurements to be conducted from a common point. Phase sensitive information is preserved by a low power optical bi-directional transmission system based around directly modulated Vertical Cavity Surface Emitting Lasers (VCSELs). The use of these techniques in combination enables a high resolution, dual plane scanning system capable of remote operation in demanding environments."

Appendix 1

List of Definitions

Monostatic, Bistatic: *Refers to the angle created by the distance between the transmit (Tx) antenna, the target and the receive (Rx) antenna. In a Monostatic radar the Tx and Rx antennas are either the same or very close together relative to the target distance creating a small angle. For a Bistatic radar the antennas are separated by a distance that is comparable or greater than the target range creating an angle up to 180 degrees.*

Multistatic: *Uses multiple Bistatic transmitter and receive paths in varying combinations to create multiple target reflections from different directions.*

Permittivity: *Of a substance is characterised by its ability to affect an electric field set up within the material. Is a measure of how the substance influences the organisation of electric charge, this will affect the speed of propagation and so the wavelength of an AC signal. Units, Farads / metre.*

Permeability: *Of a substance is characterised by its ability to affect a magnetic field set up within the material. Is a measure of how a material responds to an externally applied magnetic field. Units, Henrys / metre.*

Dielectric constant: *Also known as relative permittivity (ϵ_r). Is a measure of how a material affects or concentrates an electric field in comparison to that in a vacuum.*

Conductivity: *Is a measure of how quickly an AC signal is absorbed by a material. The higher the conductivity the more quickly the signal is absorbed and so the more opaque it appears.*

Electric field: *The force exerted by one area of electric charge on another. Units, Newtons / Coulomb. Will be dependent on the ability of a material to concentrate areas of charge.*

Ultra Wide Band (UWB): *A signal that has a fractional bandwidth in excess of 20%.*

Fringing: *“Fringing is a function of the dimensions of the patch, the height of the substrate and the dielectric constant of the substrate”. It is the degree to which the electric field extends beyond the confines of the radiating patch and as such effectively increases the dimension of the patch and will propagate differently depending on the dielectric constant of medium through which it travels. [6.22]*

Ereff: *Is the effective dielectric constant of a material and is considered as the dielectric constant of a material having identical properties in all directions. It is also a function of frequency “As the frequency of operation increases, most of the electric field lines concentrate in the substrate.” “For low frequencies the effective dielectric constant is*

essentially constant. At intermediate frequencies its values begin to monotonically increase and eventually approach the values of the dielectric constant of the substrate.”
 [6.22]

Appendix 2 Alphabetical List of Acronyms

APES.....	Amplitude & Phase Estimation
BPSK.....	Binary Phase Shift Keying
CT.....	Computer Tomography
CW.....	Continuous Wave
CWDM.....	Coarse Wavelength Division Multiplexing
DAS.....	Delay And Sum
EAM.....	Electro Absorption Modulator
EOE.....	Electrical-Optical-Electrical
EVM.....	Error Vector Magnitude
FDTD.....	Finite Difference Time Domain
GPR.....	Ground Penetrating Radar
IfSAR.....	Interferometric Synthetic Aperture
MAMI.....	Multi-static Adaptive Microwave Imaging
MIMO.....	Multi Input Multi Output
MIST.....	Microwave Imaging through Space Time
MZM.....	Mach Zehnder Modulator
NDE.....	Non-Destructive Evaluation
OSA.....	Optical Spectrum Analyser
OFDM.....	Orthogonal Frequency Division Multiplexing
QAM.....	Quadrature Amplitude Modulation
QCSE.....	Quantum Confined Stark Effect

QPSK.....	Quadrature Phase Shift Keying
R-EAT.....	Reflective Electro Absorption Transducer
RADAR.....	Radio Detection and Ranging
RCS.....	Radar Cross Section
RF.....	Radio Frequency
SNR.....	Signal to Noise Ratio
TDR.....	Time Domain Reflectometry
UWB.....	Ultra Wide Band
VCSEL.....	Vertical Cavity Surface Emitting Laser
VNA.....	Vector Network Analyser
YIG.....	Yttrium Iron Garnet